Fibroblast-Cardiomyocyte Cross-Talk in Heart Muscle Formation and Function

Doctoral Thesis

In partial fulfillment of the requirements for the degree

"Doctor rerum naturalium (Dr. rer. nat.)"

in the Molecular Medicine Study Program

at the Georg-August University Göttingen

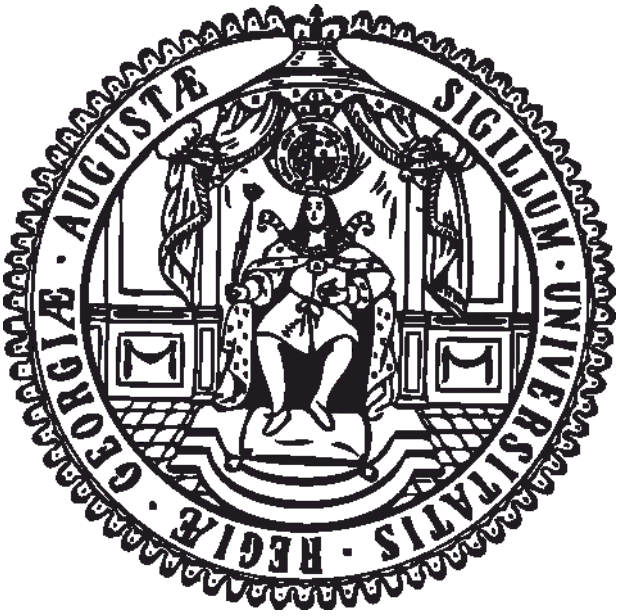

submitted by

Susanne Franziska Schlick

born in Filderstadt, Germany

Göttingen, November 2018

Members of the thesis committee

Prof. Wolfram Hubertus Zimmermann (supervisor) 1. Referee	Institute of Pharmacology and Toxicology University Medical Center Göttingen Robert-Koch-Str. 40 37075 Göttingen w.zimmermann@med.uni-goettingen.de
Prof. Ralf Dressel 2. Referee	Department of Cellular and Molecular Immunology Humboldtallee 34 37073 Göttingen, Germany rdresse@gwdg.de
Prof. Stefan Luther	Biomedical Physics MPI for Dynamics and Self-Organization Am Faßberg 17 37077 Göttingen, Germany Institute of Pharmacology and Toxicology University Medical Center Göttingen/Heart research building (DZHK) Robert-Koch-Str. 40 37075 Göttingen stefan.luther@ds.mpg.de

Members of the extended thesis committee

Prof. Rüdiger Behr	German Primate Center (Deutsches Primatenzentrum -DPZ) Kellnerweg 4 37077 Göttingen RBehr@dpz.eu
Prof. Thomas Meyer	Molecular Psychocardiology (Molekulare Psychokardiologie) Waldweg 33 37075 Göttingen thomas.meyer@med.uni-goettingen.de
Dr. rer. nat. Antje Ebert	Cardiovascular Cell Biology and Systems Medicine University Medical Center Göttingen Robert-Koch-Str. 40 37075 Göttingen antje.ebert@med.uni-goettingen.de

Date of submission of the Doctoral thesis: 06.11.2018

Date of disputation: 19.12.2018

Affidavit

Here I declare that my doctoral thesis entitled

"Fibroblast-Cardiomyocyte Cross-Talk in Heart Muscle Formation and Function"

has been written independently with no other sources and aids than quoted.

Susanne F. Schlick

Göttingen, November, 2018.

List of publications

Title	Type of publication	Date and location
Agonistic and antagonistic roles of fibroblasts and cardiomyocytes on viscoelastic stiffening of engineered human myocardium **Susanne F. Schlick***, Florian Spreckelsen*, Malte Tiburcy, Lavanya M. Iyer, Laura Zelarayan, Stefan Luther, Ulrich Parlitz, Wolfram H. Zimmermann, and Florian Rehfeldt *These authors contributed equally to this work	Research article	Prog Biophys Mol Biol. 2018 Dec 12. pii: S0079-6107(18)30159-7
X-ray diffraction imaging of cardiac cells and tissue Jan-David Nicolas, Marten Bernhardt, **Susanne F. Schlick**, Malte Tiburcy, Wolfram-H. Zimmermann, Amara Khan, Andrea Markus, Frauke Alves, Karl Toischer, Tim Salditt	Research article	Prog Biophys Mol Biol. 2018 Jun 15.: S0079-6107(18) 30064-6
Defined Engineered Human Myocardium With Advanced Maturation for Applications in Heart Failure Modeling and Repair Tiburcy M, Hudson J, Balfanz P,**Schlick S**, Meyer T, Chang Liao ML, Levent E, Raad F, Zeidler S, Wingender E, Riegler J, Wang M, Gold JD, Kehat I, Wettwer E, Ravens U, Dierickx P, van Laake LW, Goumans MJ, Khadjeh S, Toischer K, Hasenfuss G, Couture LA, Unger A, Linke WA, Araki T, Neel B, Keller G, Gepstein L, Wu JC1, Zimmermann WH.	Research article	Circulation. 2017 May 9;135(19):1832-1847.
Calcitriol enhances EHM contractile function	Poster	DGPT 2/2018, Göttingen
Effects of Vitamin D- binding protein on engineered heart muscle development and function	Talk	Meeting foundation Leducq 8/2017
Fibroblast origin determines engineered heart muscle development and function	Poster and talk (Poster prize)	Young DZHK Retreat 9/2016, Bad Aibling
Effects of Vitamin D binding protein on engineered heart muscle development and function	Talk	Meeting foundation Leducq 6/2016
Tuning hyaluronic acid deposition to enhance engineered heart muscle function	Invited talk	Dutch German Meeting 3/2016, Leiden, Holland
Hyaluronic acid deposition determines engineered heart muscle characteristics and can be pharmacologically targeted to enhance function	Invited talk	DGPT 3/2016, Berlin
Soft matter guided self-assembly of oscillating heart cells into functional macro-myocardium	Poster and talk	SFB937 Retreat 2015/2016

Table of contents

Acknowledgements

I would like to express my sincerest gratitude to Prof. Wolfram-Hubertus Zimmermann for the opportunity to conduct my Ph.D. work in his department. Apart from being the source of invaluable scientific advice and support, I have always been given the trust and encouragement to attend educational events of my personal interest, present my scientific work at various occasions and network freely with others. This freedom has been of tremendous personal benefit.

Furthermore, I want to especially thank my supervisor Dr. Malte Tiburcy for his daily supervision and guidance in the lab, as well as for all the scientific and personal support.

I would also like to thank the members of my thesis committee, Prof. Ralf Dressel (2nd referee of this work) and Prof. Stefan Luther, as well as the members of my extended committee, Dr. Antje Ebert, Prof. Rüdiger Behr and Prof. Thomas Meyer.

During this work, Prof. Susanne Lutz has been a great source of advice on fibroblasts and their biology, thank you.

This work was supported by the help of many trusted cooperation partners over the years, who I would like to acknowledge: Prof. Dirk Ziebolz, Dr. Katrin Streckfuß-Bömeke and Steffen Köhne (University Medical Center, Göttingen), the members of the SFB937 cooperative project (especially Florian Spreckelsen, Dr. Florian Rehfeldt, Prof. Ulrich Parlitz and Dr. Sebastian Stein, among many others). Prof. Jens Fischer and Petra Rompel (Institute of Pharmacology and Clinical Pharmacology, Düsseldorf).

My sincerest gratitude goes to the excellent technical and personal assistance I have received over the years, foremost by our cardiac differentiation team: Monika Hoch, Daria Reher, Andreas Schraut, Krasimira Sharkova and Iris Quentin. For support during animal studies that we conducted, I want to thank Sarah Zafar, Marcel Zoremba, and Roland Blume

For administrative and organizational help, thank you, Jutta Creydt and Silvia Magerkurth. I also greatly appreciate the help of Eva Ausmeier (SFB937) for the organization of technical assistance during my pregnancy and Dr. Lukas Cyganek and the whole team of the Stem Cell Unit, for providing a save and productive lab environment during this time.

Dear colleagues, I would like to express my deepest gratitude for all the good times, your scientific and personal advice. Foremost, to the members of my team (AG Tiburcy), who I greatly appreciate: Dr. Elif Levent, Mina Shahriyari, Luisa Peter, Paul Balfanz, Dr. Buntaro Fujita, Elina Grishina, Kashan David, Tabea Rekersbrink, Moritz Matthaei and Denise Hartung. For all the great advice and help I received, thank you: Dr. Poh Loong Soong, Dr. Sumon Sur, Dr. Tim Meyer, Dr. Norman Liaw, Dr. Svenja Hartmann, Lavanya Iyer, Dr. Sebastian Zeidler and many others! For great personal support and friendship, thank you, Dr. Monique Wölfer, Irina Trautsch and Franziska Rathjens.

I would like to mention and thank those people, who have had a great impact on my personal development and scientific career: Ulla Heilmeier and Frauke Ritter (Margaret Maltby Mentoring Program, UMG Göttingen), Dr. Ursula Hoffmann (my mentor), Dr. Steffen Burkhardt and Kerstin Grüniger (IMPRS Göttingen), Prof. Jari Ylänne, Prof. Jari Haimi, Prof. Elisa Vallius and Tiina Hakanen (University of Jyväskylä). And two very special people in my life: Dr. Benno Neufeld and Alexandra Belihart-Neufeld.

Most importantly my sincerest gratitude goes to my loving parents Maria and Wolfgang, thank you for truly everything! And to my family and all my friends, who have greatly supported me throughout all these years!

To my loving husband and our daughter.

Abstract

Cardiac fibroblasts make up a considerable fraction of the total heart cell content. How cardiac fibroblasts signaling affects heart muscle function in normal heart development and disease remains, however, largely unresolved. Engineered heart muscle (EHM) developed from human pluripotent stem cell-derived cardiomyocytes (CMs) and fibroblasts in a collagen I hydrogel can be considered a human heart surrogate, allowing for precise assessments of fibroblast-CM crosstalk under defined *in vitro* conditions. We hypothesized that EHM development and function are controlled by fibroblast-mediated cardio-instructive cues. In line with this hypothesis, we found that macroscopically contracting EHM fail to form in the absence of fibroblasts. Biophysical analyses confirmed that fibroblasts control early collagen gel compaction and stiffening, suggesting a fine-tuning function as to the biomechanical properties of the extracellular matrix (ECM) environment. Transcriptome data suggested that EHM formation in the presence of fibroblasts recapitulates important aspects of early cardiac morphogenesis, including cardiac cushion formation. In line with these findings, we identified hyaluronan (HA) as a crucial component of EHM development and function. However, excessive HA deposition resulted in functional deterioration of EHM, pointing to the need for a fine-tuning of fibroblast-mediated processes during cardiomyogenesis. By systematically comparing primary fibroblasts of different origin (skin, gingiva, cardiac) to their cardiomyogenesis-supporting activity, we found that the developmental cues needed for EHM formation were to a certain extent universally present in all tested fibroblast species. We further observed that fibroblasts from patients with dilated cardiomyopathy (DCM) elicited a pathological contractile phenotype, underscoring the relevance of fibroblast-CM crosstalk in health and disease. Collectively these findings provide strong evidence for the active role of fibroblasts in determining development, function, and disease states of the human heart.

To further improve our *in vitro* model and allow for the future use of EHM *in vivo*, we developed EHM under chemically defined conditions. We furthermore identified pluripotent stem cell (PSC)-derived cardiac fibroblast-like cells as a potential source of fibroblasts for EHM application.

List of figures

List of tables

Abbreviations

µl	microliter(s)
µm	micrometer(s)
α-SMA	α-Smooth Muscle Actin
ANG II	Angiotensin II
ANOVA	Analysis Of Variance
APC	Allophycocyanin
APS	Ammonium Persulfate
ATF6	Activating Transcription Factor 6
BMP	Bono Morphogenic Protein
bp	base pair
BSA	Bovine Serum Albumin
CACNA1c	Calcium voltage-gated channel subunit α1 C
cAMP	cyclic Adenosine Monophosphate
CD	Cluster of Differentiation
cDNA	complimentary DNA
CDS	Coding Sequence
CFB	Cardiac Fibroblast
CM	Cardiomyocyte
CO_2	Carbon Dioxide
COL1α1	Collagen type I α chain 1
CSA	Cross sectional area
CTGF	Connective Tissue Growth Factor
CTR EHM	EHM of healthy control
CVD	Cardiovascular Disease
Cx	Connexin
d	day(s)
DCM	Dilated cardiomyopathy
DCM CFB EHM	EHM of DCM affected cardiac fibroblasts
DCM CM EHM	EHM of DCM affected cardiomyocytes
DCM EHM	EHM of dilated cardiomyopathy
DDR-2	Discoidin Domain-containing Receptor 2
DEPC	Diethylpyrocarbonate
Dexa	Dexamethasone
DMEM	Dulbecco's Modified Eagle's Medium
DMSO	Dimethyl Sulfoxide
DNA	Deoxyribonucleic Acid
DNase	Deoxyribonuclease
dNTP	Deoxyribonucleotide Triphosphate
DSP	Desmoplakin

E	Embryonic day (mouse development)
EC50	Concentration at half maximal effect
ECM	Extracellular Matrix
ECT	Engineered Connective Tissue
EDTA	Ethylenediaminetetraacetic Acid
EHM	Engineered Heart Muscle
ELN	Elastin
EMT	Epithelial-Mesenchymal Transition
EndMT	Endothelial-Mesenchymal Transition
EPDC	Epicardial-Derived Cells
ER	Endoplasmic Reticulum
ES cell	Embryonic Stem Cell
EtOH	Ethanol
FACS	Fluorescence-activated cell sorting
FBLN1	Fibulin 1
FBS	Fetal Bovine Serum
FC	Flow Cytometry
FGF	Fibroblast Growth Factor
FGM3	Fibroblast Growth Medium 3
FITC	Fluorescein isothiocyanate
FSC	Forward Scatter
FSP-1	Fibroblast Specific Protein-1
Fwd	Forward primer
g	Gravitational force
GAG	Glycosaminoglycan
GAPDH	Glyceraldehyde-3-Phosphate Dehydrogenase
GFB	Gingiva Fibroblast
GFP	Green Fluorescent Protein
GMP	Good Manufacturing Practice
GO	Gene Ontology
Gy	Gray
h	hour(s)
H_2O	Water
HA	Hyaluronan
HAS	Hyaluronan Synthase
HCM	Hypertrophic Cardiomyopathy
HEPES	4-(2-Hydroxyethyl)piperazine-1-ethanesulfonic acid
HF	Heart failure
HFF	Human Foreskin Fibroblast
HMMR	Hyaluronan-mediated motility receptor
HMW	High Molecular Weight

HSA	Human Serum Albumin
HYAL	Hyaluronidase
Hz	Hertz
IF	Immune Fluorescence
IGF	Insulin-like Growth Factor
IL-6	Interleukin-6
IMDM	Iscove´s Modified Dulbecco´s Medium
IPS cell	Induced Pluripotent Stem cell
IRE-1	Serine/threonine-protein kinase/endoribonuclease IRE1
JUP	Junction plakoglobin
KO	Knockout
L	Liter
LGALS-1	Galectin-1
L-Gln	L-Glutamine
LIF	Leukemia Induced Factor
LMW	Low Molecular Weight
M	Molar
Max	Maximum
MHC	Myosin Heavy Chain
MI	Myocardial Infarction
MIM10-B	Mesodermal Induction Medium 10B
min	minute(s)
miR	microRNA
MME	Neprilysin
MMP	Matrix Metalloproteinase
MYH	Myosin Heavy Chain
MYL	Myosin Light Chain
n	Number of biological replicates
N-cadherin	Neuronal cadherin
NCD	Non-Communicable Disease
NaCl	Sodium Chloride
NaOH	Sodium Hydroxide
NEAA	Non-Essential Amino Acids
NM	Non-myocyte
nm	nanometer(s)
OB-cadherin	Osteoblast cadherin
o.n.	over night
p	p-value
P/S	Penicillin/Streptomycin
Pa	Pascal
PBS	Phosphate Buffered Saline

PCA	Principal Component Analysis
PCR	Polymerase Chain Reaction
PDGF α/ß	Platelet-Derived Growth Factor α/ß
PDGF α/ß R	Platelet-Derived Growth Factor α/ß Receptor
PDMS	Polydimethylsiloxane
PFA	Paraformaldehyde
PSC	Pluripotent Stem Cell
POSTN	Periostin
PVDF	Polyvinylidene Difluoride
qRT-PCR	Quantitative Real Time PCR
Rev	Reverse primer
RFP	Red fluorescent Protein
rHSA	recombinant Human Serum Albumin
RNA	Ribonucleic acid
RPKM	Reads Per Kilobase of transcript per Million mapped reads
rpm	Rounds per minute
RPMI	Roswell Park Memorial Institute medium
RT	Reverse Transcription
RT	Room Temperature
RYR2	Ryanodine Receptor 2
s	second(s)
SDS	Sodium dodecyl Sulfate
SDS PAGE	Sodium dodecyl Sulfate Polyacrylamide Gel Electrophoresis
SEM	Standard Error of the Mean
SERPINE1	Plasminogen activator inhibitor-1
SFMM	Serum-free maturation medium
SOC	Super Optimal broth with Catabolite repression
SPADE	Spanning-tree Progression Analysis of Density-normalized Events
SSC	Sideward Scatter
StC-SM	Stromal Cell Specification Medium
TAE	Tris base, Acetic acid and EDTA
Taq	Thermus aquaticus
TBS	Tris Buffered Saline
TBS-T	Tris Buffered Saline -Tween 20
TCF21	Transcription factor 21
tdRFP	targeted Red Fluorescent Protein
TEMED	Tetramethylethylenediamine
TGFß	Transforming growth factor ß
TGFßR	Tumor Growth Factor ß Receptor
TNFα	Tumor Necrosis Factor α
TNNI	cardiac Troponin I

TNNT	cardiac Troponin T
Tra	Holo-Transferrin, human
Tris	Trisamine
TSA	Human embryonic kidney SV40 transformed cells
TSP1	Thrombospondin 1
V	Volts
V	Volume
VCAN	Versican
WGA	Wheat germ agglutinin

1 Introduction

1.1 Cardiovascular diseases

Cardiovascular diseases (CVDs) remain the leading cause of death worldwide, both in industrial, as well as developing nations (Mendis et al., 2011). CVDs include coronary /ischemic heart disease, which is most prevalent, followed by congenital and cerebrovascular disease (stroke), as well as pathologies that underlie arrhythmias and other disorders of the myocardium (cardiomyopathies; WHO global atlas 2011 (Mendis et al., 2011), Figure 1-1).

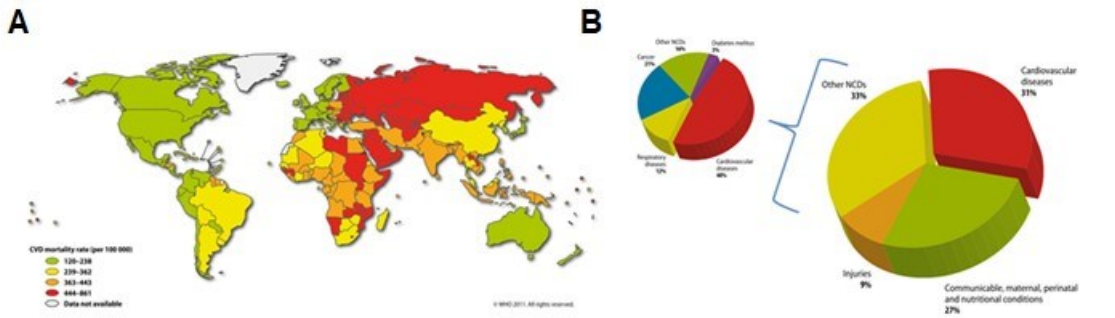

Figure 1-1 Cardiovascular disease worldwide

A Global distribution of CVD mortality rates (age standardized, per 100 000) **B** Distribution of global CVD burden (NCD - non-communicable disease). Approximately a third of NCDs are also CVDs. Taken from WHO global atlas 2011 Figures 6,7,10 (Mendis et al., 2011).

Deaths due to coronary heart disease have risen sharply since the beginning of the 20th century and peaked in the 1960s (Dalen et al., 2014) as a result of multiple risk factors (lifestyle, smoking, diabetes, hypertension) (Bentzon et al., 2014; Yusuf et al., 2004). In coronary heart disease, a buildup of plaques in the coronary arteries leads to impaired blood flow causing myocardial infarction (MI). As a consequence, areas of the myocardium undergo cellular death by apoptosis, necrosis and autophagic mechanisms (Whelan et al., 2010).

In contrast, non-ischemic cardiomyopathies are a large and diverse group of disorders that are the result of genetic predispositions, a consequence of (auto)immune reactions, or the cardiotoxicity of certain drugs. Among these are hypertrophic cardiomyopathies (HCMs) and dilated cardiomyopathies (DCMs). In HCMs, the left ventricle is found enlarged, while the latter are characterized by a dilatation of the left (or both ventricles) and myocardial fibrosis. Genetic aberrations identified in HCM and DCM typically affect the

cardiomyocyte (CM) contractile apparatus (sarcomere and cytoskeleton), ion channels, or mitochondrial proteins. Indeed, about 20% of the DCM cases can be attributed to mutations in titin (Braunwald, 2017).

1.1.1 The failing heart

The final consequence of an injured or otherwise impaired myocardium is progressive heart failure (HF), the state at which the heart has sustained excessive injury or is pathologically so impaired that it is unable to sustain the blood flow and pressure needed to supply the body with the required amount of oxygen and nutrients. HF is graded by the severity and symptoms patients present with and clinically stratified according to left ventricular ejection fraction, which is either preserved or reduced (Berliner and Bauersachs, 2017; Mosterd and Hoes, 2007; Ponikowski et al., 2016). Despite considerable efforts and advances in the pharmacological field, none of the current treatments targeting HF are curative. Thus, current therapeutics can only slow HF progression and aim to improve quality of life, while preventing hospital admission and reducing mortality (Berliner and Bauersachs, 2017; Ponikowski et al., 2016). At a terminal state, only a replacement of the diseased heart remains as therapeutic option. For transplant patients, the 1-year and 5-year survival are high with 84% and 76%, respectively, and a fifth of patients are alive 20 years after successful transplantation (Lund et al., 2014). Unfortunately, suitable donor hearts are highly limited (Johnson et al., 2014; Kittleson, 2016) and given the further increase in HF prevalence, it is clear that new therapies have to be introduced to target this challenge. This requires both novel *in vitro* systems to aid drug development (see 1.5 and 1.6) and new regenerative strategies to support or repair the diseased myocardium (1.1.2 and Figure 1-2).

1.1.2 Regenerative approaches in cardiovascular medicine

1.1.2.1 Direct reprogramming approaches

One approach in cardiovascular regenerative medicine is to target resident cells in the affected myocardium and stimulate their survival and/or proliferation (Doppler et al., 2013; Ishikawa et al., 2015) or to directly reprogram one resident cell-type into another (Figure 1-2) (Doppler et al., 2013; Luigi, Anastasia et al., 2006). This approach has been predominantly aimed at the conversion of myofibroblasts into functional CMs (Miyamoto et al., 2018; Nam et al., 2013; Song et al., 2012). First encouraging reports from *in-vivo*

models of mice reported preserved cardiac function and a reduction of adverse remodeling and fibrosis after MI (Miyamoto et al., 2018; Song et al., 2012).

1.1.2.2 Transplantation of stem cells and derivatives

Stem-cells provide an infinite source for the repair of any cell type and tissue of the body. It has thus been a primary strategy to directly deliver stem cells to the failing heart (Figure 1-2) (Doppler et al., 2013). The benefit of embryonic stem (ES) cells and induced pluripotent stem (IPS) cells have been studied extensively in animal transplantation models but there remains concern about the risk of teratoma formation when transplanting PSCs (Nelson et al., 2009; Nussbaum et al., 2007). In contrast, the use of a variety of different adult, bone marrow-derived stem cell populations and stem cells from adipose tissue have been categorized as safe, but with limited clinical improvements (Doppler et al., 2013).

Hence, a strategy has been to support the heart with *in vitro* PSC-derived CMs. This provides the myocardium with *bona fide* CMs and could circumvent the teratoma risk of näive PSC cells. Chong and colleagues demonstrated the potential use of human ES cell-derived CMs in a clinically relevant macaque model. Here, large numbers of CMs were delivered via epicardial injection. Retained cells coupled to the host myocardium and supported neovascularization of the infarct area (Chong et al., 2014). Of note, a great limitation when transplanting cells in suspension has been their effective and long-lasting engraftment onto host myocardium. Several groups have attempted to resolve this by transplanting cells together with suitable matrices (Blondiaux et al., 2017; Tang et al., 2017; Wang et al., 2017, 2018) (see also next section) an approach termed “tissue-engineering”.

1.1.2.3 Tissue engineering

In tissue engineering, one or more cell types are embedded into matrices to provide a more natural environment (Figure 1-2) and enhance cell retention after implantation (Doppler et al., 2013; Karikkineth and Zimmermann, 2013; Ogle et al., 2016) (Figure 1-2 and Figure 1-8). Tissue engineering can additionally be utilized for *in vitro* research and using PSCs, as an infinite cell source, allow for large and highly standardized screening applications (see also 1.5 and Figure 1-10).

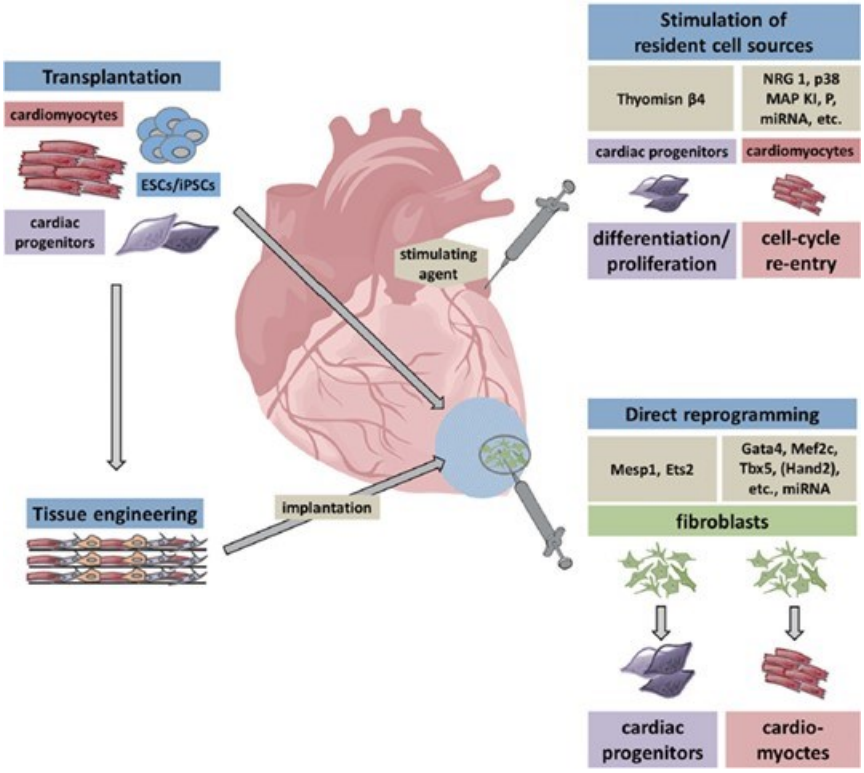

Figure 1-2 Different regenerative approaches targeting cardiac disease

The approaches in regenerative medicine to target the many types of cardiac disease are highly versatile and may ultimately be applied best in a disease specific or individualized approach. In direct cell transplantation both pluripotent/multipotent stem and progenitor cells may be used, but also cells derived from them (as in the case of EHM for instance). Cells can either be delivered via direct injection as a cell suspension or in a tissue engineering approach. Alternatively, resident cells may be stimulated to proliferate (CMs) or be reprogrammed (myofibroblasts) to differentiate into the required cell types (image taken from (Doppler et al., 2013).

In order to understand the perquisites for successful tissue engineering, an in-depth knowledge of the myocardial cell types and their interactions is required. Reciprocally, findings from engineered tissues that display organotypic functionality can be applied to decipher cell-cell and cell-matrix interactions that underlie developmental and pathological processes within the endogenous myocardium (see focus of this work 1.6).

1.2 The cellular components of the myocardium

1.2.1 Cardiomyocytes

The heart is a large muscular pump with four chambers that maintains pulmonary and systemic blood flow to support all tissues and organs with sufficient oxygen and nutrients. The CMs whose elaborate cytoskeleton with myofibrils drives contractile motion can be found in the muscular walls of the atria and ventricle in the heart. Another type of CMs,

the cardiac pacemaker cells, are an integral part of the heart's conduction system that controls the heart rate.

During embryonic development, CMs first proliferate (hyperplastic growth) and then enlarge (hypertrophic growth), resulting in an increased heart mass and size. During this development, their shape changes from a polygonal morphology to a more elongated one, as myofibrils develop and elongate parallel to the axis of the growing cell. Concurrently, the mechanical adherens junctions and desmosomes (containing cadherins and desmoplakin) assume a bipolar distribution connecting both ends of the elongated cell to adjacent cells and the ECM, together with gap junctions, in large intracellular complexes termed intercalated discs (Hirschy et al., 2006). Eventually, elongated and tightly connected CMs, form a functional syncytium (Gregorio and Antin, 2000; Severs, N., 2000). In the fully developed myocardium, the connection of the cytoskeleton to ECM and cell-cell contacts via gap junctions allows for the synchronized transmission of biomechanical and electric signals which results in the generation of directional forces across the ventricle.

1.2.2 Non-myocytes

There has been a long debate about the non-myocyte composition of the heart. Due to a lack of proper cell type specific markers, the identification of individual non-myocyte populations and their characterization has been intrinsically difficult with standard histological and fluorescence activated cell sorting (FACS) techniques. As the growth of the postnatal myocardium is mediated by hypertrophic expansion of CMs, the vast volume in the heart is occupied by CMs. However in numbers, only around 20-30% of cells in the postnatal heart are CMs (Bergmann et al., 2015; Nag, 1980; Pinto et al., 2015), the remaining cell fraction consists of endothelial cells, smooth muscle cells, cardiac fibroblasts and resident and transient immune cell populations. Recently, Pinto and colleagues used an elaborate bioinformatics algorithm, Spanning-tree Progression Analysis of Density-normalized Events (SPADE), to further stratify individual non-myocyte populations of the murine heart. They identified the predominant cell type of the heart were endothelial cells (40%) that constituted even more than 60% of non-myocytes in the heart. Of the non-myocyte population, (using platelet-derived growth factor α receptor (PDGFRα)-GFP, collagen type 1 α-chain 1 (Col1α1)-GFP, MEF-SK4 and TCF21 lineage tracing) cardiac fibroblasts only contributed 15% and cells of hematopoietic origin

between 5-10%. In the human heart they could recapitulate their findings and identified 20-30% CMs and 50% endothelial cells (Pinto et al., 2015) (Figure 1-3).

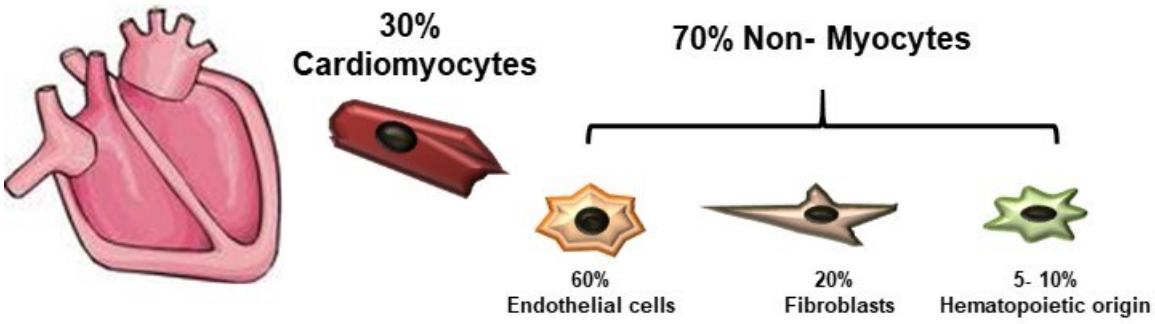

Figure 1-3 Cellular components of the myocardium

The cellular composition of the heart has been of long debate as it is intrinsically difficult to stratify the many different cell populations with appropriate markers. This figure summarizes the findings that were generated with SPADE analysis using FACS according to (Pinto et al., 2015). (Heart graphic by www.wikispaces.com/open access graphics).

1.2.3 Cardiac fibroblasts

Cardiac fibroblasts are elongated, spindle shaped cells with an elaborate endoplasmic reticulum and Golgi apparatus, reflecting their high secretory activity. They are furthermore characterized by the lack of a basement membrane (Camelliti et al., 2005; Fan et al., 2012; Souders et al., 2009). To date, cardiac fibroblasts remain poorly defined (Ivey and Tallquist, 2016): The individual use of commonly recognized markers vimentin, Discoidin domain-containing receptor 2 (DDR2), and fibroblast-specific protein 1 (FSP1) have not been sufficiently specific to faithfully characterize these cells. Recently, cardiac fibroblast populations could be better stratified from other mesenchymal cell populations by using a combination of the markers PDGFRα, collagen type I and TCF21 (Ivey and Tallquist, 2016; Ivey et al., 2018; Pinto et al., 2015; Snider et al., 2009). Myofibroblasts could furthermore be distinguished from resident fibroblast populations by using TCF21 and periostin combined in lineage tracing experiments (Kanisicak et al., 2016)

1.2.3.1 Origin and role of cardiac fibroblasts in myocardial development

Cardiac fibroblasts are predominantly derived from epicardial cells at E12.5 (embryonic day) of mouse heart development (Sullivan and Black, 2013). These cells undergo periostin- and TGFβ-dependent epithelial-to-mesenchymal transition (EMT) (Olivey et al., 2006) and subsequently differentiate into cardiac fibroblasts (Fan et al., 2012) (Figure 1-4).

Moreover, some fibroblasts arise from the endocardium through endothelial- to mesenchymal transition (endMT) (Brutsaert, 2003; Fan et al., 2012).

As the embryonic heart develops, epicardial-derived signals guide CMs into the formation of a higher order multicellular syncytium, necessary for the development of contractile forces (Takahashi et al., 2014). Ablation of signals from the epicardium such as (fibroblast-specific) PDGFα (Bax et al., 2010) and insulin-like growth factor (IGF) 2 (Li et al., 2011) lead to failure of hyperplasia and cardiac compaction (Gittenberger-de Groot et al., 2012). Interestingely, the first time cardiac fibroblasts emerge is contemporaneous with compacted myocardium and Ieda and colleagues could establish a direct connection between epicardial fibroblast-derived signals and CM development. They demonstrated that collagen I and fibronectin secreted by cardiac fibroblasts mediate the proliferation of CMs during the hyperplastic growth phase via binding to integrin ß1 receptor (Ieda et al., 2009). These findings emphasize the crucial role of fibroblast-CM crosstalk in the proper spatiotemporal development of the compacting myocardium and how fibroblast-derived ECM components directly influence CM mitotic behavior.

Eventually, following a short peak in CM and fibroblast proliferation during large structural changes of the postnatal heart (Ivey et al., 2018), the cardiac fibroblast populations ceases proliferation and remains stable. In the adult heart, the predominant function of resident cardiac fibroblasts is the maintenance and homeostasis of the ECM (see 1.3.3). Upon pathological stimuli and insults, resident cardiac fibroblasts can be reactivated and transition into myofibroblasts (Camelliti et al., 2005; Fan et al., 2012) (see section 1.3 and 1.4.2). In addition, (myo)fibroblasts can be recruited from various origins, including the bone marrow ($CD45^+$ myofibroblasts) (Ivey et al., 2018) or originate from resident fibroblasts precursors (Moore-Morris et al., 2014) and fibrocytes (Fan et al., 2012) (Figure 1-4).

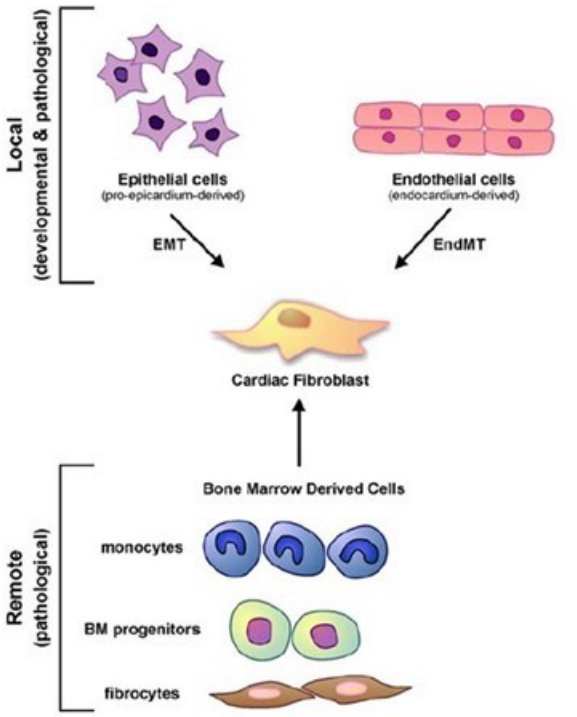

Figure 1-4 Origin of cardiac fibroblasts

In the development of the endogenous myocardium, the majority of cardiac fibroblasts arise from the cells of the pro-epicardium by epithelial-to-mesenchymal transition (EMT). Endothelial cells undergoing EMT are a second source of cardiac fibroblasts. During pathological processes other cell types such as hematopoietic progenitor cells can contribute to cardiac (myo)fibroblasts. Figure from (Fan et al., 2012).

1.3 Crosstalk between cardiac fibroblasts and cardiomyocytes

In the heart, cardiac fibroblasts can be found interspersed between CMs (Camelliti et al., 2005) allowing for the exchange of information by means of 1) direct cell-to cell contacts 2) paracrine signals (cytokines/chemokines) 3) indirect ECM-mediated signal transduction, both via biochemical (cell-ECM contacts) and biomechanical signal transmission (for an overview on the following chapter see Figure 1-5).

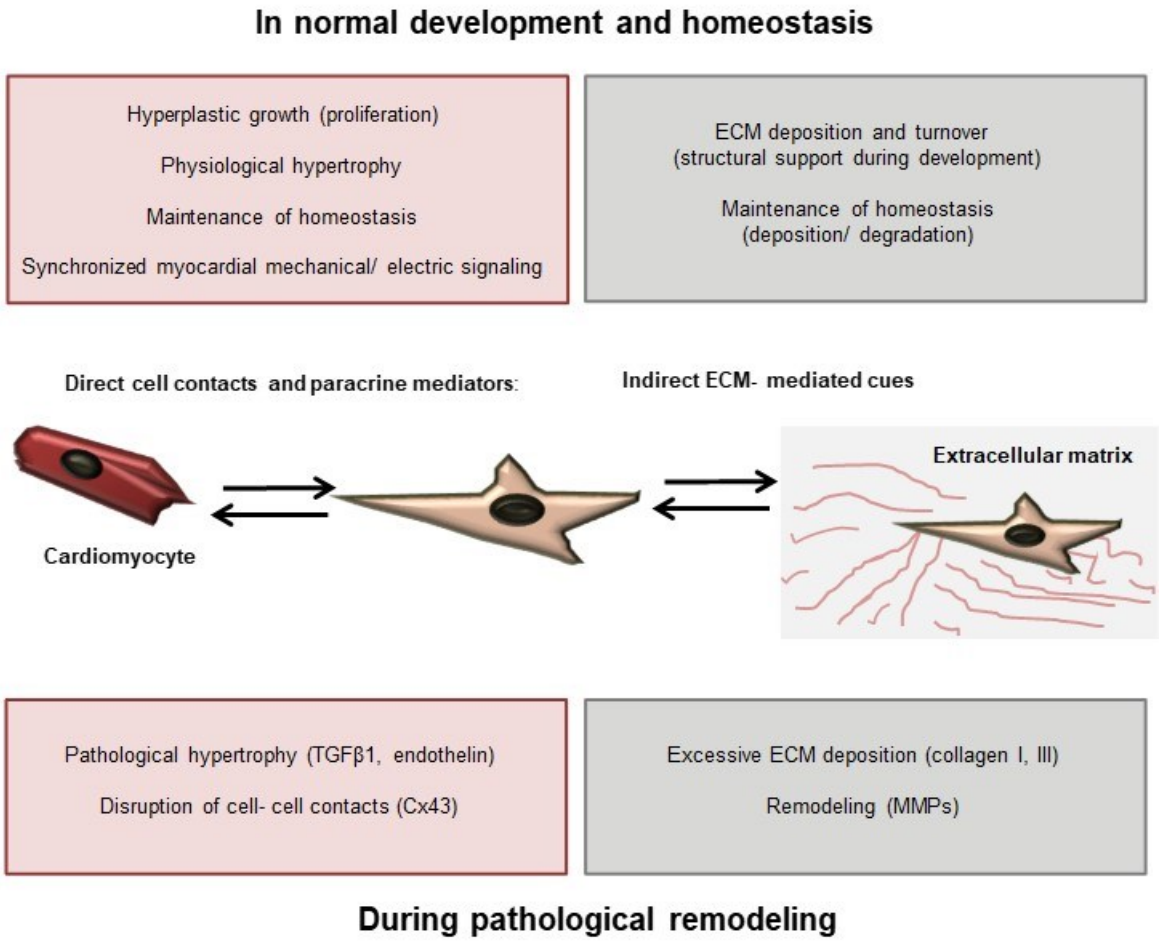

Figure 1-5 Fibroblast-cardiomyocyte communication in the myocardium

Overview on the mechanisms via which fibroblasts and CMs can communicate during physiological and pathological processes (upper/lower panel, respectively). Cardiac fibroblasts may connect to CMs via direct cell-cell contacts (both mechanically via adherens junctions and electrically via gap junctions), as depicted on the left side of the illustration (red boxes). They can furthermore influence CM behavior via paracrine signal mediators. Concurrently, cardiac fibroblasts control the integrity and viscoelasticity of the ECM (right side, grey boxes), which indirectly affects CMs. Adapted from (Sullivan and Black, 2013).

1.3.1 Direct cell-cell contacts

Although still a matter of intensive debate, there is some evidence of direct fibroblast-CM contacts in the myocardium. Fibroblasts were long thought to be electrically inert but may be crucial for the transmission of signals (for instance in the sinoatrial node (Camelliti, 2004; Gaudesius, 2003) in the myocardium. The presence of fibroblast-CM and fibroblast-fibroblast gap junctions has been suggested that would allow direct transmission of electrical signals (containing connexins 40,43 and 45) (Camelliti, 2004; Chilton et al., 2007; Gaudesius, 2003; Kohl, 2003; Kohl and Gourdie, 2014; Mahoney et al., 2016; Ongstad and Kohl, 2016). Although cardiac conduction is generally impaired in areas of firosis (Spach and Boineau, 1997), functional fibroblast-fibroblast gap junctions in the MI scar were

hypothesized to electrically connect two healthy areas of myocardium that are separated by the scar (Camelliti, 2004; Mahoney et al., 2016).

Recently, an *in vitro* study indicated that mechanical fibroblast-CM connections could potentially be established via adherens junctions (Pedrotty et al., 2008) that would allow for the direct transmission of mechanical signals between the cells in addition to the connection between cells and ECM (see 1.3.3). Further work is needed to evaluate the physiological relevance of these findings.

1.3.2 Paracrine mediators

Most is known about paracrine signaling circuits in the diseased heart involving cardiac (myo)fibroblasts and CMs. Signaling of factors such as Angiotensin II (AngII), TGFß, IGF1, different fibroblast growth factors (FGFs) and interleukin 6 (IL-6) has been extensively studied (Kakkar and Lee, 2010). Recently it has become clear, that secreted metabolites and micro RNAs (miRs) also play a crucial role in intramyocardial signaling (Bang et al., 2014, 2015; Sassi et al., 2014, 2017).

TGFß, secreted by both CM and fibroblasts is an important paracrine mediator of cellular communication (Kakkar and Lee, 2010). TGFß signaling in cardiac fibroblasts leads to myofibroblast transition followed by secretion of excessive ECM (Petrov et al., 2002) and thus fibrosis (Baum and Duffy, 2011; Weber et al., 2013). Concurrently, TGFß induces hypertrophy in CMs (Gray et al., 1998; Schultz et al., 2002). For instance, in cardiomyopathies, such as HCM, it could be demonstrated that BRAF mutations caused aberrant RAF/MAPK signaling specifically in cardiac fibroblasts. This subsequently led to enhanced secretion of TGFß, effectively stimulating hypertrophy in target CMs (Josowitz et al., 2016).

AngII acts closely together with TGFß and targets both CMs and cardiac fibroblasts. AngII-treated CMs induce TGFß signaling which stimulates fibroblasts to synthesize collagen and secrete cytokines such as IL-6 and tumor necrosis factor α (TNFα) (Sarkar et al., 2004). Autocrine signaling of IL-6 in cardiac fibroblasts causes the restructuring of the ECM via hyaluronan synthases (HASs) and the abundance of excessive hyaluronan (HA) can subsequently result in myofibroblast transformation of resident fibroblasts (Müller et al., 2014). IL-6 upregulation in turn, together with leukemia induced factor (LIF) and cardiotrophin-1 result in CM hypertrophy (Sano et al., 2000). AngII also induces FGF-2

signaling in cardiac fibroblasts which drives CM hypertrophy (Jiang et al., 2007; Pellieux et al., 2001).

Intriguingly, as a response to AngII stimulation, cardiac fibroblasts can also enhance CM hypertrophy via exosomes containing the microRNA passenger strand miR21*(Bang et al., 2014). Other micro RNAs such as miR29 also stimulate CM hypertrophy and myocardial fibrosis (Sassi et al., 2017).

1.3.3 Communication via the extracellular matrix

In the myocardium, resident cardiac fibroblasts secrete collagen types I and III followed by less abundant, collagens and proteins such as fibronectin, laminin and elastin (Fan et al., 2012). While collagens and elastins provide structural support, the ECM contains many non-structural components such as glycoproteins, (for instance fibronectin, laminins, thrombospondins and periostin), proteoglycans (such as versican and aggrecan), and glycosaminoglycans (the most common one, HA) (Rienks et al., 2014).

The ECM provides an indispensable structural scaffold for the myocardium during development. By controlling its integrity, in particular the subtypes of deposited collagen, cardiac fibroblasts can indirectly modulate CM-ECM receptor interactions and subsequent signaling. Indeed, inhibition of collagen synthesis abrogates embryonic CM myofibrillogenesis, demonstrating that these structural cues are crucial for CM sarcomere assembly and elongation (Fisher and Periasamy, 1994). The importance of structural information for CMs has also been demonstrated in experiments with decellularized cardiac ECM: The presence of structural information enhanced the upregulation of mature CM genes in fetal-like CM populations that resided on the matrix (Fong et al., 2016). Furthermore, when IPS cell-derived CMs were seeded onto decellularized human myocardial ECM they could form fully functional syncytia (Guyette et al., 2016).

In order to maintain homeostasis and allow for changes in the ECM composition, cardiac fibroblasts also produce matrix metalloproteinases (MMPs), whose temporal expression and activities are highly controlled by the secretion of tissue inhibitors of matrix metalloproteinases (TIMPs) (Fan et al., 2012), receptor-ECM binding (Olaso et al., 2002) and mechanical stimuli (Xie et al., 2014). Reciprocally, the activity of MMPs can affect cardiac fibroblasts, causing release of ECM components such as fibronectin, laminin, collagen I and also TGFß that then further stimulate collagen secretion in a positive feedback loop (Fan et al., 2012). Fibroblast-specific MMP expression, was shown to be

crucial for CMs to assume higher order structures and elongate properly in 3D coculture systems (Nichol et al., 2008), clearly emphasizing the importance of matrix remodeling for CMs development and functionality.

Cells integrate mechanical information from the surrounding ECM through integrins that bind ECM components (often within specialized signaling clusters, the focal adhesion complexes). Integrin-mediated binding of cardiac cells is important for CM proliferation and hypertrophy, but also EMT, angiogenesis and the control of cardiac fibroblast activation (Civitarese et al., 2017). There is a variety of different integrin subunits whose expression depends on the spatiotemporal development of the myocardium or its pathological state (Civitarese et al., 2017). *In vitro,* it could be demonstrated that integrins are crucial for fibroblast-mediated compaction of the ECM (Carver et al., 1995; Jokinen et al., 2004; Klein et al., 1991; Kondo et al., 2004; Schiro et al., 1991; Sur, 2016) and paracrine signals such as AngII can enhance gel contraction by cardiac fibroblasts, which can be abrogated by blockage of ß1 integrin. AngII furthermore stimulates the upregulation of ß1 subunit in treated cells (Burgess et al., 1994). In CMs, signaling through integrin ß1-binding of collagen I and fibronectin mediates hyperplastic growth (Ieda et al., 2009) and CM- specific deletion of the ß1 subunit leads to DCM and fibrosis (Shai et al., 2002).

1.4 Viscoelasticity in cardiomyocyte development and function

The ECM is strain and stretch sensitive and CMs interspersed with fibroblasts are highly responsive to changes in their viscoelastic surroundings (see also direct cell-cell contacts and how myofibroblast change viscoelasticity). Thus, by changing the properties of the ECM, fibroblasts can indirectly affect CMs behavior and function.

1.4.1 Viscoelasticity during physiological development of cardiomyocytes

During embryonic to postnatal cardiac development the stiffness of mouse ventricle increases from an elastic modulus of 12±4 up to 39±7 kPa (Jacot et al., 2010). The ideal substrate viscoelasticity is crucial for CM myofibril development and alignment, which is best at physiological values of 10 kPa substrate stiffness in 2D (Ribeiro et al., 2015). Indeed, embryonic CMs beat best when faced with an environment comparable to that of endogenous embryonic stiffness (Engler et al., 2008) and CM action potentials were found to be longest in cultures on physiological substrate stiffness of 10 kPa, which indicates a rather mature phenotype (Boothe et al., 2016). Also, in 3D gelatin matrices, CMs clearly prefer a physiological stiffness over softer and harder environments, as evidenced by

increased α-actinin and Cx43 expression, improved sarcomeric alignment and enhanced contraction force (Lee et al., 2017).

1.4.2 (Myo)fibroblasts affect myocardial viscoelasticity

Most studies so far have focused on the viscoelastic changes the heart undergoes upon pathological stimuli, but the myocardium also stiffens as a result of normal aging (Marín-García, 2007). The ECM viscoelasticity is determined by its composition which is in turn controlled by cardiac fibroblasts (an overview, see Figure 1-5 and for myofibroblasts Figure 1-6). In the healthy myocardium, the cardiac fibroblasts maintain homeostasis by carefully controlling the synthesis and deposition as well as the degradation of ECM components.

Upon pathological stimuli, resident cardiac fibroblasts transition into myofibroblasts. These are characterized by high secretory activity, in particular of collagen (Baum and Duffy, 2011; Petrov et al., 2002) and the enhanced expression of adhesion genes such as paxillin, vinculin and tensin (Baum and Duffy, 2011), as well as periostin (Kanisicak et al., 2016; Kaur et al., 2016; Snider et al., 2009). As a crucial mediator of inflammatory signaling in the heart, myofibroblasts are also highly responsive to cytokines and secrete both chemokines (IL1 α and ß, IL-6, TNF-α) and cytokines, as well as various growth factors (FGF-1 and FGF-2, TGFß, IGF-1) and other inflammatory mediators (metabolites and nitrous oxide) (Baum and Duffy, 2011. Hence, myofibroblast transition is mediated both by mechanical stimuli as well as inflammatory signaling (Baum and Duffy, 2011; Kawaguchi et al., 2011; Schroer and Merryman, 2015; Tomasek et al., 2002; Travers et al., 2016) (Figure 1-6).

The role of TGFß in this process is best understood (Baum and Duffy, 2011; Tomasek et al., 2002) (see also 1.3). Other important mediators include connective tissue growth factor (CTGF) and growth factors of the PDGF family (Travers et al., 2016). Integrins are furthermore involved in the regulation of TGFß signaling (Thannickal et al., 2003), thus connecting mechanical and paracrine signaling in the myofibroblast response (Travers et al., 2016). TGFß was shown to drive myofibroblast transition followed by enhanced collagen production and secretion (Petrov et al., 2002). TGFß also boosts α-SMA expression and thereby contractility in fibroblasts (Hinz et al., 2001). It has furthermore been shown that myofibroblast specific expression of periostin is a consequence of TGFß signaling and mechanical stretch (Kanisicak et al., 2016; Kaur et al., 2016; Snider et al., 2009), and periostin itself also regulates fibroblast to myofibroblasts conversion and boosts contractility (Elliott et al., 2012; Norris et al., 2007).

Myofibroblasts upregulate α-SMA (Baum and Duffy, 2011; Hinz et al., 2001; Tomasek et al., 2002) and embryonic smooth muscle myosin heavy chain (Frangogiannis et al., 2000; Shiojima et al., 1999) during the transition process. This allows for the development of an elaborate cytoskeleton which is connected via the fibronexus adhesion complex to fibronectin in the ECM (Baum and Duffy, 2011; Tomasek et al., 2002). Through these, contractile forces can be transmitted from myofibroblasts to the surrounding ECM. This contractile system also integrates ECM stretch and compression into intracellular signals, allowing the integration of mechanical signaling (Tomasek et al., 2002) (see also Figure 1-6).

As a consequence of myofibroblast transition, detrimental changes in ECM integrity, turnover and thus viscoelasticity result (Tomasek et al., 2002) (Figure 1-6). It could for instance be demonstrated, that expression of collagen III is upregulated upon both static and cyclic mechanical stretch (Carver et al., 1991). It has been hypothesized that under such conditions collagen III deposition would provide more elasticity while collagen I provides rigidity (Sullivan and Black, 2013). It has also been shown that increased matrix stiffness leads to enhanced gel contraction by myofibroblasts (Galie et al., 2011). To transmit mechanical stress, myofibroblasts preferentially express OB-cadherins in adherens junctions which can transmit stronger forces than N-cadherin found in CMs and resident cardiac fibroblasts and acts itself as a fibrotic stimulus enhancing transitions (Schroer and Merryman, 2015). Myofibroblasts furthermore respond to high strain as a result of ECM breakdown (Figure 1-6) (Schroer and Merryman, 2015; Travers et al., 2016). Concurrent with higher secretion of ECM components, cardiac myofibroblasts secrete more MMPs, which further degrade ECM, (left side, Figure 1-6) (Schroer and Merryman, 2015; Travers et al., 2016).

Collectively, prolonged activation of cardiac fibroblasts and transition to myofibroblasts thus lead to progressive stiffening and local changes in ECM strain that further enhance the myofibroblast response in a positive feedback loop (see in summary Figure 1-6).

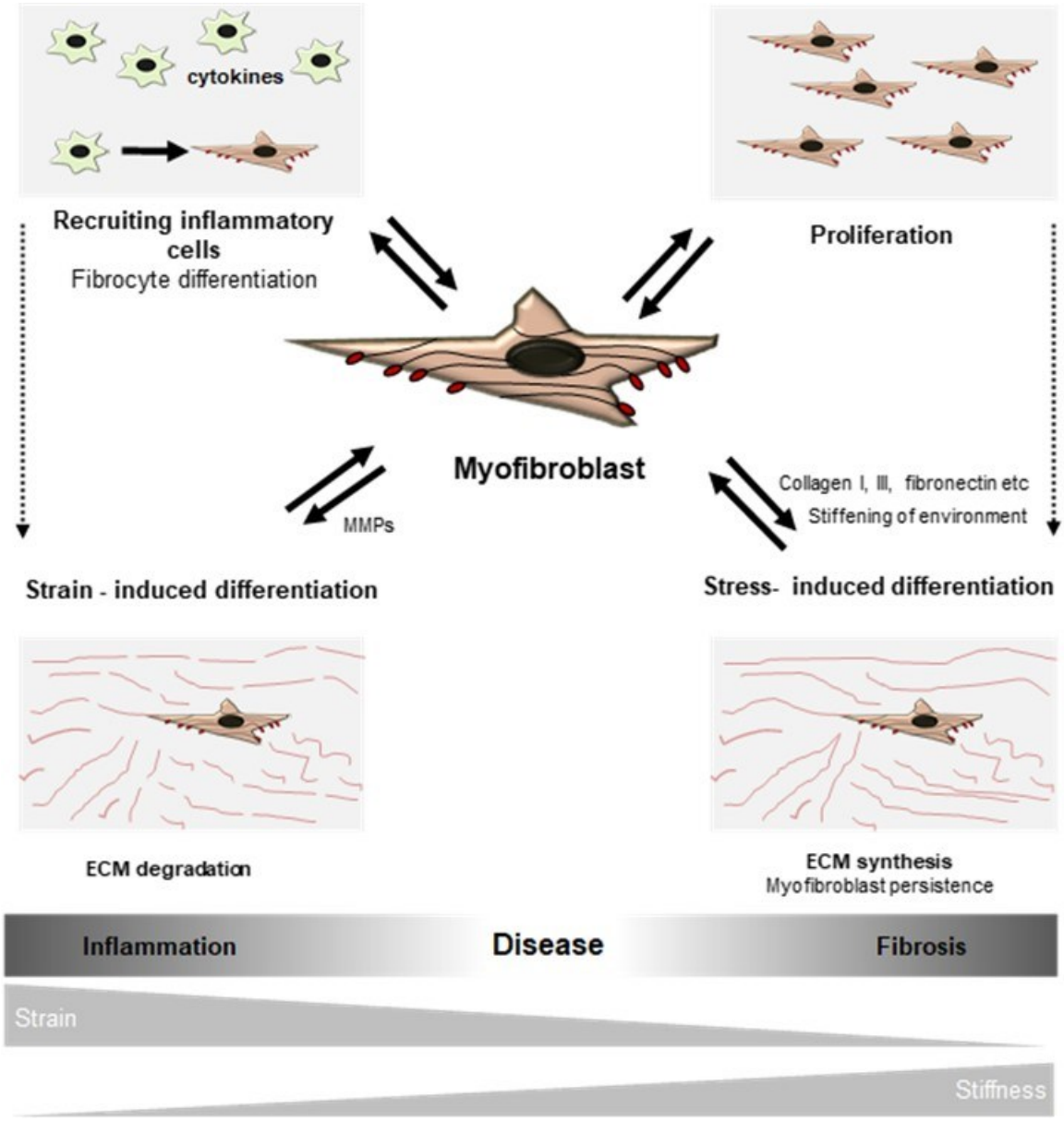

Figure 1-6 Myofibroblasts modulate and respond to viscoelastic stimuli

Fibroblast-to-myofibroblasts conversion is a highly regulated and complex process that depends on the integration of many environmental stimuli. Once activated, myofibroblasts secrete proinflammatory and profibrotic factors. These will recruit inflammatory cells and stimulate some hematopoietic progenitors to undergo fibrocyte differentiation. Myofibroblasts degrade ECM with the aid of MMPs to allow for cell migration and simultaneously also deposit new ECM with specific characteristics to replace the injured tissue. The myofibroblasts conversion process and myofibroblasts activity are highly mechanosensitive. An increase in myofibroblasts abundance typically leads to progressive stiffening of the ECM and matrix remodeling by MMPs leads to localized increase of strain. These changes in ECM viscoelastic further activate fibroblasts to undergo transition into myofibroblasts. Adapted from the reviews of (Schroer and Merryman, 2015; Travers et al., 2016).

1.5 Towards better *in vitro* models of the myocardium

The study of cellular crosstalk in the endogenous myocardium is intrinsically difficult through the complex interplay of various cell types, direct cell-cell contacts, the presence

of countless soluble mediators and the indirect control of cellular behavior by the ECM. Thus defined, yet physiological, fibroblast-CM coculture systems are necessary to simplify the study of the endogenous myocardium.

1.5.1 Limitations of 2D *in vitro* models for the study of fibroblasts

While the healthy human myocardium is estimated to be of 10 kPa, the stiffness of fibrotic heart undergoing failure is of 40-100 kPa. However, in standard 2D culture system substrate stiffness range in the GPa magnitude (Herum et al., 2017). Thus, it remains difficult to study fibroblasts *in vitro*, as 2D cell cultures on stiff non-physiological surfaces do not recapitulate the 3D environment of these cells *in vivo*. Artifical 2D culture systems thus effectively simulate a pathological environment not comparable to that of resident cardiac fibroblasts found in the healthy heart. These prerequisites have to be taken into account when interpreting findings from such studies, as the culture of cardiac fibroblasts in 2D quickly results in fibroblast-to-myofibroblast conversion (Petrov et al., 2002; Rhee, 2009; Soares et al., 2012). This limitation can be overcome by culturing fibroblasts in 3D hydrogels, for example as Engineered Connective Tissue (ECT) (Figure 1-7 A; C). Here, low α-SMA expression is indicative for a stable fibroblast phenotype (Figure 1-7 D). While fibroblasts in 2D require serum supplementation to survive, 3D ECT cultures can be maintained long-term serum-free (Figure 1-7 B), allowing *in vitro* testing under highly standardized conditions.

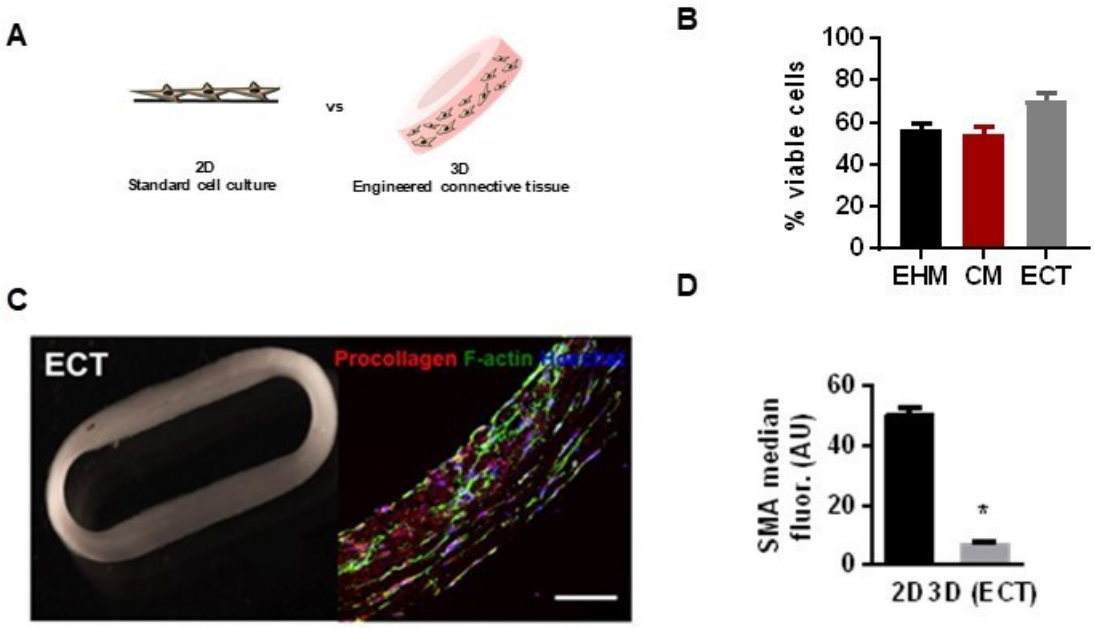

Figure 1-7 Conservation of fibroblast state in engineered connective tissue

Fibroblasts survive long-term in 3D tissue cultures under serum-free conditions: **A** Schematic of fibroblast standard 2D cultures vs fibroblasts 3D cultures within collagen I hydrogels under serum-free conditions (ECT) **B** Viability of cells after enzymatic digestion of 4-week-old tissues maintained under serum-free conditions, containing both CMs and HFFs (EHM), CMs or only HFFs (ECT). n=3/3/3. **C** ECT morphology and detailed histological analysis (Procollagen, red, F-actin in green and nuclei in blue). Scale bar 100 µm. **D** SMA^+ median fluorescence per cell (AU: arbitrary units) in fibroblasts isolated for flow cytometry from 2D and 3D culture (ECT); n≥3/group. *p<0.05 by unpaired, two-sided Student t-test). C and D: data from (Grishina, Elina, 2017).

1.5.2 Engineered Heart Muscle (EHM)

It has now become clear, that mutations in genes of the CM contractile apparatus and calcium handling machinery that underlie cardiomyopathies (Herman et al. 2012, Streckfuss-Bömeke et al. 2017) also affect cellular crosstalk of CMs with cardiac fibroblasts resulting in their proliferation and the excessive secretion of ECM (Teekakirikul et al., 2012). During neonatal to adult development, both CMs and non-myocytes in the myocardium undergo vast transcriptional changes. This is contrasted after MI; while CM transcription remains fairly quiescent, the fibroblast population gets transcriptionally reactivated into a neonatal and proliferative state (Quaife-Ryan et al., 2017). A better understanding of cardiac fibroblasts as to their pathophysiological role, may help to define novel therapeutic targets for HF treatment. Studying this in a human heart muscle model composed of defined CM and fibroblast populations in a "physiological" collagen environment, such as provided by EHM (Tiburcy et al. 2011, Tiburcy et al. 2017) may be instrumental.

1.5.2.1 EHM recapitulates *bona fide* heart development and allows the in-depth analysis of fibroblast-cardiomyocyte crosstalk

The introduction of human PSCs (Takahashi et al., 2007; Thomson et al., 1998) has enabled the translation of rodent models of heart muscle engineering (Tiburcy et al., 2017; Zimmermann et al., 2002) to the human. The required minimum cellular components for the generation of functional human EHM are PSC-derived CMs with either endogenous mesenchymal stroma cell "contaminants" or the supplementation with defined fibroblast populations (Soong et al., 2012; Streckfuss-Bomeke et al., 2013; Tiburcy and Zimmermann, 2014; Tiburcy et al., 2014, 2017) (Figure 1-8).

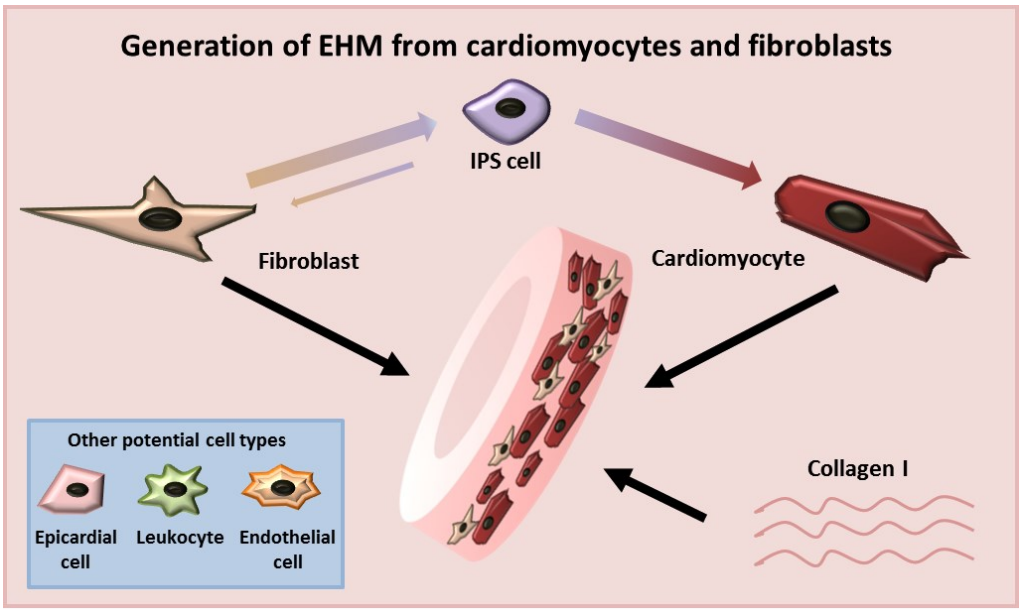

Figure 1-8 Engineered Heart Muscle

The minimal requirements for functional EHM generation are a mixture of PSC-derived cardiomyocytes and fibroblasts in a collagen hydrogel. The cell matrix mixtures are cast into molds to establish the desired geometries. Other cell types, matrix components, and culture medium supplements may be added.

CMs and fibroblasts suspended in collagen type I hydrogel co-consolidate in casting molds with the desired geometry. We prefer circular EHM geometries to allow for robust dynamic loading on central silicone poles (Figure 1-9).

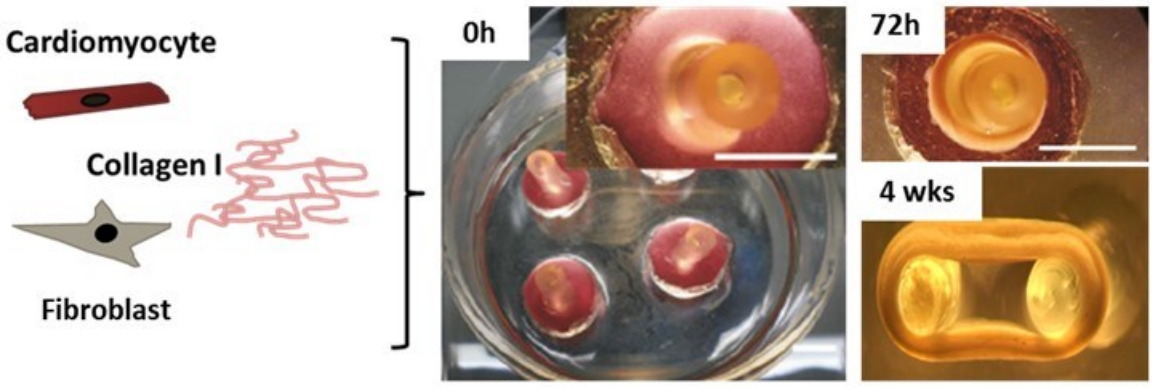

Figure 1-9 EHM generation and temporal development

EHM hydrogels undergoes rapid consolidation within hours after casting. After 72 h maximally, condensed EHM are transferred onto dynamic stretchers to facilitate auxotonic contractions and support organotypic maturation. (Images from (Tiburcy et al., 2014, 2017).

EHM recapitulates the development of *bona fide* human myocardium (Soong et al., 2012; Tiburcy et al., 2014, 2017) and can be used to study cardiac disease phenotypes (Borchert et al., 2017; Long et al., 2018; Streckfuss-Bömeke et al., 2017, 2017; Tiburcy et al., 2017).

EHM exhibit organotypic properties of postnatal human myocardium such as registered sarcomeres with M-bands, physiological responses to load (Frank-Starling mechanism) and pacing (Bowditch phenomenon) as well as a transcriptome profile indicating advanced maturation. By precise supplementation with fibroblasts, EHM can be used to define the role of these cells for heart muscle assembly and function (Tiburcy et al., 2017). This includes the investigation of distinct CM and fibroblasts pathologies and their impact on integrated heart muscle function (Figure 1-10), effectively closing the bridge between complex, yet difficult to transfer, *in vivo* animal models and highly artificial 2D human cell culture systems.

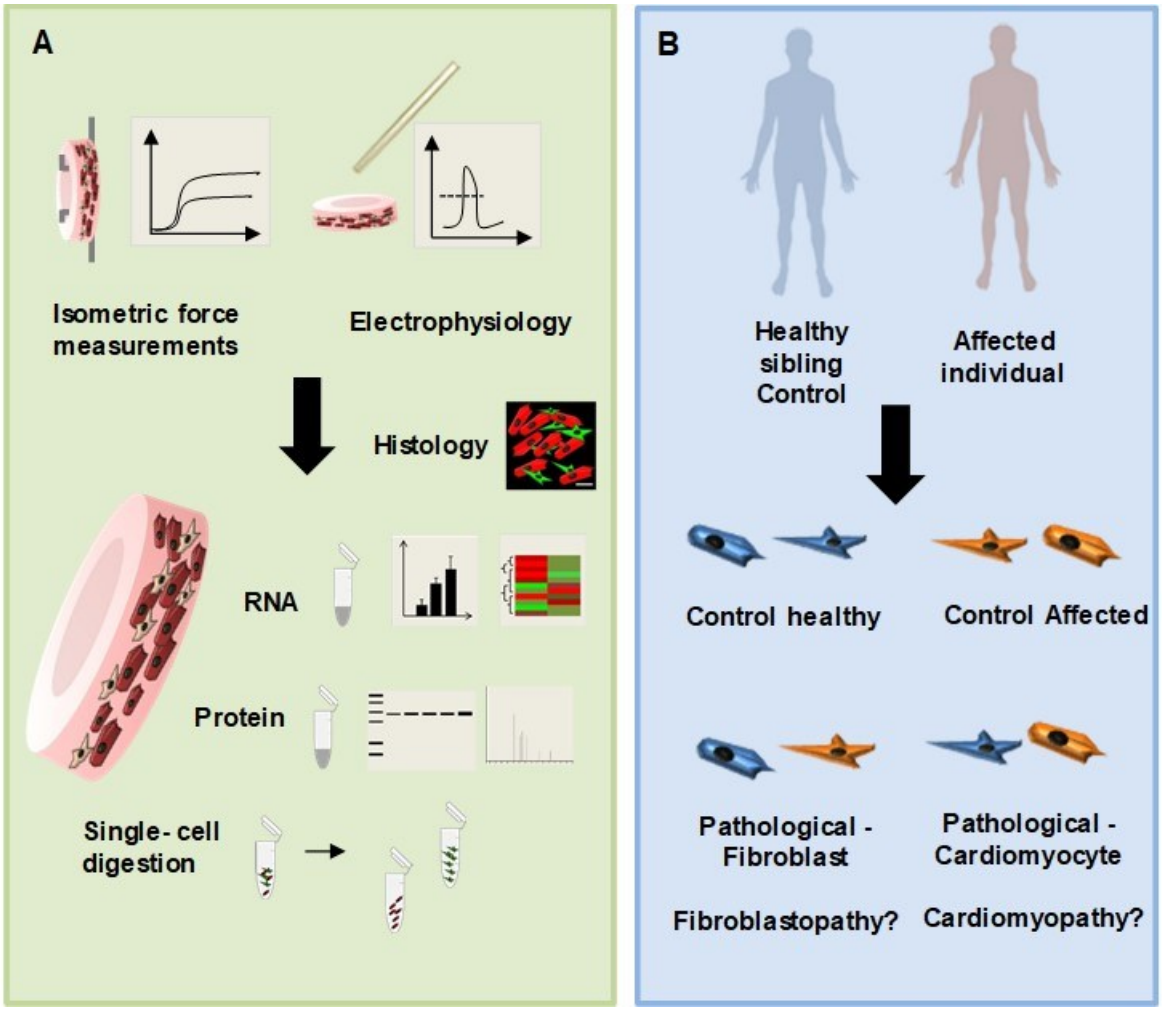

Figure 1-10 Possible *in vitro* application of EHM

A EHM recapitulate native myocardial development and can be subjected to a number of standard and advanced assays for deep phenotyping. **B** Disease modeling: EHM can be generated from IPS-derived cardiomyocytes and fibroblasts as well as from primary fibroblasts to assess cell specific phenotypes, which may ultimately allow for cell-type specific targeting of innovative therapeutics.

1.5.2.2 EHM can be used *in vivo* to replace damaged myocardium

EHM can be used as a regenerative source of myocardium for clinical application (Figure 1-11). Its beneficial effect has been demonstrated in a MI model of rats (Zimmermann et al., 2006) and is currently being investigated in larger animal models. For that, suitable fibroblast sources must be identified.

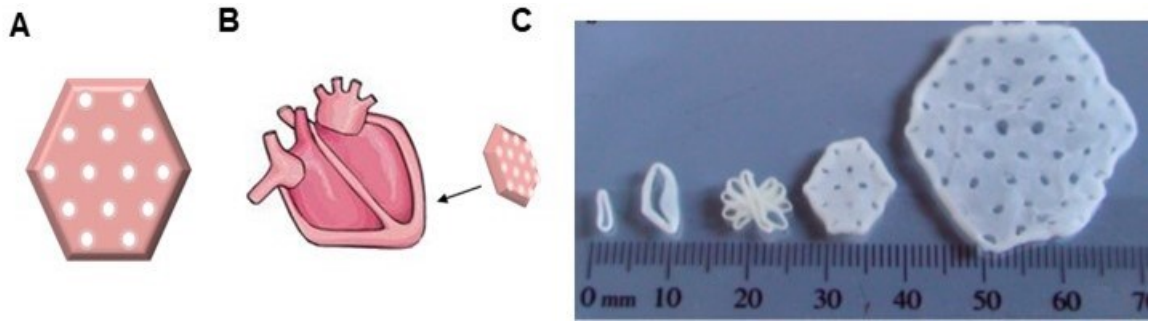

Figure 1-11 EHM as a regenerative therapeutic for cardiovascular disease

A Schematic geometry of an EHM tissue patch for implantation. **B** Patch can be implanted onto the injured myocardium. **C** Comparison of different EHM types and sizes (from left to right: small human EHM for pharmacological screening/ multi-loop fusions and patches for heart repair applications (taken from (Tiburcy et al., 2017)).

1.6 Hypotheses to be tested

The following overarching hypothesis was investigated:

Fibroblasts, by controlling the extracellular environment, are key for heart muscle assembly and homeostasis.

Specific aims of the thesis are summarized below:

1) Define the impact of fibroblasts on ECM/EHM compaction.
2) Define the viscoelastic properties of EHM.
3) Comparative analysis of different fibroblast species as to their cardio-instructive properties.
4) Modeling of fibroblast-CM specific interactions in physiological and disease models.
5) Defining suitable fibroblast sources for *in vitro* modeling and clinical application.
6) Development of chemically defined culture conditions for EHM.

2 Materials and methods

2.1 Cells

Table 2-1 List of cells

Cell type	Abbreviation in protocols	Source	Used for
HES2 RFP	RFP^+	Kindly provided by Gordon Keller (Irion et al., 2007)	CM production
hES2	HES2	(Reubinoff et al., 2000)	CM production
Human neonatal foreskin fibroblast	HFF	ATCC SCRC-1041	Feeders, EHM
Ventricular CFB vCFBv26025	CFB1	Lonza, NHCF-V Human Cardiac Fibroblast- Ventricular CC2904	EHM
Ventricular CFB vCFBv25981	CFB2	Lonza, NHCF-V Human Cardiac Fibroblast- Ventricular CC2904	EHM
Ventricular CFB vCFBv27741	CFB3	Lonza, NHCF-V Human Cardiac Fibroblast- Ventricular CC2904	EHM
Gingiva fibroblast	Patient B3 (GFB1), 6A (GFB2), 10A (GFB3), 11A (GFB4)	Kindly provided by Dirk Ziebolz Clinic for Cariology, University Medical Center (Präventive Zahnmedizin, Parodontologie und Kariologie) (Ethics votum: 16/6/09)	EHM
DCM CMs from patient	DCM CMs	Kindly provided by Katrin Streckfuß-Bömeke (Ethics votum: Az 21/1/11)	EHM
DCM control CMs	CTR CMs	Kindly provided by Katrin Streckfuß-Bömeke (Ethics votum: Az 21/1/11)	EHM
DCM CFBs from patient	DCM CFB	Kindly provided by Katrin Streckfuß-Bömeke (Ethics votum: Az 21/1/11)	EHM
Human embryonic kidney SV40 transformed cells	TSA	Sigma 96121229	Plasmid validation and virus production

2.1.1 Ventricular cardiac fibroblasts from Lonza

Cardiac fibroblasts from ventricular myocardium were obtained from Lonza (CFB). All were from non-failing hearts: CFB1: 50-year-old male, CFB2: 45-year-old male, CFB3: 52-year-old-male. CFB3 was used as a healthy control in DCM disease modeling study.

2.1.2 Dilated cardiomyopathy modeling study

Cells from a DCM patient (45-year-old male) and a healthy control donor (39-year-old female) were provided by Dr. Katrin Streckfuß-Bömeke. The patient underwent heart transplantation with an ejection fraction of ~20%. Cardiac fibroblasts (DCM CFBs) were prepared by Steffen Köhne from the ventricle of the DCM patient's heart.

Skin fibroblasts from the DCM patient were derived from punch biopsies. For reprogramming according to the Yamanaka protocol (Takahashi et al., 2007) using non-integrative Sendai virus, skin fibroblasts of DCM patient and blood of the healthy control were used, respectively. Biopsy cultures, reprogramming, IPS cell culture and CM derivation were carried out as described previously (Borchert et al., 2017). DCM CFBs were maintained in FGM3 medium (Lonza).

2.1.3 Standard cell culture conditions

All mammalian cells were grown at +37°C, 5% CO_2 and 21% O_2.

2.1.4 Human embryonic kidney SV40 transformed cells

Human embryonic kidney SV40 transformed cells (TSA) were maintained in Dulbecco's Modified Eagle Medium (DMEM) containing 10% fetal calf serum (FBS), 100 U/ml penicillin, 100 µg/ml streptomycin (P/S) and 2 mmol/L L-Glutamine (Gibco). TSA cells were used for the validation of plasmids via transfection (Turbofect) and the production of lentivirus containing target plasmids (2.3).

2.1.5 Ethics statement

The import and use of human embryonic stem (hES) cells was approved by the Robert-Koch-Institute (www.rki.de; approval #12 from 13.09.2005) to W.H. Zimmermann according to §11 Embryonic Stem Cell Act. The use of human cell material was approved by the responsible ethics committee (refer to Table 2-1).

2.1.6 Cell culture, maintenance and stock preparation

All cells were cultured as in Table 2-2. For detailed culture media and ingredients see A2.6.

Table 2-2 Overview of standard culture media for cells and tissues

Cell type	Medium	Culture conditions
Primary fibroblast cardiac	FGM3 medium (Lonza), supplemented with FGM3 bullet kit	Uncoated
Primary fibroblast skin	HFF Medium	Uncoated
Primary biopsy	HFF Medium	Synthemax coated dishes
HES2 cell	HES2 Medium	HFF feeders
PSC derived CM	CM Basal medium	Coated, Matrigel or Synthemax
CMs during selection	Selection Medium	Coated, Matrigel or Synthemax
TSA cells	TSA Medium	Uncoated
EHM- coculture of CMs and fibroblasts (2:1) in collagen	EHM Medium: Serum-free maturation medium (SFMM)	+TGFß1 culture days 1- 3 -TGFß1 culture days 4- 28
ECT- fibroblasts in collagen	EHM Medium: Serum-free maturation medium (SFMM)	+TGFß1 culture days 1- 3 -TGFß1 culture days 4- 28
CMs in collagen	EHM Medium: Serum-free maturation medium (SFMM)	+TGFß1 culture days 1- 3 -TGFß1 culture days 4- 28

For a detailed description of all used ingredients, buffers and media preparations, see A2.6.

2.1.7 Derivation of human gingiva fibroblasts from biopsies

Gingiva surgical leftovers were collected by Dr. Dirk Ziebolz (Clinic for Cariology, University Medical Center, Göttingen). Samples were provided at 4 °C within 24 h of harvest to the Institute of Pharmacology and Toxicology after pseudonymization. All samples were derived from healthy donors between 16 to 30 years of age. GFB 1,2,3 were derived from females, GFB4 from a male subject.

Tissue was washed in PBS containing P/S and 1% Fungizone (2.5 µg Amphotericin B and 2.05 µg sodium desoxycholat per ml; all Gibco). Tissue was cut into small pieces and placed on a 10 cm cell culture dishes coated with 25 µg/ml Synthemax II (Corning; see also A2.6). Per tissue piece, 5-10 µl of FBS were dropped onto the dish and tissue pieces were incubated in the drops to facilitate adhesion to the culture dish for 30 min at 37 °C and 5% CO_2. Then, HFF medium (A2.6) containing fungizone was added carefully and tissues left to adhere for 48 h. After 48 h, medium was changed. Generally, within 2 d, first epithelioid cell outgrowth could be observed, followed by fibroblasts on the edge of colonies. Epithelioid cells would die off within a week and fibroblast cells could then be subcultured

onto standard cell culture dishes without special coating. For further culture, see next section.

2.1.8 Standard cell culture techniques

2.1.8.1 Cell dissociation

Cells (fibroblasts and TSA cells) were washed one time with PBS and then incubated with TrypLE (Table 2-3) for 3-7 min, depending on cell type and confluence at 37°C and 5% CO_2. Cells were then gently dissociated from plates with standard growth medium and collected into a 50 ml tube for counting and seeding. For standard subculture, cells were also transferred directly to new culture flasks.

Table 2-3 Volumes for cell dissociation

Culture plate size	Volume (V) of TrplE used for dissociation
6- well	750 µl
T25	1 ml
T75	2.5 ml
T175	6 ml

2.1.8.2 Passaging

Cells were passaged according to confluence and experimental needs in ratios of 1:4 to 1:6.

2.1.8.3 Freezing

If not indicated otherwise, cells were dissociated by enzymatic digestion (TrypLE), resuspended in standard growth medium and counted. Cells were pelleted by centrifugation at 300 g (Heraeus Cell Culture Centrifuge; Thermo Scientific) for 5 min at room temperature and resuspended in FBS containing 10% DMSO (Sigma). Cells were transferred into cryovials (Invitrogen) and frozen at -80°C utilizing a freezing aid (Mr. Frosty, Nalgene). Subsequently, cells were transferred into a -152 °C deep freezer (Herafreeze) or the vapor phase of a nitrogen long-term storage device (Askion). Cryo-culture vials were labeled as indicated in Table 2-4.

Table 2-4 Labeling of cryovials

	Cell type	P number	Frozen by	Date	Vial content	Number/Amount of vial frozen
Example	HFF	19	SS	19.10.2017	3 X 10^6	2/5

2.1.9 Standard culture and passaging of TSA

TSA cells were maintained in DMEM with 10% FBS and P/S. Cells were subcultured at ratios of 1:4 (for transfection) to 1:20 for standard maintenance, according to cell dissociation protocol (see previous section 2.1.8).

2.1.10 Human feeder cells

HFF were maintained in DMEM with 10% FBS and P/S. HFF were irradiated with 30 Gray (Gy) γ-irradiation (STS Biobeam 8000, Germany) and plated at 2.500 cells/cm² to serve as feeder layer for HES2 cultures.

2.1.11 Culture of human embryonic stem cells

HES2 cells were kept on feeder layers of irradiated HFF cells in HES medium (Table 2-2, A2.6) and grown to 80-90% confluency. For passaging, HES2 were washed once with PBS and then incubated with TrypLE at 37 °C for 3 min. Cells were resuspended in HES medium, centrifuged at 200 g for 4 mins and finally replated in HES medium.

2.1.11.1 Derivation and culture of CMs from HES2 cells

CM differentiations were routinely performed by the technical staff of the Institute of Pharmacology and Toxicology according to a standard operating procedure (Tiburcy et al., 2017). In short, pluripotent stem cells were transferred from irradiated HFF feeder cultures onto Matrigel (1:120) for 96 h at 4.000-25.000/cm² in TESR-E8 medium (Stemcell Technologies) with 5 µmol/L ROCK-inhibitor (ROCKi, Y27632 Stemolecule). Mesodermal differentiation was induced by a combination of CHIR (CHIR99021, Stemgent), BMP4 (R&D systems), FGF-2 (Stemgent) and Activin A (R&D systems) (Table 2-5). After 72 h, the Wnt antagonist IWP4 (Stemgent) was used to induce cardiac specification (Table 2-5), followed by cardiac maturation in CM basal medium. CMs were then metabolically selected by the use of lactate in the absence of glucose (Table 2-2, A2.6) to obtain high purity CM cultures (flow cytometry for α-actinin: 95±2% n=3) for EHM generation. Cells

during differentiation and the resulting CMs were maintained in CM basal medium (Table 2-2, A2.6) until use.

Table 2-5 Small molecules for cardiac differentiation

Mesoderm induction	
CHIR	1 µmol/L
Activin A	9 ng/ml
FGF-2	5 ng/ml
BMP4	5 ng/ml
Cardiac specification	
IWP4	5 µmol/L

2.1.11.2 CM dissociation

CMs were washed twice with PBS and then incubated with Accutase dissociation solution (A2.6) for 10 min at room temperature (RT) followed by up to 15 min at 37°C, 5% CO_2, until cells were visibly detaching. Cells were resuspended in CM recovery medium, containing 5 µmol/L ROCKi. For replating, cells were centrifuged at 300 g for 5 min and resuspended in CM basal medium (A2.6) without ROCKi. Cells were then transferred onto coated plates (Matrigel 1:120 or Synthemax at 25 µg/ml). Medium was changed 24 h post plating.

2.1.12 Derivation of stroma cells from embryonic stem cells

Culture dishes were coated with laminin-521 (Biolamina) (A2.6) at least 24 h before plating. For that, the stock was diluted to 2.5 µg/ml with PBS (+ Ca^{2+}/Mg^{2+}). HES2 cells were plated at 1.3 x 10^4/cm^2 suspended in E8 medium containing 5 µmol/L ROCKi on laminin coated T75 flasks. Medium was changed daily and after 4 d, cells were treated with freshly prepared MIM10B medium for 3 more days, followed by cardiac differentiation medium at d 7 and d 9 (all media in A2.6). On d 10 of culture, cells were subsequently replated onto laminin-coated cell culture flasks in stromal cell specification medium (StC-SM) (A2.6) at 1.25 x 10^4/cm^2 and medium changed 24 h, 48 h and 96 h later. On day 15, cellular morphology was controlled for epithelial/epicardial cell shape and StC-SM Medium changed. 2 d later, medium was changed to FGM3 medium and cells grown to 90% confluence followed by passaging/freezing. Ready stroma cells were provided by technical assistants.

2.2 Engineered heart muscle (EHM)

2.2.1 Cell dissociation and casting

EHM input fibroblast and CM populations were detached using enzymatic treatment. Fibroblasts were washed once with PBS and then incubated with TrypLE until cells detached from cell culture surfaces. Cells were resuspended in CM medium and counted (2.1.8, all media in detail in A2.6). CMs were washed twice with PBS, followed by incubation with Accutase cell dissociation solution (A2.6) for 10 min at RT and then 15 min at 37 °C and 5% CO_2. CMs were collected in CM basal medium containing 5 µmol/L ROCKi (A2.6) and then counted. Cells were mixed in a defined ratio (in total 1.275 x 10^6 cells (CM:HFF 2:1), centrifuged at 300 x g and RT, and resuspended in serum-free maturation medium (SFMM) (Table 2-2 and A2.6) containing TGFß at 1 ng/ml. During centrifugation, the collagen master mix was prepared on ice (Table 2-6). Resuspended cells were mixed with the master mix and casted into EHM molds. Fresh EHM were incubated for 1 h at 37 °C, 5% CO_2 and thereafter SFMM containing TGFß was added to the tissue molds. Medium was changed 24 h after casting and after 3 d EHM were transferred, using forceps, to auxotonic stretchers (A2.5) into a 24-well format containing SFMM (without TGFß).

Table 2-6 EHM hydrogel preparation

For 4 EHM/450 µl tissue		
Master Mix (Collagen)	**Batch 1 (6.49 mg/ml) Lot 17CSA03**	**Batch 2 (6.1 mg/ml) Lot 15CSA02**
	V (µl)	V (µl)
Collagen I (Collagen Solutions)	284	305
2X RPMI	284	305
0.1 mol/L NaOH	53	57
Total	621	667
Ready EHM hydrogel		
Master Mix collagen +	665	667
Cells in SFMM (+ TGFß)	1435	1433
Total*	2100	2100
Volume (V) used per EHM/tissue	450	450

*Note that this recipe contains 300 µl additional hydrogel V to compensate for the loss during pipetting of viscous solutions. The cell input is thus 4 x 10^6 CMs and 2 x 10^6 HFFs for 4 standard EHMs.

2.2.2 EHM culture

EHM were kept in culture for 4 weeks until isometric force measurement. During this time, pharmacological treatment took place. Spontaneous beating was assessed by counting beats in a 10 s timeframe on a 37 °C heating plate under a binocular. 10 s values were extrapolated. To avoid temperature dependent bias, EHMs were sampled at random on the plate.

2.2.3 Generation of engineered connective tissues

Engineered connective tissues (ECTs) were generated from HFFs and cultured as described for EHM previously, omitting the use of CMs. The total cell count thereby was 4.25 x 10^5 /tissue.

2.2.4 Collagen I hydrogels for rheology measurements

For both shear plate rheology and destructive tensile stress measurements, cells were prepared as described for EHM generation. Tissues were generated from collagen, CMs (8.5 x 10^5 cells/tissue) and HFFs (4.25 x 10^5 /tissue). Hydrogels with both CMs and HFF (2:1) contained a total of 1.275 x 10^6 cells (CM: HFF 2:1), all in 450 µl total V/tissue. For gels without cells, only SFMM medium was used.

We used two different batches of collagen I (Table 2-6) during this work, which differed in their consolidation properties both on an absolute scale, as well as on a temporal scale (for comparison, see supplementary results section in A1).

Table 2-7 Experiments and corresponding collagen I batches

Experiment	Batch	Samples taken (time)
Shear plate rheology, time sweep	1	-
Shear plate rheology, time sweep	2	-
Cell morphological analysis	2	Cell-independent phase at: 30 min Cell-dependent phase at: 90 min
RNA sequencing	2	Cell-independent phase at: 30 min Cell-dependent phase at: 90 min

2.2.5 Replacement of B27

Table 2-8 Minimal component supplementation

Reagent	Manufacturer	Cat/PZN	Stock in 0.9% NaCl solution	Final concentration in 25X CMR	Final concentration in medium
Human serum albumin (HSA)	Baxalta (200g/l)	11128714	-	50/125 mg/ml	2/5 mg/ml
Human recombinant albumin (rHSA)	Sigma	A9731-10G	-	12.5/50/125 mg/ml	0.5 /2 /5 mg/ml
Holo- transferrin (Tra)	Sigma	T0665-100MG	5 mg/ml	250 µg/ml	10 µg/ml
Sodium selenite (SodSel)	Sigma	S9133-1MG	1 mg/ml	0.8 µg/ml	0.032 µg/ml
T3	Sigma	T6397-100MG	2 mg/ml	0.1 µg/ml	0.004 µg/ml
Liothyronin, Thyrotardin (T3)	Sanofi	50885.00.00	-	0.1 µg/ml	0.004 µg/ml
Ethanolamine (Etha)	Sigma	E9508-100ML	-	0.05 µg/ml	0.002 µl/ml or 2 µg/ml
L-Carnitine (L-Car)	Sigma	C0283-1G	-	100 µg /ml	4 µg/ml
Dexamethasone (Dexa)	Fortecortin (Merck)	81961	4 mg/ml	330 ng/ml	16 ng/ml

Preparation of minimal supplementation component for EHM culture

Supplementation was prepared as 25X stock. For that, human serum albumin (HSA, 200 g/ml; Baxalta) was diluted to a final concentration of 125 mg/ml or 50mg/ml for treatments.

In the case of supplementation based on recombinant HAS (rHSA), rHSA (Sigma) was first dissolved in 0.9% NaCl solution. Other reagents were prepared as stock solutions according to (Table 2-8) and added to a final concentration of 25X or directly weighted in as powder and supplemented. The reagents were left over night at 4 °C to dissolve and were then mixed well and sterile filtered, followed by aliquoting and freezing at -20°C.

Reagents were partially chosen based on the protocols published by the HANNA lab (adapted further from (Gafni et al., 2013), Weizmann Institute of Science), which can be accessed at https://hannalabweb.weizmann.ac.il/.

2.2.6 EHM dissociation

In order to dissociate EHM (and ECT), EHM were incubated in a 48-well format with 300 µl collagenase solution for up to 2 h at 37°C (airbath). The supernatant was subsequently collected in a 1.5 ml tube. EHM were washed once with 300 µl PBS containing 5% FBS, which was also collected into the tube on ice. Then, EHM were incubated up to 45 min with Accutase cell dissociation solution (A2.6). EHM were triturated and cells transferred into the tube. Wells were washed with PBS containing 5% FBS. The wash solution was also collected. The collected cell suspension was finally centrifuged at 4°C and 300 g for 5 min and resuspended into 950 µl PBS containing 5% FBS (resulting in a total V of 1 ml). 50 µl were used for cell counting using a CASY cell counter (Roche). The remaining cell suspension was centrifuged once more and resuspended either in ice cold 70% ethanol (EtOH) or 4% formaldehyde (FA)/PBS (Roti Histofix) for fixation.

2.2.7 Irradiation of EHM

EHM at culture day 3 were irradiated with 30 Gy (γ-irradiation, STS Biobeam 8000, Germany) in 50 ml sterile polypropylene tubes with SFMM.

2.3 Genetic modification of cells

2.3.1 Transfection of TSA cells

TSA cells were subcultured when 90% confluent in a 1:4 ratio (see 2.1.9). 24 h after seeding, cells were transfected with Turbofect reagent (ThermoScientific) according to manufacturer´s protocol. Briefly, plasmid DNA (0.18 µg/cm2) was diluted in DMEM with P/S and Turbofect (0.35 µl/cm^2) added (final V of suspension 7 µl/cm^2). The solution was vortexed and centrifuged briefly and then incubated at RT for 30 min. Transfection mix was then added to cell culture medium. 6 h post transfection medium was changed for regular TSA medium (Table 2-2). Transduction was confirmed by fluorescence microscopy (GFP) 24-48 h after transfection. Selection based on antibiotic resistance (puromycin) was usually carried out 48 h post transfection.

2.3.2 Production of Lentivirus

TSA cells were transfected with target plasmids and plasmids encoding for lentiviral envelope and packaging proteins (psPAX2 and PMD.2 by Addgene, see A2.7) in TSA medium (A2.6). 6 h after transfection medium was replaced. After 48-72 h supernatants

containing lentiviral particles were collected, sterile filtered (0.2 µm) and applied directly at 1:1 to 1:4 V/V ratios for transduction of target cells together with polybrene (Hexadimethrine bromide, Sigma) solution at a final concentration of 8 µg/ml to enhance transduction. Transduced cells were selected in the presence of puromycin (0.6 µg/ml; Gibco) for at least 72 h.

2.4 DNA manipulation

2.4.1 Cloning of HAS2-Flag

A lentiviral vector (Cumate-pLenti-Cloning-SV40-GFP; iCu2040584) encoding for the hyaluronan synthase 2 (HAS2) without a STOP codon (HAS2-noSTOP) was purchased (AbmGood). The HAS2-noSTOP sequence was PCR-amplified with primers containing specific restriction sites (NheI/BamHI) to facilitate cloning. PCR products were first size-verified by agarose gel electrophoresis and purified using the PCR cleanup kit by MachereyNagel according to manufacturer´s recommendations. Thereafter, products were controlled by Sanger sequencing (SeqLab, Göttingen; primers see A2.3). Target plasmids and inserts were both digested with NheI and BamHI (New England Biolabs). Restriction products were extracted after agarose electrophoresis and ligated over night at 4 °C (Table 2-11). Up to 5 µl of ligation reactions were used to transform 50 µl of competent bacteria (TopTen). Clones were picked with a pipet tip and first duplicated onto a clonal plate followed by colony PCR. For that, the tip with bacteria were immersed in Thermus aquaticus (Taq) polymerase ready mix (NipponGenetics), containing appropriate primers for HAS2 (A2.3), and PCR was carried out according to Table 2-9. Clones that were positive for the target insert were amplified in 5 ml LB broth. 4 ml of LB were used for DNA extraction using the MiniPrep kit of Macherey Nagel. Correct insertion was verified by restriction digests and by Sanger sequencing (SeqLab, Göttingen). After verification, the remaining 1 ml LB was used to generate larger bacterial growth cultures and DNA was once more extracted using the Midiprep Kit (Macherey Nagel). Purified plasmids were used to transfect TSA cells together with pGIPZ-GFP to estimate transduction efficiency. Transgene expression was verified by western blot. For western blot, lysates of cells expressing the control protein IGFBP5-Flag was loaded to verify antibody specificity (A1).

2.4.2 PCR, restriction digest and ligation

PCR was carried out using Thermus aquaticus (Taq) polymerase ready mix (NipponGenetics) (see Table 2-9). Optimal melting temperatures were adjusted according to the primer design or experimentally verified by gradient PCRs (52-64 °C). For colony PCR 66°C was used as melting temperature. PCR-products were Sanger sequenced (SeqLab, Göttingen) and analyzed using SerialCloner software (Open Source).

Table 2-9 PCR

Reagent	For 1X reaction (ul)
2x FastGene mix	25
Fwd primer	0.2 µmol/L
Rev primer	0.2 µmol/L
Template	up to 250 ng
H_2O	Add to total V
V total	50

PCR was started with an initial denaturation temperature of 95°C for 3 min followed by 35 amplification cycles (denaturation at 95°C for 30 s, annealing at 52- 64°C depending on the primer pair, extending at 72°C for 1 min/kb) and finished with one round of final extension at 72°C (1 min/kb).

Products and target plasmids were cut with restriction enzymes and dephosphorylated using alkaline phosphatase as described below (Table 2-10):

Table 2-10 Restriction digest of plasmids and PCR products

Reagent	For 1X reaction (µl) Plasmid	For 1X reaction (µl) Insert
Restriction enzyme 1	1	1
Restriction enzyme 2	1	1
Alkaline phosphatase	1	-
Fast digest buffer	2	1
Plasmid DNA	1 µg	-
Insert DNA	-	1 µg
H_2O	15 x V(plasmid)	7 x V (Insert)
V total	20	10

Products were either purified directly (PCR cleanup, Macherey-Nagel) or via gel electrophoresis extraction (digested plasmids with inserts >100bp, gel extraction kit by Macherey-Nagel). Products were ligated as following:

Table 2-11 Ligation scheme

Example: Plasmid 10 kb + insert 2 kb *Required mass insert (g) =* *desired insert/vector molar ratio x mass of vector (g) x ratio of insert to vector lengths*				
Ratio	1 to 3	1 to 5	1 to 7	1 to 10
bp vector	10,000	10,000	10,000	10,000
vector m (ng)	25	25	25	25
vector c (ng/µl)	25	25	25	25
vector V (µl)	1	1	1	1
bp insert	2,000	2,000	2,000	2,000
insert m (ng)	15	25	35	50
insert c (ng/µl)	25	25	25	25
insert V (µl)	0,6	1	1,4	2
10x buffer (µl)	1	1	1	1
T4 ligase (µl)	0.5	0.5	0.5	0.5
H_2O (µl)	6,9	6,5	6,1	5,5
total V in µl	10	10	10	10

Incubation 4°C o.n. Products were then used for transformation of competent bacteria.

2.4.3 Transformation and plating

50 µl of competent Bacteria (TopTen, Thermo Fisher) per construct were thawed on ice and incubated with 10-50 ng plasmid DNA for 30 min. Cell suspensions were then heat shocked for 45 s at 42°C, cooled on ice for 2 min and then incubated with 450 µl Super Optimal broth with Catabolite repression (SOC) medium (Gibco) at 37°C shaking on a heatblock (Eppendorf). Cells were then plated on agar plates containing antibiotics (Ampicillin at 100 µg/ml or Kanamycin at 50 µg/ml).

2.4.4 DNA preparation

Bacteria were grown over night (o.n) at 37°C on agar plates. Colonies were picked and resuspended in 6 ml Lysogeny broth (LB) containing either Ampicillin (100 µg/ml) or Kanamycin (50 µg/ml). These cultures were grown o.n. at 37°C shaking at 300 rpm. 6 ml pre-cultures were either directly used for plasmid extraction using the Nucleospin mini

kit (Macherey-Nagel) or alternatively resuspended into a total V of 250 ml LB, incubated 16 h at 37°C under constant shaking (300 rpm) and then used for larger yield plasmid preparation (Nucleospin Midi kit, Macherey-Nagel). Plasmids were eluted in provided elution buffer or water.

2.4.4.1 Gel electrophoresis

Agarose gels were prepared by dissolving agarose powder (Applichem) to 1% gels (1 g/ 100 ml buffer), in Tris base with acetic acid and EDTA (TAE) buffer (A2.1). Per 100 ml of gel, 8 µl of MidoriGreen (NipponGenetics) were added before the solution was poured into a gel casting system.

2.5 Staining techniques

2.5.1 Immunostaining (fluorescence)

2.5.1.1 Monolayer

Cells were fixed with 4% FA/ PBS (Roti Histofix) for 15 min RT and then washed with PBS (or stored at 4°C for several weeks in PBS) once before incubation with blocking buffer (A2.3). For intracellular antigens, permeabilization buffer (A2.1) was used, for extracellular proteins we used blocking buffer for surface proteins (A2.1) for 30 min at RT. Cells were then incubated o.n. with primary antibody (A2.3) in the appropriate blocking buffer at 4° C. The next day, cells were washed 3 times for 10 min, first with blocking buffer and then PBS, followed by incubation with secondary antibody (A2.3) and DNA staining reagent Hoechst 1:1,000 for 2 h at RT. After 3 more washes with PBS, cells were mounted using Fluoromount (SouthernBiotech).

2.5.1.2 Tissue slices

For EHM, that were embedded in Optimal Cutting Temperature (OCT) compound and had been sectioned, slides were thawed and air-dried for 30 min before applying a wax pen (liquid blocker super pap pen) to restrict the area of buffer on the objective plates. Slices were then treated and stained as described previously for monolayer cells.

2.5.1.3 Whole mount

Whole EHM were fixed in 4% FA/PBS overnight at 4°C and then washed/stored in PBS at 4°C. Tissues were then incubated with 300 µl blocking buffer (A2.1) at RT for a minimum

of 8 h followed by incubation with the primary antibody (A2.3) at 4°C for 48 h. EHM were then washed 3 times for 2 h with PBS at RT, rocking and incubated with secondary antibodies (A2.3) and DNA stain Hoechst (Invitrogen) (A2.3) at 1:1000 for another 48 h at 4°C. Finally, tissues were washed 3 times with PBS and mounted with Fluoromount (SouthernBiotech). Glass slides and coverslips were sealed after mounting with nail polish and stored at 4°C.

2.5.2 Sirius red staining

Tisses were fixed overnight with 4% FA and then underwent serial dehydration from PBS, H_20, 70% EtOH, 80% EtOH, 96% EtOH (twice) to 100% EtOH (twice), 10 min each followed by toluol (Roth) twice for 15 min before embedding in paraffin (Roth). Tissues were sectioned (4 µm, Leica RM2255) and mounted on glass slides.

For dewaxing, slides were left over night at 37 °C and then transferred into glass jars filled with graded EtOH concentrations (10 min of 100% EtOH twice, 96% EtOH twice, 80% EtOH, 70% EtOH, and then H_2O). Thereafter, slides were submersed in Mayer's Hemalaun solution (AppliChem) for 5 min followed by washing under tap water for 10 min and then incubation with Picrosirius red solution (A2.1) for 1 h. Slides were washed twice with acetic acid (5% V/V glacial acetic acid in H_2O) for 5 min, aqueous solution was removed thoroughly, and slides were then cleared in xylol (Roth) and mounted using Eukit (Roti Histokit II).

2.5.3 Fluorescence and light microscopy

Brightfield and fluorescence images were obtained with an Axiovert 200 equipped with an AxiCam MRc camera using Axiovision SE64 4.9.1 software (Zeiss). Confocal images were obtained on a Zeiss LSM710 using ZEN software (Zeiss). EHM images were taken with a Lumar binocular equipped with an AxiCam MRc camera using Axiovision SE64 4.9.1 software (Zeiss).

2.5.4 Flow cytometry

2.5.4.1 Staining for fixed intracellular antigens

Cells were pelleted at 300 x g for 5 min at 4°C. The supernatant was aspirated, the cells resuspended into blocking buffer (A2.1) and transferred into a round-bottom 96 well plate (Greiner). After 10 min incubation on ice, cells were centrifuged at 300 x g for 5 min at 4°C

and resuspended in 50 µl blocking buffer containing primary antibodies (A2.3). Cell suspensions were incubated 45 min on ice and then 150 µl of PBS were added, per well. Cells were then washed by centrifugation once more and resuspended in 50 µl blocking buffer containing secondary antibody and Hoechst 1:1,000 (Invitrogen; A2.3). After 30 min incubation on ice, 150 µl of PBS were added per well, cells were centrifuged, resuspended in blocking buffer and then spun down one more time before resuspension in 200 µl PBS. The suspensions were then transferred into flow cytometry tubes and samples were measured on a BD LSR II platform. Data was visualized using Flowing software 2.5.1 (Perttu Terho, University of Turku, 2009).

2.5.4.2 Flow cytometry of live CD90-FITC/GFP$^+$/RFP$^+$ cells

For live staining, cells were resuspended in blocking buffer for surface antigens (A2.1), centrifuged once and then resuspended in blocking buffer with Sytox stain (Invitrogen, 1:1,000; A2.3). Following incubation of 10 min at RT, cells were washed once with blocking buffer for surface antigens and finally, after centrifugation at 300 x g for 5 min, resuspended in PBS and measured directly.

Gating strategy: Cell populations were first defined in Sideward Scatter (SSC) against Forward Scatter (FSC) view (Figure 2-1, A); live and dead cells were distinguished by the use of Sytox stain, which penetrates dead cells and causes a shift to the right in the Allophycocyanin (APC) channel (Alexa Fluor 633-conjugated) (Figure 2-1, B). The unshifted live cell population was then used to gate for positive and negative cells, by comparing unstained control cells and GFP$^+$ or RFP$^+$ test populations (as an example for GFP, Figure 2-1, C and D).

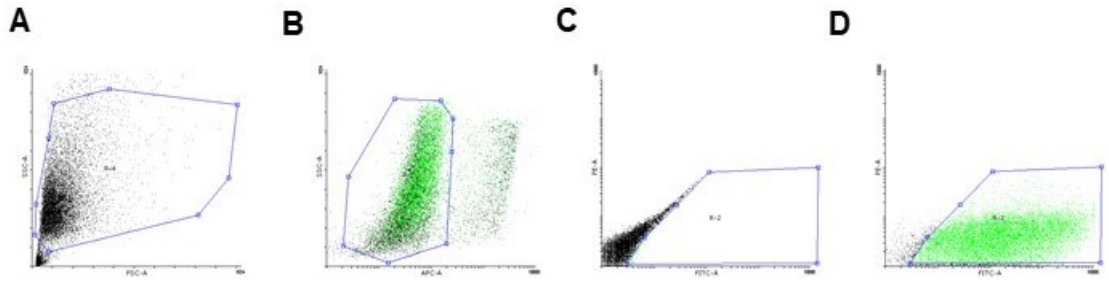

Figure 2-1 Gating strategy for flow cytometry of live cells

Example of gating for live FC of GFP analysis using appropriate controls with cells that do not express the construct. **A** SSC-A vs FSC-A gating to measure the full population of interest, followed by **B** gating for live cells using Sytox reagent (Thermo Scientific; dead cells are shifted to the right). Gating for GFP positive cells in **C** unlabeled control cells vs **D** GFP$^+$ cells.

2.5.4.3 α-actinin

Cells were stained for intracellular α-actinin (see protocol intracellular antigen staining for FC), using α-actinin antibody at 1:4,000 (Sigma, A2.3).

Gating strategy: Cell populations were determined in SSC against FSC view. Then, individual cells were determined by analysis of DNA signal width (Pacific blue channel) vs SSC, followed by determination of specific α-actinin signal, using either Fluorescein isothiocyanate (FITC) (Alexa Fluor 488-conjugated secondary antibody) or APC channel (Alexa Fluor 633-conjugated secondary antibody) and an appropriate primary IgG control for every individual sample (A2.3).

2.6 Photographs and videos

Photographs and videos were taken with a digital camera (Sony, α X5000).

2.7 Western blot

2.7.1 Sample preparation, Bradford assay

All steps were carried out on ice. Adherent cells were washed once with cold PBS. Cells were then incubated with ready protein lysis buffer (A2.1) (Bäuerle buffer with protease and phosphatase inhibitors, both Roche) and incubated for 5 min before collection of cell lysates using a cell scraper (200 µl/well of a 6-well plate). Lysates were collected into 1.5 ml tubes and vortexed vigorously followed by incubation on ice for a minimum of 1 h. Lysates were then centrifuged for 30 min at 12,000 x g. The resulting supernatants were frozen and stored at -20°C.

The concentration of protein in the lysates was determined using bovine serum albumin (BSA) assay. For that, BSA standards were prepared (0; 1; 2; 4; 8; 16 µg in 50 µl H_2O). Standards and samples were diluted in 50 µl using H_2O. Samples were distributed on a 96-well plate (flat bottom, Greiner). 200 µl of 1X RotiQuant reagent (Thermo Scientific) were added per well and samples were incubated for 5 min at RT. Standards were prepared in duplicates, samples in triplicates. Absorbance at 595 nanometer (nm) was measured using the Flexstation® 3 Multi-mode microplate reader (Molecular Devices). Protein concentration was then determined using the standard curve generated from BSA (using R^2 method in linear regression).

2.7.2 Sodium dodecyl sulfate polyacrylamide gel electrophoresis (SDS-PAGE)

Gels for electrophoresis were prepared by mixing gel buffers, 10% Sodium dodecyl sulfate (SDS), polyacrylamide solution and water. To initiate polymerization, 10% Ammonium persulfate (APS) (Sigma) and Tetramethylethylenediamine (TEMED) (Roth) were added. The solutions were gently mixed and then poured into the Mini-PROTEAN® Tetra Cell (BioRad) hand-casting system. The concentration of polyacrylamide in protein gels was either 10% or 12% (Table 2-12).

Table 2-12 SDS PAGE gels

Reagent (in ml)	**For 10%**	**For 12%**	**Stacking gel (4,4%)**
H_2O	10.0	9.0	6.5
40% Acrylamide	5.0	6.0	1
Tris pH 8.8	5.0	5.0	
Tris pH 6.8			2.5
10%SDS	0.2	0.2	0.1
10%APS	0.2	0.2	0.1
TEMED	0.008	0.008	0.01
H_2O	10.0	9.0	1
V total	**20**	**20**	**10**

Equal amounts of protein (30-40 µg) were incubated with 6X Laemmli (A2.1) sample buffer for 5 min at 95°C, briefly centrifuged and followed by loading of the supernatant containing solubilized protein. As size standard, PAGE ruler prestained (Thermo Scientific) was used. Lysates were then separated by electrophoresis, 10 min at 80 V to cross the stacking gel followed by 1.5 h at 120 V through the separation gel, using the BioRad MiniProtean electrophoresis unit.

2.7.3 Immunoblotting

2.7.3.1 Transfer

Polyvinylidene difluoride (PVDF) membranes (Protrean Bioscience) were prepared by activation in methanol, followed by a rinse in distilled H_2O and transfer buffer (A2.1). Following gel electrophoresis, proteins were transferred via semi-dry blotting (transfer buffer containing 20% methanol (A2.1), using 120 mA for 1 h (6-20 V at the time, at

constant mA setting). Following transfer, membranes were briefly rinsed in H_2O and then incubated while shaking with Ponceau solution (A2.1) for 2- 3 min. After rinsing with water, membranes were imaged using the ChemiDoc MP (BioRad) and the manufacturer´s software. Subsequently, membranes were incubated for 45 min in 5% milk/Tris buffered saline-Tween20 (TBST) (A2.1) to block unspecific binding of antibodies.

2.7.3.2 Immunodetection

Membranes were incubated with primary antibody (A2.3) o.n. at 4°C. The next day, membranes were washed 3 times for 10 min with TBST, following incubation with secondary antibody (A2.3) for 45 min at RT. After 3 more washes with TBST, each 10 min, binding of secondary horseradish peroxidase-conjugated antibodies was visualized by incubation with substrate solution (Supersignal West Femto/Thermo Scientific) in a ChemiDoc MP (BioRad). Obtained images were analyzed using ImageLab software (BioRad). Membranes were kept at -20°C.

2.8 Hyaluronan enzyme-linked immunosorbent assay

For HA determination, cells were washed twice with PBS before being incubated for 48 h with fresh growth medium. Then supernatant was collected, and HA content measured using the Hyaluronan Quantikine ELISA Kit (R&D systems), according to manufacturer´s protocols and by using the provided HA standard solutions. Firstly, standard HA solutions were prepared (20 ng/ml; 10 ng/ml; 5 ng/ml; 2.5 ng/ml; 1.25 ng/ml; 0.625 ng/ml), dissolved in Calibrator Diluent RD5-18 (R&D systems), which was also used directly as 0 ng/ml control. Standards were prepared in duplicates, samples in triplicates. Samples were diluted 1:100 from cell culture supernatants and 1:1,000 from EHM cultures. 50 µl of Assay Diluent RD1-14 (R&D systems) were loaded per well of a 96-well flat bottom ELISA plate from the manufacturer. Then, 50 µl of sample solution or prepared standards were added per well, gently mixed and incubated for 2 h at RT on an orbital shaker with gentle rocking. Thereafter, the well content was aspirated, and wells were washed altogether 5 times with 100 µl of provided washing buffer (R&D systems). 100 µl of HA conjugate (R&D systems) were then added per well and incubated for another 2 h at RT while gently shaking, followed by 5 more washes. Subsequently, empty wells were incubated for 30 min with 100 µl substrate solution (R&D systems) and finally the reaction was terminated with 100 µl stop solution (R&D systems) per well. The optical density was assessed by measuring the absorbance at 405 nanometer (nm) using the Flexstation® 3 Multi-mode microplate reader (Molecular Devices). Absorbance reads at 540 nm were subtracted from

reads at 405 nm to correct for optical imperfections on the plate, as recommended by the manufacturer. To normalize secretion to cell counts, cells were detached and counted after the supernatant was collected (from 6-well, in triplicates). Standard curves (four parameters logistic (4-PL) curve-fit) were generated using GraphPad Prism 7 software and concentration of samples determined.

2.9 Gene expression analysis

2.9.1 RNA preparation

2.9.1.1 Cells

RNA of cells and tissues was collected using Trizol reagent (Invitrogen) according to manufacturer´s protocol (see Trizol method). For 2D cell cultures, cells were either directly scraped from the cell culture plate with Trizol reagent or alternatively; centrifuged down at 300 x g, for 5 min at RT. Pellets were then snap frozen and resuspended in Trizol.

2.9.1.2 EHM

For EHM, tissues were snap frozen and then immersed in 1 ml Trizol (Invitrogen) with a steel marble for lysing using the Tissue Lyser (3 consecutive runs with 20 Hz for 3 min; Qiagen). After EHM had dissolved, the mix was centrifuged for 10 min at 5,000 x g to remove remaining fragments and fat. The supernatant was then used for RNA extraction with Trizol.

2.9.1.3 Early phase consolidation collagen I gels

To identify underlying cellular processes that play a role in the earliest consolidation stages of EHM, we generated hydrogels with CM, HFF and both cell types together (EHM) under identical conditions as previously used in shear plate rheology (23°C) and extracted RNA by the TRIZOL method. RNA was analyzed by next-generation sequencing (see 2.9.2).

2.9.1.4 Trizol method

In short, cells or tissue lysates immersed in Trizol reagent were homogenized by vortexing. Per 1 ml Trizol reagent, 200 µl of Chloroform were added (AppliChem). Tubes were closed tightly and turned upside down 5 times followed by 5 min incubation at RT. Samples were then centrifuged at 10,000-12,000 g for 15 min. The aqueous phase, containing RNA, was

transferred to fresh tubes, followed by the addition of 500 µl isopropanol (Roth) to precipitate RNA. Tubes were vortexed, left at RT for 10 min and subsequently centrifuged for 10 more min at 12,000 x g. Supernatants were discarded and 1 ml of 70% EtOH/Diethyl pyrocarbonate (DEPC) H_2O was added to wash RNA pellets. After gentle tipping of the tube to lift off and wash the RNA pellet, samples were centrifuged once more for 5 min at 12,000 x g and supernatant removed. Pellets were left to dry for 5- 10 min, until remnant liquid had evaporated, and RNA was resuspended in DEPC H_2O. RNA concentration and quality were assessed using the Nanodrop, ND-1000.

2.9.2 RNA sequencing

RNA for sequencing was prepared by the Trizol method (see 2.9.1) and analyzed by the Transcriptome and Genome Analysis Laboratory (TAL, Göttingen). Bioinformatics analysis were carried out by Dr. Sebastian Zeidler (Institute of Bioinformatics, Göttingen) and Lavanya M. Iyer (Institute of Pharmacology and Toxicology, University Medical Center, Göttingen).

2.9.2.1 Cardiomyocyte and human foreskin fibroblast comparison

Data was generated and analyzed as previously described in (Tiburcy et al., 2017). In short, RNA integrity and quality were controlled (Agilent Bioanalyzer 2100). Libraries were prepared (TruSeq Stranded Total RNA Sample Prep Kit, Illumina) and sequencing was carried out on an Illumina HighSeq-2000 platform (SR 50 bp; >25 Mio reads /sample). The resulting data was processed and transformed followed by mapping to the human genome. To determine CM- and fibroblast-specific genes, three types of PSC-derived CMs and three types of primary fibroblasts (HFF, GFB1 and CFB1, see Table 2-1) were analyzed in triplicates (for details, see (Tiburcy et al., 2017)).

For the comparison of input CM and fibroblasts in EHM, we used HES2-CM and HFF RPKM values, that had been prefiltered for CM and HFF specific gene expression (see also (Tiburcy et al., 2017)) and compared genes with highest RPKM values, respectively.

2.9.2.2 Cardiac and human foreskin fibroblast comparison

Data was generated and RPKM values were retrieved as described above. Only previously determined fibroblast-enriched genes were analyzed in this context between HFF and CFB1 cells.

2.9.2.3 Early phase consolidation of collagen I gels

This protocol can also be found in (Schlick et al., 2018) in a shortened version.

Generation of RNA-seq libraries was performed using a modified strand-specific, massively-parallel cDNA sequencing (RNA-Seq) protocol (Illumina: TruSeq Stranded Total RNA (Cat. No. RS-122-2301)). The protocol was optimized to maintain the rRNA content in the data set under 5%. (RiboMinus™ technology) The remaining whole-transcriptome RiboMinus™ RNA is suitable for direct sequencing. The ligation step was optimized to increase ligation efficiency (>94%), and PCR protocols were adjusted for an optimal final library product. The quality and RNA integrity were analyzed with the Fragment Analyzer from Advanced Analytical by (standard sensitivity RNA Analysis Kit (DNF-471)). All samples selected for sequencing exhibited an RNA integrity number over 8. For accurate quantitation of cDNA libraries, a fluorometric based system, the quantiFluor™dsDNA System from Promega were used. The size of final cDNA libraries was determined by using the dsDNA 905 Reagent Kit (Fragment Analyzer from Advanced Bioanalytical) exhibiting a sizing of 300 bp in average. Libraries were pooled and sequenced on an Illumina HiSeq 4000 (Illumina) generating 50 bp single-end reads (30-40 x 10^6 reads/sample).

Raw read and quality check:

Sequence images were transformed with Illumina software BaseCaller to BCL files, which was demultiplexed to fastq files with bcl2fastq v2.17.1.14. Quality was assessed with FastQC version 0.11.5 (Andrews, 2014).

Mapping and normalization:

Sequence reads were mapped to the human genome reference library (UCSC version hg19 using Bowtie 2.0 (Langmead and Salzberg, 2012). Then the number of mapped reads was counted for every identified gene and DESeq2 utilized to assess differential gene expression (Anders and Huber, 2010).

Gene ontology analysis:

DAVID (Huang et al., 2009a, 2009b) was used for Gene ontology (GO) analyses and VennDiagrams were created with the online tool BioVenn (Hulsen et al., 2008).

2.9.3 Quantitative real time PCR

2.9.3.1 DNAseI treatment

RNA was thawed on ice and 1 µg of RNA was used per reaction for subsequent DNAse I (Thermo Scientific) digest and reverse transcription (RT) (RT kit, Promega), as described below:

Table 2-13 DNAse I protocol

Reagent	**Per 1X reaction (in µl)**
1 µg RNA	X
10x DNase buffer	1
DNaseI	0.2
H_2O	Add up to total Vol
Vol total	10
Protocol steps	
1.	20 min 37°C
2.	Per sample, add 1 µl of 40 mmol/L EDTA
3.	10 min at 75°C

2.9.3.2 Reverse transcription

Table 2-14 RT-PCR

	Reagent	**Reagent for 1X reaction (in µl)**
Master mix 1	**dT20 Primer (500 µg/µl)***	1
	dNTPs (10 mmol/L)*	1
	H_2O	2.5
	V total	4.5
Master mix 2	**M-MLV 5X Reaction Buffer***	4
	MLV RT (200 U/µl)*	0.5
	V total	4.5
Master Mix 3 (without reverse transcriptase)	**M-MLV 5X Reaction Buffer***	4
	H_2O	0.5
	V total	4,5
qRT-PCR reaction	DNAseI treated RNA	**11**

	Reagent	Reagent for 1X reaction (in µl)
	Master Mix 1	**4.5**
	MasterMix2 (or 3 for –RT control)	**4.5**
	V total	**20**
*Primer, dNTPs, enzymes and reaction buffer are contained in the M-MLV reagent kit.		

RNA and master mix 1 were mixed before and incubated for 5 min at 65°C. Then master mix 2 (or 3) were added and samples were incubated for 50 min at 42°C followed by 15 min at 70°C. Resulting complementary DNA (cDNA) was diluted 1:5 (100 µl) and subsequently used for quantitative real time PCR (qRT-PCR). cDNA was stored at -20°C.

2.9.3.3 Quantitative real time PCR and analysis

Quantitative real time (qRT-) PCR and subsequent data analysis was carried out by Petra Rompel (HAS2 overexpression, 3.2.1).

2.10 Isometric force measurements

EHM isometric force measurements had been previously described (Zimmermann 2000). EHMs were cultured for 4 weeks. EHM were kept at 37°C on a heating plate, photographed and recorded using video capturing. Spontaneous beating frequency was determined by analyzing beats within a 10 s time window (values were then extrapolated for beats/min).

Then tissues were transferred into isolated organ baths (Föhr Medical Instruments) (A2.5). EHM were immersed in Tyrode´s buffer (A2.1), containing 2 mmol/L [Ca^{2+}] while perfused with carbogen (95% O_2, 5% CO_2), kept at a constant temperature of 37°C. EHM were prestretched carefully to an average value of 0.1 millinewton (mN) resting tension and left to equilibrate for up to 20 min. Spontaneous beating in this phase was documented. EHM were then electrically stimulated at 1.5-2 Hz (200 mA, 5 ms pulse). Subsequently, EHM were stretched (125 µm steps) until maximal force of contraction was achieved according to the Frank-Starling mechanism.

Next, EHM contractile forces in response to increasing [Ca^{2+}] were measured under constant stimulation at 1.5-2 Hz (0.2-4 mmol/L [Ca^{2+}]). After reaching maximal forces at 4 mmol/L [Ca^{2+}], the half maximal effective (EC50) calcium concentration was calculated

and Tyrode´s buffer was adjusted to individual EC50 [Ca^{2+}] values for each EHM. The force-frequency response was tested at increasing frequencies (from 1, 2 and 3 Hz for 4 min each). After evaluation of the fore-frequency response, adrenergic responses were assessed by adding 1 µmol/L isoproterenol (at 1.5- 2 Hz), followed by 10 µmol/L carbachol (A2.1). Contractile forces (Force of contraction (FOC) = Fmax – Fmin) were recorded using BMON software and subsequently analyzed using AMON software (G. Jaeckel, Hanau). EC50s [Ca^{2+}] were calculated by non-linear regression using GraphPad software.

Time to 90% contraction and time to 50% relaxation were measured on 3 consecutive single contractions (stimulated with 1.5-2 Hz at 4 mmol/l [Ca^{2+}]) and averaged.

2.10.1 Data analysis

Data was extracted to Excel (MicrosoftOffice) from Amon software as Fmin, Fmax and force of contraction (FOC) = Fmax – Fmin. Beating frequency was determined by analyzing beats in 4 s within a 1 min time window (averaging 3 measurements). EC50s [Ca^{2+}] were calculated using GraphPad Prism 7 software.

2.10.2 Cross sectional area (CSA)

EHM cross sectional area (CSA) was determined by measuring arm width and thickness, using photos from the contraction setup. Photos were scaled using the 1 mm electrode in the pictures. CSA was determined by calculation of the arm width and arm thickness as half axes of an ellipse. Image J (Open Source) was used to determine numerical measurements.

2.10.3 Tissue compaction

2.10.3.1 Analysis of tissue compaction at 1 h after casting (DCM study)

Compaction of 1 h old EHM gels was assessed by determining the gap between the polydimethylsiloxane (PDMS) tissue mold (A2.5) and the contracted gel. For this, images were taken using a digital camera and a ruler. Images were scaled from measuring the ruler with ImageJ 1.8.0 (NIH) and gaps determined accordingly.

2.10.3.2 Analysis of consolidation at 24 h and 72 h

For the analysis of compaction at 24 h and 72 h we determined the % of area that was free of collagen I hydrogels after 24 h and 72 h in circular 10 mm PDMS molds for EHM casting.

For that molds with gels were imaged with a Lumar binocular and a digital camera. Images were scaled with ImageJ software by measuring the mold diameter. Compaction was calculated by determining the % of area not occupied anymore by the gel after 24 h and 72 h. For that we determined the area free of gel divided by the whole mold area (66 mm^2; taking into account the area of the inner PDMS pole).

2.11 Rheology

2.11.1 Shear plate rheology

EHM hydrogels were prepared according to 2.2 and Table 2-6, containing either no cells, only HFFs, only CMs or both cell types. 140 µl of the suspension was then transferred onto a chromium plate and sheered using constant strain and frequency (1%, 1Hz) under a CP25-2 conical plate (cone and plate geometry with an angle of 2° and a gap height of 103 µm) in a bulk rheometer (MCR-501, Anton Paar, Austria). Here, strain is applied by shearing the hydrogel between two oscillating plates and the dynamic modulus is measured, which is a combined measurement of tensile storage (stiffness) and loss modulus of the tested gel. The loss modulus describes energy dissipated as heat, while in this setting, the storage modulus serves as an actual direct readout of gel stiffness and is thus of predominant interest.

During measurements temperature was kept at a constant 23°C and humidified atmosphere to avoid evaporative loss. Time sweep measurements were recorded (every 30 s). For analysis of stiffening behavior, slopes of the change in elastic storage modulus were analyzed and compared.

2.11.2 Destructive tensile stress measurements

EHM arm size was documented by light microscopy using a Lumar binocular (Zeiss), then EHM were fixed by two hooks in an organ bath containing PBS (no Ca/Mg) at 35°C (it was not possible to keep 37°C constant temperature in this setup). EHMs were prestretched to slack length. At this stage the motor transducer setup was zeroed and subsequently constant strain was applied at a speed of 0.025 mm/s until EHMs ruptured. Hooks were designed in-house by Dr. Tim Meyer (Figure 2-2). Data was recorded with TRIOS software.

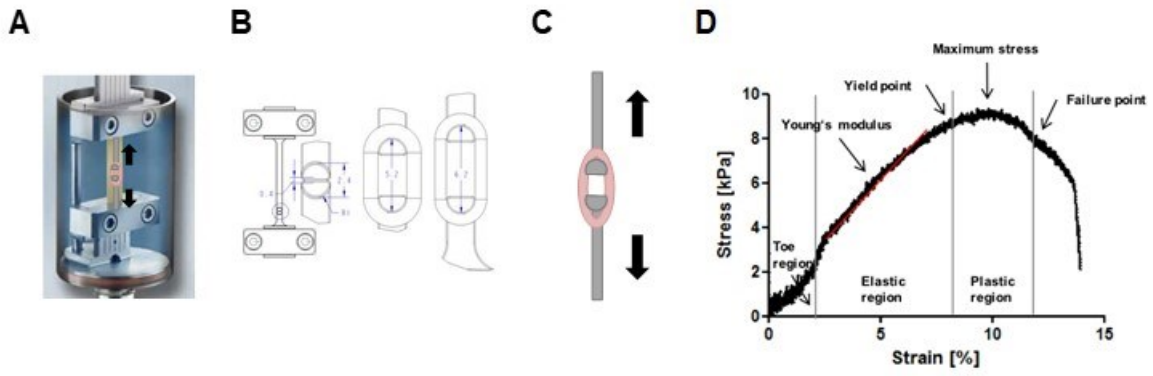

Figure 2-2 Destructive tensile stress measurement

A Setup of EHM immersed in PBS for measurement. **B** Hook design and measurements (provided by Dr. Tim Meyer). **C** Axial stress is applied to EHM tissues at constant strain rate of 0.025 mm/s. **D** Resulting stress vs strain curves in destructive tensile stress measurements (Hartmann, 2016).

2.12 Statistical analysis

Data are presented as mean±SEM. Statistical analysis was performed using GraphPad Prism 7 (GraphPad Software Inc., San Diego).

3 Results

3.1 Fibroblasts are essential for EHM formation

3.1.1 EHM is a highly defined system of cardiomyocytes and fibroblasts

To investigate the fibroblast-CM crosstalk, EHM were generated from homogenous CM populations containing >90% α-actinin$^+$ cells (95±2%; n=3) and human foreskin fibroblast (HFF) populations containing >90% CD90$^+$ cells (94±5%; n=3). We used HFFs here as a prototypic fibroblast type (Figure 3-1).

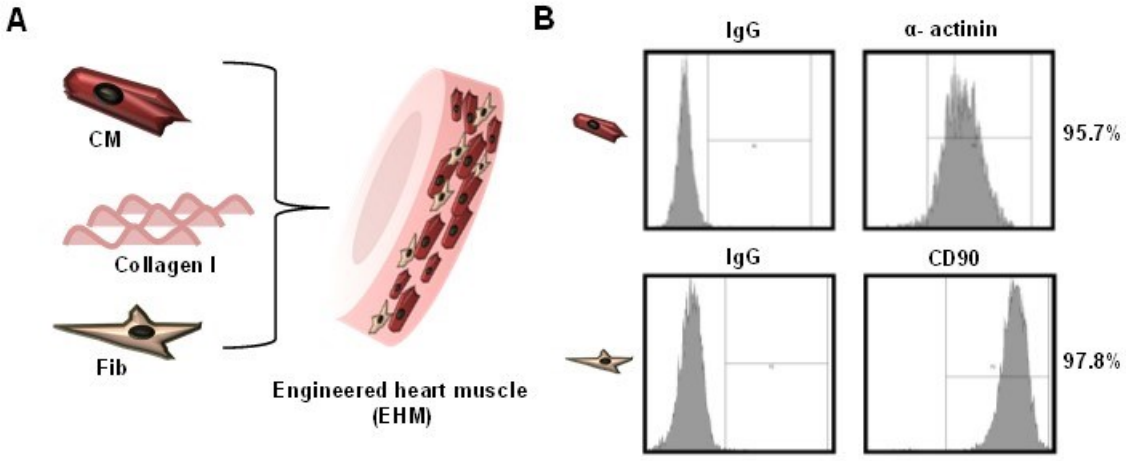

Figure 3-1 EHM generation from defined cell populations.

A Schematic of EHM content: Highly purified PSC-derived CMs and fibroblasts (Fibs) are mixed in a ratio of 2:1 in a collagen I hydrogel that develops over a time of 4 weeks into functional EHM. **B** Representative examples for flow cytometry (FC) analysis of CM and fibroblast (Fib) populations (here: HFF cells) with a typical purity of CM being >90% actinin$^+$ and >CD90$^+$ (Thy1) respectively. Data from (Schlick et al., 2018).

We analyzed RNA expression patterns of input CMs and HFFs, demonstrating distinctive cellular expression patterns, specific for both cell types (data published in (Tiburcy et al., 2017). The most predominantly expressed transcripts in CMs were found to encode for components of the sarcomere, such as cardiac troponin T (TNNT2), both troponin I 1 and 3 (TNNI1 and 3), many members of the myosin family (myosin light chain-MYL and myosin heavy chain – MYH), and sarcomeric α-actinin (Figure 3-2 A). Variants and mutations in these proteins have been associated with familial forms of DCMs (Cho et al., 2016). In line with the dependence of CM contractility on the calcium (Ca^{2+}) handling machinery, we also found high expression level of ryanodine receptor 2 (RYR2), a calcium-activated calcium release channel that plays a major role in the contractile cycle. A

dysfunction of this channel leads to detrimental pathologies of the heart (Jóna and Nánási, 2006).

The transcripts we found most abundantly expressed in fibroblasts were, as anticipated, associated with ECM generation and homeostasis (Figure 3-2 B). Here, we identified thrombospondin 1 (TSP1) mRNA as the highest expressed transcript in fibroblasts, which is important component of the ECM and involved in matrix remodeling, also after myocardial infarction (Frangogiannis, 2005). Other ECM components of interest were CD44, a structural protein that mediates HA binding, but also controls its degradation through hyaluronidases 1 and 2 (HYAL1 and 2) (Harada and Takahashi, 2007) and regulators of the ECM, such as MMP-2 and neprilysin (MME).

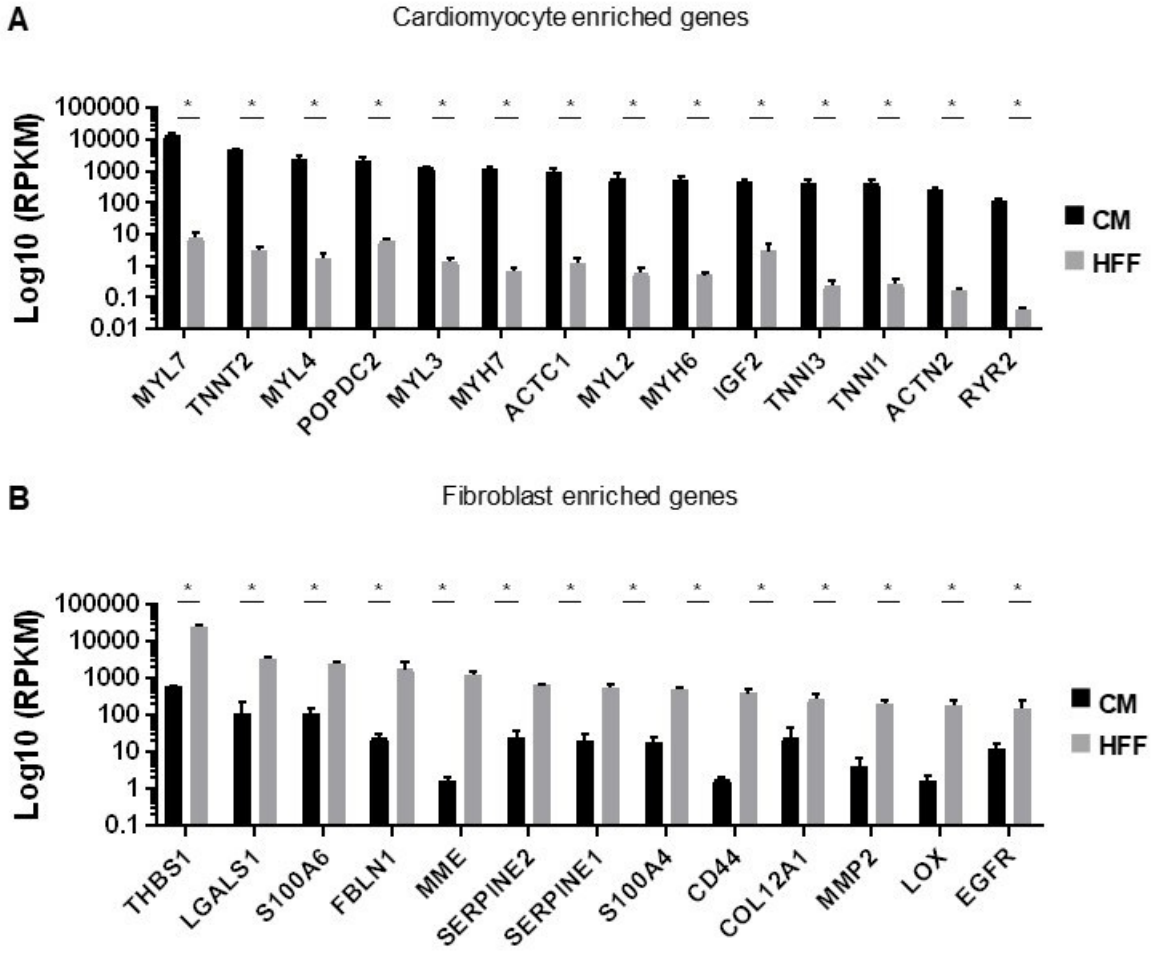

Figure 3-2 Expression profile of EHM input cell populations

Selected, highly expressed, cell-specific enriched transcripts in **A** CMs (derived from HES2) and **B** human foreskin fibroblasts (HFFs), used as prototypic fibroblast source for EHM. *p<0.05 by student´s unpaired two-tailed t-test. Values of RNA sequencing (RNAseq) data in RPKM (reads per kilobase of transcript per million

mapped reads). n=4/group and gene. Parts of these data were published in (Tiburcy et al., 2017). Figure adapted from (Schlick et al., 2018).

By combining highly purified and well characterized populations of CMs and fibroblasts in EHM, a robust 2-cell type model of the developing myocardium was generated in which crosstalk of CMs and fibroblasts can be investigated under controlled *in vitro* conditions.

3.1.2 Fibroblasts determine EHM functionality

To assess the effect of fibroblasts on the formation of the EHM syncytium, we measured the force of contraction in EHM formulations comprising only CMs or mixtures of CMs and fibroblasts as reported previously (Tiburcy et al., 2017); (Figure 3-3). CMs in collagen I hydrogels showed spontaneous beating but failed to develop a functional syncytium capable of developing considerable forces (FOC at 4 mmol/L [Ca^{2+}] in mN: 0.15±0.05 in CM only EHM vs 1.2±0.15 in CM+ HFF EHM; n=4/group). These findings confirm the important role of fibroblasts in heart muscle assembly.

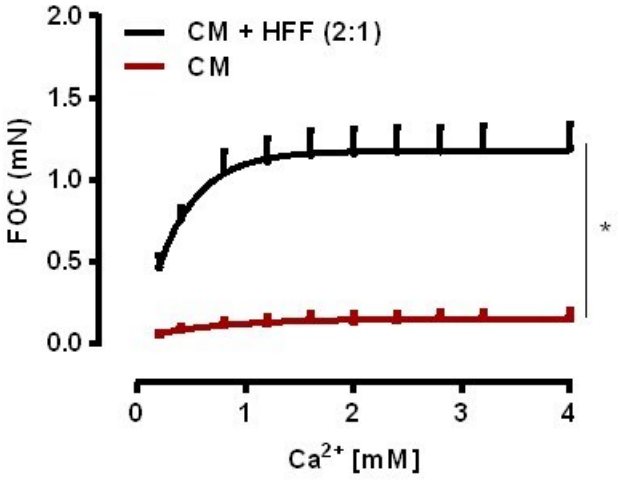

Figure 3-3 Fibroblasts are crucial for the functional development of EHM

Isometric force measurement of 4-week-old EHM. Force of contraction (FOC) in EHM constructed from CM or CM+ HFF (2:1) in collagen type I (n=4/group). FOC was measured as a function of extracellular calcium (0.2-4 mmol/L). *p<0.05 by 2-way ANOVA with Sidak´s multiple comparisons *post-hoc* test. Data from (Schlick et al., 2018).

The spatial- and temporal assembly of CMs in EHM was further analyzed by immunostaining. From day 1 until 4 weeks of EHM culture, in the presence of fibroblasts, sarcomeric proteins such as α-actinin increased in abundance and CMs underwent spatial organization into an anisotropic, aligned syncytium (Figure 3-4). This is in line with increasing force production between 2 and 4 weeks

(Tiburcy et al., 2017). Taken together with the crucial role of cardiac fibroblasts in early cardiac development and the proper spatial compaction of the developing myocardium (Camelliti et al., 2005; Takahashi et al., 2014), we aimed to further dissect the fibroblast derived-cues that govern muscle formation in EHM.

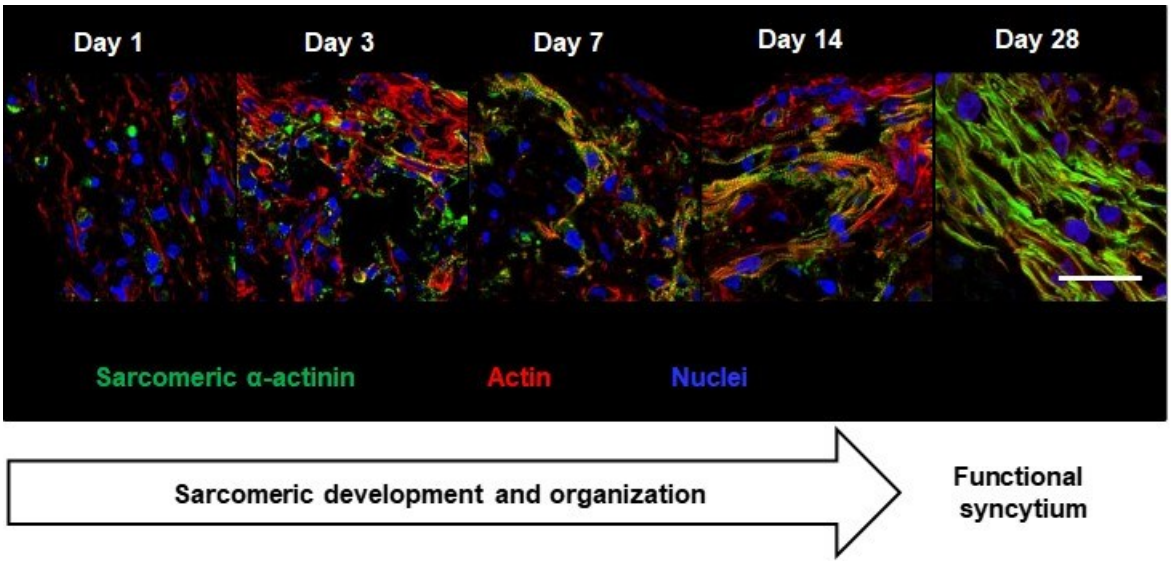

Figure 3-4 Muscle formation process in EHM

Sarcomere development during EHM maturation at indicated time points. Immunostaining for α-actinin (green) and f-actin (red), nuclei (blue). Scale bar: 50 µm. Data from (Schlick et al., 2018).

3.1.3 Biophysical cues for fibroblast-mediated muscle formation

To investigate the role of fibroblast-mediated collagen I handling during the assembly of CMs into higher order contractile units within the developing EHM, we first explored the compaction behavior of collagen I hydrogels at early days of EHM development 1 and 3 (Figure 3-5). Indeed, in line with the described capability of fibroblasts to compact gels of collagen I *in vitro* (Bell et al., 1979; Chapuis and Agache, 1992), we found that the presence of fibroblasts was clearly responsible for the consolidation of compact tissues compared to collagen I hydrogels with and without CMs. At 24 h compaction was mostly completed (in % at 24 h: Collagen I 1.5±0.9; Collagen I + CM 28.1±2.9; collagen I + HFF 61.6±2.9; collagen I + CM + HFF 70.1±0.9; at 72 h: Collagen I 5.4±1; Collagen I + CM 25.9±1.8; collagen I + HFF 78.5±2.1; collagen I + CM + HFF 70.3±3.1; n=4/4/4/4) (Figure 3-5 B). Of note, in the CM only group, the level of compaction was clearly higher than in collagen I only, which is likely the result of a small fraction of remnant stroma cells from the differentiation process. Interestingly, we also observed a continuous increase in tissue compaction in the

HFF only group indicating that there may also be "inhibitory" cross-talk between CM and fibroblasts in EHM (HFF+ CM group) (Figure 3-5 B).

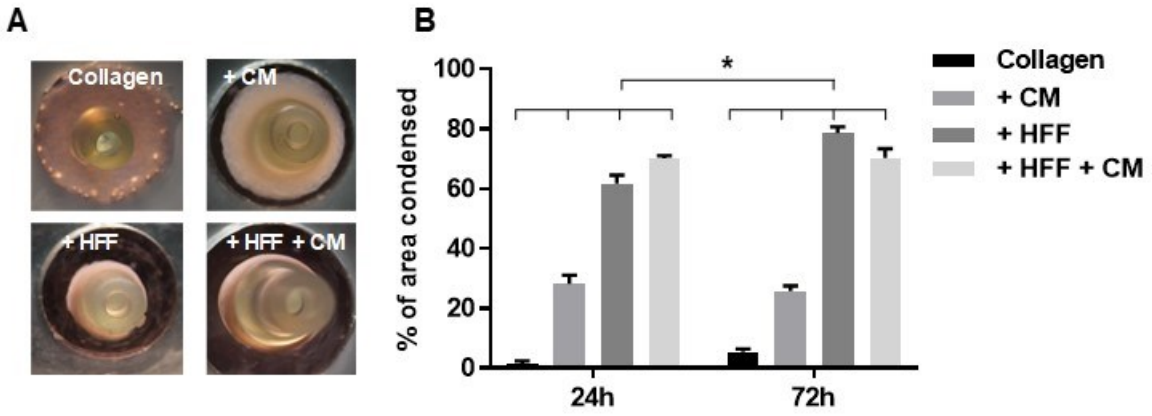

Figure 3-5 Fibroblasts drive tissue consolidation

A Representative images of hydrogels with collagen I on day 3. Diameter of casting molds: 10 mm. **B** Consolidation of tissues in PDMS molds 24 h and 72 h after casting. *p<0.05 by 2-way ANOVA with Sidak´s *post hoc* test for multiple comparisons. n=4/group at 24 h and n=9/5/8/5 at 72 h, 2 independent experiments. Data from (Schlick et al., 2018).

To further quantify fibroblast-mediated EHM compaction in more detail, we chose to utilized shear plate rheology under physiological conditions (1 Hz and 1% strain). For viscoelastic gels, the elastic modulus (a combination of storage and loss modulus) describes the deformation response of a material when it is under stress (Figure 3-6). After an initial lag-phase in which the hydrogels settled in the instrument, collagen I hydrogels underwent a gelation step in the first 30 min, which was independent of the presence of cells (Figure 3-6 B). This occurs when a solution of collagen I, which solubilized in a highly acidic solution at a pH of 2, undergoes polymerization by neutralization of the pH. After gelation, only hydrogels with cells further stiffened (Figure 3-6 B). We quantified this cell-mediated process by comparing the change in tensile storage modulus ("stiffening rate") in this phase (Figure 3-6 C). The stiffening rates of hydrogels with HFF or CMs and HFFs were significantly higher than of collagen I or collagen I with CMs (Slopes of storage moduli in Pa/min: Collagen I 0.04±0.03; Collagen I+ CMs 0.03±0.02; Collagen I + HFFs 0.53±0.07; Collagen I + CMs + HFFs 0.29±0.03; n≥ 3/group). Interestingly, hydrogels with only CMs behaved like collagen gels, while gels containing fibroblasts clearly consolidated most effectively. In the presence of both fibroblasts and CMs the consolidation was intermediate, indicating that the presence of CMs dampened fibroblast-mediated gel compaction.

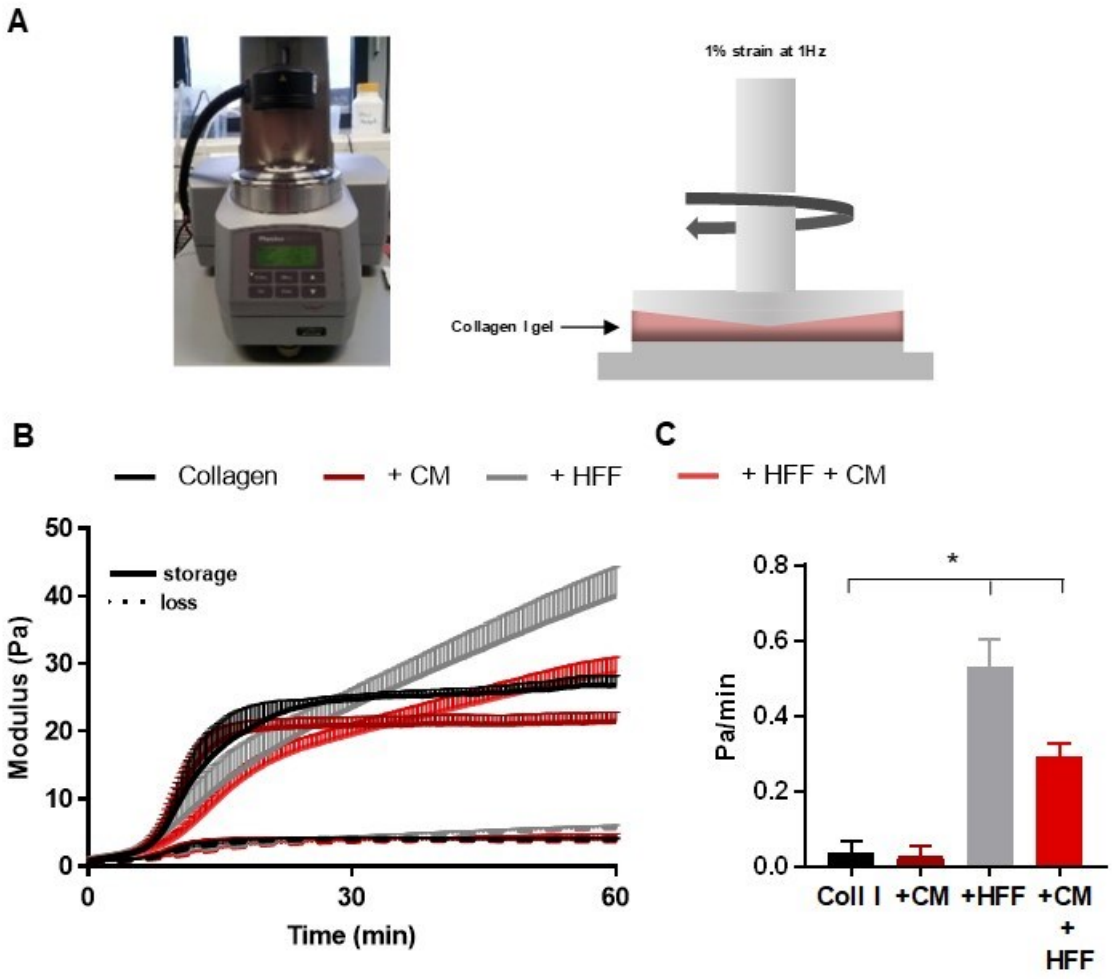

Figure 3-6 Early consolidation phase characterization of collagen I hydrogels

A Schematic overview of experimental set-up using the Anton Paar rheometer for shear plate rheology with a CP25.2. shear plate at 1% strain and 1 Hz (at 23°C). **B** Storage (Elastic) and Loss (viscous) moduli of collagen I hydrogels either without cells, with CM alone (CM), fibroblasts alone (HFF) and EHM (HFF+ CM) over time. fibroblasts were subjected to shear plate rheology and storage and loss modulus were recorded. **C** Storage modulus slopes at 40-60 min in collagen I hydrogels without cells, with CM alone (CM), fibroblasts alone (HFF) and EHM (HFF+CM). n=3/collagen and CM groups, n=4 for HFF and HFF + CM groups; *p<0.05 by 1-way ANOVA followed by Tukey´s multiple comparisons *post hoc* test. Data from (Schlick et al., 2018).

3.1.3.1 Transcriptome signatures in EHM

To unravel the impact of tissue compaction on cell phenotypes, we studied the differential transcriptome during the cell-independent gelation (up until 30 min after casting) and cell-dependent collagen compaction (30-90 min after casting) phases (Figure 3-7 A). As anticipated CM, HFF and CM+HFF (early EHM culture) sample transcriptomes were clearly distinguishable (Figure 3-7 B), as 91% of variance could be attributed to cell composition of hydrogels (PC1). Cocultures of CM:HFFs in EHM occupied a distinct cluster (PC2, 7% of variance), compared to CM and HFF only groups. This segregation indicated

transcriptome dynamics that can be specifically attributed to the coculture of the two cell types in EHM (CM:HFF 2:1). Generally, the changes in transcriptomes within the groups were small, which was expected due to the short timeframe between the two measurement points.

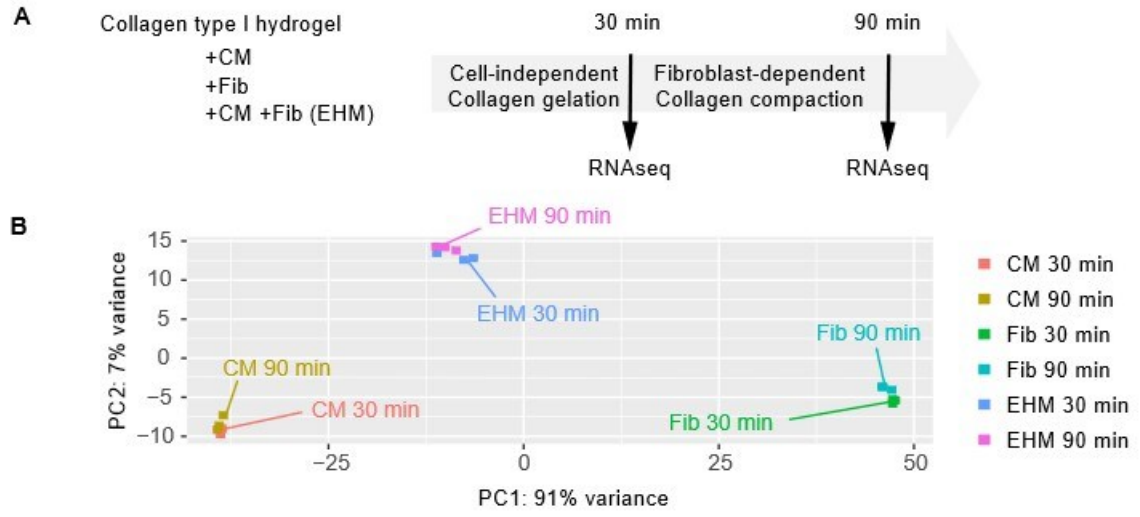

Figure 3-7 Distinct transcriptomes in EHM models

A Experimental design. Collagen I hydrogels with CMs, HFFs (Fibs) and both CMs and HFFs (2:1, EHM) were generated and RNA samples collected in the gelation process (cell-independent polymerization, 30 min after casting) and during collagen compaction, the cell-dependent phase (90 min after casting). **B** Principal component analysis (PCA) of the indicated sample groups: tissue comprised of CMs, HFFs or both (CM+HFF at a 2:1 ratio). n=3 samples/group. Data from (Schlick et al., 2018).

3.1.3.2 EHM consolidation transcriptomes resembles cardiac compaction and wound healing

The comparison of differentially expressed genes during the cell-independent and dependent phases (Figure 3-7 A) demonstrated that the HFF only group was transcriptionally more responsive (DEG: 727) compared to the CM and early EHM groups (DEGs: 106 and 107, respectively) (Figure 3-8).

The DEG overlap was larger between the EHM and HFF groups (434) than the EHM and CM groups (48 genes; Figure 3-8). The CM and HFF groups shared only 13 commonly regulated DEGs, which may be due to the fibroblast-like component in the CM group (on average 96% α-actinin$^+$ CM preparation, n=3 batches). 202 genes were regulated in all three groups (CM, HFF and CM + HFF), indicating similarities in tissue compaction associated transcriptome regulation (termed here “General tissue formation processes”).

Using gene ontology (GO) analyses we scrutinized the cell type-dependent processes (Figure 3-8). Among the general tissue formation processes (Figure 3-8 B), we found responses to BMP signaling, (cardiac) epithelial to mesenchymal transition (EMT) and endocardial cushion formation, together with biosynthetic processes of EHM polysaccharides and the regulation of wound healing. In the fibroblast (HFF) group transcriptional changes involved processes such as ECM organization and general heart development (Figure 3-8 A). Of note, both TGFß and PDGFß signaling could be specifically identified. TGFß signaling is stimulated in EHM in the presence of exogenous TGFß1 supplemented with the culture medium to enhance EHM compaction (Tiburcy et al., 2017). In the CM group (Figure 3-8 C), GO term analyses suggest cellular and in particular endoplasmic-reticulum (ER) stress in response to the 3D environment. With only four unique GOs in EHM (not shown) and the large overlap of DEG in EHM and fibroblast samples it appears that the fibroblast fraction is highly responsive to the changes in tissue compaction. Of note, we identified many regulatory RNAs of the micro and noncoding family in the DEGs of the EHM (CM:HFF 2:1) group (45 up- and 405 downregulated genes, including 210 micro/long non-coding RNAs).

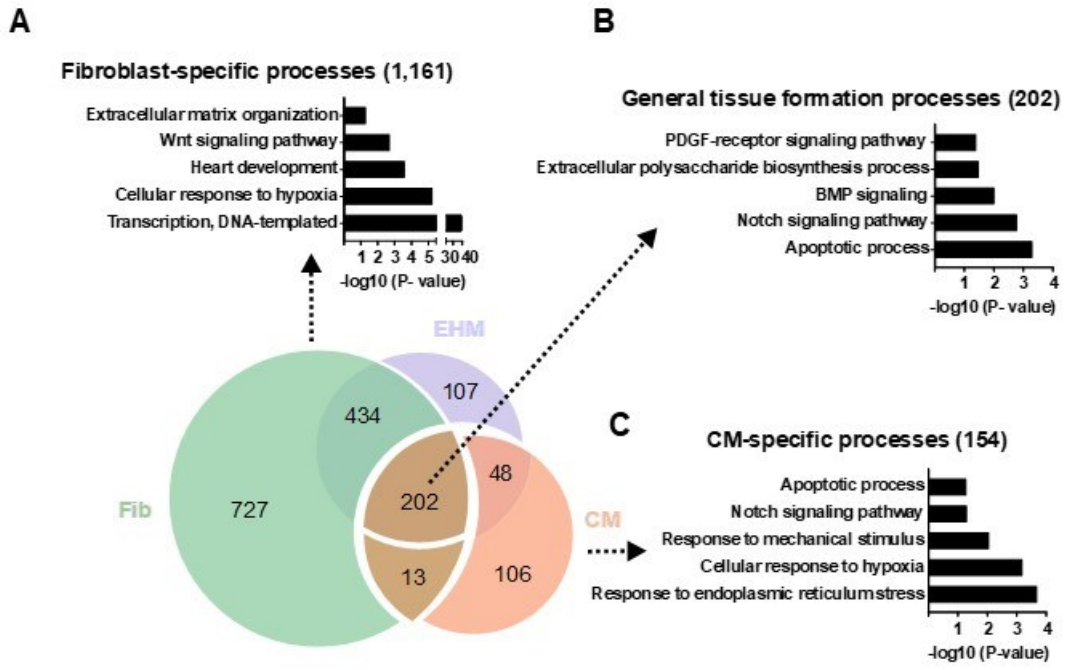

Figure 3-8 Regulated biological processes during fibroblast-mediated collagen I compaction

Venn diagram of genes that are differentially regulated (DEGs) as a result of fibroblast-specific collagen I compaction. Selected gene ontology (GO) terms of regulated genes that are **A** fibroblast-specific (EHM and HFF only group), **B** regulated in all groups or **C** CM-specific. Data from (Schlick et al., 2018).

Among the DEGs regulated in all groups, we found regulators of early cardiac morphogenesis and endocardial cushion/cardiac jelly formation (HAS1, HAS2, BMP2 and TGFß (Figure 3-9 A). During cardiac development, cardiac compaction and jelly formation are guided by the developing fibroblast(-like cell) population (Ieda et al., 2009; Takahashi et al., 2014) and crucially dependent upon HA synthesis by the HASs, particularly HAS2 (Camenisch et al., 2000, 2001; Meran et al., 2011; Missinato et al., 2015; Porsch et al., 2013), which is regulated via BMP2 signaling (Ma, 2005). Furthermore, PDGFß can stimulate HA production also by CMs (Hellman et al., 2010) and the PDGF receptors are crucial for EMT during cardiac early development (Smith et al., 2011). In the fibroblast-specific group (Figure 3-9 B), we identified genes of ECM turnover and anchorage (ELN (elastin), DSP, and JUP) and the master transcriptional regulator SOX9 that is involved in heart development and associated with a majority of fibrotic processes (collagen I deposition) in the heart (Hanley et al., 2008; Lacraz et al., 2017).

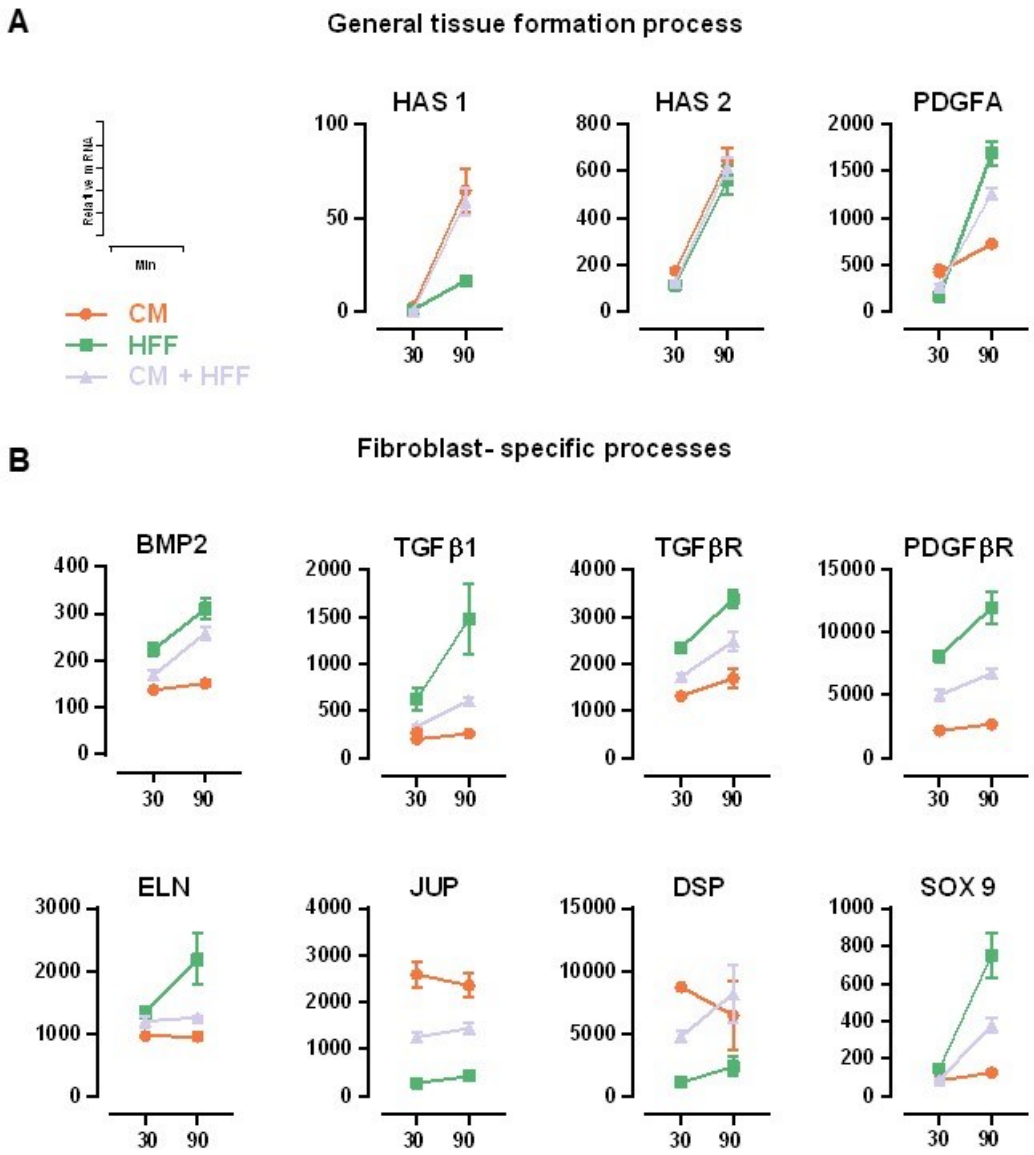

Figure 3-9 Selected genes regulated during the cell-dependent phase

Trajectory of transcriptional alterations during the cell-independent collagen I gelation and cell-dependent collagen I compaction phases of early tissue development. **A** DEG present in all groups. **B** Selected DEG from the fibroblasts containing groups (HFF, EHM (CM:HFF 2:1). Ordinates indicate relative RPKM values. Data from (Schlick et al., 2018).

3.1.3.3 Fibroblasts remodel the ECM and determine EHM viscoelasticity

Next, we analyzed the morphology of tissues with CM, HFFs or both cell types (EHM) after 4 weeks (Figure 3-10 A and B). In line with our results at 1 and 3 days, we found that only collagen I gels with HFFs had formed compacted tissues as measured by the thickness of arms (in mm: Collagen I 5.1±0.27; Collagen I + CM 4.8±0.24; Collagen I + HFF 1.1±0.06; Collagen I + CM + HFF 1.3±0.03; n=12/9/10/12; Figure 3-10 B).

We further evaluated the viscoelastic properties of tissues with CM, HFFs or both cell types (EHM; Figure 3-10 C) by destructive tensile stress measurements. The linear phase of the generated strain vs stress curve was used to calculate the Young´s modulus. Tissues with HFF were significantly stiffer than either collagen I hydrogels or collagen I hydrogels populated with CMs only. There was no difference in stiffness between either collagen I with and without CMs; HFF populated as well as HFFs and CMs (EHM) populated collagen hydrogels were clearly stiffer (Young´s modulus in kPa: Collagen I 0.07±0.06; Collagen I + CM 0.02±0.01; Collagen I + HFF 2.2±0.37; Collagen I + CM + HFF 0.89±0.13; n=6/5/9/11; Figure 3-10 C).

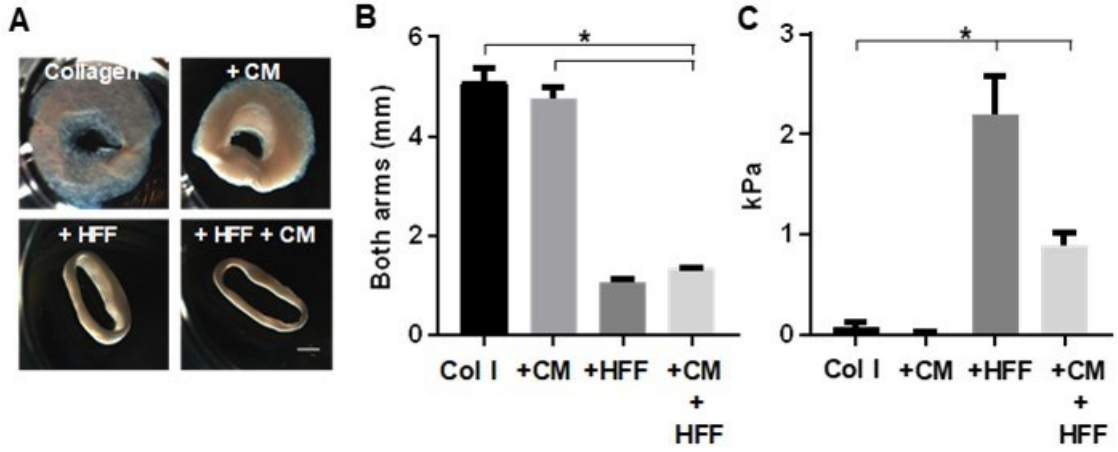

Figure 3-10 Fibroblasts are major determinants of EHM viscoelasticity

A Images of constructed cell-free or cell containing tissues at 4 weeks (scale bar: 1 mm; applies to all panels). **B** Tissue arm thickness used to calculate the Young´s modulus of collagen I (Col I) without cells, with CMs, with HFFs or with both CMs and HFFs after 4 weeks (n=12/9/10/12). **C** EHMs were prestretched and tension applied at 0.025 mm/s (n=6/5/9/11). *p<0.05 by 1-way ANOVA followed by Tukey´s multiple comparisons *post hoc* test. Data from (Schlick et al., 2018).

In order to evaluate the structure of ECM, we compared Sirius red staining of 4-week-old hydrogels (Figure 3-11), which clearly indicated that collagen I used as EHM input material had been remodeled extensively and replaced during the 4 weeks of culture when fibroblasts were present (compare collagen I hydrogel loose lattice with highly compacted ECM of collagen I containing HFFs and both HFFs and CMs). This small level of compaction observed in CM only gels can likely be attributed to the presence of contaminant stroma cells found in HES2- derived CM preparations.

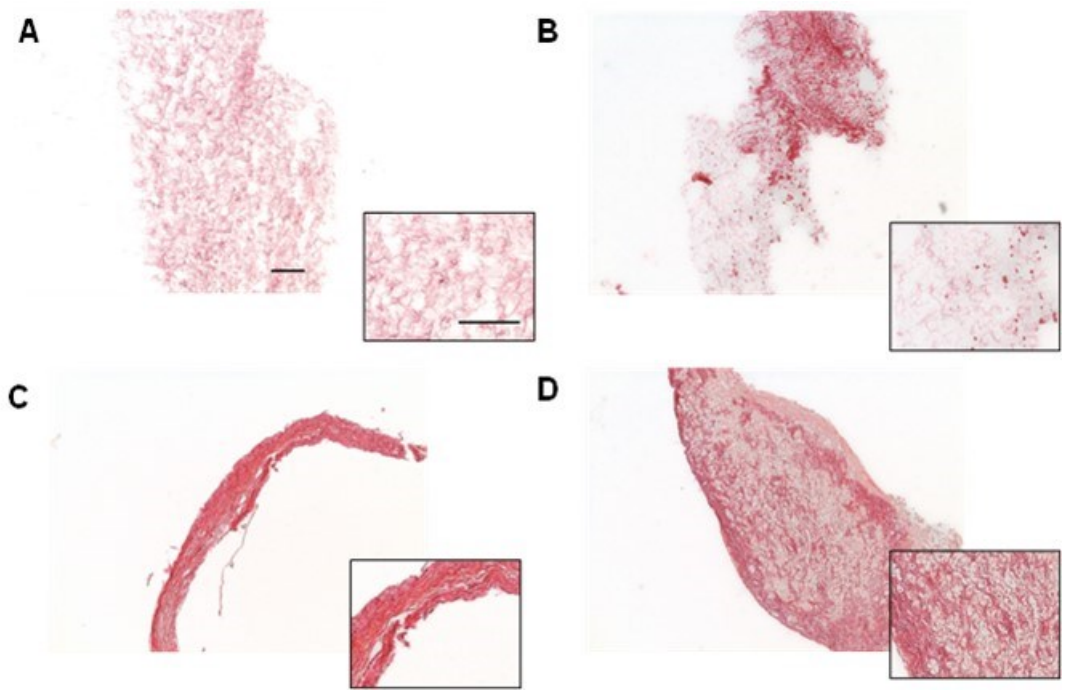

Figure 3-11 Collagen remodeling in 4-week-old collagen I hydrogels

Collagen I hydrogels with and without cells were generated and cultivated for 4 weeks and then stained with Sirius red. **A** Collagen I without cells. **B** CMs in collagen I. **C** HFF in collagen I. **D** EHM (CM:HFF 2:1). Scale bar 100 to 400 µm (in magnified view). Data from (Schlick et al., 2018).

Collectively, these data demonstrate the crucial role of HFFs during the early phase of EHM compaction and long-term tissue development where they control tissue viscoelasticity and ECM integrity.

3.1.4 Fibroblasts from different origin support EHM formation

Since most of the experiments so far were performed with HFF as prototype for fibroblasts, we asked whether our observations were universal across all fibroblasts cell types or HFF-specific mechanisms. Firstly, we chose to compare HFFs with endogenous cardiac fibroblasts (CFBs) derived from the ventricle of healthy patients (organ donors, Lonza) and we hypothesized that these cells may be more likely to reconstitute an organotypic EHM for *in vitro* modeling of native myocardium. Additionally, we chose fibroblasts derived from the gingiva of patients (GFBs). These cells can be obtained to generate patient-specific EHMs for *in vitro* use and potentially for clinical applications (Figure 3-12 A), see also section 3.3.1 for in depth analysis.

We generated EHM from HFFs, CFBs (3 different patients, CFB1-3) and GFBs (4 patients, GFB1-4). All fibroblasts tested were able to support the formation of functional syncytia with some evidence of differences to the functional outcome (Figure 3-12 B): EHMs

generated from HFFs performed significantly better than either GFBs and CFB EHMs, while there was no difference in EHMs containing GFBs and CFBs (FOC at 4 mmol/L [Ca^{2+}]: HFF 1.01±0.06; GFB 0.67±0.04; CFB 0.61±0.04; n=58/31/59; Figure 3-12 B). The analysis of CSA revealed that EHM with CFBs were thicker compared to EHM containing HFFs and GFBs (CSA in mm^2: HFF 0.7±0.03; GFB 0.7±0.04; CFB 1.2±0.07; n=46/20/39; Figure 3-12 C).

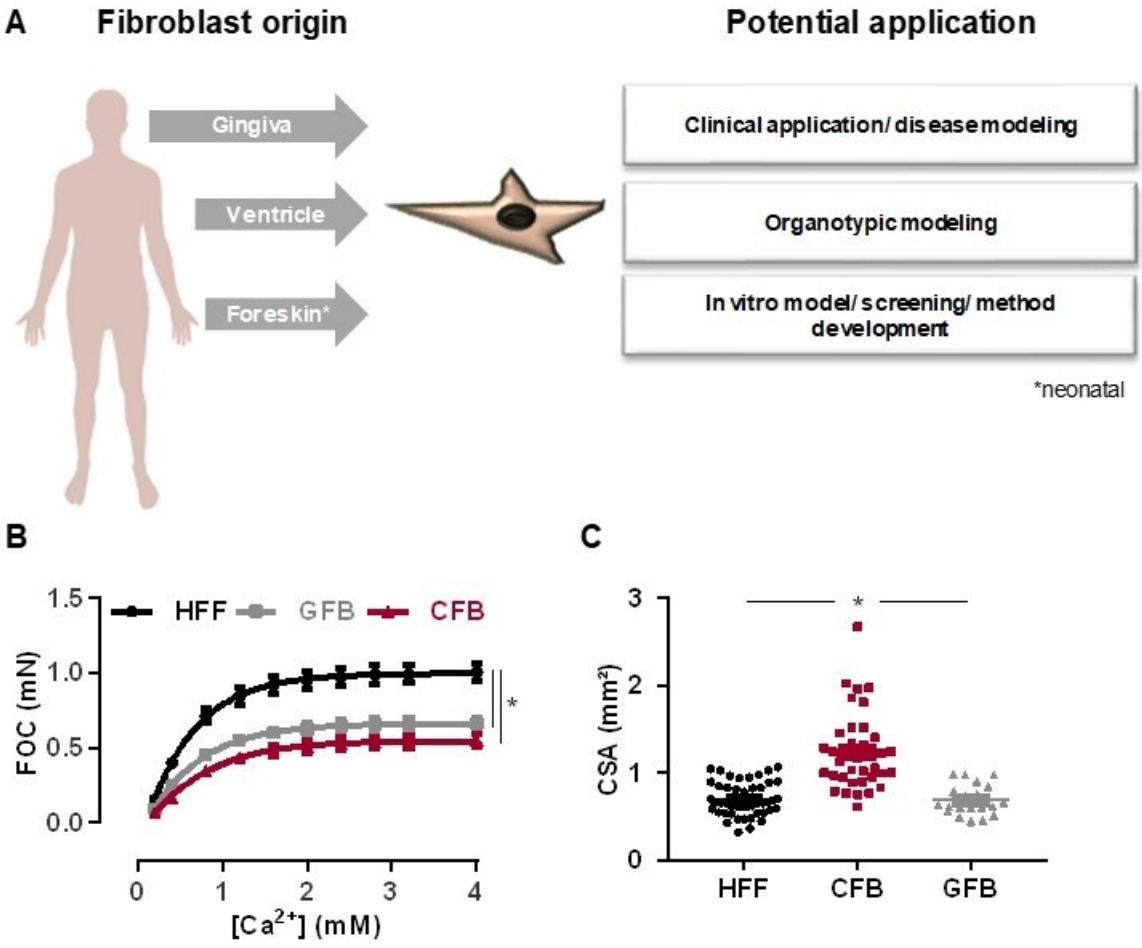

Figure 3-12 Fibroblast origin affects EHM function and appearance

A Origin of primary fibroblasts used in this study and their potential application. Patient-specific gingiva fibroblasts could be obtained from biopsies. Ventricular cardiac fibroblasts (CFBs) (Lonza) from healthy patients can be used for organotypic modeling. HFF provide a large, homogenous cell population which is ideal for method development and screening purposes. **B** EHM were generated from fibroblasts of different origin and compared after 4 weeks of culture. Pooled data from EHM with HFF, CFB, or GFB. FOC at increasing extracellular calcium (0.2-4 mmol/L) was compared. *p<0.05 by 2-way ANOVA and Tukey´s multiple comparisons *post hoc* test (n=58/31/59). **C** CSA in EHM with HFF, CFB, or GFB. *p<0.05 by 1-way ANOVA followed by Tukey´s multiple comparisons *post hoc* test (n=46/20/39).

To assess the variability between fibroblasts from the same source, we compared EHM constructed with CFB from 3 different individuals. CFB1 performed consistently poorer than all other groups (FOC at 4 mmol/L [Ca^{2+}] in mN: HFF 1.0±0.07; CFB1 0.43±0.05;

CFB2 0.78±0.08; CFB3 0.59±0.08; n=45/24/15/8; Figure 3-13 A). Morphologically, all CFB EHMs were significantly enlarged in CSA compared to HFF controls (CSA in mm^2: HFF 0.7±0.03; CFB1 1.4±0.1; CFB2 1.1±0.1; CFB3 1.1±0.1; n=42/20/10/9), without obvious difference between individual CFB EHMs, indicating small patient-specific, but larger cell source-specific variances in EHM phenotype (Figure 3-13 B; compare also Figure 3-29 for EHM with GFB from 4 different individuals).

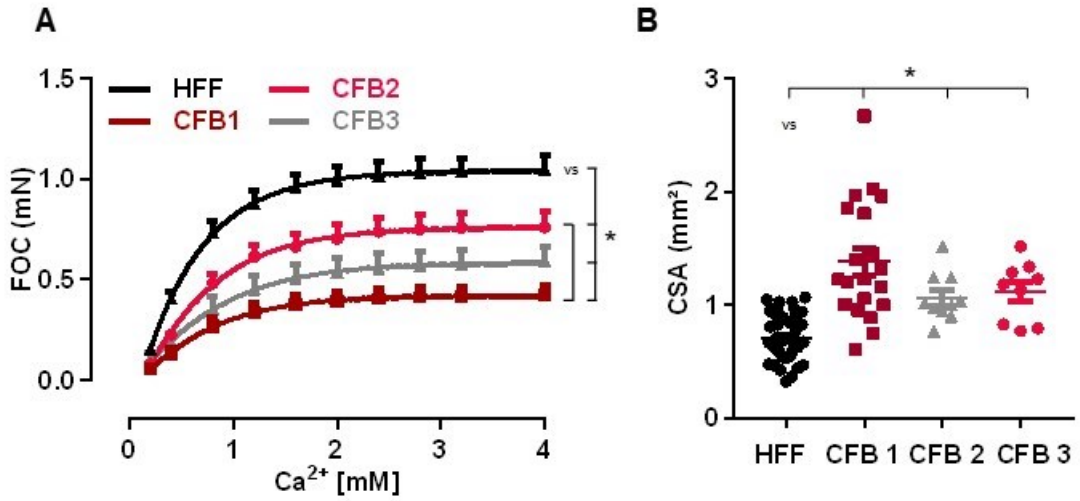

Figure 3-13 Low patient-dependent variability of EHM function and morphology

A Isometric force analysis of EHM containing fibroblasts from different sources (HFF, CFB from 3 different individuals) after 4 weeks of culture; n=45/24/15/8 (HFF/CFB1-3). FOC at increasing extracellular calcium (0.2-4 mmol/L) was compared. *p<0.05 by 2-way ANOVA with Tukey multiple comparison *post hoc* test. **B** CSA in EHM with HFF and CFB from 3 different individuals n=42/20/10/9 (HFF/CFB1-3). *p<0.05 by 1-way ANOVA followed by Tukey´s multiple comparisons *post hoc* test.

3.1.4.1 EHM of cardiac fibroblasts from one patient represent a pathological phenotype

In subsequent experiments, we analyzed CFB1 EHMs in more detail, as they likely represented a pathological phenotype. We evaluated the EC50 for [Ca^{2+}] of tissues which was increased in CFB1 EHMs, indicating lower calcium sensitivity (in mmol/L: HFF 0.5±0.03; CFB1 0.6±0.04; n=19/11) (Figure 3-14 A). All EHMs responded to a similar extent to adrenergic stimulation with the receptor agonist isoproterenol (1µmol/L) (at EC50 and 1.5 Hz, FOC increase in %: HFF 94±18; CFB1 85±15; n=20/12) (Figure 3-14 B).

Subsequently, we enzymatically digested EHMs. When evaluating the resulting cellular content of HFF vs CFB1s we observed that, while the CM content was unchanged between groups (α-actinin$^+$ cells) (Myocyte count x 10^5: HFF 2.1±0.52; CFB1 2.4±0.24; n=6/group)

CFB1 EHMs yielded higher non-myocyte cell counts (non-myocyte count x 10^5: HFF 6.4±0.4; CFB1 8.3±1.4, n=6/group) (Figure 3-14 C), concurrent with the significant increase in CSA (Figure 3-13 B). Finally, the analysis of EHM responses to strain revealed no significant differences between groups (Figure 3-14 D), indicating no major difference in matrix stiffness.

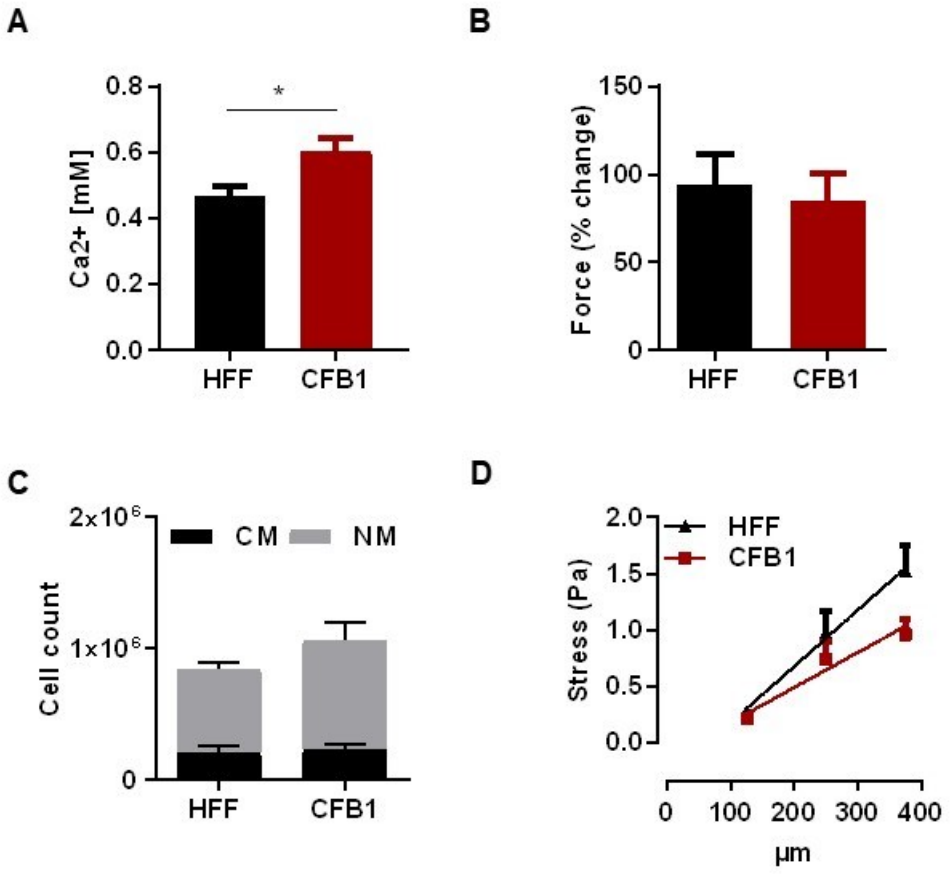

Figure 3-14 Cardiac fibroblast EHM are distinct in cellular composition

4-week-old HFF EHM vs CFB1 (n=20/12). **A** EC50 for [Ca^{2+}] and **B** % increase in FOC at EC50 to 1 µmol/L isoproterenol. 3 independent experiments. A and B *p<0.05 by unpaired t-test. n=19/11 **C** Cellular content of EHMs. n=6/6 in 2 independent experiments. **D** Stress (Force per CSA of tissue) vs strain response in different tissues. n=12/8. 2 independent experiments.

Further analysis of cryosections revealed clear differences in α-actinin abundance and spatial organization (Figure 3-15) between the groups, which was concurrent with the developed forces of these EHMs (Figure 3-13 A). Wheat germ agglutinin (WGA) staining of sialic acid and N-acetyl glucosamine indicated a more diffuse ECM network in CFB1 tissue when compared to HFF controls (Figure 3-15).

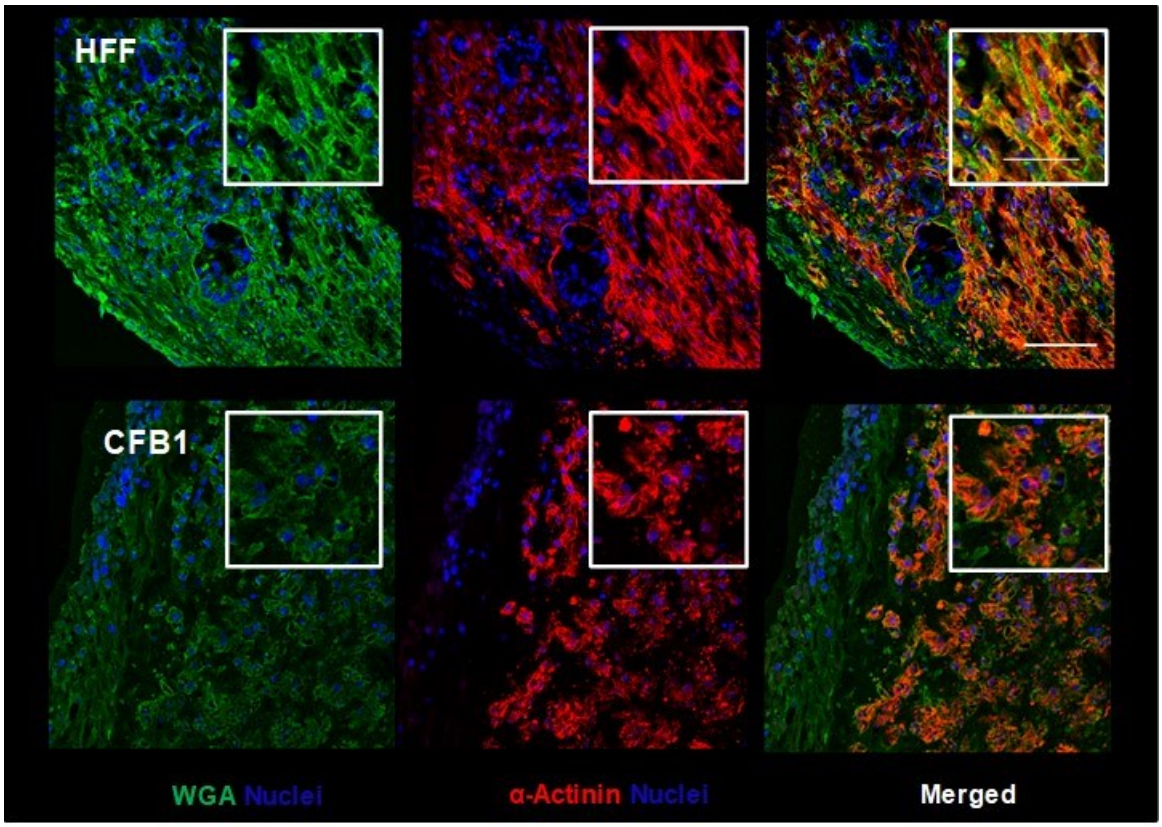

Figure 3-15 Cardiomyocyte alignment and sarcomeric abundance in EHM of fibroblasts from different origin

Representative cryosections of HFF vs CFB1 EHM. Immunostaining for α-actinin (red), wheat germ agglutinin (WGA) (red) and nuclei (blue). Scale bar 100 µm and 50 µm in magnified view. Scales apply for all images.

3.1.4.2 Cardiac fibroblasts transcriptome reveals cardiac origin and myofibroblast characteristics

We analyzed CFB1-specific gene expression and found that transcription factors GATA4 and TCF21 were highly expressed in CFB1 cells compared to HFF (RPKM in CFB1 vs HFF GATA4 10±0.3 vs 0.01±0.01; TCF21 7.7±0.1 vs 0.3±0.01; n=3): GATA4 is of high importance in mammalian embryonic heart development and TCF21 is known as a marker of cardiac fibroblasts. Thereby the expression of both markers in CFB1 compared to HFF confirmed the cardiac origin of these cells. Furthermore, CFB1 expressed higher levels of periostin and CTGF when compared to HFF (RPKM in CFB1 vs HFF: POSTN 1376±53 vs 3±0.2 and CTGF 868±1 vs 141±4; n=3/group) (Figure 3-16 B), indicating a myofibroblast phenotype of CFB1 cells. In contrast, THY1 was highly expressed in HFFs vs CFB1 (RPKM in CFB1 vs HFF: 72±9 vs 3±0.3; n=3/group), which was in line with subsequent live FC analysis of CD90 (THY1) expression (n=1/group) (Figure 3-16 C and D).

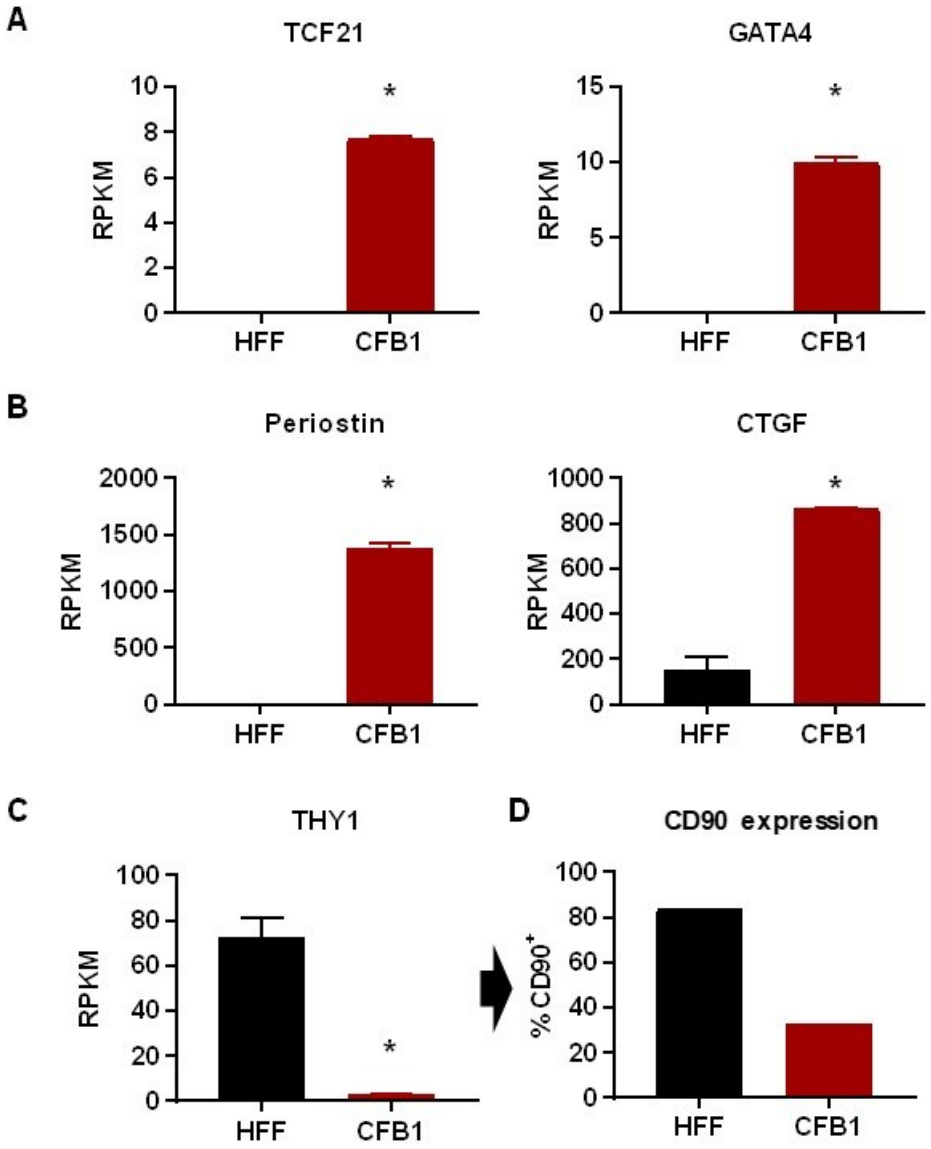

Figure 3-16 CFB1-specific genes reflect cardiac origin and a myofibroblast phenotype

Selected, highly expressed, CFB1-specific genes that represent **A** cardiac transcription factors and **B** ECM genes. **C** THY1 expression in HFF vs CFB1 cells. *$p<0.05$ by unpaired t-test comparing HFF vs CFB1. n=3/group. These data were published in (Tiburcy et al., 2017). **D** Live FC analysis of $CD90^+$ cell populations in HFF and CFB1 cultures. n=1/group.

In conclusion, we could demonstrate that all fibroblasts were able to constitute functional EHM, however the cues provided by HFF appeared more optimal as to functional and structural outcome as compared to GFBs and CFBs (Figure 3-12).

In-depth analysis of EHM morphology and functionality indicated that CFB1 EHM could represent a pathological phenotype (Figure 3-13 and Figure 3-14). In agreement with the functional data we obtained previously, we confirmed the cardiac origin of CFB1 cells on

transcriptome level and found that CFB1 cells represent a myofibroblast phenotype. Collectively, these findings all indicated that in CFB1 EHM, fibroblast-specific signaling mechanisms to guide proper alignment and development of CMs was impaired. We thus investigated this phenotype further.

3.2 Fibroblast-cardiomyocyte crosstalk in EHM

3.2.1 Excessive deposition of hyaluronan leads to EHM dysfunction

The analysis of morphology, histology, and contractile function of CFB1 EHM indicated that these fibroblasts were suboptimal to support EHM formation and maturation compared to HFF (Figure 3-13 A). The apparent "swelling" of ECM in CFB1 EHM, as evidenced by a larger CSA (Figure 3-13 B), led us to hypothesize that excessive H_2O may have been retained in the ECM, interfering with EHM development and contractile function. Analysis of ECM distribution by WGA staining (Figure 3-15) suggested an involvement of hyaluronic acid (HA) (Figure 3-17). This large molecular mass glycosaminoglycan is attached exclusively via non-covalent interactions with other proteins of the ECM (Rienks et al., 2014), sequesters water and thereby confers structure and stability to tissues.

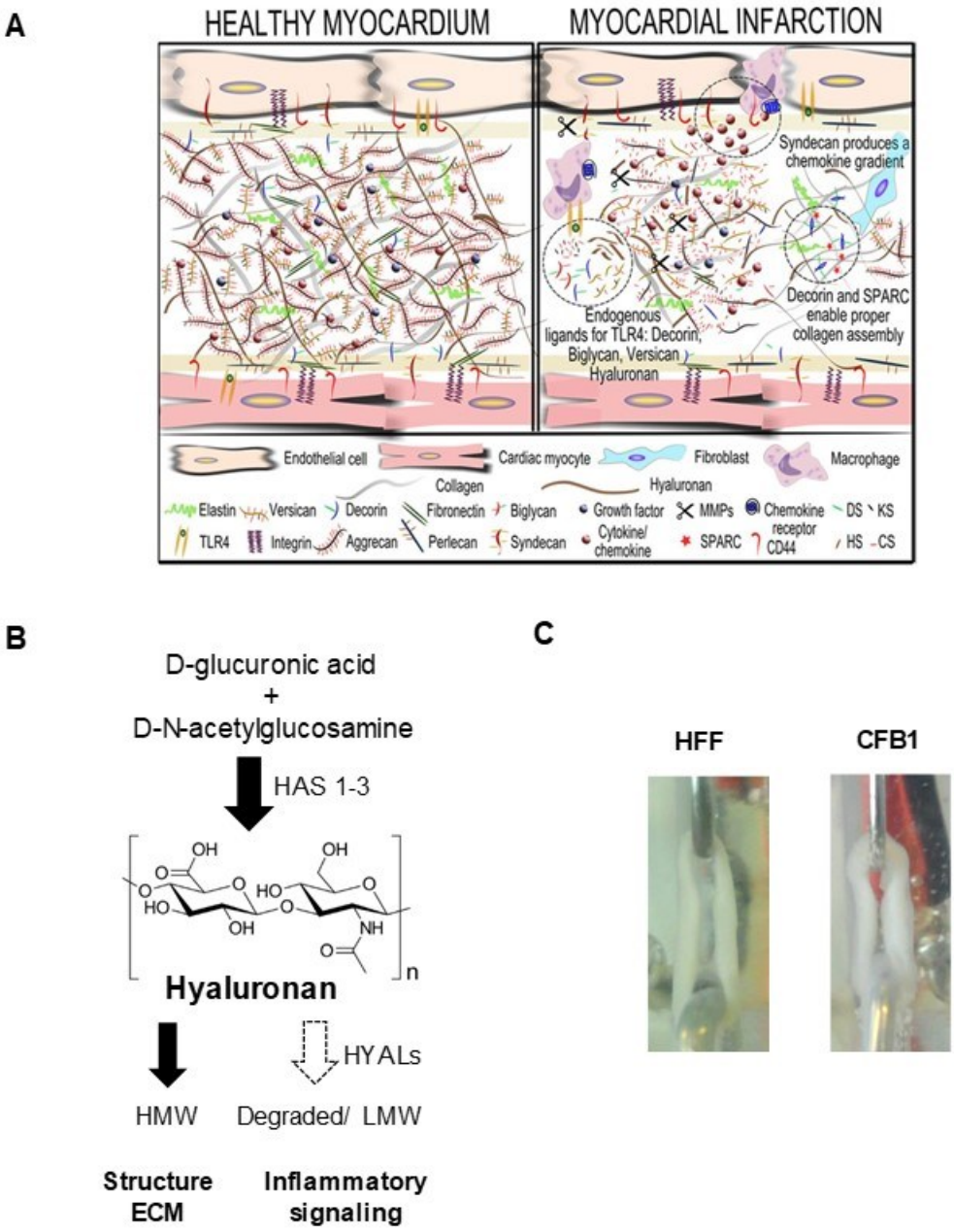

Figure 3-17 The role of hyaluronan and its chemical structure

A Schematic overview of HA in ECM (Rienks et al., 2014). **B** The chemical structure of HA allows for the large H_2O-binding capacity of HA polymers. HA is constituted of repeating disaccharide molecules of D-glucuronic acid and D-N-acetylglucosamine, bound via alternating ß-1,4 and ß-1,3 glycosidic bonds (graphic taken from (Rienks et al., 2014)). HA is synthesized by hyaluronan synthases (HAS) 1-3. Hyaluronidase enzymes degrade HA by cutting the enzymatic bond. High and low molecular weight (HMW and LMW) HA play distinctive biological roles. **C** Representative images of HFF EHM vs CFB1 EHM.

Excessive HA deposition is found in fibrosis and associated with contractile pathophysiologies of the heart (Chowdhury et al., 2013, 2017; Hellström, 2007; Waldenström et al., 1991). Thus, based on our earlier findings that the HA biosynthesis system is regulated during early consolidation of tissues, we hypothesized that HA is a key mediator of EHM development and hence function.

The HA content of the ECM is determined by HA synthesis and degradation. HA is synthesized by the HASs. We thus first investigated the abundance of transcripts encoding for HAS enzymes in the different fibroblasts (Figure 3-18 B). HAS1-3 have distinct spatiotemporal expression patterns during development (Tien and Spicer, 2005) and HAS2, the predominant synthase in human, plays an important role in the heart. Its knockout results in failure of cardiac cushion formation (Camenisch et al., 2001). Indeed, while there was no difference in HAS1 expression (in RPKM: HFF 0.02±0.14; CFB1 0.02±0.14; CMs 0.12±0.04; n=3/group), HAS2 transcript abundance was markedly higher in CFB1 cells and CFB1 also expressed significantly more HAS3 than other cell types (HAS2 in RPKM: HFF 5.3±2.4; CFB1 27.8±0.3; CM 3.9±1; and HAS3 in RPKM: HFF 0.3±0.08; CFB1 10.1±0.2; CM 0.4±0.1; n=3/group).

While HA is synthesized by the HAS enzymes, homeostasis is achieved via its controlled degradation by hyaluronidases (HYALs). For instance, a lack of HYAL2 leads to congenital heart defects and heart failure (Chowdhury et al., 2017). We could not detect any differences in transcript abundance in the two investigated fibroblast entities (Figure 3-18 C) (HYAL1 in RPKM in: HFF 0.6±0.2; CFB1 0.3±0.1; CM 4.2±1.6; HYAL2 in RPKM in: HFF 10.0±0.3; CFB1 11.2±0.2; CM 6±0.9; HYAL3 in RPKM: HFF 2±0.01; CFB1 2.5±0.4; CM 1.4±0.02 and HYAL4 in RPKM all fibroblasts 0; CM 0.1±0.02; n=3/group). Of note, HYAL expression was generally lower in CMs compared to fibroblasts.

Furthermore, ECM components that bind HA were evaluated (Figure 3-18 D): Versican (VCAN) transcript abundance was significantly higher in CFB1 compared to HFF (VCAN in RPKM in: HFF 2.4±0.07; CFB1 355±1; CM 92±10; n=3/group). VCAN and HA functionally cooperate in the ECM. In $VCAN^{-/-}$ mice, HA can be detected but is highly disorganized which results in septal and cushion defects resembling the $HAS2^{-/-}$ phenotype. (Hatano et al., 2012). In contrast, aggrecan RPKM values were lower than 1 in all cell types and thereby excluded from analysis, indicating that aggrecan expression in 2D cells is generally very low.

The presence of HA-mediated motility receptor (HMMR) is crucial for HA-mediated EMT in development (Missinato et al., 2015). We found HMMR transcript significantly upregulated in CFB1 cells (HMMR in RPKM in: HFF 37±13; CFB1 178±5; CM 11±3; n=3/group). In contrast, the HA receptor CD44 which is also required for HA degradation by HYAL1 and HYAL2 (Harada and Takahashi, 2007), was downregulated in CFB1 cells

(CD44 in RPKM: HFF 454±110; CFB1 97±3; CM 1.4±0.1; n=3/group) (Figure 3-18 D). Of note, CD44 levels were significantly lower in CMs compared to both fibroblast species.

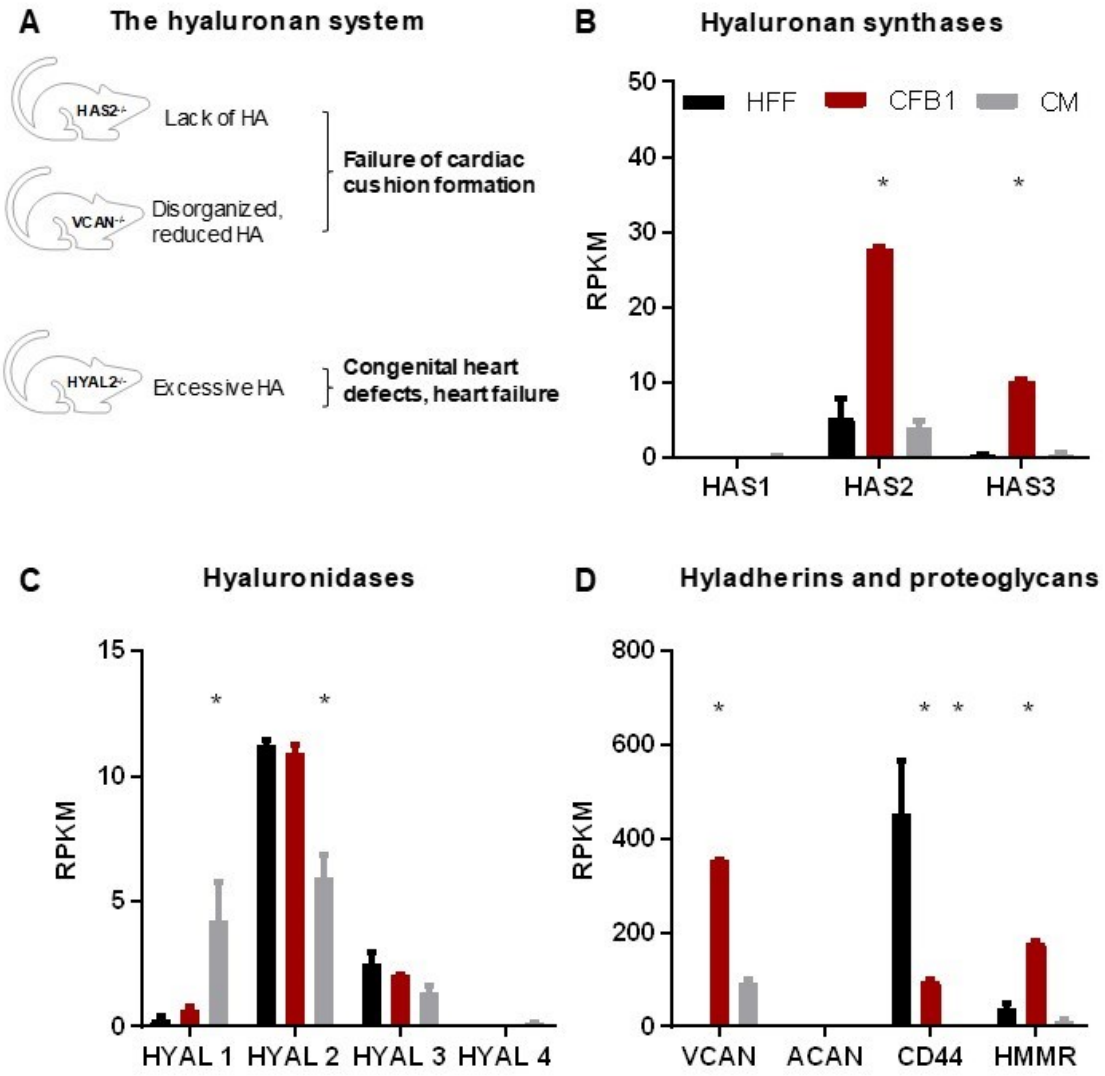

Figure 3-18 Expression of genes involved in hyaluronan metabolism in HFF and CFB1

A Hyaluronan (HA) in the heart. Selected phenotypes of knockout mice for hyaluronan synthase 2 (HAS2; HA biosynthesis), versican (VCAN; HA binding in ECM) and hyaluronidase 2 (HYAL2; HA degradation) emphasize the importance of a controlled HA content in the myocardial ECM for proper myocardial development and homeostasis (References, see main text). Gene expression in HFF, CFB1 and HES2-derived CMs **B** of HAS enzymes. **C** Transcript abundance for the HA degrading enzymes HYAL 1-4. **D** Expression of HA-binding components of the ECM: VCAN and aggrecan (ACAN) are proteoglycans whereas CD44 and HA-mediated motility receptor (HMMR) are hyaladherins. *p<0.05 by 2-way ANOVA with Dunnett's multiple comparisons *post hoc* test vs HFF control). n=3/group.

From these findings, we hypothesized that an increased expression of HAS enzymes (in particular of HAS2) combined with lower expression of CD44 and thus low HYAL activity may result in excessive HA deposition in the ECM of CFB1 EHM. This could be responsible for the pathological phenotype we observed in CFB1 EHMs.

We validated HAS2 expression with qRT-PCR (Figure 3-19), which indicated higher HAS2 expression in CFB1 vs HFF cells (mRNA levels compared to S18 control mRNA: HFF vs CFB1: 0.4±0.3 vs 5.0±1.2; n=3/group). However, the difference was not significant.

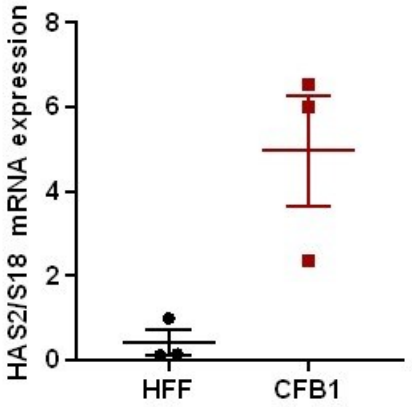

Figure 3-19 Validation of RNAseq data for HAS2 with qRT-PCR

Expression of HAS2 mRNA normalized to ribosomal S18 mRNA in HFF and CFB1 cells grown in 2D. n=3/group. Statistical analysis using unpaired t-test with Welch correction between HFF and CFB1. RT reaction and qRT-PCR carried out by Petra Rompel, lab of Prof. Jens Fischer, Department of Pharmacology, Düsseldorf.

To test if the HA content affects EHM function, we aimed to restore the optimal HA content in CFB1 EHM by treatment with increasing concentrations of hyaluronidase (HYAL). Interestingly, HYAL treatment boosted CFB1 EHM function in a concentration dependent manner (Figure 3-20 B). At higher HYAL concentrations, a detrimental effect on functionality was observed (relative increase compared to CFB1 control at 4 mmol/L $[Ca^{2+}]$: Control: 0.96±0.2; 0.015 U/ml 0.9±0.3; 0.15 U/ml 1.8±0.2; 1.5 U/ml 3.4±0.7; 15 U/ml 1.1; 150 U/ml 0.4; n=11/3/4/4/1/1) (Figure 3-20 B). HYAL treatment also reduced CSA to levels comparable to HFF EHMs (CSA in mm^2: Control: 2±0.1; 0.015U/ml: 1.1±0.1; 0.15 U/ml: 0.8±0.1; 1.5 U/ml: 0.8±0.1; 15U/ml 1; 150 U/ml 0.6; n=12/3/4/3/1/1) (Figure 3-20 C).

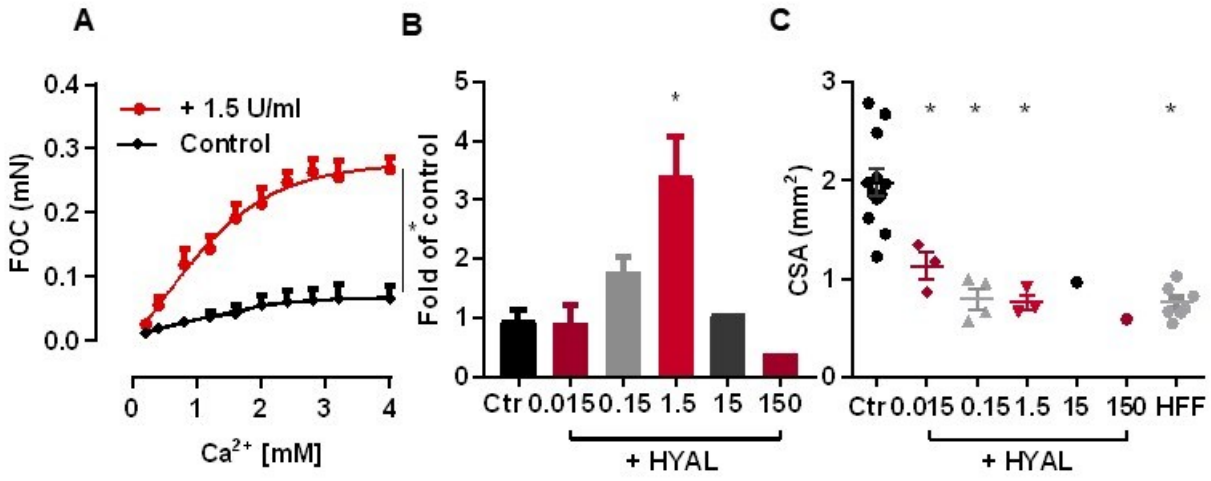

Figure 3-20 CFB1 EHM function can be enhanced by hyaluronidase (HYAL) treatment

A FOC of control and CFB1 EHM treated with 1.5 U/ml HYAL for 4 weeks, n=4/3 (Control/treated). **B** FOC normalized to average of respective control CFB EHM. n= 11/3/4/4/1/1. *p<0.05 by 1-way ANOVA followed by Dunnett´s multiple comparisons *post hoc* test comparing treated EHM to untreated controls. **C** CSA of HFF vs CFB1 EHM. n=12/3/4/3/1/1. *p<0.05 by 1-way ANOVA followed by Dunnett´s multiple comparisons *post hoc* test comparing treated EHM to untreated controls. B-C, data of 2 independent experiments.

Immunostaining of CFB1 EHMs treated with HYAL revealed that sarcomeric organization and CM alignment were improved compared to controls (Figure 3-21), which is in line with the observed enhancement in contractile performance in these tissues (Figure 3-20). Our findings indicate that excessive HA in CFB1 EHM contributes to the observed phenotype.

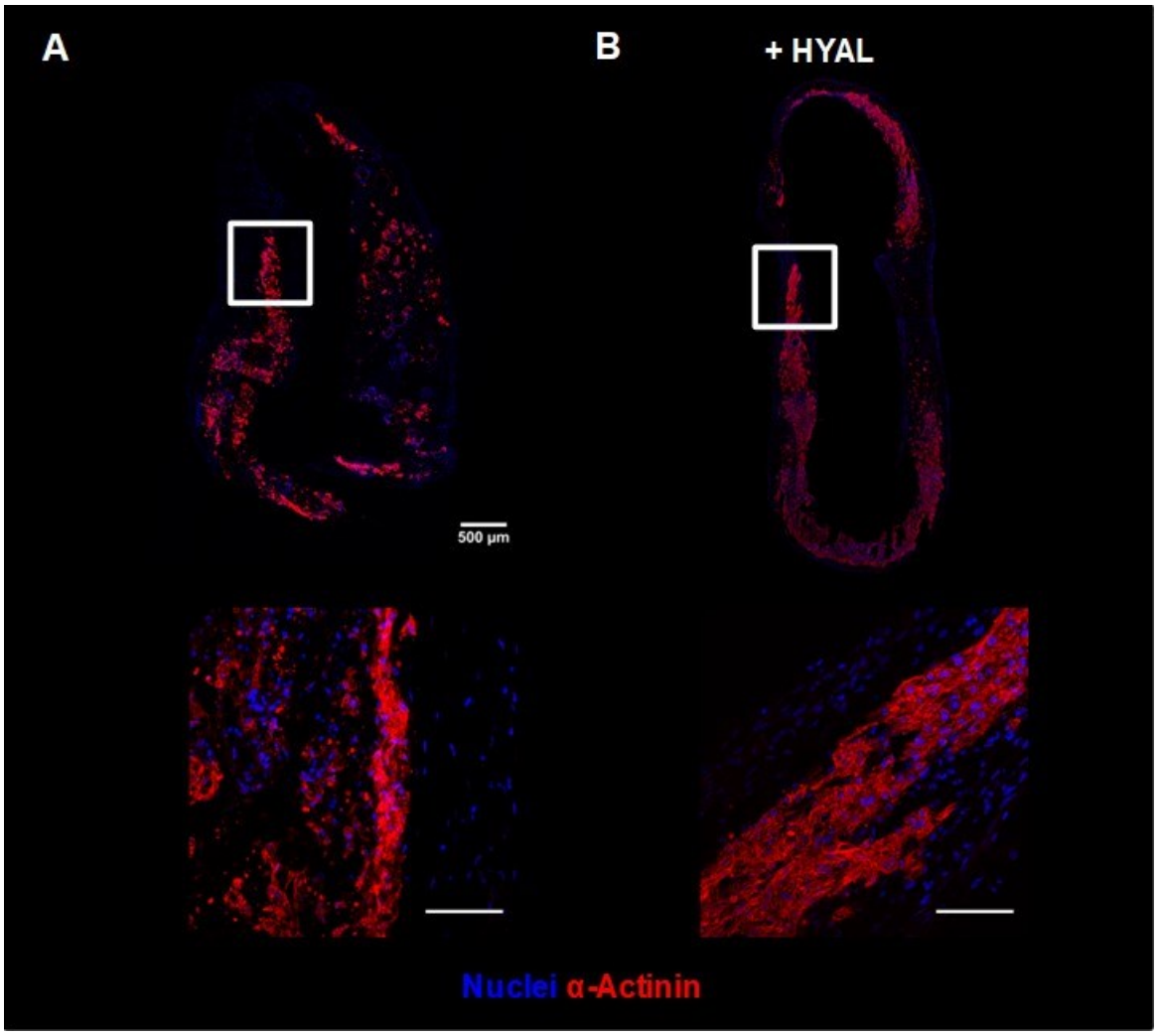

Figure 3-21 Hyaluronidase treatment improves CM morphology and alignment

Cross sections of **A** untreated CFB1 EHM and **B** HYAL (0.15 U/ml) treated CFB1 EHMs stained for sarcomeric actinin (red) and with Hoechst (blue nuclei). Scale bars: 500 µm and 100 µm in magnified views.

Of note, when comparing HFF, GFB1 and CFB1 EHM cellular content (Figure 3-14), we observed that the non-myocyte content in CFB1 EHMs seemed increased when compared to HFF EHMs. We thus further hypothesized, that, proliferative behavior may somehow contribute to the phenotype development.

To test this, we irradiated CFB1 EHM with 30 Gy at day 3 and measured FOC and CSA after 4 weeks (Figure 3-22 A). Interestingly, irradiation improved the contractile function of CFB1 EHM (FOC at 4 mmol/L $[Ca^{2+}]$ in mN: Control: 0.07±0.02 vs irradiated 0.2±0.04). As expected, irradiation reduced cell numbers in treated EHMs, although this effect was not significant (Figure 3-22 C), concurrent with a reduction in CSA (CSA in mm^2: Control 2.2±0.3 vs Irradiated 1.2±0.1; n = 4/group) (Figure 3-22 B and D).

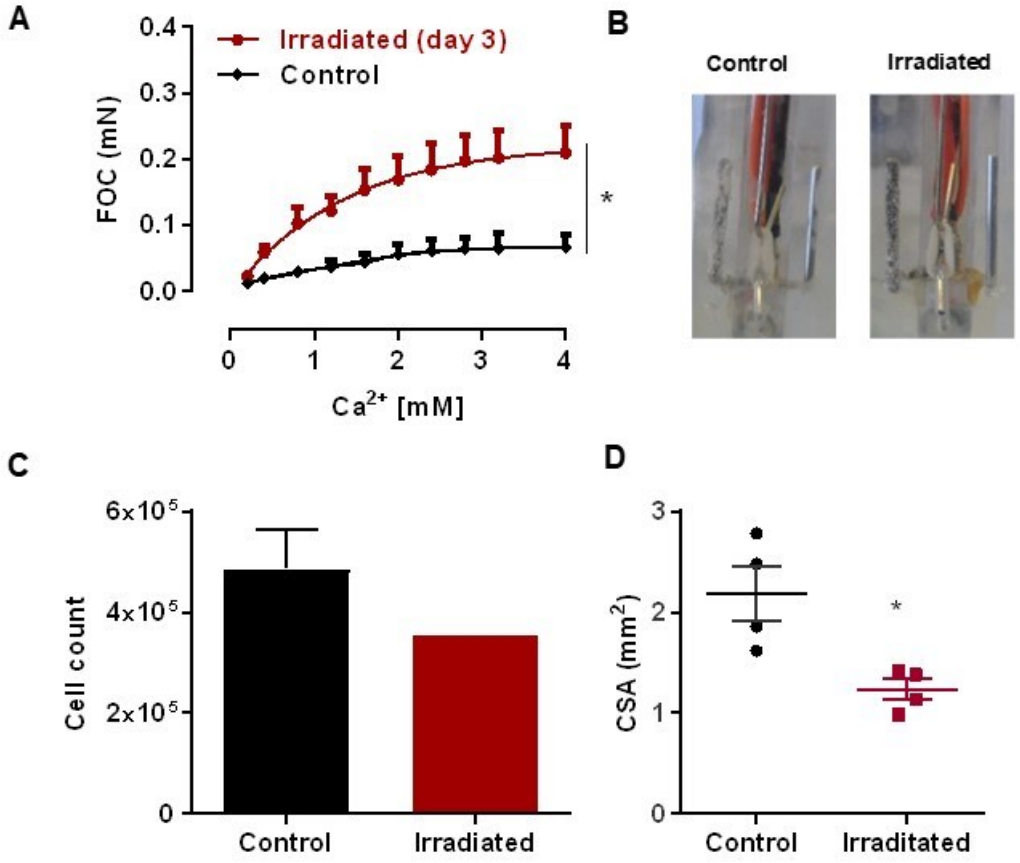

Figure 3-22 The HA phenotype can be modulated by anti-proliferative treatment

A CFB EHM were irradiated with 30 Gy on day 3 of culture before transfer to stretchers. Forces of contraction were assessed after 4 weeks of culture. *p<0.05 by 2-way ANOVA followed by Sidak´s multiple comparisons *post hoc* test. n=4/4 **B** EHM morphology at 4 weeks. **C** Cell count after enzymatic digestion of EHM (n=3 for controls, n=2 for irradiated group). **D** CSA analysis of CFB EHM without and with irradiation. n=4/4. *p<0.05 by unpaired t-test.

Taken together, both HYAL treatment and irradiation to abolish proliferative capacity in CFB1 EHM improved CFB1 EHM function, suggesting that HA content in CFB1 EHM and proliferation of non-myocytes in these tissues are collectively involved in the development of the observed pathophysiological phenotype (contractile failure and EHM swelling).

In order to validate our findings and gain insight into the underlying mechanisms, we generated HFFs overexpressing HAS2 by transduction with a lentiviral overexpression construct (kindly provided by the lab of Prof. Jens Fischer in Düsseldorf) (Figure 3-23). We generated virus particles by transfection of TSA cells with packaging plasmids and our plasmid of interest with the HAS2 insert (and without as control). Virus production was

confirmed using LentiGo sticks from Takara. After selection, we validated that HAS2 expression was increased in cells with the HAS2-constructs compared to control constructs with cells from the second transduced colony (HAS2-2) expressing the highest levels of HAS2 (mRNA HAS2/S18 ribosomal mRNA expression: Control 1 0.9±0.2; Control 2 1.1±0.07; HAS2-1 389±39; HAS2-2 830±51; n=3/group) (Figure 3-23 B). Concurrent with these findings, the secretion of HA was highest in HAS2-2 cells > HAS2-1 > control 1 +2 (HA secretion in ng/10^5 cells in 48 h: Control 1 116±19; control 2 142±13; HAS2-1 327±38; Has2-2 447±48; n=3/group) (Figure 3-23 C).

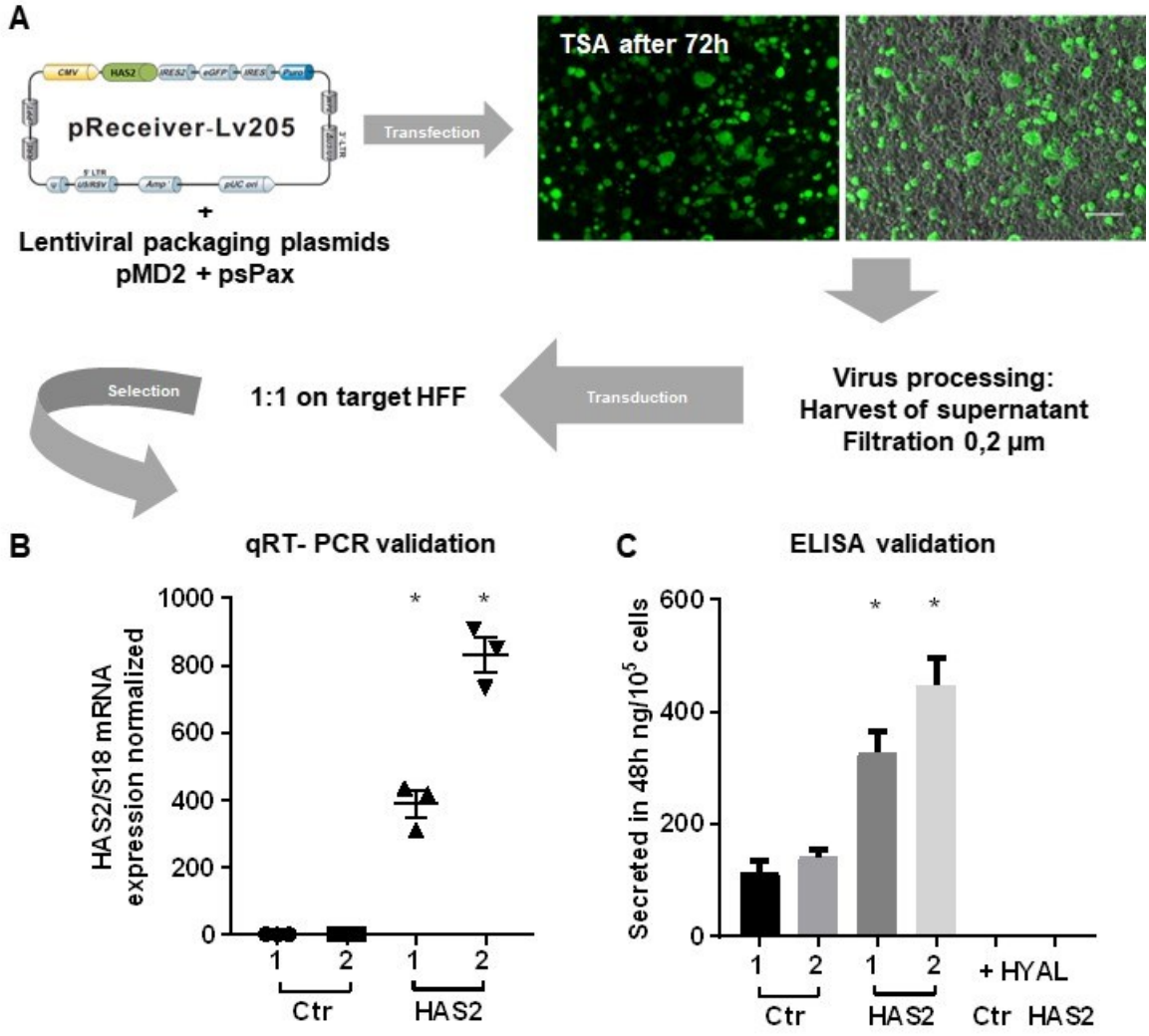

Figure 3-23 Generation of stable HAS2-overexpressing fibroblasts

A Construct and transduction protocol. TSA cells were transfected with target plasmid containing HAS2 (or no ORF for controls) and 2 lentiviral packaging plasmids. Virus was then used to generate HFF with a stable overexpression of HAS2 **B** Validation of HAS2 overexpression by qRT-PCR. n=3/group. *p<0.05 by 1-way ANOVA with Dunnetts´s multiple comparisons *post hoc* test of treatments vs control 1 and control 2, *p<0.05). **C** HA secretion quantified by ELISA. n=3/group. *p<0.05 by 1-way ANOVA with Dunnetts´s multiple comparisons *post hoc* test of overexpression and HYAL treatments vs control 1 and 2, *p<0.05). qRT-PCR was

carried out in cooperation with Prof. Jens Fischer (Department of Pharmacology, Duesseldorf) and carried out by Petra Rompel.

After confirming the overexpression of HAS2 in 2D, we generated EHM from these cells and assessed HA secretion and functionality, as well as morphology, after 4 weeks of culture (Figure 3-24). EHM with HAS2-1 HFFs secreted around three times as much HA in 48 h as control EHMs (HA secretion in ng/EHM in 48 h: Control 1 456±44; control 2 482±54; HAS2-1 1442±18; n=3/group). However, when assessing forces, HAS2-overexpressing EHM did not perform differently from respective controls (Figure 3-24 B). HAS2 overexpressing EHM treated with 1.5 U/ml HYAL developed even lower FOC than control groups (FOC in mN at 4 mmol/L: Control 1 0.9±0.17; control 2 1.0±0.1; HAS2-1 0.89±0.2; HAS2-1 + HYAL 0.6±0.1, n=4/4/3/3), although this was not significant. Morphologically, no difference between groups in CSA and total cell output following enzymatic digestion could be detected (CSA in mm^2: Control 1 1.2±0.16; control 2 1.5±0.15; HAS2-1 1.2±0.14; HAS2-1 + HYAL 1.1±0.07; n=4/4/3/3) (Cell output x 10^5: Control 1 6.7±1.1; control 2 10±0.5; HAS2-1 6.5±2.1; HAS2-1 + HYAL 8.6±2.2; n=4/4/3/3) (Figure 3-24 C, D and E).

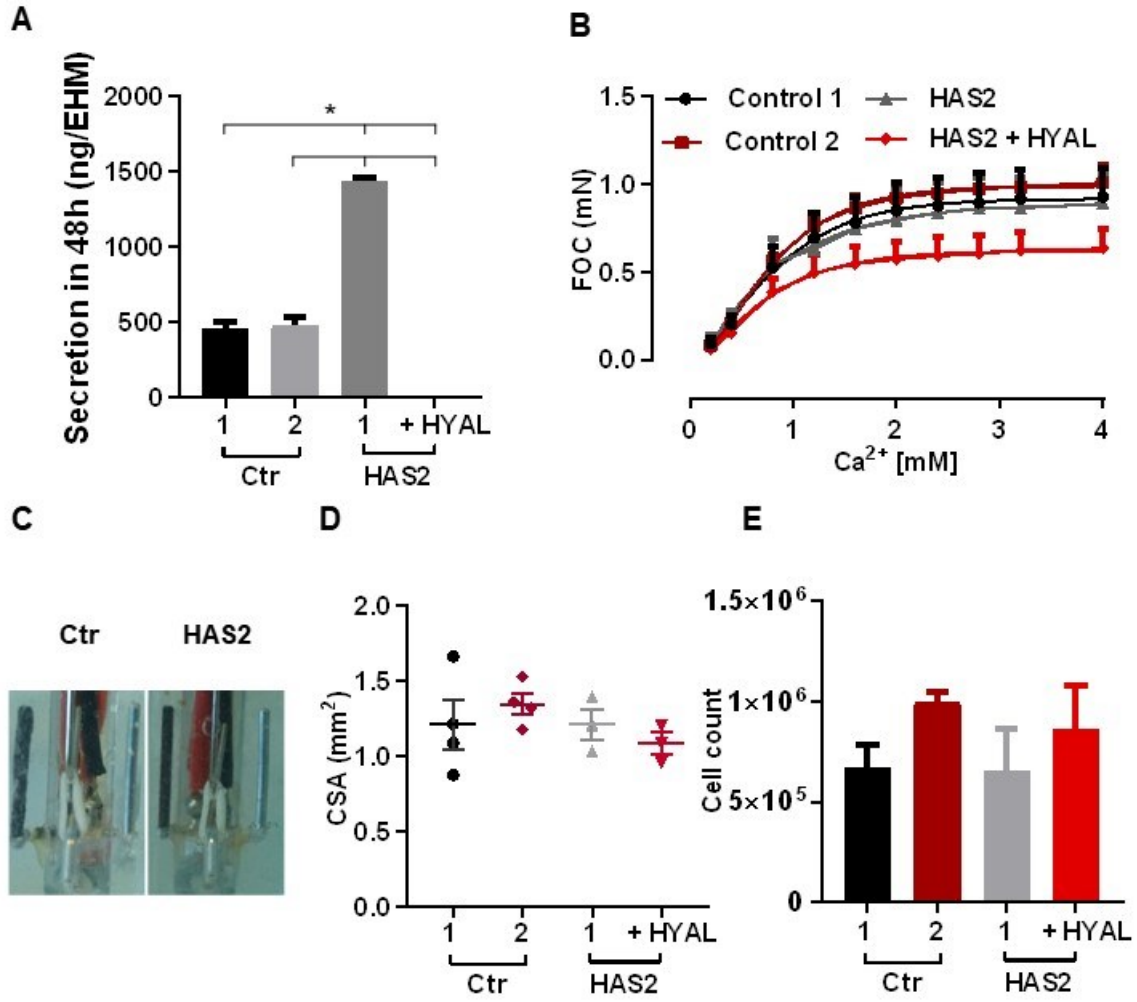

Figure 3-24 Analysis of EHM from HAS2-overexpressing fibroblasts

EHM was generated from cells overexpressing HAS2 and controls **A** ELISA of 48 h supernatants of EHM. *p<0.05 by 1-way ANOVA with Tukey´s multiple comparisons *post hoc* test. n=3/group. **B** Forces of 4-week-old EHM. **C** Representative images of control vector 1 and HAS2 overexpressing HFF EHMs. **D** CSA of 4-week old EHM **E** Cell counts after enzymatic digestion, from 4-week-old EHM after contraction analysis n=4/4/3/3 (Control1/control 2/HAS2-1/HAS2-1 + 1.5 U/ml HYAL).

Contrary to our hypothesis, we did not observe a pathological phenotype (reduced FOC and swelling as in CFB1 EHM) upon application of HAS2-overexpressing HFFs (Figure 3-24 B and D), suggesting fundamental differences in the HFF and CFB1 entities.

3.2.2 Dilated cardiomyopathy fibroblasts in EHM

IPS-derived CMs have been utilized to recapitulate DCM, HCM and long QT syndrome phenotypes *in vitro* (Karakikes et al., 2015; Sun et al., 2012). Collectively, however, these models have so far neglected the role of other cell types and the surrounding 3D environment in cardiac pathologies (Bang et al., 2014; Cartledge et al., 2015; Gaudesius, 2003; Ieda et al., 2009). As the role of cardiac fibroblasts both in development and

pathology of the myocardium is becoming increasingly appreciated, better models that take cellular crosstalk into account need to be established. EHM of IPS- derived CMs has recently been used to model DCM with an underlying mutation in RBM20 protein (Streckfuss-Bömeke et al., 2017). However, also the predominant focus of this work was on the DCM-affected CMs which were cocultured with non-organotypic HFFs.

We thus sought to generate a comprehensive DCM-disease model that also involved fibroblasts of affected individuals (Figure 3-25 A). Compared to EHM generated from the CMs of the healthy donor (CTR EHM and DCM CFB EHM), tissues containing DCM-affected CMs (DCM CM EHM and DCM EHM) did not produce any measurable forces (we define FOC< 0.03 mN as background in isometric force measurements) (Figure 3-25 B). Interestingly, there was also a significant decrease in contractile performance when disease-affected cardiac fibroblasts were used (FOC in mN at 4 mmol/L [Ca^{2+}]: CTR 0.9±0.1; DCM CFB 0.3±0.06; DCM CM and DCM <0.1; n=3/3/3/4) (Figure 3-25 B). These data suggest that apart from the obvious dysfunction of disease-affected CMs, CFBs also clearly contribute to the contractile pathophysiology of DCM.

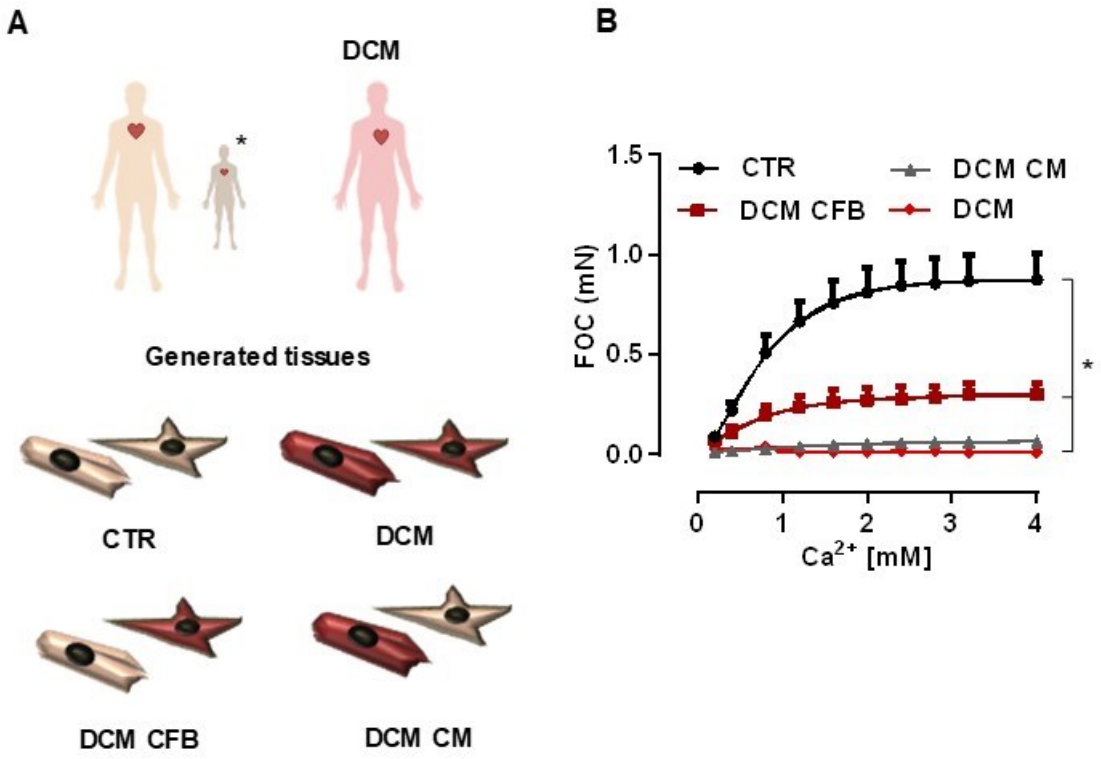

Figure 3-25 Modeling of DCM in EHM: Elucidating fibroblast- and CM-specific effects

A Experimental outline for the modeling of DCM in EHM. Both IPS-derived CMs and CFBs from a DCM-affected individual (red) were obtained and cocultured in EHM with IPS-derived CM of a healthy donor (nude) and CFBs from a healthy individual* (CFB3 obtained from Lonza) (dark nude). **B** FOC of 4-week-old EHMs.

*p<0.05 by 2-way ANOVA with Tukey´s multiple comparisons *post hoc* test. n=3/3/4/4 (CTR; DCM CFB; DCM CM; DCM).

We previously demonstrated the crucial role of fibroblasts in early tissue consolidation, compaction during maturation and the resulting viscoelasticity in 4-week-old EHM. We thus further scrutinized these fibroblast-specific characteristics in our DCM model. We found significant differences in early tissue consolidation between the groups: EHM containing DCM-affected CFBs condensed significantly stronger than those with CFBs of the healthy proband (Gap from mold in mm: CTR 0.4±0.07; DCM CFB 1.0±0.01; DCM CM 0.4±0.03; DCM 1.1±0.05; n=3/3/3/4) (Figure 3-26 A). After 4 weeks, EHM containing DCM-affected CFBs had completely bent the silicone poles they resided on suggesting a myofibroblastic phenotype (Figure 3-26 B). In DCM CM EHM, we observed a partial condensation (Pole distance in mm: CTR 2.4±0.06; DCM CFB 0±0; DCM CM 0.6±0.1; DCM 0±0; n=3/3/3/4). We further evaluated the viscoelasticity of 4-week-old EHMs and found that all EHMs containing DCM-affected cells were significantly stiffer than CTR EHMs (Figure 3-26 D). Between these three groups, however, we could not observe significant differences (slope of the stress vs strain curve: CTR 0.002±0.0005; DCM CFB 0.008±0.002; DCM CM 0.008±0.0001; DCM 0.009±0.001; n=3/3/3/4) (Figure 3-26 C). Collectively, these data suggest a pro-fibrotic profile of DCM-affected CFBs. Interestingly, in combination with CMs of our DCM patient also CFBs from a healthy donor seem to develop a similar phenotype (see DCM CM EHM in Figure 3-26 B), which may result from DCM-affected remnant stroma cells of impure CM preparations (Figure 3-27).

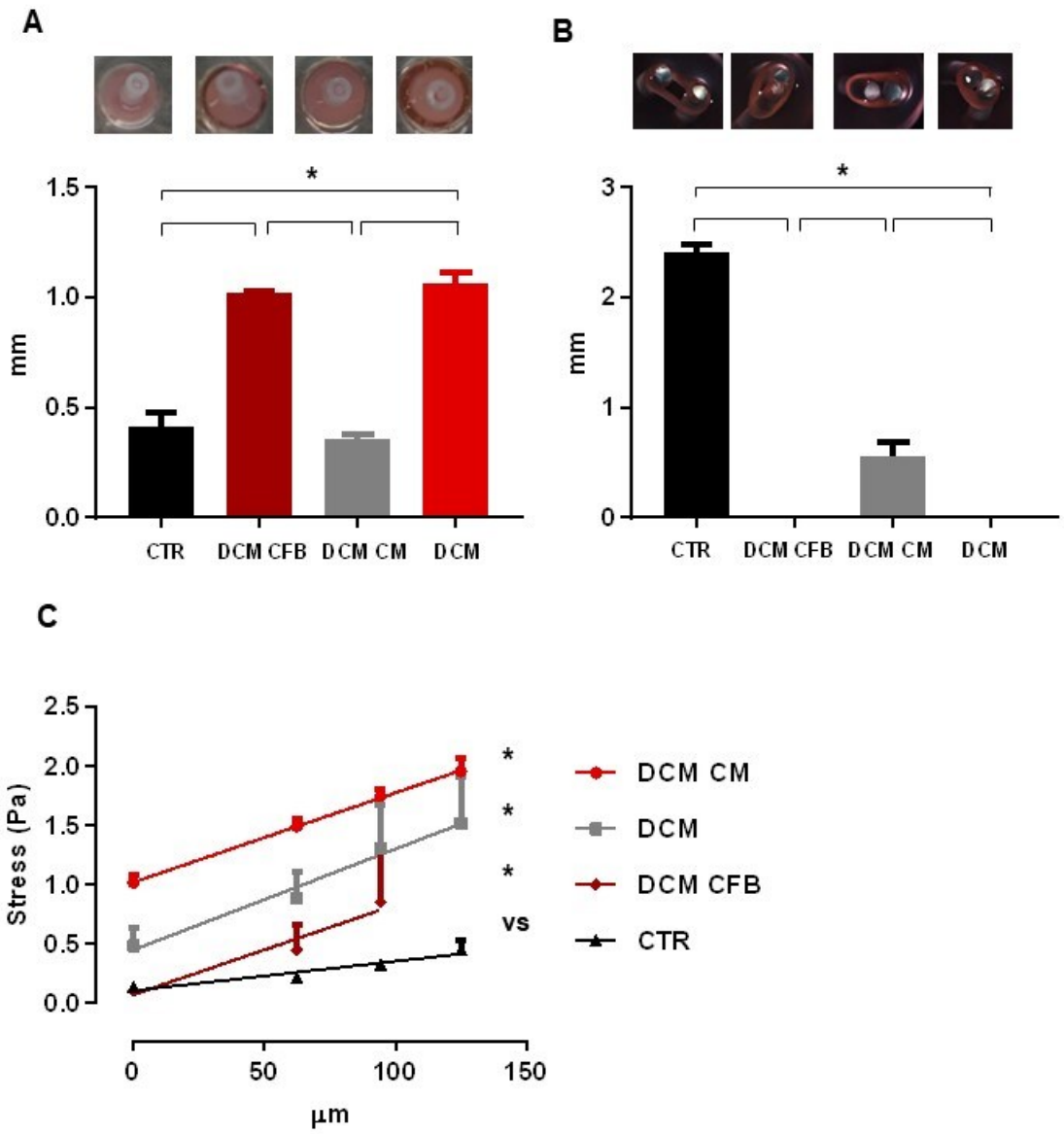

Figure 3-26 Modeling DCM in EHM: Fibroblast-specific characteristics of EHM

A Degree of consolidation of EHMs one hour after casting measured by the gap between mold and consolidated hydrogel in mm. *p<0.05 by 1-way ANOVA with Tukey´s multiple comparisons *post hoc* test. n=3/3/4/4. **B** In 4-week-old EHM we measured the distance of flexible PDMS poles, EHM tissues resided on. *p<0.05 by 1-way ANOVA with Tukey´s multiple comparisons *post hoc* test. n=3/3/4/4. **C** Stress vs strain in EHM. *p<0.05 by 1-way ANOVA and Tukey´s multiple comparisons test of slopes. n=3/3/4/3 for (CTR/DCM CFB/DCM CM/DCM). All slopes of tested groups were significant vs the CTR group but not among each other.

Based on these findings, we further investigated the non-myocyte population of EHMs. For that we analyzed the expression of the myofibroblast marker α-SMA. We detected α-SMA$^+$ cells in all EHMs, yet tissues generated with the CMs of the healthy donor contained significantly less SMA$^+$ cells when compared to EHM of DCM-affected CMs (α-SMA in % of viable output cells: CTR 49±3; DCM CFB 50±2; DCM CM 72±1; DCM 78±4; n=3/3/3/4)

(Figure 3-27 A). Of note, the addition of DCM-affected CFB did not affect SMA$^+$ populations when compared to CTR EHM.

Flow cytometry analyses revealed that concurrent with functional performance, EHM generated from DCM-affected CFBs and CMs contained significantly lower numbers of α-actinin$^+$ cells (CMs) than control EHM (α-actinin in % of viable output cells: CTR 23±2 DCM CFB 14±1 DCM CM 8±0.6 DCM 2±0.3; n=3/3/3/4). Of note, cellular input populations of DCM-affected CMs used to generate these tissues were already lower in α-actinin content at casting (original input for CTR CMs vs DCM CMs 85 vs 69% α actinin$^+$) (Figure 3-27 B). Interestingly, the presence of healthy CFBs in DCM CM EHMs seems to have a beneficial effect on CM retention when compared to DCM EHMs. Collectively, FC and cell content analysis revealed that also the total amount of α-SMA$^+$ cells found in DCM EHM was significantly increased compared to CTR EHMs (α-SMA$^+$ non-myocytes in x 10^5: CTR 1.8±0.2 DCM CFB 1.8±0.4 DCM CM 2.9±0.9 DCM 4.9±1; n=3/3/3/4) (Figure 3-27 C).

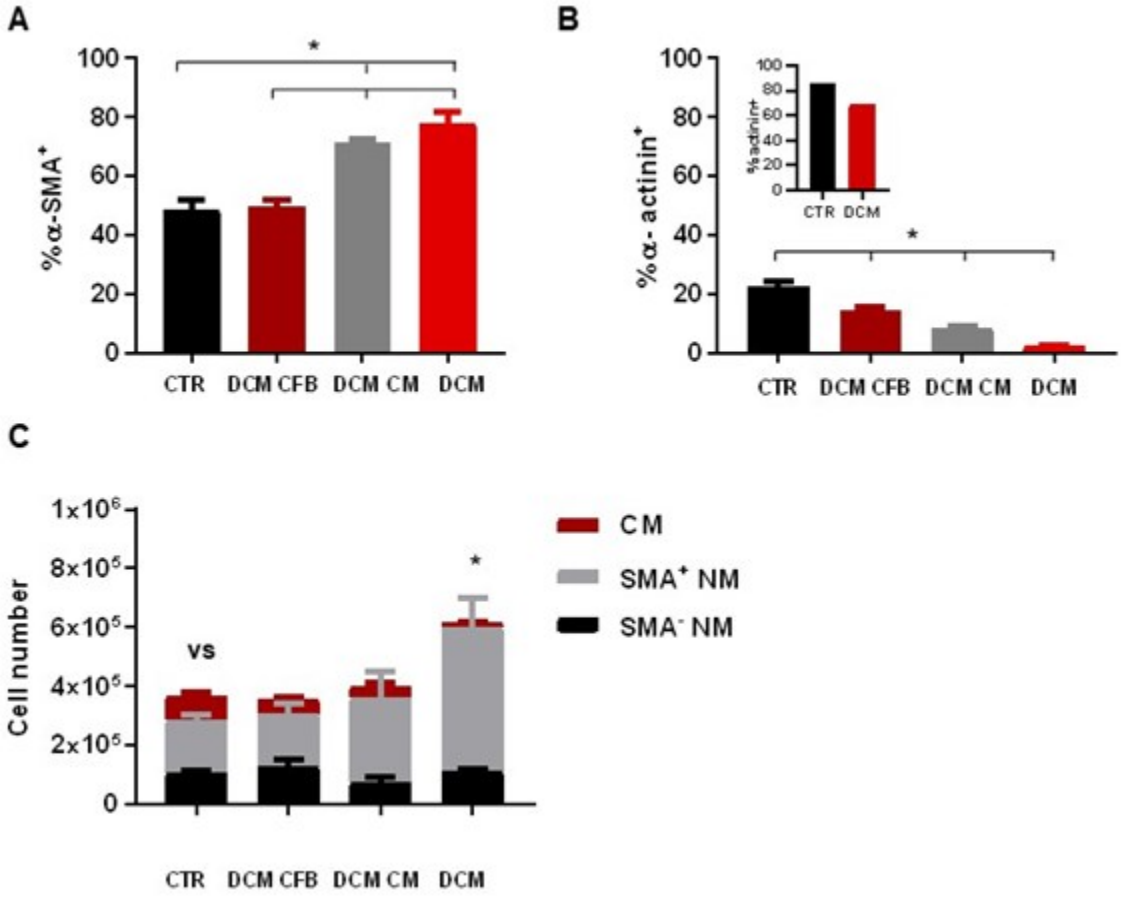

Figure 3-27 Modeling DCM in EHM: Cellular content of EHM

A Proportion of actinin$^+$ cells after enzymatic digestion of EHMs and FACS analysis. In the small inset, the purity of input CM populations is depicted. **B** % of SMA$^+$ cells in digested EHM. **C** Total cellular content with

actinin$^+$ CMs and actinin$^-$ non-myocytes that were either α-SMA$^+$ or α-SMA$^-$ in viable cells from digested EHM after FACS. A-C, *p<0.05 by 1-way ANOVA with Tukey´s multiple comparisons *post hoc* test. n=3/3/3/4 (CTR/DCM CFB/DCM CM/DCM).

In conclusion, these findings emphasize that the DCM phenotype in EHM is a result of both CM dysfunction and the presence of DCM-affected CFBs. Our results suggest, that both DCM-affected CFBs and DCM-stroma cells harbor myofibroblast characteristics that interfere with proper EHM functional development.

3.3 Towards fully defined EHM for pharmacological testing and clinical application – focus on fibroblasts

With the emphasis on fibroblasts, several aspects have to be considered for better control of EHM application in *in vitro* platforms and as potential HF therapeutic:

First, suitable sources of fibroblasts need to be accurately defined for the following: 1) patient-specific disease modeling and *in vitro* screening, 2) safe and feasible application of EHM *in vivo* as therapeutic. Second, a complete understanding of culture medium, supplements and their biological action is essential for the large-scale production and subsequent application of EHM in the clinics.

3.3.1 Non-myocytes pose a bottleneck for cardiac tissue engineering application in the clinics

3.3.1.1 A patient-specific fibroblast source for functional EHM

In the context of disease-modeling and *in vitro* investigation of EHM, patient-specific and easily obtainable yet well characterized fibroblasts are of great importance. We first investigated the potential to derive sufficient amounts of fibroblasts from gingiva of patients. Outgrowth cultures were easily obtained within 1-2 weeks post explantation from gingival biopsies (average time until first fibroblast culture outgrowth was observable was 13±1 days; n=6) (Figure 3-28 D). Cultures could be passaged at least 5 times and at 90% confluence yielded 30.000±1.600 cells/cm^2 (n=4) (Figure 3-28 E). Depending on tissue sizes and quality, at P1 we generally were able to obtain at least two T25 flasks/patient, that could then be passaged further at ratios of up to 1:5. It has been hypothesized that for cardiac repair 1 billion cells would be necessary to sufficiently regenerate a dysfunctional MI scar (Gepstein, 2002). We observed that EHM patches can be generated from cell preparations containing only 10% fibroblasts, thus 100 x 10^6

fibroblasts would be required to generate such a large tissue graft (approximate to 12X T175). Accordingly, this would require 5 passages.

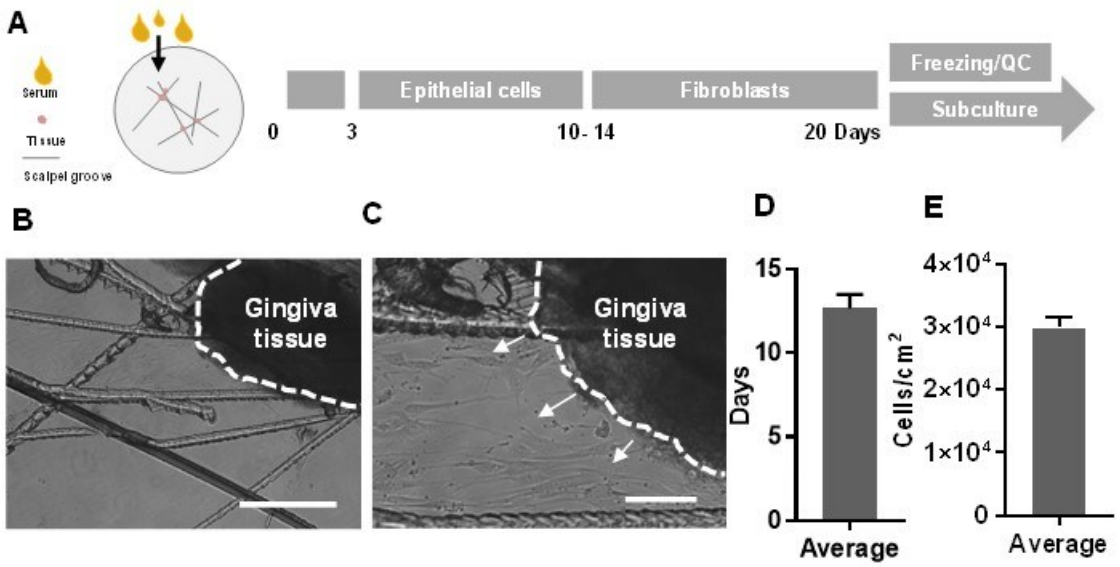

Figure 3-28 Generation of primary fibroblasts from human gingiva

A Schematic of cell harvest procedure. **B** Cellular outgrowth from attached gingiva tissue after several days in culture on Synthemax II surface (Corning). Scale bars: 500 µm in **B** and 100 µm in **C**. **D** Outgrowth time (n=6 independent patients) and **E** potential yield/cm^2 (4 patients) at 90% confluency in culture dishes.

For proof of principle, we generated EHM composed of CM and GFB from 4 subjects (GFB1-4). We found that EHM containing GFB1-4 developed significant lower forces than HFF EHMs in line with our observations with CFBs. There were no significant differences as to maximal contractile performance between EHM with GFB1-4 (FOC at 4 mmol/L [Ca^{2+}] in mN: HFF 1.1±0.1; GFB1 0.71±0.1; GFB2 0.52±0.1 GFB3 0.55±0.1; GFB4 0.7±0.1; n=22/12/4/4/4) (Figure 3-29 A). These findings were in line with morphological analyses: GFB EHMs were similar to each other and control HFF (CSA in mm2: HFF 0.6±0.04; GFB1 0.7±0.06; GFB2 0.6±0.06; GFB3 0.7±0.1; GFB4 0.8±0.08; n=11/8/4/4/4) (Figure 3-29 B).

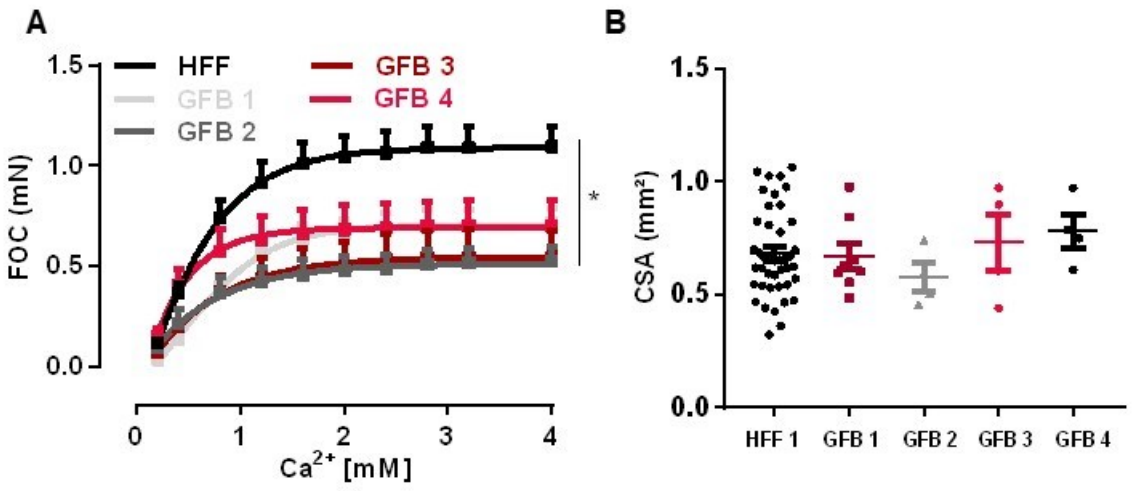

Figure 3-29 Patient-specific variances in EHM from gingiva fibroblasts

A FOC of 4-week old EHM from different GFB patients 1-4 compared to HFF controls (n =22/12/4/4/4 for HFF/GFB1-4). *p<0.05 by 1-way ANOVA with Tukey´s multiple comparisons *post hoc* test. **B** CSA of EHMs. (n = 11/8/4/4/4 for HFF/GFB1-4.

Collectively, these findings suggest, that patient-specific fibroblasts can be easily generated and used for individualized EHM studies *in vitro* and potentially even for *in vivo* application. We observed minimal variances in resulting EHMs between patients, indicating that our system is robust. However, the use of patient-specific cells requires intensive quality control and is time and cost-intensive.

3.3.1.2 PSC-derived non-myocytes offer new potential for EHM generation in clinical context

The need of primary fibroblasts for tissue engineering may now be circumvented as significant progress has been made in the development of protocols to derive epicardium and cardiac fibroblast-like cells from PSCs (Bao et al., 2017; Iyer et al., 2015; Tan et al., 2016; Witty et al., 2014). These cells were characterized by the expression of markers such as DDR2, periostin and PDGFRα (Iyer et al., 2015) (compare to Figure 3-16 of CFB1 specific transcription we identified in RNAseq).

For this study, RFP$^+$ HES2 cells were differentiated (see 2.1.12, cells were provided readily differentiated) into fibroblasts to produce non-myocyte populations that could be utilized in EHM. We found, that HES2 RFP$^+$-derived cardiac fibroblast-like cells (PSC-CFBs) were able to support EHM formation to a similar degree as neonatal HFFs (FOC at 4 mmol/L [Ca^{2+}] in mN: HFF controls 0.84±0.1; PSC-CFBs 0.72±0.2; n=7/6) (Figure 3-30 A). They demonstrated a slightly decreased [Ca^{2+}] sensitivity (EC50 [Ca^{2+}] in mmol/L: HFF 0.4±0.02

vs PSC-CFBs 0.5±0.01; n=7/6), while adrenergic responsiveness was comparable to HFF controls (Figure 3-30 B) (% increase FOC at EC50: HFF 64±3 vs PSC-CFBs 67±6; n=7/6) (Figure 3-30 C). Furthermore, we found that CSA in PSC-CFB EHMs was significantly increased (in mm^2: 1.6±0.15 vs 0.8±0.07 in HFF EHM; n=7/6) (Figure 3-30 D) concurrent with a higher cellular content that we measured after enzymatic digestion (viable cell counts x 10^5: 8.5±1.1 vs 5.5±0.7 in HFF EHM; n=5/6) (Figure 3-30 F).

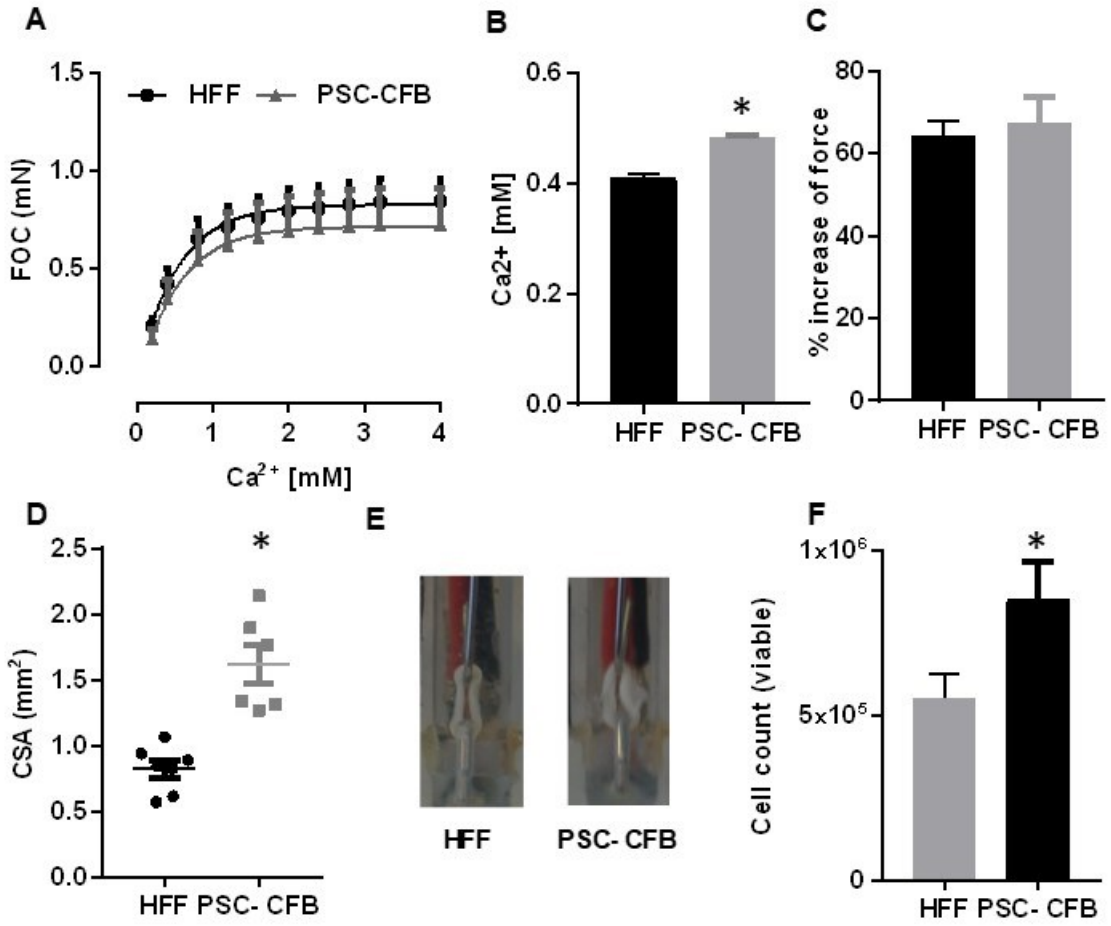

Figure 3-30 EHM can be generated from PSC-derived cardiac fibroblast-like cells

A EHM were generated from HFF and HES2 RFP^+-derived cardiac fibroblast like cells (PSC-CFBs) using the standard protocol. After 4 weeks FOC was assessed. **B** EC50 of [Ca2+] for HFF vs PSC-CFBs. (n=7/6). **C** Response to 1 µmol/L isoproterenol at EC50 and 1.5 Hz stimulation. **D** CSA of HFF and PSC-CFB EHM. (n=7/6). **E** Representative images of the two EHM groups. **F** Cellular content of EHM. For B, D, and F statistical analysis using unpaired t-test, two-tailed, *p<0.05 n=6/HFF and 5/PSC-CFB group.

In summary, we show that EHMs can be robustly generated from PSC-CFBs. In light of developing new *in vitro* models and their potential clinical application, these cells need further characterization. In EHM of HFFs, we found that fibroblasts do generally not proliferate (Tiburcy et al., 2017). The increased cell content of PSC-CFB EHMs thus

suggests that some proliferation may have taken place, which could pose a safety issue for transplanted EHMs (see next section).

3.3.1.3 Anti-proliferative treatment does not impair EHM function

To ensure safety of clinical applications of the EHM, potential cellular overgrowth through remnant PSCs (formation of potential teratoma and other cancer) and infections must be well controlled. One such option is the irradiation of a tissue. Thus, we next investigated whether irradiation would adversely affect EHM functionality. We found that EHM treated at day 3 with 30 Gy were similar in function to untreated controls (FOC at 4 mmol/L [Ca^{2+}] in mN: Control 0.83±0.2; Irradiated 0.9±0.1; n=3/10) (Figure 3-31 A). Irradiated EHMs were slightly decreased in CSA, possibly due to reduced levels of proliferation (CSA in mm^2: Control 0.7±0.1; Irradiated 0.4±0.03; n=4/10) (Figure 3-31 B). This difference was significant when comparing irradiated and control EHM. In line with arrested proliferation, we were unable to detect any $Ki67^+$ cell population in irradiated EHM ($Ki67^+$ cells in %: Control 4±0.9; Irradiated 0±0; n=4/10) (Figure 3-31 D). Concurrent with these findings, non-myocyte content in both treated groups was significantly reduced compared to untreated controls (Non-myocytes x 10^5: Control 4.3±0.6; Irradiated 1.2±0.2; CMs x 10^5: Control 1.3±0.1; Irradiated 0.9±0.2; n=4/10) (Figure 3-31 C). Taken together, our irradiation strategy would ensure high *in vitro* reproducibility of PSC-CFB EHMs and provide for a safe method for clinical applications of the EHM.

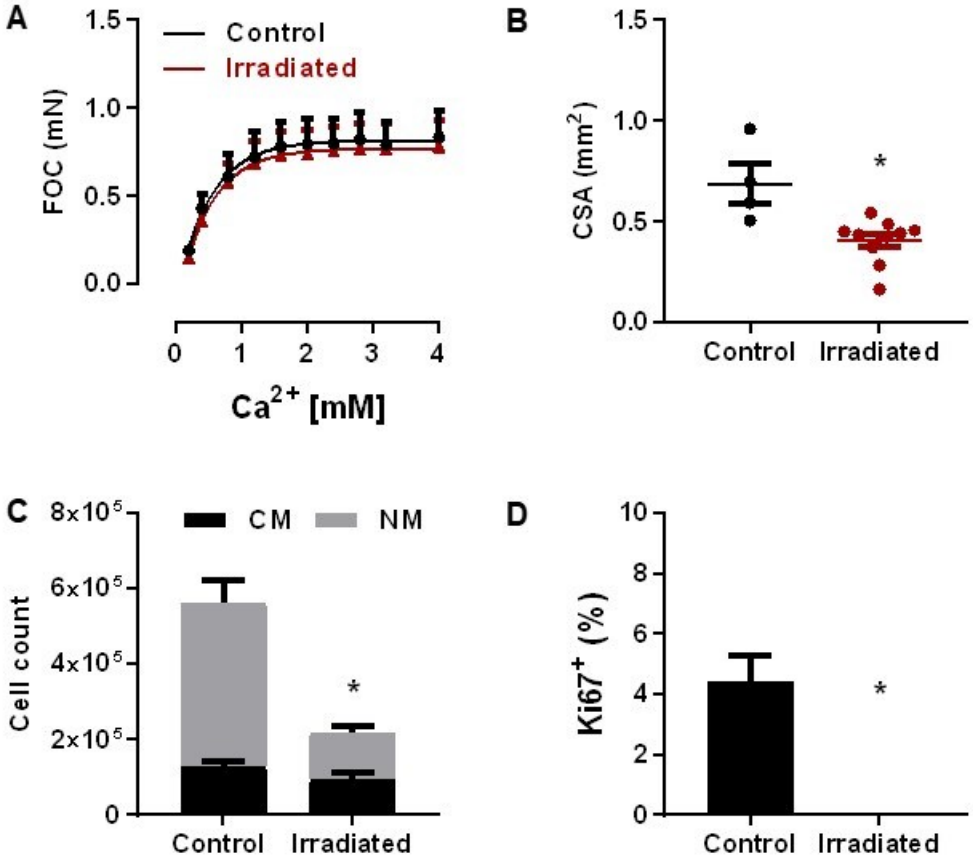

Figure 3-31 EHM function and content upon anti-proliferative treatment

A HFF EHM were irradiated on day 3 with 30 Gy and subsequently cultured for 4 more weeks before functional assessment, compared to control HFF EHM. n=3/10 (Control vs irradiated). **B** CSA in tissues. *p<0.05 by Welch´s test comparing control vs treated EHMs. n=3/10 (Control vs irradiated). **C** Cellular content of EHMs. *p<0.05 by unpaired t- test. n=4/10 (Control vs irradiated). **D** Proliferation in EHM assessed by Ki67$^+$ FACS. n=4/10 (Control vs irradiated). *p<0.05 by Mann-Whitney test.

3.3.2 EHM can be generated under chemically defined conditions

Next, to better understand cell-cell specific processes in EHM, we aimed at further defining our experimental model. While we were able to demonstrate that fibroblasts alone in ECT (Figure 1-7) and EHM can be robustly generated under serum-free conditions (Tiburcy et al., 2017), a further definition of the culture medium components would be required to ensure reproducibility. One such component of high complexity is B27. We thus aimed at defining the minimal requirements of B27 for EHM reconstitution.

First, we compared B27 control to EHM supplemented serum albumin (recombinant (rHSA) or purified serum albumin (HSA)), as bovine serum albumin is the major component of B27. Indeed, we found that albumin alone could support EHM development

and function in a concentration dependent manner with optimal support at 5 mg/ml and HAS being superior to rHSA (fold of control FOC at 4 mmol/L [Ca^{2+}]: Control B27 1±0.09; no supplement 0.5±0.06; rHSA 0.5 mg/ml 0.5±0.07; rHSA 2.5 mg/ml 0.8±0; rHSA 5 mg/ml 0.9±0.07; HSA 2 mg/ml 0.7±0.08; HSA 5 mg/ml 1.5±0.02; n=20/4/8/4/4/4) (Figure 3-32 A). The use of albumin derived from serum, however, is suboptimal for highly standardized applications.

We thus combined rHSA next with triiodothyronine (T3), transferrin (Tra) and sodium selenite (SoSel), L-carnitine (L-Car) and ethanolamine (Etha) or dexamethasone (Dexa). Many of these factors were tested before with data on their supportive function in EHM (Naito et al., 2006) and fibroblast culture as well as stem cell-differentiation Although none of the tested factors significantly enhanced EHM force production (Figure 3-32 B), they also did not reduce EHM function compared to respective controls. At this point we did not investigate further, more subtle differences (for instance calcium handling) in EHM and focused on their most prominent and integrative function, i.e., force of contraction developed under optimally preloaded isometric conditions.

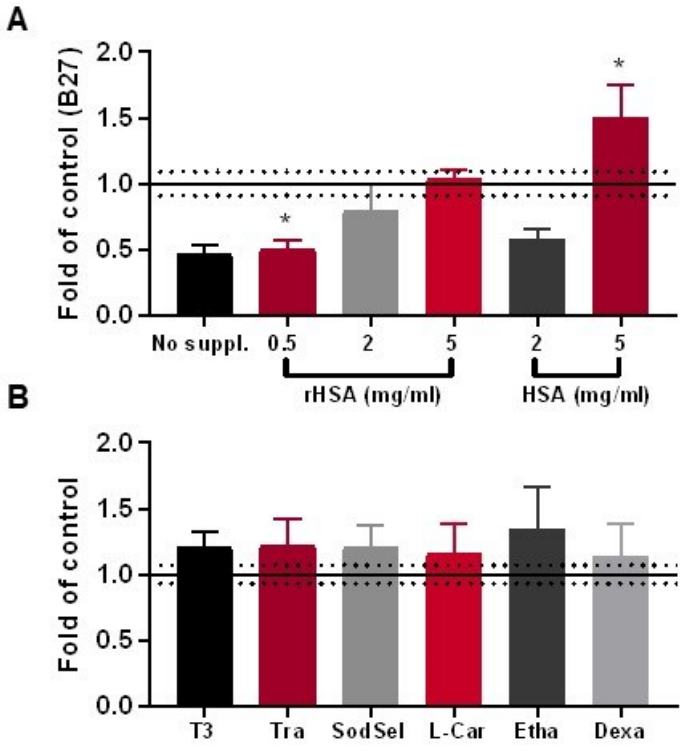

Figure 3-32 Essential components of EHM culture

Comparison of FOC at 4 mmol/L [Ca^{2+}] in 4-week-old EHM. **A** Data from EHM exposed to no supplement (no B27) and either recombinant (rHSA) or serum-derived human albumin (HSA) compared to control conditions defined in Tiburcy et al. 2017 (including B27); n=20/4/8/4/4/4. **B** Screening of additional factors included in B27 for EHM development supporting effects: Transferrin (Tra), sodium selenite (SodSel), L-Carnitine (L-

Car), ethanolamine (Etha), dexamethasone (Dexa). Data is displayed as fold difference in FOC from control EHM constructed according to the defined serum-free protocol reported by our group previously (Tiburcy et al. 2017), without B27 but with 5 mg/ml rHSA. The solid and dotted lines display the control mean±SEM. *p<0.05 by 1-way ANOVA with Tukey's multiple comparisons *post hoc* test.

From the earlier findings of Parikh et al., we investigated the combined addition of rHSA, T3 and Dexa, hypothesizing that these two ingredients could potentially support both CM development or even maturation and fibroblast maintenance in our system.

Indeed, rHSA in combination with both T3 and Dexa enhanced EHM function significantly (FOC at 4 mmol/L [Ca^{2+}] in mN: Control B27 0.25±0.04; rHSA 0.26±0.02; rHSA + T3 0.2±0.03; rHSA + T3 + Dexa 0.39±0.08; n=4/4/4/4) (Figure 3-33 A). Supplementation of EHM culture with rHSA and additional factors reduced spontaneous beating frequency, which was significant when combining T3 and Dexa, compared to both B27 and rHSA controls (in beats/min: B27 69±8; rHSA 56±3; RHSA + T3 51±2; rHSA + T3 + Dexa 35±5; n=4/group) (Figure 3-33 B). In tissues supplemented with rHSA, rHSA with T3 and in combination with Dexa, we also found that during isometric force measurements, the time until 90% contraction was reduced (time of contraction at 4 mmol/L [Ca^{2+}] and 1.5 Hz stimulation in ms: B27 172±4; rHSA 180±2; rHSA + T3 166±1; rHSA + T3 + dexa 153±4; n=4/group) (Figure 3-33 C). The trend in time until 50% relaxation of individual peaks was opposed (time until relaxation at 4 mmol/L [Ca^{2+}] and 1.5 Hz in ms: B27 100±2; rHSA 104±4; rHSA + T3 112±3; rHSa + T3 + Dexa 119±4; n=4/group) (Figure 3-33 D). In summary, these findings indicate vast changes in the calcium handling machinery of EHM supplemented with rHSA, T3 and Dexa.

Analysis of cellular composition revealed that rHSA +T3 and Dexa EHM contained less CMs but increased numbers of fibroblasts - this difference was significant when compared to B27 controls (RFP^+ CM x 10^5: B27 2.7±0.5; rHSA 1.8±0.1; rHSA + T3 2.1±0.3; rHSA + T3 + Dexa 1±0.1; and GFP^+ HFF x 10^5: B27 1.4±0.07; rHSA 1.9±0.2; rHSA + T3 2.2±0.4; rHSA + T3 + Dexa 2.8±0.1; n=3/4/4/4) (Figure 3-33 E).

Collectively, we could define minimal EHM supplementation that can sustain full EHM development and functionality. Indeed, even the use of albumin was sufficient to allow the generation of functional tissues.

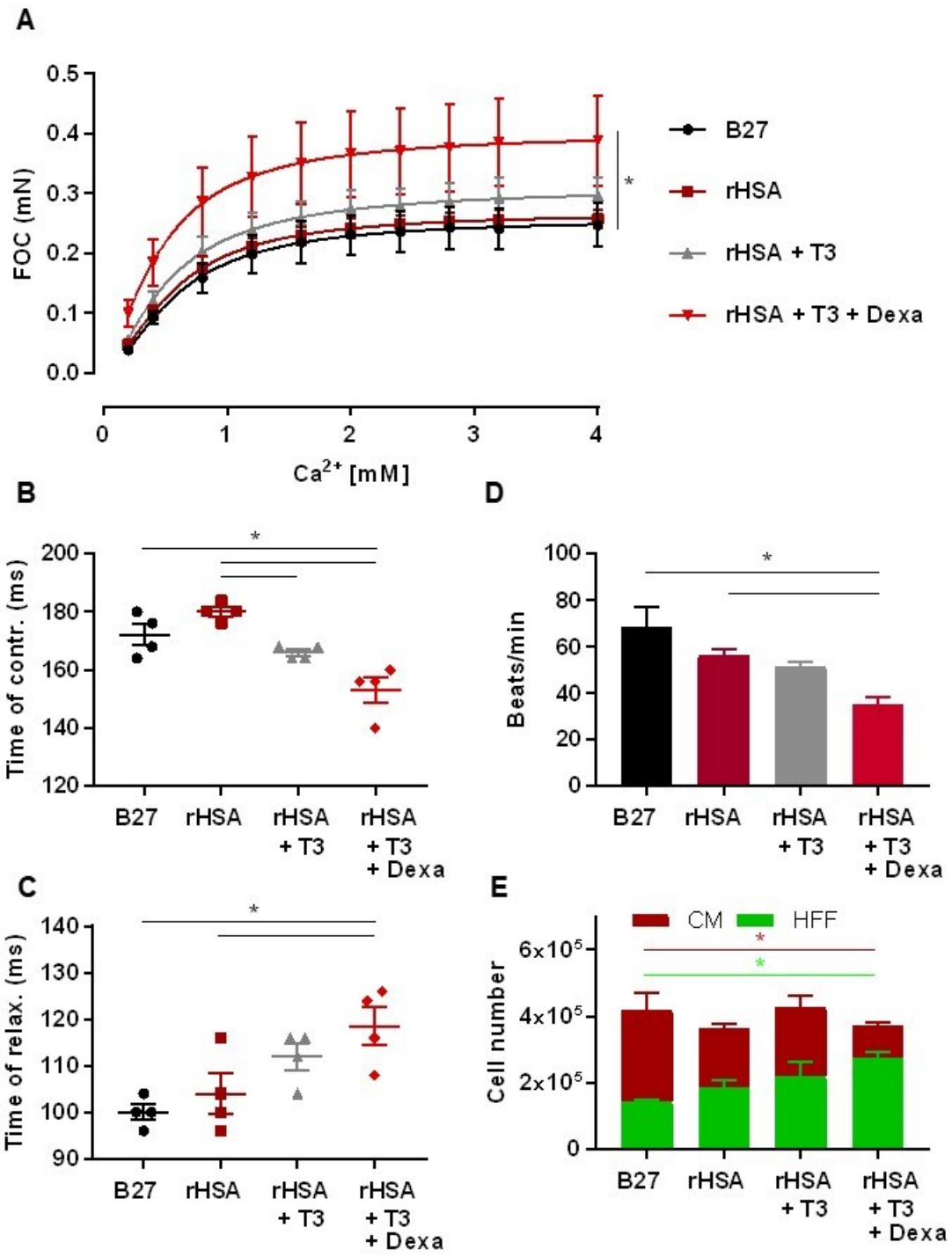

Figure 3-33 Minimal supplementation of EHM with albumin, T3 and dexamethasone

A FOC at 0.2-4 mmol/L [Ca^{2+}] in 4-week-old EHM supplemented with either B27 or rHSA in combination with Triiodothyronine (T3) and Dexamethasone (Dexa). *p<0.05 by 2-way ANOVA with Tukey's multiple comparisons *post hoc* test to compare defined supplement groups with B27 control. **B** Spontaneous beating frequency of EHM. n=4/group. **C** Contraction time at 4 mmol/L [Ca^{2+}] of EHMs and **D** Relaxation time at 4 mmol/L [Ca^{2+}]. For B-D: *p<0.05 by 1-way ANOVA with Tukey's multiple comparisons *post hoc* test. **E** Cellular content of EHM (RFP^+ CMs and GFP^+ HFFs). Difference in CM and HFF content: *p<0.05 by 1-way ANOVA with multiple comparisons *post hoc* test. n=3/4/4/4 (B27/rHSA/rHSA + T3/ rHSA+ T3 + Dexa).

In conclusion, while the defined and controlled derivation of primary fibroblasts is challenging, PSC-derived non-myocytes are now available for the use in EHM. Potential risks posed by remnant mesodermal progenitor or pluripotent stem cells in EHM can be diminished by radiation treatment without functional loss. These findings, taken together with the option of minimal and chemically defined supplementation, are very promising for the improvement of EHM as a defined *in vitro* model of fibroblast-CM crosstalk within the myocardium and its future application in the clinics.

4 Discussion

The role of cardiac fibroblasts in development and disease has become increasingly appreciated. Through the intrinsic complexity of the myocardium, however, the study of fibroblast-CM crosstalk has been hampered by the availability of suitable *in vitro* model systems.

In this work, we hypothesized that fibroblasts, by controlling the extracellular environment, are key for heart muscle assembly and homeostasis.

By utilizing the EHM model, which enables the reduction of the complex myocardium to a controlled 2-cell type system, we could specifically address 3 major questions and observed the following:

1. The role of fibroblasts for EHM development:
    - Fibroblast, but not cardiomyocytes compact the collagen I hydrogel environment during EHM formation.
    - Collagen I compaction leads to an activation of fibroblasts with subsequent ECM synthesis and assembly
    - The cardioinstructive cues necessary for EHM formation are to a certain degree universal to fibroblasts of different origin
2. Fibroblast-specific signaling to support healthy and diseased myocardium:
    - A tightly controlled HA content is crucial for proper EHM development and function
    - Fibroblast from DCM patients contribute to contractile failure of EHM
3. Optimization of EHM culture
    - PSC-derived fibroblast-like cells support EHM formation similarly as primary fibroblasts
    - rHSA, T3, and Dexa were identified as cardiomyogenesis-supporting factors in EHM

4.1 The role of fibroblasts in EHM development

The developing epicardium provides the necessary cues for cardiac compaction and guides the assembly of CMs into higher order contractile units (Takahashi et al., 2014). Cardiac fibroblasts were shown to first arise during cardiac compaction and their presence is a perquisite for hyperplastic growth of CMs during this phase (Ieda et al., 2009). The

endogenous role of fibroblasts is recapitulated in the generation of cardiac tissue constructs, where they are necessary to compact matrix and drive CM development (Kensah et al., 2013; Liau et al., 2011; Naito et al., 2006; Sur, 2016; Tiburcy et al., 2017; Wang et al., 2016; Zhang et al., 2017). Indeed, in the absence of suitable fibroblasts or comparable yet undefined stroma cell populations, engineered myocardial tissue does not consolidate and fails to form functional syncytia comprised of electromechanically integrated CMs. These findings could be confirmed in the present study, which demonstrated that that fibroblasts are essential for the early EHM compaction process.

During development, epicardium-derived cardiac fibroblasts interact with CMs via paracrine modulators (Bang et al., 2014; Cartledge et al., 2015). The ablation of paracrine signaling from the epicardium leads to a failure of the compaction process (Bax et al., 2010; Gittenberger-de Groot et al., 2012; Li et al., 2011). However, our lab has previously demonstrated, that paracrine signaling alone was insufficient for CMs in collagen I hydrogel supplemented with other matrix components such as Matrigel to drive compaction of tissue and form functional syncytia (Sur, 2016). Instead, these findings suggest the need for structural or biomechanical cues provided by the surrounding ECM during development. We thus investigated how fibroblasts affected the ECM of EHMs. Comparing 4-week old tissues without cells, with only CMs, HFFs or both cell types (EHM), we could appreciate the ECM consolidation process was highly dependent on the presence of fibroblasts. In earlier studies of rat engineered heart tissues, upregulation of collagen I and III transcripts, evidence of collagen I synthesis by electron microscopy, and the detection of increased levels of transcripts from MMPs 2 and 14 during development supported that extensive ECM modulation had taken place *in vitro*. Furthermore, already at culture day 12, CMs in this model were aligned in an anisotropic manner and tissues demonstrated phenotypic properties of native neonatal myocardium (Tiburcy et al., 2011). Thus, fibroblast-mediated ECM compaction in EHM likely coincides with functional development of CMs.

In addition, viscoelastic properties of the three-dimensional ECM environment in EHM is a key determinant for spatiotemporal maturation of CMs, a finding supported also in 2D and 3D models of CM maturation (in 2D: (Boothe et al., 2016; Engler et al., 2008; Ribeiro et al., 2015); in 3D (Lee et al., 2017). We evaluated the viscoelastic properties of EHM after 4-weeks of culture. Fibroblast only tissues showed the most profound stiffening as compared to cell-free, CM-containing, and EHM (CM+HFF) hydrogels. These findings were concurrent with the profound ECM structural changes that tissue constructs had

undergone, as evidenced by Sirius red staining. Notably, with a Young's modulus of 1-3 kPa, EHM are still rather soft compared to the endogenous myocardium, which ranges from 10 kPa in embryonic to 40 kPa in postnatal hearts (Jacot et al., 2010). This discrepancy has also been observed in other microtissues of collagen with cardiac fibroblasts (van Spreeuwel et al., 2017) and may for instance be explained by a different collagen I/III ratio of *in vitro* tissue constructs compared to endogenous myocardium and also the type of measuring method and mathematical model used.

Collectively our findings emphasize the fibroblast´s impact on integrity and viscoelasticity of the ECM. The maturation and mechanical development of cocultured CMs in EHM is driven and accompanied by the dynamical changes the ECM undergoes over time. For future studies, tuning of the EHM stiffness should be evaluated as a potential measure to further mature CMs. Application of external mechanical stress through dynamic stretching has already been extensively used to optimize the stress-strain behavior and thus functionality of EHM (Liaw and Zimmermann, 2016; Tiburcy et al., 2017).

4.1.1 Fibroblasts, but not cardiomyocytes, compact the collagen I hydrogel environment during EHM formation

From our findings of 4-week-old tissues we next sought to better understand the compaction of early developing EHM. In our previous work, we observed that proper collagen I compaction, which occurs within a timescale of hours post-casting (Tiburcy et al., 2014), was necessary to obtain functional EHM (Tiburcy et al., 2017). From our data, we could identify 3 distinct phases of collagen I hydrogel stiffening. First, collagen I hydrogels would settle in the instrument (lag), followed by a pH-dependent gelation step, independent of cellular content and finally a plateau, when the pH dependent reaction slowed (Figure 4-1)(Schlick et al., 2018). These observations were in line with the well-described properties of pH-dependent polymerization of collagen type I hydrogels: As a result of changes from acidic to physiological conditions, dimer and trimer collagen molecules are nucleated (lag phase), followed by a linear growth during which fibrillogenesis takes place that eventually reaches a plateau (equilibrium of fibrillogenesis and fibril breakdown) (Djabourov et al., 1993). In the presence of fibroblasts, collagen I compaction did not reach equilibrium and stiffening was further enhanced.

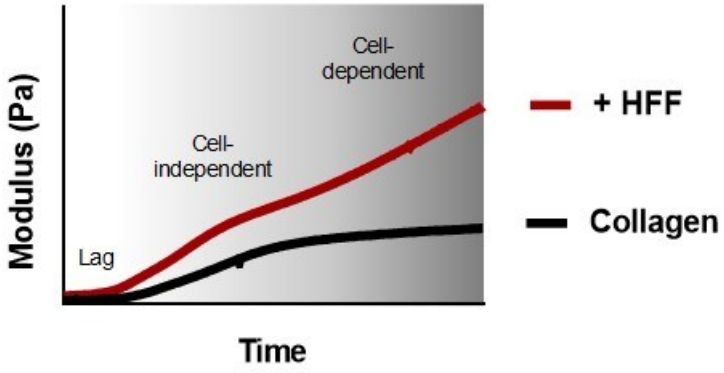

Figure 4-1 Temporal phases of collagen I polymerization

The polymerization of collagen I hydrogels with and without cells (here HFFs) in shear plate rheology can be divided into three stages. First the gel settles in the instrument (lag), then pH-dependent polymerization takes place (cell-independent), followed by a cell-dependent polymerization in the presence of fibroblasts. Figure modified from (Schlick et al., 2018).

The cell-driven collagen gel contraction is thought to be mediated by three consecutive processes that compact the collagen fibers and expel water: First, cell traction forces: Fibroblasts attach to the ECM and compact collagen fibrils into thicker fibers through tension mediated from the integrin-containing adhesion complexes. Secondly, within fibroblasts, active cell contraction involving myosin motors and the actin cytoskeleton transmit tension onto the surrounding gel. Finally, on a time-scale of hours, cell elongation and spreading of fibroblasts that attached to collagen I pulls fibers along the cells, effectively ridding the gel further of water (Dallon and Ehrlich, 2008).

The initial collagen I-fibroblast interaction is predominantly mediated by the integrins which can be found in focal adhesions. A major role in gel contraction is attributed to α2ß1-integrin, which is upregulated when fibroblast are exposed to a 3D collagen I environment (Jokinen et al., 2004; Klein et al., 1991; Schiro et al., 1991), and to a lesser degree α1ß1 (Carver et al., 1995; Jokinen et al., 2004; Zhang, 2006), α10ß1 (Tulla et al., 2001; Varas et al., 2007) and α11ß1-integrins (Varas et al., 2007). In line with the findings of others (Carver et al., 1995; Kondo et al., 2004), our lab has previously demonstrated that the integrin subunits α1, α2 and ß1 were predominantly expressed on fibroblasts and their blockage impaired the consolidation of both mouse and human EHM (Sur, 2016). Of note, we also observed a dosage-dependent effect on collagen I stiffness as doubling the input HFF cell number resulted in a markedly increased slope of storage modulus/time (n=1, see A1). In the work of Streeuwel and colleagues, increasing fibroblasts density in microtissues accelerated the early compaction process, but did not affect final elasticity of the tissues. Together with our findings, this suggests, that during initial gel contraction,

the extent to which a gel is compacted is dependent upon the number of cells that can bind collectively to the matrix via direct receptor-ECM interactions and contract the tissues through cytoskeletal rearrangements (van Spreeuwel et al., 2017). Thus, a higher number of cells will result in more effective gel contraction.

Cardiac tissues have also been generated from fibrin/Matrigel gels (Mannhardt et al., 2016; Schaaf et al., 2014). In fibrin-only gels, using an experimental setup very similar to ours, consolidation was shown to require cell-ECM binding and subsequent cytoskeletal dynamics, as it could be inhibited by treating fibroblasts with blebbistatin, demonstrating intracellular requirement for myosin II motor proteins and the actin cytoskeleton (Jansen et al., 2013). This second phase of cell-mediated gel contraction requires further investigation in our EHM model.

In the work of others, it was observed that gel contraction resulting from morphological changes of embedded cells generally appears much later (Dallon and Ehrlich, 2008). For instance, fibroblasts in contracted collagen I gels extend dendritic like protrusions only after hours and days (Rhee, 2009; Rhee and Grinnell, 2007) and also Jansen and colleagues found in their work, that fibrin gel polymerization had completed after 1 h, but the cellular morphology of fibroblasts changed on a timescale of several hours (6 h) (Jansen et al., 2013). Thus, as anticipated, during early gel consolidation, we could not detect distinct morphological differences in HFF and CM cell populations (see A1).

In EHM, consolidation was finished by 24 h. Indeed, it has previously been demonstrated that fibroblasts in collagen I gels immediately initiate gel compaction and that this process is mostly finished within the first 24 h (Yang et al., 2015; Zhang, 2006). Accordingly, the initial gel compaction we observe is a temporally very restricted process that involves cell-hydrogel binding and cytoskeletal rearrangements on a short time-scale. The large morphological changes involving the elongation of CMs and upregulation and assembly of α-actinin into functional sarcomeres take place on a timescale of days to weeks although the earliest signs of sarcomeric formation can be observed already at day 1 and 3 of EHM culture.

In summary, we could demonstrate, and for the first time quantify, fibroblast-dependent collagen compaction in EHM. Further maturation over several weeks of culture depends on fibroblast-mediated modeling of the ECM and *de novo* synthesis of ECM components resulting in changes in the viscoelasticity of developing tissues beginning at consolidation with 29 Pa (EHM at 60 min) to 0.9 kPa in 4-week-old EHM. These changes coincide with

CM elongation and spatial alignment that confer syncytium functionality. Interestingly, we found that fibroblast-mediated gel consolidation and subsequent stiffening over the 4-week culture time of EHMs was attenuated by the presence of CMs. We hypothesize that this may result from the "softer" characteristic of cells compared to the stiffer matrix, or be the consequence of cellular crosstalk between CMs and fibroblasts, both which require further investigation.

4.1.2 Collagen I compaction leads to an activation of fibroblasts with subsequent ECM synthesis and assembly

To better understand the cell-specific processes in early consolidating tissues, we analyzed the transcriptome changes of collagen I hydrogels with HFF, CMs and both cell types between cell-independent and dependent phase (Figure 3-7/Figure 3-8/Figure 3-9).

Interestingly, GO analyses suggested similar processes in EHM as observed in embryonic cardiac jelly formation and endocardial cushion development, which include HA synthesis (Camenisch et al., 2000, 2001). The EHM collagen matrix thus appears to mimic the environment of the early developing myocardium. In line with our hypothesis that fibroblast-mediated processes dominate tissue compaction, we found that fibroblasts responded strongest to the stiffening environment with enhanced transcription of ECM-related genes and genes of general tissue formation processes.

Among key factors in the fibroblast-specific group we identified SOX9, a master regulator of the fibrotic response in the heart (Lacraz et al., 2017) and TGFß which controls ECM contraction and synthesis (Chen et al., 2005; Dobaczewski et al., 2011; Lijnen et al., 2003; Montesano and Orci, 1988). Other genes identified played a role in glycosaminoglycan biosynthesis and wound contractile processes (VCAN, PDGFß and its receptor). Also, anchorage proteins (junction plakoglobin (JUP) and desmoplakin (DSP)) were specifically regulated in the fibroblast group. Collectively, all these factors clearly emphasize the fibroblast-specific function of ECM-binding and subsequent contraction during consolidation in EHM. Of note, BMP2 was also specifically regulated in the fibroblast-group, a factor that is important for HA-mediated cardiac jelly formation and thus endocardial cushion development (Ma, 2005). This is also the case for VCAN, which cooperates with HA in cardiac development (Hatano et al., 2012) (see also 4.2.1 on the role of HA in endogenous myocardium and EHM).

GO terms unique to CMs (154 DEGs in the CM only and EHM group) were indicative for ER stress, which is in line with earlier findings of our group that demonstrated an increase in caspase activity and CM-specific apoptosis (and anoikis) during early formation of EHM (Tiburcy et al., 2011, 2017). Surprisingly, around half of the DEGs in EHM were comprised of micro- and long non-coding-RNA species(Schlick et al., 2018). RNAs of this family have been reported to be transported between cells by means of exosomes (Bang et al., 2014; Fatima et al., 2017; Hayashi and Hoffman, 2017). This axis of fibroblast-CM crosstalk will be the subject of further work in the EHM model.

Collectively, these data illustrate how early EHM development recapitulates *bona fide* heart formation at the stages of cardiac jelly formation and compaction, involving HA biosynthetic processes in both cell types, while ECM assembly and contractile processes could be clearly attributed to the fibroblast fraction of tissues. The reshaping of the viscoelastic matrix activates predominantly the fibroblast fraction in EHM in a reciprocal manner and is itself controlled by the presence of CMs.

4.1.3 All fibroblasts can provide cardioinstructive cues

We observed cardioinstructive properties in all fibroblasts, irrespective of their origin, i.e., skin, gingiva or heart. These data are in agreement with observations of other groups that have utilized various sources fibroblasts to generate functional cardiac tissue constructs, for instance from whole heart preparations (Conradi et al., 2015; Jackman et al., 2018; Tiburcy et al., 2011; Zimmermann et al., 2002, 2006), or PSC-derived CM preparations from differentiations at various levels of purity (Lemoine et al., 2017; Mannhardt et al., 2016; Naito et al., 2006). In this case, remnant mesodermal cells with fibroblast-like function have likely mediated tissue contraction and development. Finally, our finding that neonatal fibroblasts (HFF) supported the formation of functionally superior EHM compared to EHM containing fibroblasts from adults (GFB, CFB) is in line with the data of others (Liau et al., 2017). Here, cocultures with fetal rather than adult cardiac fibroblasts resulted in significantly higher expression of α-actinin and also connexin 43, concurrent with functional superiority, in cardiac tissue patches (Liau et al., 2017). It has also been observed that “younger” fibroblasts are more effective in contracting collagen I gels (Wilson et al., 2011), which may facilitate initial EHM development. Furthermore, it has been shown that fibroblasts of different origin differentially express MMPs (Lindner et al., 2012). Resulting variances in matrix-remodeling capabilities of different fibroblasts

may result in changes in EHM functionality since the presence of MMPs controls proper CM development in tissues (Nichol et al., 2008).

4.2 Fibroblast-specific signaling to support healthy and diseased myocardium

Utilizing EHM as *in vitro* model of fibroblast-specific signaling in the myocardium, we investigated the contribution of primary cardiac fibroblasts to pathological phenotypes.

4.2.1 A tightly controlled hyaluronan content is crucial for EHM development and function

The presence of HA is critical for cardiac cushion development (Camenisch et al., 2001; Ma, 2005; Shirai et al., 2009) and pericardial EMT (Shirai et al., 2009). In contrast, an excessive accumulation of HA results in severe cardiac pathologies with fibrosis, including hypertrophy and myofibril disarrangement in CMs (Chowdhury et al., 2013, 2017). The HA content of the ECM is tightly regulated during development, homeostasis and disease by the complex interplay between HA synthesis by HAS enzymes and degradation by HYALs. Our data of CFB1 EHMs suggest that the same accounts for EHM development.

Analysis of the CFB (from patient 1) transcriptome revealed increased levels of HASs, while no difference in HYAL expression was detected compared to HFF cells. Taken together with low levels of CD44, which is necessary for HYAL-mediated degradation of HA (Harada and Takahashi, 2007), excessive HA deposition in CFB1 EHM was implied. Coincidentally a higher abundance of HA-binding proteoglycans such as VCAN could enhance binding and thus incorporation of HA in the ECM of CFB1 EHMs (Keller et al., 2012). In line with our hypothesis, HYAL treatment of EHMs reduced CSA and concurrently boosted function in a dose-dependent manner. When treating EHM with higher concentrations of HYAL, function progressively deteriorated suggesting that there is also a minimal level of extracellular HA required during development.

HA is crucially involved in all structural changes of the myocardium and found upregulated upon MI injury (Müller et al., 2014; Waldenström et al., 1991), where it plays an important role in myofibroblast regulation (Müller et al., 2014). Although analysis of CFB1-EHM viscoelastic properties did not indicate a fibrotic phenotype, RNAseq analysis revealed a higher expression of myofibroblast markers periostin (Snider et al., 2009) and CTGF (Leask et al., 2003; Lin et al., 2013). Of note, in periostin knock-out cells, HA secretion is reduced and it has been demonstrated that periostin-integrin interaction

controls HAS2 activity via PI3K signaling (Ghatak et al., 2014). These findings indicate a direct regulation between periostin and HA. Upon myofibroblast differentiation, more HA is detected in media of fibroblasts *in vitro*, which is not necessarily only associated with an increase in synthesis, rather a decrease in HA degradation (Jenkins et al., 2004). These findings would be in line with comparable HYAL levels but different levels of VCAN and CD44 in CFB1 and HFF control cells.

While HFF cells are proliferative in 2D, they do not outgrow CMs in EHM (Tiburcy et al., 2017; Zimmermann et al., 2006). Indeed this quiescent behavior of dermal fibroblasts in 3D collagen matrices has been described and investigated and it could be demonstrated that cells in surroundings of physiological stiffness normally undergo a mitotic stop (Nishiyama et al., 1990). Although they were of comparable stiffness as HFF EHMs, CFB1 EHM contained higher numbers of non-myocytes. Excessive cell numbers were shown to impair CM development as observed in other cardiac tissue models (van Spreeuwel et al., 2017), which may also apply for EHM. There is a close connection between HA and non-myocyte proliferation: HA is initially required for TGFß-dependent myofibroblast transition and maintenance of the fibrotic phenotype (Webber et al., 2009a, 2009b) and HA stimulates TGFß-dependent proliferative activity (Meran et al., 2011). Thus, myofibroblasts sustain their phenotype and proliferative capacity in an autocrine TGFß- and HA-dependent feedback loop (Webber et al., 2009a). Intriguingly, in HYAL2-deficienct mice, HA accumulates which results in higher non-myocytes populations (Chowdhury et al., 2017). Reciprocally, inhibition of HAS2 also leads to a reduction of proliferation (Chao and Spicer, 2005). Notably, similarly to HYAL, anti-proliferative treatment in EHM did boost function and restored CSA to levels, comparable to HFF EHMs. However, at this point, we are unable to segregate whether proliferation was the consequence of high HA levels or whether proliferating non-myocytes resulted in the secretion of higher levels of HA within EHM. Both mechanisms may contribute to the CFB1 phenotype.

To investigate our phenotype further, we first generated HAS2-Flag overexpressing constructs (A2.7), but failed to confirm the successful overexpression of HAS2-Flag (see A1). We then generated stable HAS2-overexpressing HFFs with a commercial vector and validated HAS2 overexpression on mRNA levels and resulting HA secretion. Interestingly, RNA transcript levels were greatly increased (600X in HAS2-overexpressing HFFs vs controls compared to only 6-8X in CFB1 cells vs HFFs). In contrast, HA secretion in 2D was only 3X higher in HAS2-overexpressing cells when compared to controls. These findings suggest that much higher levels of HAS2 mRNA do not necessarily lead to

comparable HA output, likely due to intrinsic regulation of HAS2 activity with endogenous antisense RNA HAS2-AS1 (Chao and Spicer, 2005) or HA degradation by HYALs. Next, we generated EHM from these cells: Although we confirmed increased HA secretion in HAS2-overexpressing EHMs, we could not recapitulate our previous phenotype suggesting the need to establish 1) whether a certain HA concentration range is supportive for EHM development and 2) whether the HFF-background may affect HA synthesis and retention in this model through other members of the HA system (for instance VCAN, CD44).

4.2.2 Fibroblasts from DCM patients contribute to contractile failure EHM

Initial studies of DCM disease modeling in EHM focused on defects in cardiomyocytes, such as observed in subjects with mutations in the RBM20 gene (Streckfuss-Bömeke et al., 2017). Whether DCM phenotypes could also be associated with a fibroblast dysfunction has not been studied, so far. To address this, we combined DCM-affected CFBs and CMs in our EHM model. Decreased contractile performance in EHM with DCM-fibroblasts was in agreement with an earlier hypothesis that heart failure can be a consequence of a fibroblastopathy (Tiburcy and Zimmermann, 2014).

As a high prevalence of fibrosis is typically found in DCM pathologies (Ohtani et al., 1995; Unverferth et al., 1986), we investigated this matter in more detail: Within an hour after casting, the presence of DCM CFBs had resulted in significantly more consolidated gels. This indicated a contractile, potentially myofibroblast phenotype since myofibroblasts were shown to exert stronger contractile forces on gels than resident cardiac fibroblasts (Wrobel et al., 2002). And indeed, 4-week-old EHM of DCM CFBs had contracted so forcefully, that the PDMS poles they were placed on had been bent maximally. That was also the case for EHM with DCM CMs, suggesting that DCM remnant stroma cells retained similar, pathological characteristics. In agreement with these observations, analysis of viscoelasticity revealed that the presence of DCM-affected cells had resulted in higher tissue stiffness, indicating fibrotic ECM modulation.

High levels of mechanical strain in cardiac fibroblasts were found to result in myofibroblast activation and subsequent ECM remodeling that progressively stiffens the ECM in a positive feedback loop (Baum and Duffy, 2011; Schroer and Merryman, 2015; Tomasek et al., 2002; Travers et al., 2016). Thus, in consolidating DCM-affected EHM a stiffer environment could further enhance fibrotic modulation of the ECM. Furthermore, in EHMs that progressively condensed the poles, cells were subjected to high mechanical load while tissue movement was restrained (static stretch). These processes could

adversely affect CM development, as optimal load and auxotonic (not static) stretching of EHMs are essential for CM development and thus optimal functionality in EHM (Abilez et al., 2018; Zimmermann, 2013; Zimmermann et al., 2006).

Notably, in agreement with a myofibroblast phenotype, α-SMA content in 4-week-old EHMs of DCM CMs and EHM with both DCM CMs and DCM fibroblasts was increased, but not in EHMs of DCM fibroblasts. α-SMA content alone thus cannot fully explain the fibrotic behavior of DCM-affected CFBs.

Further analysis of cellular content revealed: CM content of EHMs containing DCM-affected CMs and CFBs was reduced, which was concurrent with a trend in functional deterioration. Impure DCM-CM preparations can partially explain this finding. However less CMs were recovered when either healthy or DCM-affected CMs were coculture with DCM-affected CFBs, demonstrating fibroblast-specific mechanisms that adversely affected CM retention.

Of note, EHM of DCM-affected CMs did not develop measurable forces. These findings were anticipated as previous studies had demonstrated the contractile dysfunction of DCM-affected CMs in 2D (Sun et al., 2012) and EHM (Streckfuss-Bömeke et al., 2017).

In summary, our data demonstrate the suitability and importance of physiological *in vitro* systems to study CM- and fibroblast-specific processes in the myocardium. By using EHM of both DCM-affected CMs and cardiac fibroblasts we were able to distinguish cell-specific contributions to the contractile and fibrotic pathophysiology of DCM and our findings further emphasized the underestimated role of cardiac fibroblasts in this context.

4.3 Optimization of EHM culture

To gain a comprehensive understanding of the role of nonmyocytes in cardiac tissue engineering and of endogenous cardiac fibroblasts in the myocardium, better *in vitro* systems are needed. Future applications of fibroblasts in EHM both in the context of *in vitro* screening and clinical application require: 1) the determination of suitable fibroblast sources, 2) safe application of the tissue constructs in preclinical models and 3) improved and chemically defined culture conditions for resulting EHMs.

4.3.1 PSC-derived fibroblast-like cells support EHM formation similarly as primary fibroblasts

Although primary fibroblasts could clearly support EHM development and patient-specific variances were low, for robust *in vitro* disease models including large-scale screening applications and the potential use of EHM *in vivo*, larger amounts of well characterized non-myocytes are required. These needs can now be met by the directed differentiation of cardiac fibroblast(-like) cells (characterized by the expression of markers such as DDR2, PDGF receptor α, or periostin (Bao et al., 2017; Hewitt et al., 2011; Iyer et al., 2015, 2015; Witty et al., 2014)) from PSCs.

EHM from PSC-derived cardiac fibroblast-like cells performed similarly to EHM containing HFF. Of note, morphological analysis and enzymatic digestion revealed a higher cellular content, suggesting that proliferation, potentially by remnant PSCs, had occurred. Uncontrolled growth of PSCs and teratoma formation have been observed both in other tissue engineering approaches and when using PSCs *in vivo* (Nelson et al., 2009; Nussbaum et al., 2007). In order to both abolish cellular proliferation and rid EHM of potential pathogens, we previously tested γ-ray irradiation of HFF EHM, which preserved function while completely abolishing Ki67 activity. We thus suggest this treatment also for PSC-CFB EHMs.

In summary, this preliminary data indicates that PSC-derived cardiac fibroblast-like cells could serve as a reproducible and stable source of fibroblasts for EHM. Their large-scale production in combination with biological safety treatment could allow a future therapeutic application of EHM.

4.3.2 Further definition of EHM culture supplements

Our standard defined EHM culture conditions utilize B27 supplementation (Tiburcy et al. 2017). To our surprise we observed that both recombinant and serum-derived albumin alone could replace B27 and support the development of functional EHM. However, two additional factors, T3 and dexamethasone, appeared to support maturation of the calcium handling machinery as evidenced by shortened contraction and prolonged relaxation time. The general observation that albumin, T3 and corticoids enhance maturation is in line with previous reports (Naito et al., 2006; Parikh et al., 2017; Yang et al., 2014). We furthermore found that the addition of Dexa specifically supported fibroblasts in EHM,

which is in agreement with the use of Dexa in defined growth media for fibroblast maintenance (Bettger et al., 1981; Phillips and Cristofalo, 1980; van der Valk et al., 2010).

5 Conclusion and outlook

By utilizing EHM, a model system resembling structural, molecular, and functional properties of postnatal myocardium (Tiburcy et al. 2017), we demonstrated the crucial role of fibroblasts in early EHM formation and subsequent maturation of functional cardiac tissue constructs. Fibroblasts controlled the compaction of the collagen type I hydrogel environment, the main EHM ECM component, and appeared to be activated by ECM stiffening to provide cardioinstructive cues. Fibroblasts of different origin supported cardiomyogenesis in EHM suggesting a common cardioinstructive function. As a potential specific cardioinstructive fibroblast-derived ECM factor HA was identified. The requirement for a tight regulation of its ECM content was demonstrated as an important parameter for optimal EHM function. Furthermore, we showed that EHM can serve as a powerful tool to study the pathophysiological role of fibroblast-CM crosstalk with evidence for a specific role of fibroblasts in DCM associated contractile dysfunction. Finally, with the definition of a protocol for scalable derivation of fibroblasts from iPSC and rHSA, T3, and Dexa as important culture medium supplements we further optimized the EHM technology for applications in disease modelling, drug development, and potentially also for heart repair.

6 Bibliography

Abilez, O.J., Tzatzalos, E., Yang, H., Zhao, M.-T., Jung, G., Zöllner, A.M., Tiburcy, M., Riegler, J., Matsa, E., Shukla, P., et al. (2018). Passive Stretch Induces Structural and Functional Maturation of Engineered Heart Muscle as Predicted by Computational Modeling. Stem Cells Dayt. Ohio *36*, 265–277.

Anders, S., and Huber, W. (2010). Differential expression analysis for sequence count data. Genome Biol. *11*, R106.

Andrews, Si. (2014). FastQC: a quality control tool for high throughput sequence data. http://www.bioinformatics.babraham.ac.uk/projects/fastqc. *Babraham Bioinformatics*.

Bang, C., Batkai, S., Dangwal, S., Gupta, S.K., Foinquinos, A., Holzmann, A., Just, A., Remke, J., Zimmer, K., Zeug, A., et al. (2014). Cardiac fibroblast–derived microRNA passenger strand-enriched exosomes mediate cardiomyocyte hypertrophy. J. Clin. Invest. *124*, 2136–2146.

Bang, C., Antoniades, C., Antonopoulos, A.S., Eriksson, U., Franssen, C., Hamdani, N., Lehmann, L., Moessinger, C., Mongillo, M., Muhl, L., et al. (2015). Intercellular communication lessons in heart failure: Communication in heart failure. Eur. J. Heart Fail. *17*, 1091–1103.

Bao, X., Lian, X., Qian, T., Bhute, V.J., Han, T., and Palecek, S.P. (2017). Directed differentiation and long-term maintenance of epicardial cells derived from human pluripotent stem cells under fully defined conditions. Nat. Protoc. *12*, 1890–1900.

Baum, J., and Duffy, H.S. (2011). Fibroblasts and Myofibroblasts: What Are We Talking About?: J. Cardiovasc. Pharmacol. *57*, 376–379.

Bax, N.A.M., Bleyl, S.B., Gallini, R., Wisse, L.J., Hunter, J., van Oorschot, A.A.M., Mahtab, E.A.F., Lie-Venema, H., Goumans, M.-J., Betsholtz, C., et al. (2010). Cardiac malformations in Pdgfrα mutant embryos are associated with increased expression of WT1 and Nkx2.5 in the second heart field. Dev. Dyn. Off. Publ. Am. Assoc. Anat. *239*, 2307–2317.

Bell, E., Ivarsson, B., and Merrill, C. (1979). Production of a tissue-like structure by contraction of collagen lattices by human fibroblasts of different proliferative potential in vitro. Proc. Natl. Acad. Sci. *76*, 1274–1278.

Bentzon, J.F., Otsuka, F., Virmani, R., and Falk, E. (2014). Mechanisms of Plaque Formation and Rupture. Circ. Res. *114*, 1852–1866.

Bergmann, O., Zdunek, S., Felker, A., Salehpour, M., Alkass, K., Bernard, S., Sjostrom, S.L., Szewczykowska, M., Jackowska, T., dos Remedios, C., et al. (2015). Dynamics of Cell Generation and Turnover in the Human Heart. Cell *161*, 1566–1575.

Berliner, D., and Bauersachs, J. (2017). Current Drug Therapy in Chronic Heart Failure: the New Guidelines of the European Society of Cardiology (ESC). Korean Circ. J. *47*, 543.

Bettger, W.J., Boyce, S.T., Walthall, B.J., and Ham, R.G. (1981). Rapid clonal growth and serial passage of human diploid fibroblasts in a lipid-enriched synthetic medium supplemented with epidermal growth factor, insulin, and dexamethasone. Proc. Natl. Acad. Sci. *78*, 5588–5592.

Blondiaux, E., Pidial, L., Autret, G., Rahmi, G., Balvay, D., Audureau, E., Wilhelm, C., Guerin, C.L., Bruneval, P., Silvestre, J.-S., et al. (2017). Bone marrow-derived mesenchymal stem cell-loaded fibrin patches act as a reservoir of paracrine factors in chronic myocardial infarction. J. Tissue Eng. Regen. Med. *11*, 3417–3427.

Boothe, S.D., Myers, J.D., Pok, S., Sun, J., Xi, Y., Nieto, R.M., Cheng, J., and Jacot, J.G. (2016). The Effect of Substrate Stiffness on Cardiomyocyte Action Potentials. Cell Biochem. Biophys. *74*, 527–535.

Borchert, T., Hübscher, D., Guessoum, C.I., Lam, T.-D.D., Ghadri, J.R., Schellinger, I.N., Tiburcy, M., Liaw, N.Y., Li, Y., Haas, J., et al. (2017). Catecholamine-Dependent ß-Adrenergic Signaling in a Pluripotent Stem Cell Model of Takotsubo Cardiomyopathy. J. Am. Coll. Cardiol. *70*, 975–991.

Braunwald, E. (2017). Cardiomyopathies: An Overview. Circ. Res. *121*, 711–721.

Brutsaert, D.L. (2003). Cardiac Endothelial-Myocardial Signaling: Its Role in Cardiac Growth, Contractile Performance, and Rhythmicity. Physiol. Rev. *83*, 59–115.

Burgess, M.L., Carver, W.E., Terracio, L., Wilson, S.P., Wilson, M.A., and Borg, T.K. (1994). Integrin-mediated collagen gel contraction by cardiac fibroblasts. Effects of angiotensin II. Circ. Res. *74*, 291–298.

Camelliti, P. (2004). Fibroblast Network in Rabbit Sinoatrial Node: Structural and Functional Identification of Homogeneous and Heterogeneous Cell Coupling. Circ. Res. *94*, 828–835.

Camelliti, P., Borg, T.K., and Kohl, P. (2005). Structural and functional characterisation of cardiac fibroblasts. Cardiovasc. Res. *65*, 40–51.

Camenisch, T.D., Spicer, A.P., Brehm-Gibson, T., Biesterfeldt, J., Augustine, M.L., Calabro, A., Kubalak, S., Klewer, S.E., and McDonald, J.A. (2000). Disruption of hyaluronan synthase-2 abrogates normal cardiac morphogenesis and hyaluronan-mediated transformation of epithelium to mesenchyme. J. Clin. Invest. *106*, 349–360.

Camenisch, T.D., Biesterfeldt, J., Brehm-Gibson, T., Bradley, J., and McDonald, J.A. (2001). Regulation of cardiac cushion development by hyaluronan. Exp. Clin. Cardiol. *6*, 4–10.

Cartledge, J.E., Kane, C., Dias, P., Tesfom, M., Clarke, L., Mckee, B., Al Ayoubi, S., Chester, A., Yacoub, M.H., Camelliti, P., et al. (2015). Functional crosstalk between cardiac fibroblasts and adult cardiomyocytes by soluble mediators. Cardiovasc. Res. *105*, 260–270.

Carver, W., Nagpal, M.L., Nachtigal, M., Borg, T.K., and Terracio, L. (1991). Collagen expression in mechanically stimulated cardiac fibroblasts. Circ. Res. *69*, 116–122.

Carver, W., Molano, I., Reaves, T.A., Borg, T.K., and Terracio, L. (1995). Role of the α1ß1 integrin complex in collagen gel contraction in vitro by fibroblasts. J. Cell. Physiol. *165*, 425–437.

Chao, H., and Spicer, A.P. (2005). Natural antisense mRNAs to hyaluronan synthase 2 inhibit hyaluronan biosynthesis and cell proliferation. J. Biol. Chem. *280*, 27513–27522.

Chapuis, J.F., and Agache, P. (1992). A new technique to study the mechanical properties of collagen lattices. J. Biomech. *25*, 115–120.

Chen, Y., Shi-wen, X., van Beek, J., Kennedy, L., McLeod, M., Renzoni, E.A., Bou-Gharios, G., Wilcox-Adelman, S., Goetinck, P.F., Eastwood, M., et al. (2005). Matrix Contraction by Dermal Fibroblasts Requires Transforming Growth Factor-ß/Activin-Linked Kinase 5, Heparan Sulfate-Containing Proteoglycans, and MEK/ERK. Am. J. Pathol. *167*, 1699–1711.

Chilton, L., Giles, W.R., and Smith, G.L. (2007). Evidence of intercellular coupling between co-cultured adult rabbit ventricular myocytes and myofibroblasts: Coupling of ventricular myocytes and myofibroblasts. J. Physiol. *583*, 225–236.

Chong, J.J.H., Yang, X., Don, C.W., Minami, E., Liu, Y.-W., Weyers, J.J., Mahoney, W.M., Van Biber, B., Cook, S.M., Palpant, N.J., et al. (2014). Human embryonic-stem-cell-derived cardiomyocytes regenerate non-human primate hearts. Nature *510*, 273–277.

Chowdhury, B., Hemming, R., Hombach-Klonisch, S., Flamion, B., and Triggs-Raine, B. (2013). Murine Hyaluronidase 2 Deficiency Results in Extracellular Hyaluronan Accumulation and Severe Cardiopulmonary Dysfunction. J. Biol. Chem. *288*, 520–528.

Chowdhury, B., Xiang, B., Liu, M., Hemming, R., Dolinsky, V.W., and Triggs-Raine, B. (2017). Hyaluronidase 2 Deficiency Causes Increased Mesenchymal Cells, Congenital Heart Defects, and Heart Failure. Circ. Cardiovasc. Genet. *10*, e001598.

Civitarese, R.A., Kapus, A., McCulloch, C.A., and Connelly, K.A. (2017). Role of integrins in mediating cardiac fibroblast–cardiomyocyte cross talk: a dynamic relationship in cardiac biology and pathophysiology. Basic Res. Cardiol. *112*.

Conradi, L., Schmidt, S., Neofytou, E., Deuse, T., Peters, L., Eder, A., Hua, X., Hansen, A., Robbins, R.C., Beygui, R.E., et al. (2015). Immunobiology of Fibrin-Based Engineered Heart Tissue: EHT Immunobiology. STEM CELLS Transl. Med. *4*, 625–631.

Dalen, J.E., Alpert, J.S., Goldberg, R.J., and Weinstein, R.S. (2014). The Epidemic of the 20th Century: Coronary Heart Disease. Am. J. Med. *127*, 807–812.

Dallon, J.C., and Ehrlich, H.P. (2008). A review of fibroblast-populated collagen lattices. Wound Repair Regen. *16*, 472–479.

Djabourov, M., Lechaire, J.P., and Gaill, F. (1993). Structure and rheology of gelatin and collagen gels. Biorheology *30*, 191–205.

Dobaczewski, M., Chen, W., and Frangogiannis, N.G. (2011). Transforming growth factor (TGF)-ß signaling in cardiac remodeling. J. Mol. Cell. Cardiol. *51*, 600–606.

Doppler, S.A., Deutsch, M.-A., Lange, R., and Krane, M. (2013). Cardiac regeneration: current therapies—future concepts. J. Thorac. Dis. *5*, 683–697.

Elliott, C.G., Wang, J., Guo, X., Xu, S. -w., Eastwood, M., Guan, J., Leask, A., Conway, S.J., and Hamilton, D.W. (2012). Periostin modulates myofibroblast differentiation during full-thickness cutaneous wound repair. J. Cell Sci. *125*, 121–132.

Engler, A.J., Carag-Krieger, C., Johnson, C.P., Raab, M., Tang, H.-Y., Speicher, D.W., Sanger, J.W., Sanger, J.M., and Discher, D.E. (2008). Embryonic cardiomyocytes beat best on a matrix with heart-like elasticity: scar-like rigidity inhibits beating. J. Cell Sci. *121*, 3794–3802.

Fan, D., Takawale, A., Lee, J., and Kassiri, Z. (2012). Cardiac fibroblasts, fibrosis and extracellular matrix remodeling in heart disease. Fibrogenesis Tissue Repair *5*, 15.

Fatima, F., Ekstrom, K., Nazarenko, I., Maugeri, M., Valadi, H., Hill, A.F., Camussi, G., and Nawaz, M. (2017). Non-coding RNAs in Mesenchymal Stem Cell-Derived Extracellular Vesicles: Deciphering Regulatory Roles in Stem Cell Potency, Inflammatory Resolve, and Tissue Regeneration. Front. Genet. *8*.

Fisher, S.A., and Periasamy, M. (1994). Collagen Synthesis Inhibitors Disrupt Embryonic Cardiocyte Myofibrillogenesis and Alter the Expression of Cardiac Specific Genes in Vitro. J. Mol. Cell. Cardiol. *26*, 721–731.

Fong, A.H., Romero-López, M., Heylman, C.M., Keating, M., Tran, D., Sobrino, A., Tran, A.Q., Pham, H.H., Fimbres, C., Gershon, P.D., et al. (2016). Three-Dimensional Adult Cardiac

Extracellular Matrix Promotes Maturation of Human Induced Pluripotent Stem Cell-Derived Cardiomyocytes. Tissue Eng. Part A *22*, 1016–1025.

Frangogiannis, N.G. (2005). Critical Role of Endogenous Thrombospondin-1 in Preventing Expansion of Healing Myocardial Infarcts. Circulation *111*, 2935–2942.

Frangogiannis, N.G., Michael, L.H., and Entman, M.L. (2000). Myofibroblasts in reperfused myocardial infarcts express the embryonic form of smooth muscle myosin heavy chain (SMemb). Cardiovasc. Res. *48*, 89–100.

Gafni, O., Weinberger, L., Mansour, A.A., Manor, Y.S., Chomsky, E., Ben-Yosef, D., Kalma, Y., Viukov, S., Maza, I., Zviran, A., et al. (2013). Derivation of novel human ground state naive pluripotent stem cells. Nature *504*, 282–286.

Galie, P.A., Westfall, M.V., and Stegemann, J.P. (2011). Reduced serum content and increased matrix stiffness promote the cardiac myofibroblast transition in 3D collagen matrices. Cardiovasc. Pathol. Off. J. Soc. Cardiovasc. Pathol. *20*, 325–333.

Gaudesius, G. (2003). Coupling of Cardiac Electrical Activity Over Extended Distances by Fibroblasts of Cardiac Origin. Circ. Res. *93*, 421–428.

Gepstein, L. (2002). Derivation and Potential Applications of Human Embryonic Stem Cells. Circ. Res. *91*, 866–876.

Ghatak, S., Misra, S., Norris, R.A., Moreno-Rodriguez, R.A., Hoffman, S., Levine, R.A., Hascall, V.C., and Markwald, R.R. (2014). Periostin Induces Intracellular Cross-talk between Kinases and Hyaluronan in Atrioventricular Valvulogenesis. J. Biol. Chem. *289*, 8545–8561.

Gittenberger-de Groot, A.C., Winter, E.M., Bartelings, M.M., Jose Goumans, M., DeRuiter, M.C., and Poelmann, R.E. (2012). The arterial and cardiac epicardium in development, disease and repair. Differentiation *84*, 41–53.

Gray, M.O., Long, C.S., Kalinyak, J.E., Li, H.T., and Karliner, J.S. (1998). Angiotensin II stimulates cardiac myocyte hypertrophy via paracrine release of TGF-beta 1 and endothelin-1 from fibroblasts. Cardiovasc. Res. *40*, 352–363.

Gregorio, C.C., and Antin, P.B. (2000). To the heart of myofibril assembly. Trends Cell Biol. *10*, 355–362.

Grishina, Elina (2017). The role of RAF1 mutations in human cardiomyocytes and stroma cells. Master thesis. Institute of Pharmacology and Toxicology, Göttingen University.

Guyette, J.P., Charest, J.M., Mills, R.W., Jank, B.J., Moser, P.T., Gilpin, S.E., Gershlak, J.R., Okamoto, T., Gonzalez, G., Milan, D.J., et al. (2016). Bioengineering Human Myocardium on Native Extracellular MatrixNovelty and Significance. Circ. Res. *118*, 56–72.

Hanley, K.P., Oakley, F., Sugden, S., Wilson, D.I., Mann, D.A., and Hanley, N.A. (2008). Ectopic SOX9 Mediates Extracellular Matrix Deposition Characteristic of Organ Fibrosis. J. Biol. Chem. *283*, 14063–14071.

Harada, H., and Takahashi, M. (2007). CD44-dependent Intracellular and Extracellular Catabolism of Hyaluronic Acid by Hyaluronidase-1 and -2. J. Biol. Chem. *282*, 5597–5607.

Hartmann, S. (2016). Modulation of Cardiac Fibroblast to Myofibroblast Transition by Rho Associated Kinases ROCK1 and ROCK2. Doctoral thesis. Institute of Pharmacology and Toxicology, University Göttingen.

Hatano, S., Kimata, K., Hiraiwa, N., Kusakabe, M., Isogai, Z., Adachi, E., Shinomura, T., and Watanabe, H. (2012). Versican/PG-M is essential for ventricular septal formation subsequent to cardiac atrioventricular cushion development. Glycobiology *22*, 1268–1277.

Hayashi, T., and Hoffman, M.P. (2017). Exosomal microRNA communication between tissues during organogenesis. RNA Biol. *14*, 1683–1689.

Hellman, U., Malm, L., Ma, L.-P., Larsson, G., Mörner, S., Fu, M., Engström-Laurent, A., and Waldenström, A. (2010). Growth Factor PDGF-BB Stimulates Cultured Cardiomyocytes to Synthesize the Extracellular Matrix Component Hyaluronan. PLoS ONE *5*.

Hellström, M. (2007). Hyaluronan and the receptor CD 44 in the heart and vessels: a study in normal and pathological conditions. Univ.

Herum, K.M., Lunde, I.G., McCulloch, A.D., and Christensen, G. (2017). The Soft- and Hard-Heartedness of Cardiac Fibroblasts: Mechanotransduction Signaling Pathways in Fibrosis of the Heart. J. Clin. Med. *6*.

Hewitt, K.J., Shamis, Y., Hayman, R.B., Margvelashvili, M., Dong, S., Carlson, M.W., and Garlick, J.A. (2011). Epigenetic and Phenotypic Profile of Fibroblasts Derived from Induced Pluripotent Stem Cells. PLoS ONE *6*.

Hinz, B., Celetta, G., Tomasek, J.J., Gabbiani, G., and Chaponnier, C. (2001). Alpha-smooth muscle actin expression upregulates fibroblast contractile activity. Mol. Biol. Cell *12*, 2730–2741.

Hirschy, A., Schatzmann, F., Ehler, E., and Perriard, J.-C. (2006). Establishment of cardiac cytoarchitecture in the developing mouse heart. Dev. Biol. *289*, 430–441.

Huang, D.W., Sherman, B.T., and Lempicki, R.A. (2009a). Bioinformatics enrichment tools: paths toward the comprehensive functional analysis of large gene lists. Nucleic Acids Res. *37*, 1–13.

Huang, D.W., Sherman, B.T., Zheng, X., Yang, J., Imamichi, T., Stephens, R., and Lempicki, R.A. (2009b). Extracting biological meaning from large gene lists with DAVID. Curr. Protoc. Bioinforma. *Chapter 13*, Unit 13.11.

Hulsen, T., de Vlieg, J., and Alkema, W. (2008). BioVenn – a web application for the comparison and visualization of biological lists using area-proportional Venn diagrams. BMC Genomics *9*, 488.

Ieda, M., Tsuchihashi, T., Ivey, K.N., Ross, R.S., Hong, T.-T., Shaw, R.M., and Srivastava, D. (2009). Cardiac Fibroblasts Regulate Myocardial Proliferation through β1 Integrin Signaling. Dev. Cell *16*, 233–244.

Irion, S., Luche, H., Gadue, P., Fehling, H.J., Kennedy, M., and Keller, G. (2007). Identification and targeting of the ROSA26 locus in human embryonic stem cells. Nat. Biotechnol. *25*, 1477.

Ishikawa, K., Fish, K., Aguero, J., Yaniz-Galende, E., Jeong, D., Kho, C., Tilemann, L., Fish, L., Liang, L., Eltoukhy, A.A., et al. (2015). Stem Cell Factor Gene Transfer Improves Cardiac Function After Myocardial Infarction in Swine clinical perspective. Circ. Heart Fail. *8*, 167–174.

Ivey, M.J., and Tallquist, M.D. (2016). Defining the Cardiac Fibroblast. Circ. J. Off. J. Jpn. Circ. Soc. *80*, 2269–2276.

Ivey, M.J., Kuwabara, J.T., Pai, J.T., Moore, R.E., Sun, Z., and Tallquist, M.D. (2018). Resident fibroblast expansion during cardiac growth and remodeling. J. Mol. Cell. Cardiol. *114*, 161–174.

Iyer, D., Gambardella, L., Bernard, W.G., Serrano, F., Mascetti, V.L., Pedersen, R.A., Talasila, A., and Sinha, S. (2015). Robust derivation of epicardium and its differentiated smooth muscle cell progeny from human pluripotent stem cells. Dev. Camb. Engl. *142*, 1528–1541.

Jackman, C.P., Ganapathi, A.M., Asfour, H., Qian, Y., Allen, B.W., Li, Y., and Bursac, N. (2018). Engineered cardiac tissue patch maintains structural and electrical properties after epicardial implantation. Biomaterials *159*, 48–58.

Jacot, J.G., Martin, J.C., and Hunt, D.L. (2010). Mechanobiology of cardiomyocyte development. J. Biomech. *43*, 93–98.

Jansen, K.A., Bacabac, R.G., Piechocka, I.K., and Koenderink, G.H. (2013). Cells Actively Stiffen Fibrin Networks by Generating Contractile Stress. Biophys. J. *105*, 2240–2251.

Jenkins, R.H., Thomas, G.J., Williams, J.D., and Steadman, R. (2004). Myofibroblastic Differentiation Leads to Hyaluronan Accumulation through Reduced Hyaluronan Turnover. J. Biol. Chem. *279*, 41453–41460.

Jiang, Z.-S., Jeyaraman, M., Wen, G.-B., Fandrich, R.R., Dixon, I.M.C., Cattini, P.A., and Kardami, E. (2007). High- but not low-molecular weight FGF-2 causes cardiac hypertrophy in vivo; possible involvement of cardiotrophin-1. J. Mol. Cell. Cardiol. *42*, 222–233.

Johnson, R.J., Bradbury, L.L., Martin, K., Neuberger, J., and UK Transplant Registry (2014). Organ donation and transplantation in the UK-the last decade: a report from the UK national transplant registry. Transplantation *97 Suppl 1*, S1–S27.

Jokinen, J., Dadu, E., Nykvist, P., Käpylä, J., White, D.J., Ivaska, J., Vehviläinen, P., Reunanen, H., Larjava, H., Häkkinen, L., et al. (2004). Integrin-mediated Cell Adhesion to Type I Collagen Fibrils. J. Biol. Chem. *279*, 31956–31963.

Jóna, I., and Nánási, P.P. (2006). Cardiomyopathies and sudden cardiac death caused by RyR2 mutations: Are the channels the beginning and the end? Cardiovasc. Res. *71*, 416–418.

Josowitz, R., Mulero-Navarro, S., Rodriguez, N.A., Falce, C., Cohen, N., Ullian, E.M., Weiss, L.A., Rauen, K.A., Sobie, E.A., and Gelb, B.D. (2016). Autonomous and Non-autonomous Defects Underlie Hypertrophic Cardiomyopathy in BRAF-Mutant hiPSC-Derived Cardiomyocytes. Stem Cell Rep. *7*, 355–369.

Kakkar, R., and Lee, R.T. (2010). Intramyocardial Fibroblast Myocyte Communication. Circ. Res. *106*, 47–57.

Kanisicak, O., Khalil, H., Ivey, M.J., Karch, J., Maliken, B.D., Correll, R.N., Brody, M.J., Lin, S.-C.J., Aronow, B.J., Tallquist, M.D., et al. (2016). Genetic lineage tracing defines myofibroblast origin and function in the injured heart. Nat. Commun. *7*, 12260.

Karakikes, I., Ameen, M., Termglinchan, V., and Wu, J.C. (2015). Human Induced Pluripotent Stem Cell-Derived Cardiomyocytes: Insights into Molecular, Cellular, and Functional Phenotypes. Circ. Res. *117*, 80–88.

Karikkineth, B.C., and Zimmermann, W.-H. (2013). Myocardial tissue engineering and heart muscle repair. Curr. Pharm. Biotechnol. *14*, 4–11.

Kaur, H., Takefuji, M., Ngai, C.Y., Carvalho, J., Bayer, J., Wietelmann, A., Poetsch, A., Hoelper, S., Conway, S.J., Möllmann, H., et al. (2016). Targeted Ablation of Periostin-Expressing Activated Fibroblasts Prevents Adverse Cardiac Remodeling in Mice. Circ. Res. *118*, 1906–1917.

Kawaguchi, M., Takahashi, M., Hata, T., Kashima, Y., Usui, F., Morimoto, H., Izawa, A., Takahashi, Y., Masumoto, J., Koyama, J., et al. (2011). Inflammasome Activation of Cardiac Fibroblasts Is Essential for Myocardial Ischemia/Reperfusion InjuryClinical Perspective. Circulation *123*, 594–604.

Keller, K.E., Sun, Y.Y., Vranka, J.A., Hayashi, L., and Acott, T.S. (2012). Inhibition of Hyaluronan Synthesis Reduces Versican and Fibronectin Levels in Trabecular Meshwork Cells. PLoS ONE *7*.

Kensah, G., Roa Lara, A., Dahlmann, J., Zweigerdt, R., Schwanke, K., Hegermann, J., Skvorc, D., Gawol, A., Azizian, A., Wagner, S., et al. (2013). Murine and human pluripotent stem cell-derived cardiac bodies form contractile myocardial tissue in vitro. Eur. Heart J. *34*, 1134–1146.

Kittleson, M.M. (2016). Changing Role of Heart Transplantation. Heart Fail. Clin. *12*, 411–421.

Klein, C.E., Dressel, D., Steinmayer, T., Mauch, C., Eckes, B., Krieg, T., Bankert, R.B., and Weber, L. (1991). Integrin alpha 2 beta 1 is upregulated in fibroblasts and highly aggressive melanoma cells in three-dimensional collagen lattices and mediates the reorganization of collagen I fibrils. J. Cell Biol. *115*, 1427–1436.

Kohl, P. (2003). Heterogeneous Cell Coupling in the Heart: An Electrophysiological Role for Fibroblasts. Circ. Res. *93*, 381–383.

Kohl, P., and Gourdie, R.G. (2014). Fibroblast–myocyte electrotonic coupling: Does it occur in native cardiac tissue? J. Mol. Cell. Cardiol. *70*, 37–46.

Kondo, S., Kagami, S., Urushihara, M., Kitamura, A., Shimizu, M., Strutz, F., Müller, G.A., and Kuroda, Y. (2004). Transforming growth factor-β1 stimulates collagen matrix remodeling through increased adhesive and contractive potential by human renal fibroblasts. Biochim. Biophys. Acta BBA - Mol. Cell Res. *1693*, 91–100.

Lacraz, G.P.A., Junker, J.P., Gladka, M.M., Molenaar, B., Scholman, K.T., Vigil-Garcia, M., Versteeg, D., de Ruiter, H., Vermunt, M.W., Creyghton, M.P., et al. (2017). Tomo-Seq Identifies SOX9 as a Key Regulator of Cardiac Fibrosis During Ischemic Injury. Circulation *136*, 1396–1409.

Langmead, B., and Salzberg, S.L. (2012). Fast gapped-read alignment with Bowtie 2. Nat. Methods *9*, 357.

Leask, A., Holmes, A., Black, C.M., and Abraham, D.J. (2003). Connective Tissue Growth Factor Gene Regulation: Requirements for its induction by transforming growth factor ß2 in fibroblasts. J. Biol. Chem. *278*, 13008–13015.

Lee, S., Serpooshan, V., Tong, X., Venkatraman, S., Lee, M., Lee, J., Chirikian, O., Wu, J.C., Wu, S.M., and Yang, F. (2017). Contractile force generation by 3D hiPSC-derived cardiac tissues is enhanced by rapid establishment of cellular interconnection in matrix with muscle-mimicking stiffness. Biomaterials *131*, 111–120.

Lemoine, M.D., Mannhardt, I., Breckwoldt, K., Prondzynski, M., Flenner, F., Ulmer, B., Hirt, M.N., Neuber, C., Horváth, A., Kloth, B., et al. (2017). Human iPSC-derived cardiomyocytes cultured in 3D engineered heart tissue show physiological upstroke velocity and sodium current density. Sci. Rep. *7*.

Li, P., Cavallero, S., Gu, Y., Chen, T.H.P., Hughes, J., Hassan, A.B., Brüning, J.C., Pashmforoush, M., and Sucov, H.M. (2011). IGF signaling directs ventricular cardiomyocyte proliferation during embryonic heart development. Dev. Camb. Engl. *138*, 1795–1805.

Liau, B., Christoforou, N., Leong, K.W., and Bursac, N. (2011). Pluripotent stem cell-derived cardiac tissue patch with advanced structure and function. Biomaterials *32*, 9180–9187.

Liau, B., Jackman, C.P., Li, Y., and Bursac, N. (2017). Developmental stage-dependent effects of cardiac fibroblasts on function of stem cell-derived engineered cardiac tissues. Sci. Rep. *7*, 42290.

Liaw, N.Y., and Zimmermann, W.-H. (2016). Mechanical stimulation in the engineering of heart muscle. Adv. Drug Deliv. Rev. *96*, 156–160.

Lijnen, P., Petrov, V., Rumilla, K., and Fagard, R. (2003). Transforming growth factor-beta 1 promotes contraction of collagen gel by cardiac fibroblasts through their differentiation into myofibroblasts. Methods Find. Exp. Clin. Pharmacol. *25*, 79–86.

Lin, C.-H., Yu, M.-C., Tung, W.-H., Chen, T.-T., Yu, C.-C., Weng, C.-M., Tsai, Y.-J., Bai, K.-J., Hong, C.-Y., Chien, M.-H., et al. (2013). Connective tissue growth factor induces collagen I expression in human lung fibroblasts through the Rac1/MLK3/JNK/AP-1 pathway. Biochim. Biophys. Acta BBA - Mol. Cell Res. *1833*, 2823–2833.

Long, C., Li, H., Tiburcy, M., Rodriguez-Caycedo, C., Kyrychenko, V., Zhou, H., Zhang, Y., Min, Y.-L., Shelton, J.M., Mammen, P.P.A., et al. (2018). Correction of diverse muscular dystrophy mutations in human engineered heart muscle by single-site genome editing. Sci. Adv. *4*.

Luigi, Anastasia, Maurilio Sampaolesi, Nadia Papini, Diego Oleari, Giuseppe Lamorte, Cristina Tringali, Eugenio, Monti, Daniela Galli, Guido Tettamanti, Giulio Cossu, and Bruno Venerando (2006). Reversine-treated fibroblasts acquire myogenic competence in vitro and in regenerating skeletal muscle..pdf.

Lund, L.H., Edwards, L.B., Kucheryavaya, A.Y., Benden, C., Christie, J.D., Dipchand, A.I., Dobbels, F., Goldfarb, S.B., Levvey, B.J., Meiser, B., et al. (2014). The Registry of the International Society for Heart and Lung Transplantation: Thirty-first Official Adult Heart Transplant Report—2014; Focus Theme: Retransplantation. J. Heart Lung Transplant. *33*, 996–1008.

Ma, L. (2005). Bmp2 is essential for cardiac cushion epithelial-mesenchymal transition and myocardial patterning. Development *132*, 5601–5611.

Mahoney, V.M., Mezzano, V., Mirams, G.R., Maass, K., Li, Z., Cerrone, M., Vasquez, C., Bapat, A., Delmar, M., and Morley, G.E. (2016). Connexin43 contributes to electrotonic conduction across scar tissue in the intact heart. Sci. Rep. *6*.

Mannhardt, I., Breckwoldt, K., Letuffe-Brenière, D., Schaaf, S., Schulz, H., Neuber, C., Benzin, A., Werner, T., Eder, A., Schulze, T., et al. (2016). Human Engineered Heart Tissue: Analysis of Contractile Force. Stem Cell Rep. *7*, 29–42.

Marín-García, J. (2007). Aging and the Heart: A Post-Genomic View (Springer Science & Business Media).

Mendis, S., Puska, P., and Norrving, B. (2011). Global atlas on cardiovascular disease prevention and control (Geneva: World Health Organization in collaboration with the World Heart Federation and the World Stroke Organization).

Meran, S., Luo, D.D., Simpson, R., Martin, J., Wells, A., Steadman, R., and Phillips, A.O. (2011). Hyaluronan Facilitates Transforming Growth Factor-β1-dependent Proliferation via CD44 and Epidermal Growth Factor Receptor Interaction. J. Biol. Chem. *286*, 17618–17630.

Missinato, M.A., Tobita, K., Romano, N., Carroll, J.A., and Tsang, M. (2015). Extracellular component hyaluronic acid and its receptor Hmmr are required for epicardial EMT during heart regeneration. Cardiovasc. Res. *107*, 487–498.

Miyamoto, K., Akiyama, M., Tamura, F., Isomi, M., Yamakawa, H., Sadahiro, T., Muraoka, N., Kojima, H., Haginiwa, S., Kurotsu, S., et al. (2018). Direct In Vivo Reprogramming with Sendai Virus Vectors Improves Cardiac Function after Myocardial Infarction. Cell Stem Cell *22*, 91-103.e5.

Montesano, R., and Orci, L. (1988). Transforming growth factor beta stimulates collagen-matrix contraction by fibroblasts: implications for wound healing. Proc. Natl. Acad. Sci. U. S. A. *85*, 4894–4897.

Moore-Morris, T., Guimarães-Camboa, N., Banerjee, I., Zambon, A.C., Kisseleva, T., Velayoudon, A., Stallcup, W.B., Gu, Y., Dalton, N.D., Cedenilla, M., et al. (2014). Resident fibroblast lineages mediate pressure overload–induced cardiac fibrosis. J. Clin. Invest. *124*, 2921–2934.

Mosterd, A., and Hoes, A.W. (2007). Clinical epidemiology of heart failure. Heart *93*, 1137–1146.

Müller, J., Gorressen, S., Grandoch, M., Feldmann, K., Kretschmer, I., Lehr, S., Ding, Z., Schmitt, J.P., Schrader, J., Garbers, C., et al. (2014). Interleukin-6-dependent phenotypic modulation of cardiac fibroblasts after acute myocardial infarction. Basic Res. Cardiol. *109*, 440.

Nag, A.C. (1980). Study of non-muscle cells of the adult mammalian heart: a fine structural analysis and distribution. Cytobios *28*, 41–61.

Naito, H., Melnychenko, I., Didié, M., Schneiderbanger, K., Schubert, P., Rosenkranz, S., Eschenhagen, T., and Zimmermann, W.-H. (2006). Optimizing Engineered Heart Tissue for Therapeutic Applications as Surrogate Heart Muscle. Circulation *114*, I-72-I–78.

Nam, Y.-J., Song, K., Luo, X., Daniel, E., Lambeth, K., West, K., Hill, J.A., DiMaio, J.M., Baker, L.A., and Bassel-Duby, R. (2013). Reprogramming of human fibroblasts toward a cardiac fate. Proc. Natl. Acad. Sci. *110*, 5588–5593.

Nelson, T.J., Martinez-Fernandez, A., Yamada, S., Perez-Terzic, C., Ikeda, Y., and Terzic, A. (2009). Repair of Acute Myocardial Infarction by Human Stemness Factors Induced Pluripotent Stem Cells. Circulation *120*, 408–416.

Nichol, J.W., Engelmayr, G.C., Cheng, M., and Freed, L.E. (2008). Co-culture induces alignment in engineered cardiac constructs via MMP-2 expression. Biochem. Biophys. Res. Commun. *373*, 360–365.

Nishiyama, T., Horii, I., Nakayama, Y., Ozawa, T., and Hayashi, T. (1990). A Distinct Characteristic of the Quiescent State of Human Dermal Fibroblasts in Contracted Collagen Gel as Revealed by No Response to Epidermal Growth Factor Alone, But a Positive Growth Response to a Combination of the Growth Factor and Saikosaponin b1. Matrix *10*, 412–419.

Norris, R.A., Damon, B., Mironov, V., Kasyanov, V., Ramamurthi, A., Moreno-Rodriguez, R., Trusk, T., Potts, J.D., Goodwin, R.L., Davis, J., et al. (2007). Periostin regulates collagen fibrillogenesis and the biomechanical properties of connective tissues. J. Cell. Biochem. *101*, 695–711.

Nussbaum, J., Minami, E., Laflamme, M.A., Virag, J.A.I., Ware, C.B., Masino, A., Muskheli, V., Pabon, L., Reinecke, H., and Murry, C.E. (2007). Transplantation of undifferentiated murine embryonic stem cells in the heart: teratoma formation and immune response. FASEB J. Off. Publ. Fed. Am. Soc. Exp. Biol. *21*, 1345–1357.

Ogle, B.M., Bursac, N., Domian, I., Huang, N.F., Menasché, P., Murry, C.E., Pruitt, B., Radisic, M., Wu, J.C., Wu, S.M., et al. (2016). Distilling complexity to advance cardiac tissue engineering. Sci. Transl. Med. *8*, 342ps13.

Ohtani, K., Yutani, C., Nagata, S., Koretsune, Y., Hori, M., and Kamada, T. (1995). High prevalence of atrial fibrosis in patients with dilated cardiomyopathy. J. Am. Coll. Cardiol. *25*, 1162–1169.

Olaso, E., Labrador, J.-P., Wang, L., Ikeda, K., Eng, F.J., Klein, R., Lovett, D.H., Lin, H.C., and Friedman, S.L. (2002). Discoidin Domain Receptor 2 Regulates Fibroblast Proliferation and Migration through the Extracellular Matrix in Association with Transcriptional Activation of Matrix Metalloproteinase-2. J. Biol. Chem. *277*, 3606–3613.

Olivey, H.E., Mundell, N.A., Austin, A.F., and Barnett, J.V. (2006). Transforming growth factor-ß stimuluates epithelial- to mesenchymal transformation in the proepicardium. Dev. Dyn. Off. Publ. Am. Assoc. Anat. *235*, 50–59.

Ongstad, E., and Kohl, P. (2016). Fibroblast-Myocyte Coupling in the Heart: Potential Relevance for Therapeutic Interventions. J. Mol. Cell. Cardiol. *91*, 238–246.

Parikh, S.S., Blackwell, D.J., Gomez-Hurtado, N., Frisk, M., Wang, L., Kim, K., Dahl, C.P., Fiane, A., Tønnessen, T., Kryshtal, D.O., et al. (2017). Thyroid and Glucocorticoid Hormones Promote Functional T-Tubule Development in Human-Induced Pluripotent Stem Cell–Derived Cardiomyocytes Novelty and Significance. Circ. Res. *121*, 1323–1330.

Pedrotty, D.M., Klinger, R.Y., Badie, N., Hinds, S., Kardashian, A., and Bursac, N. (2008). Structural coupling of cardiomyocytes and noncardiomyocytes: quantitative comparisons using a novel micropatterned cell pair assay. Am. J. Physiol. Heart Circ. Physiol. *295*, H390-400.

Pellieux, C., Foletti, A., Peduto, G., Aubert, J.-F., Nussberger, J., Beermann, F., Brunner, H.-R., and Pedrazzini, T. (2001). Dilated cardiomyopathy and impaired cardiac hypertrophic response to angiotensin II in mice lacking FGF-2. J. Clin. Invest. *108*, 1843–1851.

Petrov, V.V., Fagard, R.H., and Lijnen, P.J. (2002). Stimulation of Collagen Production by Transforming Growth Factor-ß1 During Differentiation of Cardiac Fibroblasts to Myofibroblasts. Hypertension *39*, 258–263.

Phillips, P.D., and Cristofalo, V.J. (1980). A procedure for the serum-free growth of normal human diploid fibroblasts. J. Tissue Cult. Methods *6*, 123–126.

Pinto, A.R., Ilinykh, A., Ivey, M.J., Kuwabara, J.T., D'Antoni, M., Debuque, R.J., Chandran, A., Wang, L., Arora, K., Rosenthal, N., et al. (2015). Revisiting Cardiac Cellular Composition. Circ. Res. CIRCRESAHA.115.307778.

Ponikowski, P., Voors, A.A., Anker, S.D., Bueno, H., Cleland, J.G.F., Coats, A.J.S., Falk, V., González-Juanatey, J.R., Harjola, V.-P., Jankowska, E.A., et al. (2016). 2016 ESC Guidelines for the diagnosis and treatment of acute and chronic heart failure: The Task Force for the diagnosis and treatment of acute and chronic heart failure of the European Society of Cardiology (ESC). Developed with the spec. Eur. J. Heart Fail. *18*, 891–975.

Porsch, H., Bernert, B., Mehić, M., Theocharis, A.D., Heldin, C.-H., and Heldin, P. (2013). Efficient TGFß-induced epithelial–mesenchymal transition depends on hyaluronan synthase HAS2. Oncogene *32*, 4355–4365.

Quaife-Ryan, G.A., Sim, C.B., Ziemann, M., Kaspi, A., Rafehi, H., Ramialison, M., El-Osta, A., Hudson, J.E., and Porrello, E.R. (2017). Multicellular Transcriptional Analysis of Mammalian Heart Regeneration. Circulation *136*, 1123–1139.

Reubinoff, B.E., Pera, M.F., Fong, C.Y., Trounson, A., and Bongso, A. (2000). Embryonic stem cell lines from human blastocysts: somatic differentiation in vitro. Nat. Biotechnol. *18*, 399–404.

Rhee, S. (2009). Fibroblasts in three dimensional matrices: cell migration and matrix remodeling. Exp. Mol. Med. *41*, 858–865.

Rhee, S., and Grinnell, F. (2007). Fibroblast mechanics in 3D collagen matrices. Adv. Drug Deliv. Rev. *59*, 1299–1305.

Ribeiro, A.J.S., Ang, Y.-S., Fu, J.-D., Rivas, R.N., Mohamed, T.M.A., Higgs, G.C., Srivastava, D., and Pruitt, B.L. (2015). Contractility of single cardiomyocytes differentiated from pluripotent stem cells depends on physiological shape and substrate stiffness. Proc. Natl. Acad. Sci. U. S. A. *112*, 12705–12710.

Rienks, M., Papageorgiou, A.-P., Frangogiannis, N.G., and Heymans, S. (2014). Myocardial Extracellular Matrix: An Ever-Changing and Diverse Entity. Circ. Res. *114*, 872–888.

Sano, M., Fukuda, K., Kodama, H., Pan, J., Saito, M., Matsuzaki, J., Takahashi, T., Makino, S., Kato, T., and Ogawa, S. (2000). Interleukin-6 Family of Cytokines Mediate Angiotensin II-induced Cardiac Hypertrophy in Rodent Cardiomyocytes. J. Biol. Chem. *275*, 29717–29723.

Sarkar, S., Vellaichamy, E., Young, D., and Sen, S. (2004). Influence of cytokines and growth factors in ANG II-mediated collagen upregulation by fibroblasts in rats: role of myocytes. Am. J. Physiol. Heart Circ. Physiol. *287*, H107-117.

Sassi, Y., Ahles, A., Truong, D.-J.J., Baqi, Y., Lee, S.-Y., Husse, B., Hulot, J.-S., Foinquinos, A., Thum, T., Müller, C.E., et al. (2014). Cardiac myocyte-secreted cAMP exerts paracrine action via adenosine receptor activation. J. Clin. Invest. *124*, 5385–5397.

Sassi, Y., Avramopoulos, P., Ramanujam, D., Grüter, L., Werfel, S., Giosele, S., Brunner, A.-D., Esfandyari, D., Papadopoulou, A.S., Strooper, B., et al. (2017). Cardiac myocyte miR-29 promotes pathological remodeling of the heart by activating Wnt signaling. Nat. Commun. *8*, 1614.

Schaaf, S., Eder, A., Vollert, I., Stöhr, A., Hansen, A., and Eschenhagen, T. (2014). Generation of Strip-Format Fibrin-Based Engineered Heart Tissue (EHT). In Cardiac Tissue Engineering, (Humana Press, New York, NY), pp. 121–129.

Schiro, J.A., Chan, B.M.C., Roswit, W.T., Kassner, P.D., Pentland, A.P., Hemler, M.E., Eisen, A.Z., and Kupper, T.S. (1991). Integrin α2β1 (VLA-2) mediates reorganization and contraction of collagen matrices by human cells. Cell *67*, 403–410.

Schlick, S.F., Spreckelsen, F., Tiburcy, M., Iyer, L.M., Zelarayan, L.C., Luther, S., Parlitz, U., Zimmermann, W.H., and Rehfeldt, F. (2018). Agonistic and antagonistic roles of fibroblasts and cardiomyocytes on viscoelastic stiffening of engineered human myocardium. Prog. Biophys. Mol. Biol. pii: S0079-6107(18)30159-7. doi: 10.1016/j.pbiomolbio.2018.11.011.

Schroer, A.K., and Merryman, W.D. (2015). Mechanobiology of myofibroblast adhesion in fibrotic cardiac disease. J. Cell Sci. *128*, 1865–1875.

Schultz, J.E.J., Witt, S.A., Glascock, B.J., Nieman, M.L., Reiser, P.J., Nix, S.L., Kimball, T.R., and Doetschman, T. (2002). TGF-β1 mediates the hypertrophic cardiomyocyte growth induced by angiotensin II. J. Clin. Invest. *109*, 787–796.

Severs, N. (2000). The cardiac muscle cell. BioEssays 22188–199 © 2000 John Wiley Sons Inc.

Shai, S.-Y., Harpf, A.E., Babbitt, C.J., Jordan, M.C., Fishbein, M.C., Chen, J., Omura, M., Leil, T.A., Becker, K.D., Jiang, M., et al. (2002). Cardiac Myocyte-Specific Excision of the β1 Integrin Gene Results in Myocardial Fibrosis and Cardiac Failure. Circ. Res. *90*, 458–464.

Shiojima, I., Aikawa, M., Suzuki, J., Yazaki, Y., and Nagai, R. (1999). Embryonic smooth muscle myosin heavy chain SMemb is expressed in pressure-overloaded cardiac fibroblasts. Jpn. Heart J. *40*, 803–818.

Shirai, M., Imanaka-Yoshida, K., Schneider, M.D., Schwartz, R.J., and Morisaki, T. (2009). T-box 2, a mediator of Bmp-Smad signaling, induced hyaluronan synthase 2 and Tgfβ2 expression and endocardial cushion formation. Proc. Natl. Acad. Sci. U. S. A. *106*, 18604–18609.

Smith, C.L., Baek, S.T., Sung, C.Y., and Tallquist, M.D. (2011). Epicardial-derived cell epithelial-to-mesenchymal transition and fate specification require PDGF receptor signaling. Circ. Res. *108*, e15-26.

Snider, P., Standley, K.N., Wang, J., Azhar, M., Doetschman, T., and Conway, S.J. (2009). Origin of Cardiac Fibroblasts and the Role of Periostin. Circ. Res. *105*, 934–947.

Soares, C.P., Midlej, V., de Oliveira, M.E.W., Benchimol, M., Costa, M.L., and Mermelstein, C. (2012). 2D and 3D-Organized Cardiac Cells Shows Differences in Cellular Morphology, Adhesion Junctions, Presence of Myofibrils and Protein Expression. PLoS ONE *7*.

Song, K., Nam, Y.-J., Luo, X., Qi, X., Tan, W., Huang, G.N., Acharya, A., Smith, C.L., Tallquist, M.D., Neilson, E.G., et al. (2012). Heart repair by reprogramming non-myocytes with cardiac transcription factors. Nature *485*, 599–604.

Soong, P.L., Tiburcy, M., and Zimmermann, W.-H. (2012). Cardiac differentiation of human embryonic stem cells and their assembly into engineered heart muscle. Curr. Protoc. Cell Biol. Editor. Board Juan Bonifacino Al *Chapter 23*, Unit23.8.

Souders, C.A., Bowers, S.L.K., and Baudino, T.A. (2009). Cardiac Fibroblast: The Renaissance Cell. Circ. Res. *105*, 1164–1176.

Spach, M.S., and Boineau, J.P. (1997). Microfibrosis produces electrical load variations due to loss of side-to-side cell connections: a major mechanism of structural heart disease arrhythmias. Pacing Clin. Electrophysiol. PACE *20*, 397–413.

van Spreeuwel, A.C.C., Bax, N.A.M., van Nierop, B.J., Aartsma-Rus, A., Goumans, M.-J.T.H., and Bouten, C.V.C. (2017). Mimicking Cardiac Fibrosis in a Dish: Fibroblast Density Rather than Collagen Density Weakens Cardiomyocyte Function. J Cardiovasc. Transl. Res. *10*, 116–127.

Streckfuss-Bomeke, K., Wolf, F., Azizian, A., Stauske, M., Tiburcy, M., Wagner, S., Hubscher, D., Dressel, R., Chen, S., Jende, J., et al. (2013). Comparative study of human-induced pluripotent stem cells derived from bone marrow cells, hair keratinocytes, and skin fibroblasts. Eur. Heart J. *34*, 2618–2629.

Streckfuss-Bömeke, K., Tiburcy, M., Fomin, A., Luo, X., Li, W., Fischer, C., Özcelik, C., Perrot, A., Sossalla, S., Haas, J., et al. (2017). Severe DCM phenotype of patient harboring RBM20 mutation S635A can be modeled by patient-specific induced pluripotent stem cell-derived cardiomyocytes. J. Mol. Cell. Cardiol.

Sullivan, K.E., and Black, L.D. (2013). The role of cardiac fibroblasts in extracellular matrix-mediated signaling during normal and pathological cardiac development. J. Biomech. Eng. *135*, 071001.

Sun, N., Yazawa, M., Liu, J., Han, L., Sanchez-Freire, V., Abilez, O.J., Navarrete, E.G., Hu, S., Wang, L., Lee, A., et al. (2012). Patient-Specific Induced Pluripotent Stem Cell as a Model for Familial Dilated Cardiomyopathy. Sci. Transl. Med. *4*, 130ra47.

Sur, S. (2016). Control of cardiogenesis and homeostasis by cardiac fibroblasts. Doctoral thesis. Institute of Pharmacology and Toxicology, University Göttingen.

Takahashi, K., Tanabe, K., Ohnuki, M., Narita, M., Ichisaka, T., Tomoda, K., and Yamanaka, S. (2007). Induction of pluripotent stem cells from adult human fibroblasts by defined factors. Cell *131*, 861–872.

Takahashi, M., Yamagishi, T., Narematsu, M., Kamimura, T., Kai, M., and Nakajima, Y. (2014). Epicardium is required for sarcomeric maturation and cardiomyocyte growth in the ventricular compact layer mediated by transforming growth factor ß and fibroblast growth factor before the onset of coronary circulation. Congenit. Anom. *54*, 162–171.

Tan, Y., Han, P., Gu, Q., Chen, G., Wang, L., Ma, R., Wu, J., Feng, C., Zhang, Y., Wang, L., et al. (2016). Generation of clinical-grade functional cardiomyocytes from human embryonic stem cells in chemically defined conditions. J. Tissue Eng. Regen. Med.

Tang, J., Cui, X., Caranasos, T.G., Hensley, M.T., Vandergriff, A.C., Hartanto, Y., Shen, D., Zhang, H., Zhang, J., and Cheng, K. (2017). Heart Repair Using Nanogel-Encapsulated Human Cardiac Stem Cells in Mice and Pigs with Myocardial Infarction. ACS Nano *11*, 9738–9749.

Teekakirikul, P., Padera, R.F., Seidman, J.G., and Seidman, C.E. (2012). Hypertrophic cardiomyopathy: Translating cellular cross talk into therapeutics. J. Cell Biol. *199*, 417–421.

Thannickal, V.J., Lee, D.Y., White, E.S., Cui, Z., Larios, J.M., Chacon, R., Horowitz, J.C., Day, R.M., and Thomas, P.E. (2003). Myofibroblast Differentiation by Transforming Growth Factor-β1 Is Dependent on Cell Adhesion and Integrin Signaling via Focal Adhesion Kinase. J. Biol. Chem. *278*, 12384–12389.

Thomson, J.A., Itskovitz-Eldor, J., Shapiro, S.S., Waknitz, M.A., Swiergiel, J.J., Marshall, V.S., and Jones, J.M. (1998). Embryonic stem cell lines derived from human blastocysts. Science *282*, 1145–1147.

Tiburcy, M., and Zimmermann, W.-H. (2014). Modeling myocardial growth and hypertrophy in engineered heart muscle. Trends Cardiovasc. Med. *24*, 7–13.

Tiburcy, M., Didie, M., Boy, O., Christalla, P., Doker, S., Naito, H., Karikkineth, B.C., El-Armouche, A., Grimm, M., Nose, M., et al. (2011). Terminal Differentiation, Advanced Organotypic Maturation, and Modeling of Hypertrophic Growth in Engineered Heart Tissue. Circ. Res. *109*, 1105–1114.

Tiburcy, M., Meyer, T., Soong, P.L., and Zimmermann, W.-H. (2014). Collagen-Based Engineered Heart Muscle. In Cardiac Tissue Engineering: Methods and Protocols, M. Radisic, and L.D. Black III, eds. (New York, NY: Springer New York), pp. 167–176.

Tiburcy, M., Hudson, J.E., Balfanz, P., Schlick, S., Meyer, T., Liao, M.-L.C., Levent, E., Raad, F., Zeidler, S., Wingender, E., et al. (2017). Defined Engineered Human Myocardium with Advanced Maturation for Applications in Heart Failure Modelling and Repair. Circulation *135*, 1832–1847.

Tien, J.Y.L., and Spicer, A.P. (2005). Three vertebrate hyaluronan synthases are expressed during mouse development in distinct spatial and temporal patterns. Dev. Dyn. Off. Publ. Am. Assoc. Anat. *233*, 130–141.

Tomasek, J.J., Gabbiani, G., Hinz, B., Chaponnier, C., and Brown, R.A. (2002). Myofibroblasts and mechano-regulation of connective tissue remodelling. Nat. Rev. Mol. Cell Biol. *3*, 349–363.

Travers, J.G., Kamal, F.A., Robbins, J., Yutzey, K.E., and Blaxall, B.C. (2016). Cardiac Fibrosis. Circ. Res. *118*, 1021–1040.

Tulla, M., Pentikäinen, O.T., Viitasalo, T., Käpylä, J., Impola, U., Nykvist, P., Nissinen, L., Johnson, M.S., and Heino, J. (2001). Selective Binding of Collagen Subtypes by Integrin α1I, α2I, and α10I Domains. J. Biol. Chem. *276*, 48206–48212.

Unverferth, D.V., Baker, P.B., Swift, S.E., Chaffee, R., Fetters, J.K., Uretsky, B.F., Thompson, M.E., and Leier, C.V. (1986). Extent of myocardial fibrosis and cellular hypertrophy in dilated cardiomyopathy. Am. J. Cardiol. *57*, 816–820.

van der Valk, J., Brunner, D., De Smet, K., Fex Svenningsen, Honegger, P., Knudsen, L.E., Lindl, T., Noraberg, J., Price, A., Scarino, M.L., et al. (2010). Optimization of chemically defined cell culture media – Replacing fetal bovine serum in mammalian in vitro methods. Toxicol. In Vitro *24*, 1053–1063.

Varas, L., Ohlsson, L.B., Honeth, G., Olsson, A., Bengtsson, T., Wiberg, C., Bockermann, R., Järnum, S., Richter, J., Pennington, D., et al. (2007). Alpha10 integrin expression is up-regulated

on fibroblast growth factor-2-treated mesenchymal stem cells with improved chondrogenic differentiation potential. Stem Cells Dev. *16*, 965–978.

Waldenström, A., Martinussen, H.J., Gerdin, B., and Hällgren, R. (1991). Accumulation of hyaluronan and tissue edema in experimental myocardial infarction. J. Clin. Invest. *88*, 1622–1628.

Wang, Q., Yang, H., Bai, A., Jiang, W., Li, X., Wang, X., Mao, Y., Lu, C., Qian, R., Guo, F., et al. (2016). Functional engineered human cardiac patches prepared from nature's platform improve heart function after acute myocardial infarction. Biomaterials *105*, 52–65.

Wang, Q., Wang, H., Li, Z., Wang, Y., Wu, X., and Tan, Y. (2017). Mesenchymal stem cell-loaded cardiac patch promotes epicardial activation and repair of the infarcted myocardium. J. Cell. Mol. Med. *21*, 1751–1766.

Wang, W., Tan, B., Chen, J., Bao, R., Zhang, X., Liang, S., Shang, Y., Liang, W., Cui, Y., Fan, G., et al. (2018). An injectable conductive hydrogel encapsulating plasmid DNA-eNOs and ADSCs for treating myocardial infarction. Biomaterials *160*, 69–81.

Webber, J., Meran, S., Steadman, R., and Phillips, A. (2009a). Hyaluronan Orchestrates Transforming Growth Factor-ß1-dependent Maintenance of Myofibroblast Phenotype. J. Biol. Chem. *284*, 9083–9092.

Webber, J., Jenkins, R.H., Meran, S., Phillips, A., and Steadman, R. (2009b). Modulation of TGFß1-Dependent Myofibroblast Differentiation by Hyaluronan. Am. J. Pathol. *175*, 148–160.

Weber, K.T., Sun, Y., Bhattacharya, S.K., Ahokas, R.A., and Gerling, I.C. (2013). Myofibroblast-mediated mechanisms of pathological remodelling of the heart. Nat. Rev. Cardiol. *10*, 15–26.

Whelan, R.S., Kaplinskiy, V., and Kitsis, R.N. (2010). Cell Death in the Pathogenesis of Heart Disease: Mechanisms and Significance. Annu. Rev. Physiol. *72*, 19–44.

Witty, A.D., Mihic, A., Tam, R.Y., Fisher, S.A., Mikryukov, A., Shoichet, M.S., Li, R.-K., Kattman, S.J., and Keller, G. (2014). Generation of the epicardial lineage from human pluripotent stem cells. Nat. Biotechnol. *32*, 1026–1035.

Wrobel, L.K., Fray, T.R., Molloy, J.E., Adams, J.J., Armitage, M.P., and Sparrow, J.C. (2002). Contractility of single human dermal myofibroblasts and fibroblasts. Cell Motil. Cytoskeleton *52*, 82–90.

Xie, J., Zhang, Q., Zhu, T., Zhang, Y., Liu, B., Xu, J., and Zhao, H. (2014). Substrate stiffness-regulated matrix metalloproteinase output in myocardial cells and cardiac fibroblasts: Implications for myocardial fibrosis. Acta Biomater. *10*, 2463–2472.

Yang, T.-H., Thoreson, A.R., Gingery, A., An, K.-N., Larson, D.R., Zhao, C., and Amadio, P.C. (2015). Collagen Gel Contraction as a Measure of Fibroblast Function in Carpal Tunnel Syndrome. J. Biomed. Mater. Res. A *103*, 574–580.

Yang, X., Rodriguez, M., Pabon, L., Fischer, K.A., Reinecke, H., Regnier, M., Sniadecki, N.J., Ruohola-Baker, H., and Murry, C.E. (2014). Tri-iodo-l-thyronine promotes the maturation of human cardiomyocytes-derived from induced pluripotent stem cells. J. Mol. Cell. Cardiol. *72*, 296–304.

Yusuf, S., Hawken, S., Ôunpuu, S., Dans, T., Avezum, A., Lanas, F., McQueen, M., Budaj, A., Pais, P., Varigos, J., et al. (2004). Effect of potentially modifiable risk factors associated with myocardial infarction in 52 countries (the INTERHEART study): case-control study. The Lancet *364*, 937–952.

Zhang, Z.-G. (2006). Interactions of primary fibroblasts and keratinocytes with extracellular matrix proteins: contribution of 2 1 integrin. J. Cell Sci. *119*, 1886–1895.

Zhang, W., Kong, C.W., Tong, M.H., Chooi, W.H., Huang, N., Li, R.A., and Chan, B.P. (2017). Maturation of human embryonic stem cell-derived cardiomyocytes (hESC-CMs) in 3D collagen matrix: Effects of niche cell supplementation and mechanical stimulation. Acta Biomater. *49*, 204–217.

Zimmermann, W.-H. (2013). Biomechanical regulation of in vitro cardiogenesis for tissue-engineered heart repair. Stem Cell Res. Ther. *4*, 137.

Zimmermann, W.-H., Schneiderbanger, K., Schubert, P., Didié, M., Münzel, F., Heubach, J.F., Kostin, S., Neuhuber, W.L., and Eschenhagen, T. (2002). Tissue Engineering of a Differentiated Cardiac Muscle Construct. Circ. Res. *90*, 223–230.

Zimmermann, W.-H., Melnychenko, I., Wasmeier, G., Didié, M., Naito, H., Nixdorff, U., Hess, A., Budinsky, L., Brune, K., Michaelis, B., et al. (2006). Engineered heart tissue grafts improve systolic and diastolic function in infarcted rat hearts. Nat. Med. *12*, 452–458.

Appendix

A1. Supplementary results

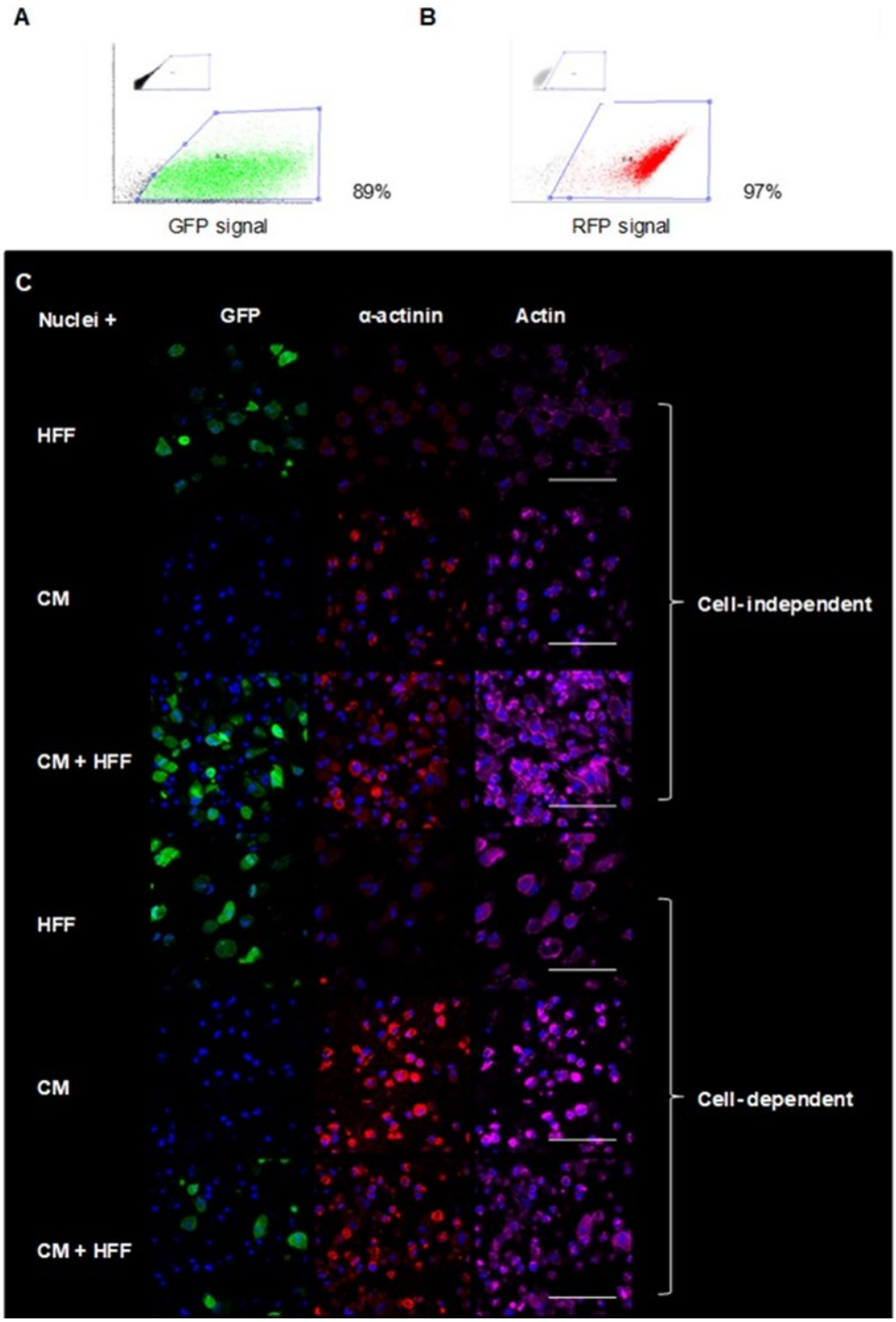

Figure A 1 Cell morphology during early EHM early consolidation

To investigate if changes in stiffness are correlated with changes in cell morphology, we generated hydrogels with GFP$^+$-HFFs and RFP$^+$-CMs. This allowed us to clearly distinguish fibroblasts and CM populations based on their endogenous fluorescence signal. **A** Purity of GFP$^+$-HFF (GFP fluorescence) and **B** RFP$^+$-CM (RFP-

fluorescence) populations used for tissue generation/hydrogel cultures was tested by flow cytometry (representative flow cytometry plots are depicted). **C** Whole mount histology of collagen I hydrogels containing either RFP$^+$-CMs, GFP$^+$-HFFs, or mixtures of both at a 2:1 ratio either 30 or 90 minutes post reconstitution, which represent phases of cell-independent and cell-dependent hydrogel condensation; green: endogenous GFP, red: immunofluorescence staining for α-sarcomeric actinin, magenta: f-actin (phalloidin-labelling); note that the RFP, but not the GFP signal is lost during 4% FA treatment; scale bars: 100 µm.

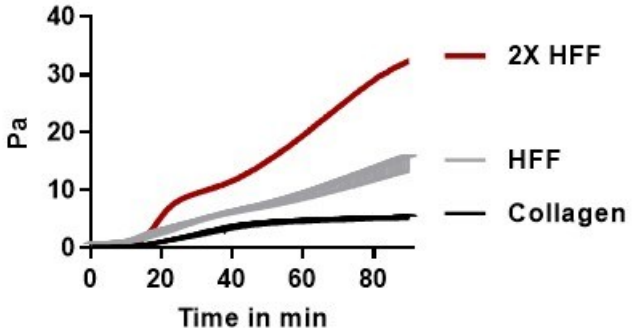

Figure A 2 Fibroblast dosage affects stiffening of collagen I gel

Time sweep of polymerizing collagen I gel (storage modulus) with standard concentration of HFF and doubled HFF content (2X HFF), compared to collagen I hydrogel without cells. n=3/3/1 (Collagen I/+HFF/+2X HFF).

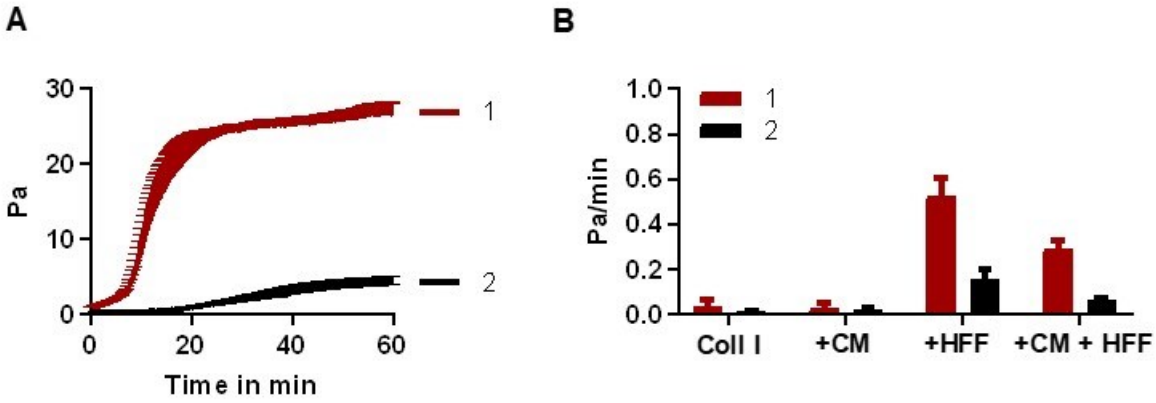

Figure A 3 Comparison of different collagen I batches

A Time sweep of polymerizing collagen I gels (storage modulus) without cells (batch 1 and 2). n=4/3 (Batch 1/2). **B** Slopes of storage moduli in cell-dependent polymerization phase. Batch 1 n=3/4/3/4; Batch 2 n=3/3/4/3; (Collagen/+HFF/+CM/+HFF+CM). Parts of data from (Schlick et al., 2018).

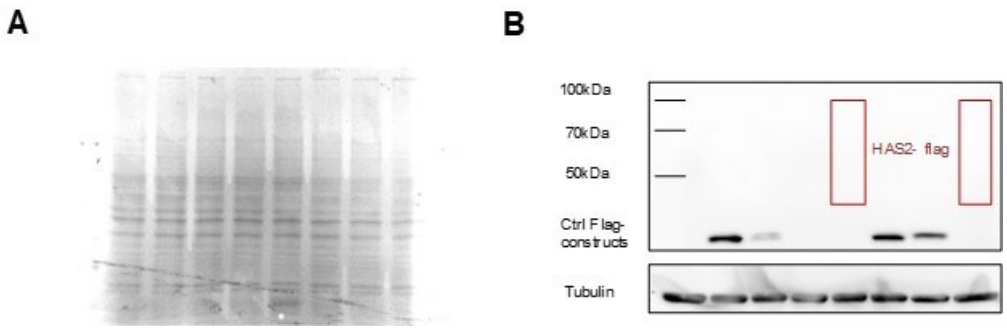

Figure A 4 HAS2-Flag expression in TSA cells

Protein abundance in TSA cells 72 h after transfection with HAS2-flag sequence encoding plasmids. **A** Ponceau stain indicates equal loading without evidence for a particularly enhanced protein band. **B** Western blot of several constructs with control Flag-expressing proteins. In cells transfected with HAS2-Flag containing constructs no flag expression could be detected (red boxes), suggesting instability or lack of expression of the HAS2-flag protein. This was observed despite confirmation of a correctly cloned HAS2-Flag sequence by Sanger sequencing.

A2. Supplementary material

A2.1. Chemicals and buffers for molecular techniques

Chemicals

Table A 1 List of chemicals

Chemical	Manufacturer	Catalogue number
1,4 Dithiotreitol (DTT)	Roth	6908.2
2-[4-(2-hydroxyethyl)-1- piperazinyl]-ethanesulfonic acid (HEPES)	Roth	3908.3
Acetic acid	Roth	T179.2
Ammoniumpersulfate (APS)	Roth	9592.3
Ampicilin sodium salt	Sigma	A9518
Bovine Serum Albumin	Sigma	A3311
Bromphenol blue	Sigma Aldrich	B0126
Calcium chloride dihydrate ($CaCl_2$ X $2H_2O$)	Carl Roth GmbH & Co. KG	52391
Carbachol (Carbamoyl choline chloride)	Sigma	C4382
Complete Mini Protease Inhibitor EDTA free	Roche	11836170001
Deoxycholic acid	AppliChem	A2835.0025
Diethyl pyrocarbonate (DEPC)	Sigma	159220
Dimethyl sulfoxide (DMSO)	AppliChem / Sigma	A3672,0100 / D2650
EGTA	Sigma	E3889
Ethanol	Roth	0911.6
Ethanol molecular grade	Roth	P076.1
Ethylenediaminetetraacetic acid (EDTA)	Roth	8040.1
Eukit (Roti-Histokit II)	Roth	T160
Glacial acetic acid	Roth	3738
Glucose	Carl Roth GmbH & Co. KG	X997.2
Glycerol	Roth	3783.2
Glycine	Roth	3908.2
Hydrochloric acid (HCl) 25%	Roth	4625.2
Isoproterenol (Isoprenaline hydrochloride)	Sigma	I5627
Kanamycin/Streptomycin	Sigma	K4000
L-Ascorbic acid (for Tyrode)	Roth	3525.1
L-ascorbic acid 2 phosphate sesquimagnesium (L-AAP)	Sigma	A8960
Lysogeny broth (LB) powder	Sigma	L3022
Mayer´s haemalaun solution	AppliChem	T865
Methanol	Roth	4627.5

Chemical	Manufacturer	Catalogue number
Milk powder	Roth	T145.4
Phosphatase inhibitor, PhosSTOP	Roche	000000004906845001
Picrosirius red- Direct Red 80	Sigma	365548 or 43665
Polybrene	Sigma	107689-10G
Ponceau S	Carl Roth GmbH & Co. KG	5938.1
Potassium chloride (KCl)	Roth	P017.2
Potassium hydrogenphosphate monobasic (KH_2PO_4)	Roth	T875.1
Rotiphorese gel 30/ 30% Acrylamide-solution	Roth	3029.1
Rotiphorese gel 40% Acrylamide-solution	Roth	7748
Saturated aqueous solution of picric acid (1.3% in water)	Sigma	P6744-1GA
Sodium (di-) hydrogenphosphate dihydrate (Na_2HPO_4 X $2H_2O$)	Carl Roth GmbH & Co. KG	4984.1
Sodium Chloride (NaCl)	Roth	6771.1
Sodium Deoxycholate	AppliChem	30970
Sodium dodecyl sulfate (SDS)	Roth	2326.2
Sodium hydroxide solution (NaOH)	Carl Roth GmbH & Co. KG	0993.1
Sodium lactate	Sigma	71723
Tetramethylethylenediamine (TEMED)	Roth	2367.3
Toluol	Roth	7591
Trasylol	Bayer	34579.01.00
Triton X100	AppliChem	A4975
Trizma base (Tris-HCl)	Roth	4855.2
Tween 20	AppliChem	A49740100
Xylol	Roth	3791
ß-Mercaptoethanol	Sigma	31350-010

Buffers

Table A 2 Buffers and solutions

Buffer	Composition/ Recipe	Protocol
6X Laemmli buffer	0.35 mol/L Tris pH 6.8 30% Glycerol (w/v) 10% SDS (w/v) 9.3% Dithiotreitol (DTT) (w/v) 0.02% Bromphenol blue (w/v)	WesternBlot, SDS-PAGE sample loading buffer
Acetic acid solution 5% (v/v)	5% glacial acetic acid in 1l H2O	Sirius red staining

Buffer	Composition/ Recipe	Protocol
Bäuerle buffer	4.77 g/l HEPES 20.45 g/l NaCl 200 g/l glycerol 0.2 g/l $MgCl_2$ 0.186 g/l EDTA 0.038 g/l EGTA 10 g/l NP-40	Protein extraction for WesternBlot
Blocking buffer, permeabilizing	500 ml PBS 25 ml FBS 5 g Bovine Serum Albumin (BSA) 2.5 ml Triton X-100	FC; IF
Blocking buffer, surface proteins	PBS 5-10%FBS	FC; IF
Blocking solution/ Antibody solution	Milk powder 5%(w/v) in TBST	Western Blot
Carbachol stock 10 mmol/L	10 mmol/L in 300 µmol/L L-AAP	Isometric force measurement
DEPC H_2O	1 ml DEPC in 1 l H_2O, leave o.n. at RT, then autoclave	RNA extraction
Isoproterenol stock 1 mmol/L	1 mmol/L in 300 µmol/L L-AAP	Isometric force measurement
Phosphate buffered saline (PBS)	24 mmol/L NaCl 0.27 mmol/L KCl 0.81 mmol/L Na_2HPO_4 X 2 H_2O 0.15 mmol/L KH_2PO_4 pH 7.4	IF, washing cells for protein and RNA preparations. For cell culture use, see Gibco PBS
Picrosisurs red in Saturated aqueous solution of picric acid	1 g/l in H_2O	Sirius red staining
Ponceau S solution	0.1% Ponceau S (w/v); 0.5% acetic acid (v/v)	Western Blot
Protein preparation buffer ready	Bäuerle buffer 750 µl + CI 150 µl and PI 100 µl	Protein extraction for Western Blot
Ready phosphatase inhibitor solution (PI)	Tablet dissolved in 1 ml H_2O	Protein extraction for Western Blot
Ready protease inhibitor solution (CI)	Tablet dissolved in 1.5 ml H_2O	Protein extraction for Western Blot
Running-Buffer for SDS-PAGE	0.1% SDS 25 mmol/L Tris (30.3 g/l) 192 mmol/L Glycine (144 g/l)	Western Blot
Separating gel buffer	1.5 M Tris-HCl pH 8.8 (181.7 g/l)	Western Blot
Stacking gel buffer	0.5 M Tris-HCl, pH 6.8 (60.56 g/l)	Western Blot
TAE (50X)	242.2 g/l TrisBase 18.6 g/l EDTA 57.1 ml/l glacial acetic acid	Agarose gel-electrophoresis
TBS-Tween (TBST)	0.05 % Tween in TBS	Western Blot

Buffer	Composition/ Recipe	Protocol
Transfer buffer 20% methanol	25 mmol/L Tris 192 mmol/L Glycin 20% Methanol	Western Blot
Tris buffered saline (TBS)	100 mmol/L Tris 150 mmol/L NaCl pH 7.5	Western Blot

Buffers for isometric force measurement

Table A 3 Buffers for isometric force measurement

Buffer	Composition/ Recipe
$CaCl_2$ stock (2.25 mol/l)	165.57 g $CaCl_2$ x $2H_2O$ (MW = 147.02) 500 ml H_2O
$MgCl_2$ stock (1.05 mol/l)	106.83 g $MgCl_2$ x$6H_2O$ (MW = 203.01) 500 ml H_2O
Tyrode Solution I	175 g NaCl 10 g KCl 2.22 ml $CaCl_2$ stock 25 ml $MgCl_2$ stock In 1 l H_2O
Tyrode Solution II	50 g $NaHCO_3$ in 1l
Tyrode Solution III	5.8 g NaH_2PO_4 in 1l
Tyrode´s buffer complete	For 1 l 1 g glucose (cell culture grade) 100 mg L-ascorbic acid (Roth) 40 ml Tyrode solution I 38 ml Tyrode solution II 10 ml Tyrode solution III

A2.2. Labware, consumables and kits

Labware

Table A 4 Labwear

Labwear	Manufacturer
12-well plates	Greiner, Sarstedt, Thermo Scientific
6-well plates	Greiner, Sarstedt, Thermo Scientific
6-well cell culture plates	Greiner, Sarstedt, Thermo Scientific
96-well plates, round bottom, straight bottom	Greiner, Sarstedt, Thermo Scientific
Duran glass petri dishes (60x20 mm)	Duran
Canules	B.Braun
Cell culture dish (6, 10 cm)	Greiner, Sarstedt, Thermo Scientific
Cell culture flasks (T25,75,175)	Greiner, Sarstedt, Thermo Scientific

Cell scraper (16 mm)	Sarstedt
Cryotubes 1.8 ml	Nunc, Greiner
Filter tips (0.5-10 µl, 2-200 µl, 1000 µl)	Labsolute
MrFrosty® Freezing container	Thermo Scientific
Pipet tips (0.5-10 µl, 2-200 µl, 1000 µl)	Greiner
Pipets, serological (5 ml, 10 ml, 25 ml)	Sarstedt
Reaction tubes (1.5 ml, 2 ml)	Eppendorf
Reaction tubes (15 ml, 50 ml)	Greiner
Sterile filter 0,2 and 0,45 µm	Sartorius
Syringe 1,2,5,10,20 and 50 ml	Henke-Sass, Wolf,Braun

Other consumables

Table A 5 Other consumables

Consumable	Manufacturer	Catalogue number	Corresponding protocol
BAM HI	New England Biolabs	R0136S	Cloning of HAS2-Flag
DNA ladder 1 kb ruler	Thermo Scientific	SM0321	Agarose gel electrophoresis
DNA ladder 100 bp plus	Thermo Scientific	SM0321	Agarose gel electrophoresis
DNAseI	Thermo Scientific	18047019	cDNA synthesis
Immobilon Western Chemiluminescent HRP Substrate	Merck Millipore	WBKLS0500	Western Blot
LentiGo stick	Takara Clontech	631243	Virus production and transduction of cells
MidoriGreen	Nippon Genetics	MG04	Agarose gel electrophoresis
NHE I	New England Biolabs	R0131S	Cloning of HAS2-Flag
Nitrocellulose Membrane	Protran Bioscience	10 401396	Western Blot
PAGE ruler prestained, (10 to 170kDa)	Thermo Scientific	26617	Western Blot
Reverse transcriptase	Promega	M3681	cDNA synthesis
Rotiquant	Thermo Scientific	K015	Bradford assay
Silicone Elastomer Kit	Dow Corning	Sylgard®185	Generation of EHM mold
Supersignal West Femto	Pierce Thermo Scientific	34095	Western Blot
Tag polymerase 2X mix	Nippon Genetics	LS27	Colony PCR, cloning of HAS2-Flag

Consumable	Manufacturer	Catalogue number	Corresponding protocol
Trypan blue stain 0.4%	Thermo Scientific	T10282	Cell counting, live/dead exclusion
Whatman Blotting Paper	Whatman	10 426 669	Western Blot

Kits

Table A 6 Kits

Kit name	Manufacturer	Catalogue number	Corresponding protocol
cDNA Synthese: QuantiTect Reverse Trabscription Kit	Qiagen	205313	cDNA (Petra Rompel)
Gel extraction and PCR clean up	Macherey Nagel	740986.20	Cloning of HAS2-flag
Hyaluronan Quantikine ELISA kit	R&D Systems	DHYAL0	ELISA
Plasmid isolation (Mini, Midi) Nucelospin kits	Macherey Nagel	AX20 and AX100 740499.250	Cloning of HAS2-flag
Platinum SYBR Green qPCR SuperMix-UDG	Invitrogen	11733-046	qRT-PCR (Petra Rompel)

A2.3. Antibodies

Table A 7 Primary and secondary antibodies

Target Protein	Antibody specification/Cat	Source	Manufacturer	Dilution	Dilution in WB
Primary Antibodies					
α-sarcomeric Actinin	A7811	Mouse	Sigma	1:1000 IF, 1:100 whole mount 1:4000 FC	
α-Tubulin	T6199/T8203	Mouse	Sigma		1:3.000
BUV395 Mouse anti Human CD90	5E10/563804	Mouse	BD	5 µl/test	
FLAG	M2, monoclonal/F1804/F3165	Mouse	Sigma		1:200
IgG Isotype control	SAB3701169	Rabbit	Sigma	1:2000	
IgG1	MAB002	Mouse	R&D Systems	1:100	
Ki67	SP6/16667	Rabbit	Abcam	1:100 in FC	
Other primary binding reagents					
Wheat Germ Agglutinin – 488 labeled tagged	W11261	-	Invitrogen		
Secondary Antibodies					
anti-Mouse-Alexa 488	A11001	Goat	Invitrogen/Life Technologies	1:1000 IF/FC	
anti-Mouse-Alexa 546	A11003	Goat	Invitrogen/Life Technologies	1:1000 IF/ FC	
anti-Mouse-Alexa 633	A21050	Goat	Invitrogen/Life Technologies	1:1000 IF/ FC	
anti-Rabbit-Alexa 488	A11008	Goat	Invitrogen/Life Technologies	1:1000 IF/ FC	
anti-Rabbit-Alexa 546	A11010	Goat	Invitrogen/Life Technologies	1:1000 IF/ FC	
anti-Rabbit-Alexa 633	A-21071	Goat	Invitrogen/Life Technologies	1:1000 IF/ FC	
HRP conjugated Mouse IgG	P0260	Goat	Dako		1:10.000

Target Protein	Antibody specification/Cat	Source	Manufacturer	Dilution	Dilution in WB
HRP conjugated Rabbit IgG	P0448	Goat	Dako		1:5.000
Other staining reagents					
Hoechst	H3570/33342		Invitrogen/BD	1:1000 IF/ FC	
Phalloidin 488	A22284		Invitrogen	1:100 IF	
Phalloidin 546	A22283		Invitrogen	1:100 IF	
Phalloidin 633	A22284		Invitrogen	1:100 IF	
Sytox Red Dead Cell Stain 633	S34859		Invitrogen /Molecular Probes	1:1000 FC	

IF (Immune fluorescence), FC (Flow cytometry)

A2.4. Plasmids, primers, competent bacteria

Table A 8 Plasmids for the production of lentivirus in TSA cells

Plasmid	Description of vector	Manufacturer/Source
Cumate-pLenti-Blank-SV40-GFP	Cumate repressible vector without insert	AbmGood ICu008
GIPZ	Lentiviral vector	Open Biosystems
HAS2 Lentiviral Vector (Cumate) Cumate	pLenti-Cloning-SV40-GFP), see appendix	AbmGood iCu2040584
pCDNA3	pCDNA3	Invitrogen
pCDNA3 HAS2 flag	pCDNA3 containing HAS2-Flag CDS	Cloned by S. Schlick (see A2.4)
pGIPZ modified-HAS2 flag	pGIPZ containing HAS-flag CDS	Cloned by S. Schlick (see A2.4)
pMD2.G	Vector encoding lentivirus envelope proteins	Addgene 12259, source Didié Trono lab
pReceiver-Lv205	Lentiviral plasmid (control) EX-NEG-Lv205	GeneCopeia, gift of the Department of Pharmacology (Fischer lab), Düsseldorf Petra Rompel
pReceiver-Lv205 with HAS2 insert	Lentiviral plasmid with HAS2 insert for constitutive overexpression EX-U0330-Lv205	GeneCopeia, gift of the Department of Pharmacology (Fischer lab), Düsseldorf Petra Rompel

Bacteria, competent

Table A 9 Competent bacteria

Bacteria	Manufacturer/source	Genotype
TOP10	Produced inhouse	F– mcrA Δ(mrr-hsdRMS-mcrBC) Φ80lacZΔM15 ΔlacX74 recA1 araD139 Δ(ara leu) 7697 galU galK rpsL (StrR) endA1 nupG

Primer

Primers were designed using standard settings of PrimerBLAST. Primers for cloning were generated using SerialCloner software (adaptor function). All primers listed were targeting human genes.

Table A 10 Primers

Target gene	Fwd/Rev	Sequence (5'→3')
18S	Fwd	GCAATTATTCCCCATGAACG
18S	Rev	GGCCTCACTAAACCATCCAA
HAS2	Fwd	GTGGATTATGTACAGGTTTGTGA
HAS2	Rev	TCCAACCATGGGATCTTCTT
HAS2 (cloning-Flag tag)	Fwd	tacaagctagctggcATGCATTGTGA
HAS2 (cloning-Flag tag)	Rev	caaagtggatccTACATCAAGCACC
HAS2 (sequencing)	Fwd	TCGCAACACGTAACGCAAT
HAS2 (sequencing)	Rev	ACTTCTCTTTTTCCACCCCATTT

A2.5. Technical devices, machines and software

Technical devices

Table A 11 Technical devices

Device	Manufacturer
Agarose gel casting system and electrophoresis unit	Generic
Axiovert 40CFL microscope with HBO100 lamp and Axiocam ICm 1	Zeiss
Biovortexer MHX (E)	Xenox
CASY Model TT	Roche
Centrifuge 5417C	Eppendorf
Centrifuge 5417R	Eppendorf
Centrifuge 5810R	Eppendorf
Centrifuge Megafuge 1.0R	Thermo Scientific
Centrifuge MIKRO 22R	Hettich GmbH & Co. KG

Device	Manufacturer
Freezer (-20°C)	Liebherr
Freezer -152	Heraeus, Thermo Scientific
Freezer Hera freeze (-80°C)	Heraeus, Thermo Scientific
Fridge	Liebherr
Heating block	Eppendorf
Incubator for cell culture, Hera Cell 150	Heraeus, Thermo Scientific
Isometric force measurement apparatus	Föhr Medical Instruments (FMI)
Laminar flow cabinet Hera Safe	Heraeus, Thermo Scientific
Magnet stirrer MR3001	Heidolph Instruments GmbH & Co.KG
Mini-PROTEAN® Tetra Cell (electrophoresis unit) and hand casting system	BioRad
NanoDrop® ND-100 spectrophotometer	Peqlab
Neubauer counting chamber, improved	Brand GmbH & Co. KG
P25T Powerpack	Biometra
Personal computers	Dell, HP Compaq 6715b
pH meter	Sartorius
Pipets (0,1-2.5µL; 2-20µL; 20-200µL; 100-1000µL) Eppendorf Research Series 2100	Eppendorf/Sartorius/Gilson/Peqlab
Power supply unit Powerpack P25T	Biometra
Precision balance	Sartorius
Refrigerator (4°C)	Liebherr
Rheometer RSA-G2 (destructive tensile stress measurement)	TA Instruments
Rheometer AntonPaar MCR-501 (shear plate))	AntonPaar
Rotator PROMAX 2020	Heidolph Instruments GmbH & Co.KG
Shaking device “Rocky“	Schütt Labortechnik
StepOnePlus Real Time PCR	Applied Biosystems (qRT-PCR in Düsseldorf)
Thermomixer comfort	Eppendorf

Custom made tissue culture molds

PDMS was prepared according to the manufacturer´s protocol. In short, polymerization reagent and silicone were mixed in a 1:10 (5 ml and 45 ml) ratio. The solution was inverted till it was homogenous, centrifuged briefly to remove bubbles and then loaded either by pouring or with a cannula into stretcher molds. The solution was allowed to settle for several hours at RT (o.n.) and then baked in the drying cabinet at 60°C until it was polymerized and solidified properly (non-stick test). Negative molds were provided by the workshop (UMG, and custom-made).

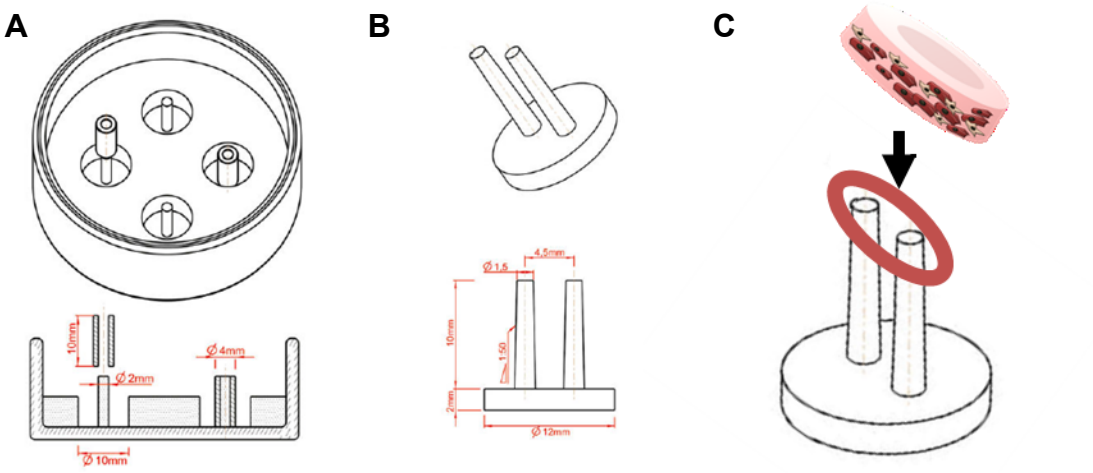

Figure A 5 EHM PDMS molds and auxotonic stretchers

A Standard EHM mold, V per tissue 450 µl. Central hollow poles can be removed for EHM to be transferred onto stretchers. **B** Auxotonic PDMS stretcher, both images taken from (Tiburcy et al., 2014). **C** Positioning of EHM onto auxotonic stretchers (carried out manually).

Contraction setup

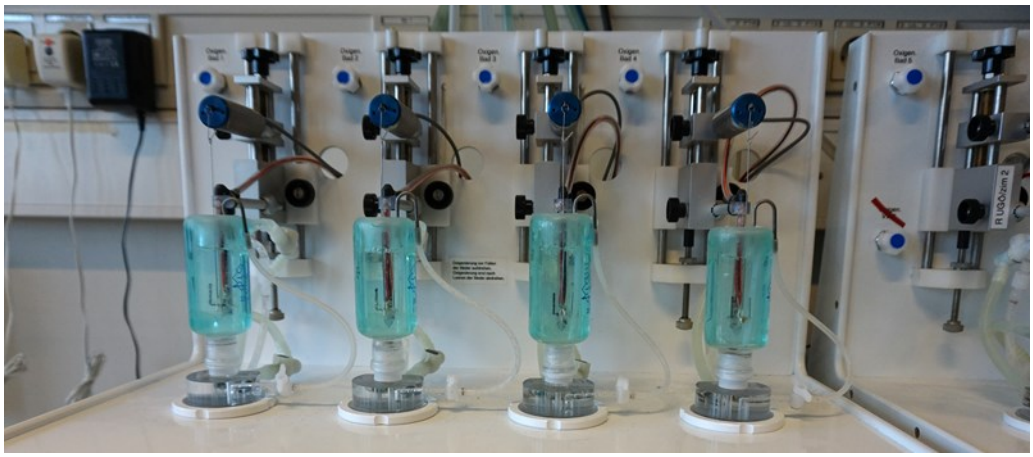

Figure A 6 Organ bath apparatus for isometric force measurements

The isolated organ bath apparatus was designed and constructed by FMI. It consists of 16 individual organ baths with a 20 ml buffer reservoir. The hollow glass mantle is warmed by a steady flow of prewarmed 37°C warm water containing anti-microbial supplements. EHM can be stimulated electrically. Forces are measured via force transducers. The force of contraction (FOC) is calculated by $Force_{max} - Force_{min}$ exerted by the EHM. For isometric force measurements, EHMs were immersed in Tyrode´s solution containing a basal concentration of 0.2-4 mmol/L $[Ca^{2+}]$ during measurements.

Software

Table A 12 Software

Software	Manufacturer	Purpose
Adobe Photoshop CS	Adobe	Image processing
AxioVision 4.8	Zeiss	Imaging
FACS DIVA	BD	Flow cytometry
Flowings	University of Turku	Flow cytometry analysis
Gimp	Open source/freeware	Image processing
GraphPad Prism 7	GraphPad Software Inc., San Diego	Data analysis, generation of figures
ImageJX2	Open source/freeware	Image processing
Linux Ubuntu	Canonical	Operating system
Microsoft Office (PowerPoint, Excel, Word) 2010 and 2013	Microsoft	Data management, generation of documents and presentations
Microsoft Windows 7, 8, and 10	Microsoft	Operating system
ND-1000 v3.7.0	Peqlab	Nanodrop
Rheometer AntoonPaar Rheoplus	AntonPaar	Rheology
SerialCloner	Open source	Cloning
TRIOS	TA Instruments	Rheology, tensile stress
Zotero	Open source/freeware	Citations, bibliography

A2.6. Primary cells, cell lines and cell culture

Basic cell culture ingredients

Table A 13 Reagents for cell culture

Base media/Chemicals/growth factors/inhibitors	Cat	Manufacturer
100X penicillin/streptomycin (10.000 U/ml)	15140	Life technologies/Gibco
100X penicillin/streptomycin, -20°C	15140	Life technologies/Gibco
100X sodium pyruvate (NaP) (100 mmol/L)	11360	Life technologies/Gibco
10X PBS	70011044	Life technologies/Gibco
10X RPMI powder	52800-035	Life technologies/Gibco
Accutase Solution	SCR005,	Milipore
Acid-soluble Collagen	01APA006	Collagen Solutions
Activin A	338-AC	R&D systems
B27- insulin supplement	A1895601	Life technologies/Gibco
B27 supplement	17504-044	Life technologies/Gibco

BD Matrigel Basement Membrane Matrix Growth Factor Reduced	354230	BD
FGF (for stem cell differentiation)	130-093-841	Stemgent
CHIR	04-0004	Stemgent
Collagenase from Clostridium histolyticum Type I	C0130	Sigma
DMEM for TSA cells	42430-082	Life technologies/Gibco
DNaseI	260913	Calbiochem
DNaseI	3750	Calbiochem
Dulbecco's Modified Eagle Medium (DMEM) (Glutamax)	61965-059	Life technologies/Gibco
EDTA 0.5 mmol/L, 2 mmol/L	In-house	
Fibroblast Basal Medium (FBM)	CC-3131	Lonza
Fetal bovine serum (FBS)	11573397	Life technologies/Gibco
FGF (for EHM culture)	AF-100-18B	Peprotech
FGM-3 SingleQuots	CC-4525	Lonza
Fungizone/Amphotericin B	11510496	Life technologies/Gibco
IGF	AF-100-11	Peprotech
IMDM (Glutamax)	21980-065	Life technologies/Gibco
IWP4	04-0036	Stemgent
Knockout DMEM	10829-018	Life technologies/Gibco
Knockout serum replacement (KOSR)	10828-028	Life technologies/Gibco
Laminin-521 (100 µg/ml)	LN521-03	Biolamina
L-ascorbic acid 2 phosphate sesquimagnesium salt hydrate (L-AAP)	A8960	Sigma
L-Glutamine, 100X (200 mmol/L)	35050061	Life technologies/Gibco
Matrigel Basement Membrane Matrix Growth Factor Reduced	354230	BD
Non-essential amino acids (NEAA) 100X (10 mmol/L)	11140050	Life technologies/Gibco
PBS (+$CaCl_2$/+$MgCl_2$)	14040-091	Life technologies/Gibco
PBS without $CaCl_2$/$MgCl_2$	14190144	Life technologies/Gibco
Polybrene	107689	Sigma
Polybrene - Hexadimethrine bromide	H9268	Sigma
Puromycin	A1113803	Life technologies/Gibco
Retinoic acid	R2625	Sigma
Rock inhibitor Y27632 (ROCKi)	04-0012-10	Stemolecule
RPMI 1640 (Glutamax)	61870-044	Life technologies/Gibco
RPMI 1640 without glucose, without HEPES	11879020	Life technologies/Gibco
StemPro® Accutase® Cell Dissociation Reagent	A11105-01	Life technologies/Gibco
Synthemax II	CLS3535	Corning via Sigma

TeSR™-E8™ Kit	05940	Stem Cell Technologies
TGFβ1	AF-100-21C	Peprotech
TrypLE	12604	Life technologies/Gibco
Trypsin 2.5%,	15090-046	Life technologies/Gibco
$VEGF_{165}$	AF-100-20	Peprotech
Versene	15040-033	Life technologies/Gibco

Cell culture media and working solutions

Solution/buffer	Recipe/Instructions	Protocol
10X RPMI	RPMI powder dissolved in H_20 10.4g in 10ml	Generation of EHM
2X RPMI	2 ml 10X RPMI, 7 ml H_20, 200 µl of 100X P/S solution and 800 µl B27 minus insulin	Generation of EHM
Accutase cell dissociation solution	Accutase solutionAccutase Solution 0.025% Trypsin 20 µg/ml DNaseI	Subculture of CMs
Collagenase solution	2 g/l PBS (+ Ca^{2+} and Mg^{2+}) with 20% FBS	EHM dissociation
DNaseI	1 mg/ml in H_2O	Cell and EHM dissociation
DNaseI stock solution	100 µg/ml in H_2O	CM dissociation
EDTA 0.5 mmol/L	Add 1 ml of the 0.5 mol/L EDTA stock solution (pH 8.0) into 1 l PBS with 0.9 g NaC	HES dissociation
EDTA 0.5 mol/L stock	18.6 g/L EDTA in H_2O	
FGF-2 stock	10 µg/ml in PBS containing 0.1% rHSA	Generation of EHM, EHM culture
IGF-1 stock	100 µg/ml in PBS containing 0.1% rHSA	Generation of EHM, EHM culture
IWP4 stock solution	5 mmol/L IWP4 in DMSO	Cardiac specification
L-AAP stock at 300 mmol/L	L-AAP dissolved in H_2O	Standard cell culture
Laminin coating solution	Dilution of stock (100 µg/ml) to 2.5 µg/ml in PBS (+ Ca^{2+} and Mg^{2+})	Stromal cell differentiation
Matrigel coating solution	1 ml Matrigel thawed on ice, diluted 1:120 in PBS (Gibco)	CM differentiation and replating
Polybrene stock	8 mg/ml in H_2O	Transduction of cells
Retinoic acid solution	For 100 mmol/L: 50 mg in 1.67ml DMSO For 1 mmol/L stock dilute 1:100 in 100% EtOH	Stromal cell differentiation
Rock Inhibitor (Stemolecule Y27632) Stock solution	10 mmol/L in DMSO	Dissociation and subculture of PSC cells and CMs

Synthemax II coating solution	Dilute stock 1:40 in H_20 (25 µg/ml)	Derivation of primary cells
Synthemax II stock	10 ml H_20 in 1 vial (1 mg/ml)	Derivation of primary cells
TGFß1 stock	5 µg/ml in PBS containing 0.1% rHSA	Generation of EHM, EHM culture
$VEGF_{165}$ stock	5 µg/ml in PBS containing 0.1% rHSA	Generation of EHM, EHM culture

All cell culture media and supplements from powder or unsterile solutions were sterile filtered through 0.2 µm filters (Sartorius). All growth factor stocks and enzyme solutions were kept at -20°C for storage. Coating solutions for cell culture dishes were kept at 4°C once prepared.

Table A 14 Cell culture media and supplements

Medium/Buffer	Recipe	Protocol
Cardiac fibroblast culture medium (FGM3 Medium)	FBM medium containing all supplements (FGM3 bullet kit)	Culture of cardiac fibroblasts
Cardiac specification medium	CM basal medium 5 µmol/l IWP4	Cardiac specification
CM basal medium	RPMI 1640 with Glutamax 100 U/ml / 100 µg/ml P/S 1 mmol/l of sodium pyruvate 2% B27 supplement 200 µmol/L L-AAP	CM maintenance and differentiation, stromal cell differentiation
HES2 medium	Kockout DMEM 20% Knock-out serum replacement (KOSR) 10 ng/ml FGF-2	Culture of HES2 cells
HFF/GFB culture medium	DMEM Glutamax 15% FBS 100 U/ml P/S	HFF and GFB culture
Lactate selection medium	RPMI without Glucose 100 U/ml / 100 µg/ml P/S 2.2 mmol/L Na lactate 0.1 mmol/L 2-mercaptoethanol	CM differentiation, metabolic selection after cardiac specification
Mesodermal induction medium (MIM10-B)	CM basal medium 1 µmol/L CHIR 10 ng/ml BMP4 9 ng/ml Activin A 5 ng/ml FGF-2	Stromal cell differentiation
Serum free maturation medium (EHM Medium)	IMDM Glutamax 100 U/ml / 100 µg/ml P/S 0.1 mmol/L NEAA 300 µmol/L L-AAP 4% B27 minus insulin	EHM generation, EHM long-term culture

	5 ng/ml $VEGF_{165}$ 10 ng/ml FGF-2 100 ng/ml IGF-1 5 ng/ml TGFβ1 (days 1-3)	
Stromal cell specification medium (StC-SM; prepare fresh)	CM basal medium 50 ng/ml BMP4 4 µmol/L retinoic acid 1 µmol/L CHIR	Stromal cell differentiation
TSA culture medium	DMEM (for TSA) 10% FBS 100 U/ml / 100 µg/ml P/S 2 mmol/L L-Glutamine	TSA culture

All cell culture media were kept at 4°C. Media that did not contain FBS were prepared fresh every time for use. Media with FBS were kept up to 2 weeks.

A2.7. Vector maps

Standard and commercial vectors

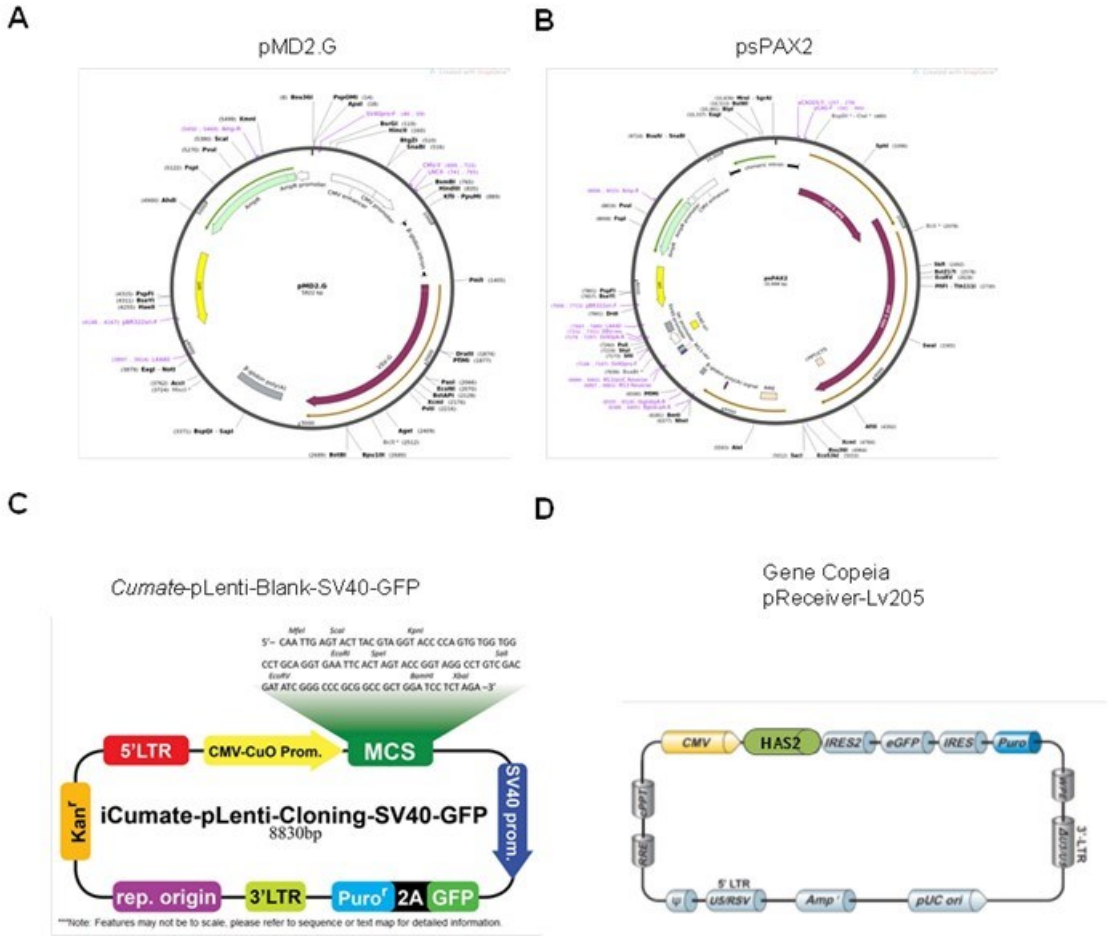

Figure A 7 Maps of commercial vectors

A Lentiviral envelope plasmid pMD2.G vector by Addgene (Lab of Didié Trono). **B** Lentiviral packaging plasmid psPAX2 vector by Addgene (Lab of Didié Trono). **C** Cumate-p-Lenti_Blank-SV40-GFP from AbmGood used for generation of GFP^+ HFF cells. **D** GeneCopeia pReceiver-Lv205 vector with/without HAS2 insert used for the generation of HAS2-overexpressing HFF.

Vectors containing HAS2-Flag

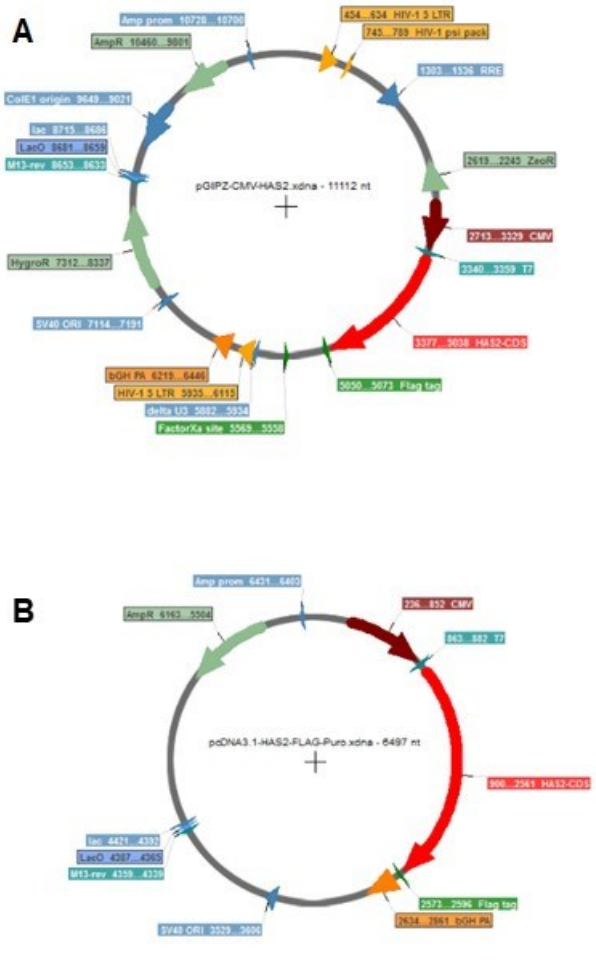

Figure A 8 Vectors generated for HAS2-Flag overexpression

A pGIPZ-based vector and **B** pcDNA3.1 based vector with HAS2-Flag CDS.